Amphiphilic Polymer-Based Fluorescent Probes for Enantioselective Recognition of Amino Acids and Amino Alcohols

Shifeng Nian
Bengbu, China

B.S. Chemistry, University of Science and Technology of China, 2013

M.S. Chemistry, University of Virginia, 2016

A Dissertation presented to the Graduate Faculty
of the University of Virginia in Candidacy for the Degree of
Doctor of Philosophy

Department of Chemistry

University of Virginia
May, 2018 Degree **will be Conferred**

Abstract

Amphiphilic polymer-based fluorescent probes were synthesized by conducting atom transfer radical polymerization of *N*-isopropylacrylamide in the presence of a 3,3'-diformyl-1,1'-BINOL-based diinitiator. The probes were soluble in both water and common organic solvents and had unique solution properties such as lower critical solution temperature (LCST) and cononsolvency.

Optically pure polymer probes in combination with Zn^{2+} in aqueous solution (BICINE buffer at pH = 8.80) showed highly enantioselective fluorescence enhancement in the presence of a number of amino acids. It was found that chloroform can be used to extract the aqueous polymer-Zn^{2+}-amino acid solution and the resulting chloroform extract maintained the highly enantioselective fluorescence response. Thus, the enantiomeric composition of a chiral amino acid can be determined in the two immiscible solvents of water and chloroform. The aqueous polymer-Zn^{2+}-amino acid solution showed LCST at 34 ^{o}C above which the polymer-Zn^{2+}-amino acid adduct precipitated out. Measuring the fluorescence of the precipitate redissolved in the aqueous buffer solution showed the retention of the high enantioselectivity. Both the chloroform extraction and the thermo-induced precipitation have allowed the fluorescence response of the sensor toward amino acids to be measured away from the original substrate solution. These two strategies should minimize the interference by other reaction components on the fluorescence measurement when the sensor is applied to analyze the asymmetric reaction screening experiments.

Optically pure polymer probes in combination with Zn^{2+} in water and methanol showed highly enantioselective fluorescence enhancement in the presence of five amino alcohols. In addition, optically pure and racemic probes exhibited a unique cononsolvency property. Mixing

an aqueous solution of an optically pure polymer probe and Zn^{2+} with a dichloromethane solution of (*S*)- or (*R*)-amino alcohols led to the formation of polymer films at the interface of the water and dichloromethane phases. The polymer films were separated and showed highly enantioselective fluorescence enhancement in DMSO solution. The cononsolvency of this PNIPAM-based BINOL probes allows the sensor-substrate adduct to be readily separated from the original solution which should greatly reduce the interference of other components on the fluorescence measurement when the substrate is produced from a catalyst screening experiment.

When the polymers were treated with a mixture of the enantiomers of an amino alcohol, no fluorescence enhancement was observed unless one of the enantiomers was in excess of the other. This large nonlinear effect allows the racemic polymer probe to be used to determine the *ee* of the amino alcohol which represents the first example to use a racemic fluorescent probe to determine the *ee* of a chiral molecule.

Acknowledgement

I would like to give my deepest appreciation to my graduate advisor, Prof. Lin Pu, for his continuous guidance and help during my studies.

I would also like to thank Prof. Gunnoe, Prof. Hilinski, Prof. Zhang and Prof. He for being my Committee member and giving me advice on my research.

I also want to thank my undergraduate advisor, Dr. Guoqing Zhang, who gave me a lot of support and help during my PhD career.

I wish to express my gratitude to all my groupmates who helped me a lot on my research project.

Last but not least, I would like to thank my parents for always believing in me and encouraging me to finish my Doctoral Degree.

Table of Contents

List of Figures

List of Schemes

List of Tables

Chapter 1. Enantioselective fluorescent recognition of chiral molecules

1.1. Introduction

Chirality is a geometric property of some molecules and ions and exists universally in nature.[1] A molecule is chiral if it is not superimposable on its mirror image, and the mirror image of the molecule is called enantiomer or optical isomer. The two enantiomers of a chiral molecule have identical physical and chemical properties in most cases, however, their functions in biological systems can be very different because of the chiral environment in the body.[2] Most biologically active molecules are chiral, including amino acids, proteins, sugars and nucleic acids.[3] These molecules may behave differently as plant growth regulators, insect pheromones, and enzyme substrates in living system.[4] In addition, most modern drugs are enantiopure, as one enantiomer of a chiral molecule often has higher efficacy and lower toxicity than the other enantiomer.[5,6] The synthesis of enantiopure drugs requires the discovery of new chiral catalysts or chiral reagents. Therefore, the development of techniques for the determination of enantiomeric composition of substance has become a major research area, as these techniques are not only useful in the analysis of enantiomeric purity of biological analytes but also very promising in the high throughput screening (HTS) of chiral catalysts, reagents and drugs in pharmaceutical industry.[7]

Enantiomeric excess (*ee*) is often used to quantify the ratio of two enantiomers in a mixture as defined by the equation: $ee = ([R]-[S])/([R]+[S])$, where [R] and [S] are the respective fraction of two enantiomers in a mixture.[8] Currently, there are several techniques that are able to determine the enantiomeric content in analytes or reactions, such as high-performance liquid chromatography (HPLC), gas chromatography (GC), nuclear magnetic resonance (NMR) and capillary electrophoresis (CE).[9–15] However, the instruments used for these techniques are

usually expensive and the methods are time-consuming in most cases. As a result, low-cost, real-time and simple techniques are needed for the rapid determination of *ee*.

Optical methods, especially those based on fluorescence techniques, have drawn extensive attention of researchers due to the advantages of fluorescence methods such as simplicity, high sensitivity, readily available instrumentation and real-time analysis.[16–18] Therefore, fluorescence methods have been widely used for the enantioselective recognition of chiral organic molecules.[19] In the following content, enantioselective fluorescent recognition of various chiral substrates, such as chiral amines, amino alcohols and amino acids will be summarized and the applications of these fluorescent methods will be described.

1.2. Enantioselective fluorescent recognition of chiral amines and amino alcohols

Chiral amines and amino alcohols are important building blocks for developing new pharmaceutical drugs due to their abundant structural diversity and inherent ability for hydrogen bonding.[20] Therefore, development of efficient fluorescent method for enantioselective recognition of chiral amines and amino alcohols would be very useful for the screening of asymmetric catalysts to carry out the synthesis of the enantiopure compounds.

1.2.1. 1,1'-Bi-2-naphthol (BINOL)-based fluorescent probes

BINOL-based organic compounds are the most extensively used enantioselective fluorescent probes. Iwanek and Mattay reported the first enantioselective fluorescent recognition of chiral amines by (*S*)- or (*R*)-BINOL (**1.1**) in 1992. The fluorescence of (*S*)-**1.1** or (*R*)-**1.1** could be enantioselectively quenched by a series of chiral amines (**1.2**-**1.5**) in acetonitrile (Figure **1.1**).[21] The enantioselectivity could be due to the formation of different charge separated excited ionic pairs between BINOL and two enantiomers in acetonitrile.

However, the enantioselectivity is low (less than 16%), probably because most of the BINOL molecules were quenched by radiationless decay, and only a small portion of the excited BINOL molecules was quenched by the formation of the excited ionic pairs.

Figure 1.1. Structure of BINOL and chiral amines

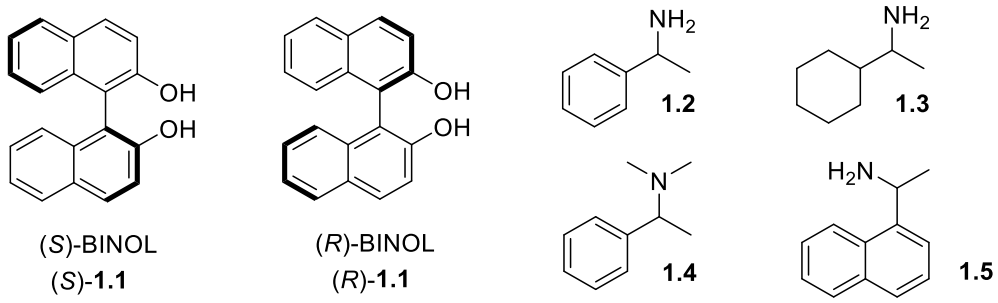

In the past two decades, our laboratory has carried out extensive study on using BINOL to develop enantioselective fluorescent sensor.[19,22–24] For example, Pugh et al. synthesized a series of BINOL-based dendrimers for the enantioselective fluorescent recognition of amino alcohols.[25–27] It was found that the dendrimer **1.8** with longer branching chains (Figure **1.2**) led to the higher fluorescence intensity in a benzene:hexane (20:80) mixed solvent, which was a much more sensitive sensor compare with **1.6** and **1.7** when used to interact with amino alcohols. Chiral amino alcohols **1.9-1.11** could efficiently quench the fluorescence of **1.8**. The quenching is enantioselective and the two enantiomers led to a 1.18-fold difference in fluorescence intensity.

Figure 1.2. Structure of dendrimers and chiral amino alcohols. Reprinted (adapted) with permission from (*J. Org. Chem*. **1999**, 64 (20), 7528–7536). Copyright (1999) American Chemical Society.

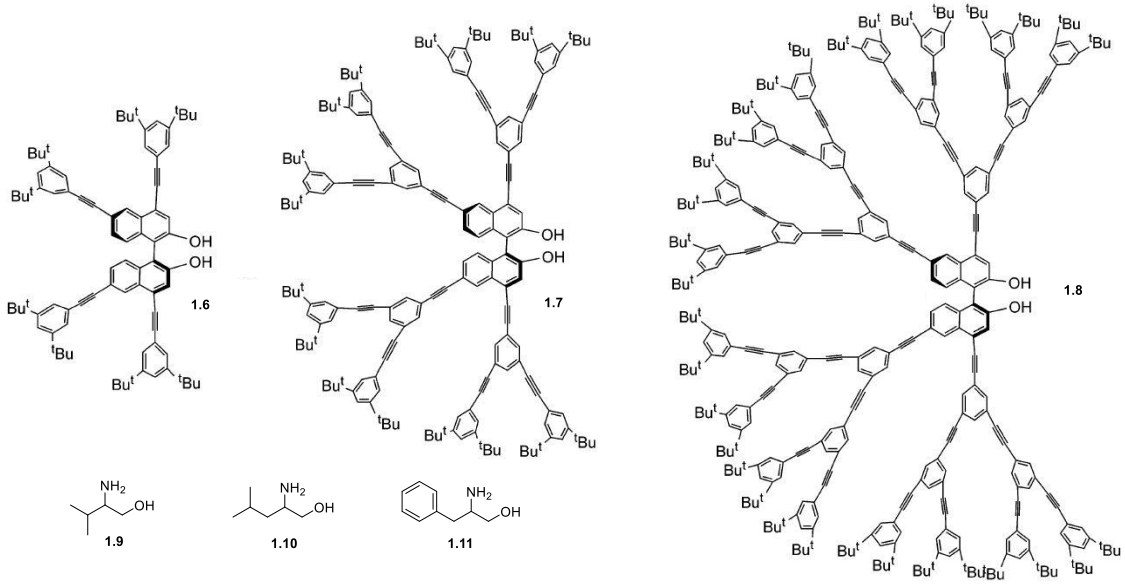

Yu et al. reported the synthesis of BINOL-based trifluoromethyl ketone molecule (**1.12**) for the enantioselective fluorescent recognition of chiral diamine *trans*-1,2-diaminocyclohexane (*S*,*S*)-**1.13** and (*R*,*R*)-**1.13** in CH_2Cl_2.[28] (*S*)-**1.12** was non-emissive in CH_2Cl_2. However, addition of (*R*,*R*)-**1.13** led to dramatic fluorescence enhancement with dual emissions at 370 (λ_1) and 438 (λ_2) nm (Figure **1.3**, blue line). The addition of (*S*,*S*)-**1.13** led to similar fluorescence enhancement at λ_1, however, the fluorescence enhancement at λ_2 is much weaker (Red line). Therefore, the concentration of **1.13** can be determined by using the fluorescence intensity at λ_1, and the *ee* of **1.13** can be calculated by using the fluorescence intensity difference at λ_2.

Figure 1.3. Enantioselective fluorescent recognition of **1.13** by (*S*)-**1.12**. Reprinted (adapted) with permission from (*J. Am. Chem. Soc*., **2012**, 134 (50), 20282–20285). Copyright (2012) American Chemical Society

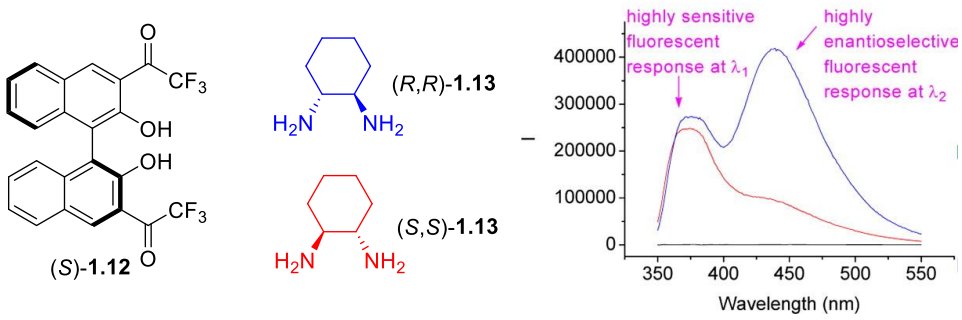

Wang et al. further modified the structure of (*S*)-**1.12** to make (*S*)-**1.14** with long perfluoro chains.[29] (*S*)-**1.14** was soluble in perfluorohexanes and had highly enantioselective fluorescent response toward various amino alcohols (**1.9**, **1.10**, **1.15**, **1.16**) and diamine (**1.13**) after the amino alcohols dissolved in minimum amount of CH_2Cl_2 and mixed with the perfluorohexane solution of (*S*)-**1.14**. The products generated from two enantiomers of a chiral substrate would precipitate out of the solution with different particle size and the two enantiomers could be distinguished even by naked eyes (Figure **1.4**). This is the first highly enantioselective fluorescent probe applied in the fluorous phase.

Figure 1.4. Enantioselective fluorescent recognition of amino alcohols by (*S*)-**1.14**. Reprinted (adapted) with permission from (*J. Am. Chem. Soc.*, **2015**, 137 (11), 3747–3750). Copyright (2015) American Chemical Society.

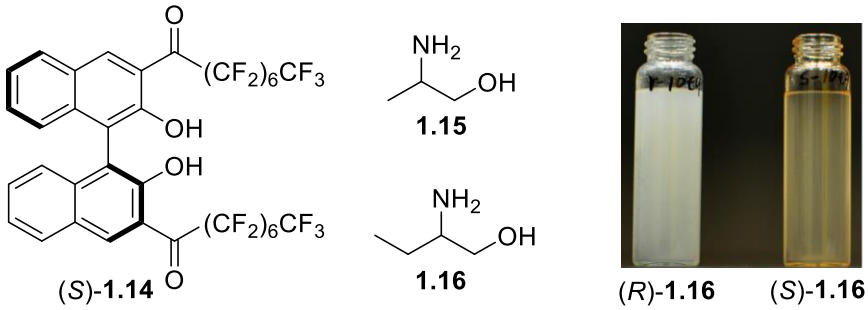

Huang et al. synthesized the BINOL-based chiral dialdehyde **1.17** for the enantioselective recognition of diamine (**1.13**) and various amino alcohols (**1.11**, **1.15**, **1.18**) in the presence of Zn^{2+} in methanol.[30] (*R*)-**1.17** itself had little fluorescence in methanol, and would

have a much higher fluorescence enhancement toward (*S*,*S*)-**1.13** and (*S*)-amino alcohols than their enantiomers. Song et al. studied enantioselective fluorescence enhancement mechanism.[31] The aldehyde group in **1.17** quenched its fluorescence due to the excited state proton transfer from hydroxide group to aldehyde. After the reaction between **1.17** and amino alcohol, the imine product still had little fluorescence due to proton transfer and *cis-trans* isomerization of the imine bond at excited state. Zn^{2+} coordination toward the product played a key role in fluorescence enhancement because the formed rigid Zn^{2+} complex could inhibit the proton transfer and *cis-trans* isomerization processes. ESI-MS revealed the formation of the dimeric structure **1.19** (Figure **1.5**), which had much higher fluorescence intensity in methanol compared with **1.17**. NMR study showed that the product after the reaction between (*R*)-**1.15** and (*S*)-**1.17** was more favored to form structure 1.19 and exhibited strong fluorescence intensity. The other product resulted from (*S*)-**1.15** would less likely to form dimeric structure and the fluorescence intensity is much weaker.

Figure 1.5. BINOL-based chiral dialdehyde probes and formation of Zn^{2+} complex

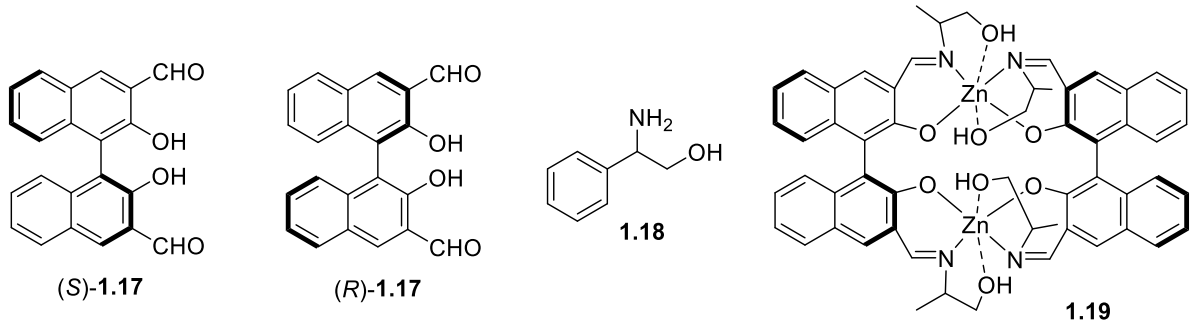

BINOL-based polymer sensors were also employed in the enantioselective fluorescent recognition of amino alcohols. Compared with small molecule sensors, polymer sensors may have higher enantioselectivity due to conjugation and energy transfer among each subunit and multiple chiral centers in the polymer. Zhang et al. reported the synthesis of the polymer sensor (*S*)-**1.20** by coupling BINOL dialdehyde sensors with *p*-phenylene linkers (Figure **1.6**).[32] (*S*)-

1.17 had large fluorescent response toward leucinol **1.10** in CH_2Cl_2, but the enantioselectivity is low. The enantiomeric fluorescence enhancement ratio (*ef*) is only 1.1 [$ef = (I_R - I_0)/(I_S - I_0)$, where I_R is the fluorescence intensity after the addition of (*R*)-amino alcohol, I_S is the fluorescence intensity after the addition of (*S*)-amino acid, I_0 is the fluorescence intensity of the background]. However, for (*S*)-**1.20**, the *ef* value is 5.4, which demonstrated a much large enantioselectivity. The enhanced enantioselectivity is probably due to the energy migration along such a chiral conjugated polymer chain. The fluorescent recognition requires a cumulative effect of the enantiomers along the polymer chain. Only when all of the binding sites of the polymer interact with the substrates can there be a large fluorescence enhancement, which should contribute to the increased enantioselectivity.

Figure 1.6. Structure of the polymer fluorescent probe (*S*)-**1.20**

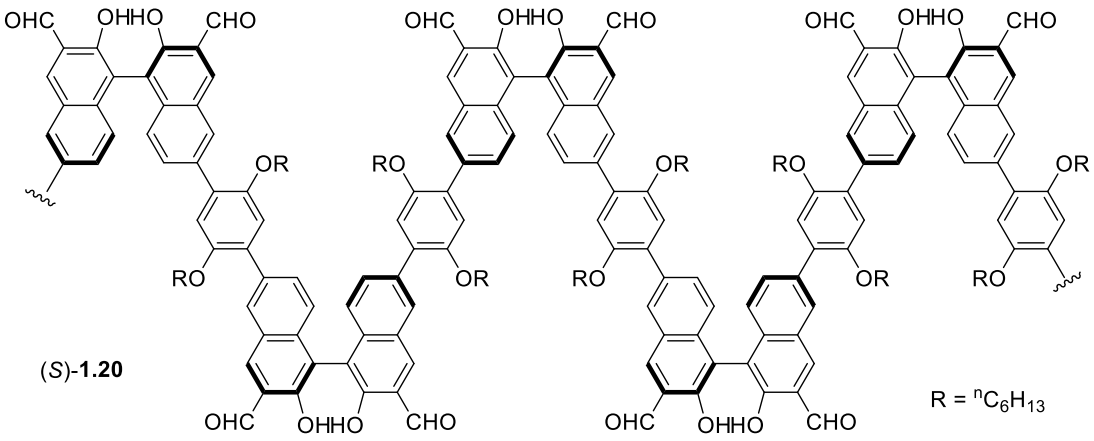

Wang et al. developed a BINOL-monoaldehyde-based polymer sensor for enantioselective recognition of prolinol (**1.21**), a secondary amino alcohol.[33] The monoaldehyde small molecule (*S*)-**1.22** had large fluorescent response toward **1.21** in CH_2Cl_2, but the *ef* value is less than 1.2, representing very low enantioselectivity. After free radical polymerization, multiple monoaldehyde units were attached on a single carbon backbone to form a polymer sensor (*S*)-**1.23** (Figure **1.7**), which has much lower fluorescence intensity

compared with (*S*)-**1.22** due to the photoinduced electron transfer (PET) between adjacent subunits and excited proton transfer process. However, (*S*)-**1.23** showed a much higher enantioselective fluorescent response toward **1.21** than (*S*)-**1.22** with *ef* = 3.7, which could be due to cumulative inhibition of PET and proton transfer as well as the multiple steric centers of the polymer sensor.

Figure 1.7. Structure of polymer fluorescent probe (*S*)-**1.23**

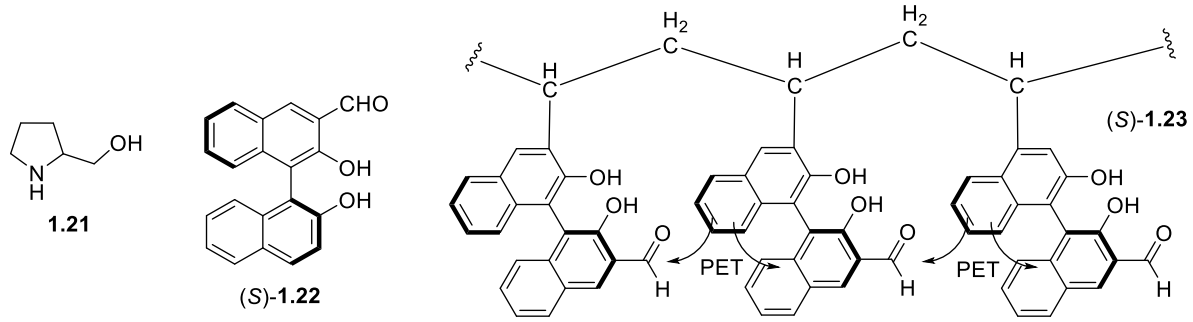

1.2.2. Other fluorescent probes

There are a lot of fluorescent probes applied in the enantioselective recognition of amino alcohols besides BINOL-base probes. Reetz et al. synthesized enantiopure 2,15-dihydroxy-hexahelicene **1.24** (Figure **1.8**) and used it for the enantioselective recognition of various amines and amino alcohols (**1.3**, **1.4**, **1.9**, **1.11**, **1.15**, **1.25-1.27**).[34] The fluorescence intensity of **1.24** was enantioselectively quenched by the two enantiomers of the substrates. **1.15** gave the best results with over 2- fold enantioselectivity.

Figure 1.8. Structure of fluorescent probe **1.24**

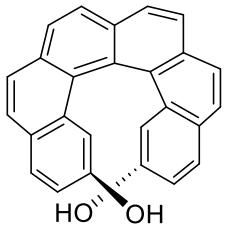

1.24

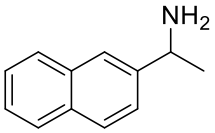

1.25

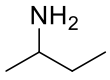

1.26

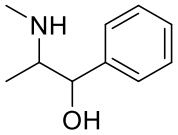

1.27

Liu et al. synthesized a 1,8-bis(3-*tert*-butyl-9-acridyl)naphthalene *N*,*N*′-dioxide compound **1.28** for enantioselective recognition of chiral amino alcohols.[35] **1.28** has weak fluorescence intensity, however, it forms a complex with $Sc(OTf)_3$, which exhibited strong fluorescence intensity. Two enantiomers of amino alcohols (**1.10**, **1.15**, **1.16**, **1.29**, **1.30**) can enantioselectively quench the Sc-**1.28** complex due to the ligand displacement mechanism.

Figure 1.9. Structure of fluorescent probe **1.28**

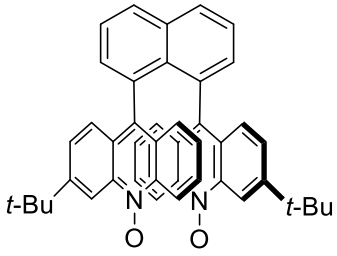

1.28

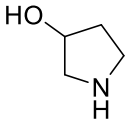

1.29

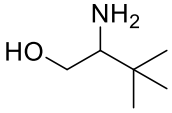

1.30

Xu et al. synthesized chiral polymer **1.31** incorporating (*R*,*R*)-salen-type unit. Reduction of imine bonding using $NaBH_4$ gave chiral polymer **1.32**.[36] The two polymer probes can be used for the enantioselective recognition of phenylglycinol **1.18**. Addition of (*S*)-**1.18** led to higher fluorescence enhancement than its enantiomer, probably due to the stronger interaction between the probe and (*S*)-**1.18**. The *ef* values are 1.84 and 2.05 for **1.31** and **1.32**, respectively. The linear relationship between fluorescence intensity and *ee* of **1.18** made it useful in the *ee* measurement.

Figure 1.10. Structure of polymer fluorescent probe **1.31** and **1.32**

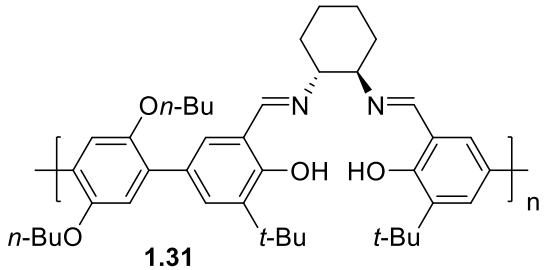

1.31

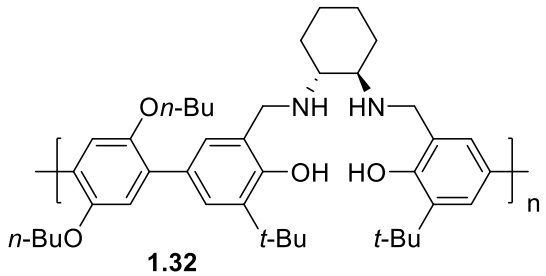

1.32

1.3. Enantioselective fluorescent recognition of amino acids and their derivatives

Amino acids play a crucial role in nature. L-amino acids are building blocks of proteins and important metabolic intermediates in biological processes.[37,38] In recent years, more and more natural D-amino acids have been discovered in humans, animals and plants.[39,40] They are also associated with a variety of biological functions. For example, D-Serine was found to be an endogenous neuromodulator at glutamatergic synapses.[41] Therefore, mapping the distribution of L- and D- amino acids in biological systems is of great importance to further understand the role of amino acids. D-amino acids was also found in food due to high temperature, extreme pH processing conditions or microbial contamination. Thus, the D/L ratio of amino acids can be used to examine the quality of food.[42,43] The significance of L- and D-amino acids attracts researchers to develop the methods for enantioselective recognition of amino acids, and fluorescence method is one of the most powerful ways.

1.3.1. BINOL-based fluorescent probes

In 2004, Lin et al. reported the use of chiral bisbinaphthyl macrocycle **1.33** (Figure **1.11**) in the enantioselective fluorescent recognition of *N*-protected amino acid derivatives.[44] Compound **1.33** has weak fluorescence intensity due to the excited state proton transfer from hydroxide group to amine group.[45] Amino acid derivatives had strong hydrogen bonding

interaction with **1.33** in aprotic solvent, and the carboxylic acid group could protonate amine group, inhibiting the proton transfer process. As a result, enhanced fluorescence intensity would be observed after adding amino acid derivatives. (*R*)-**1.33** has highly enantioselective fluorescent response toward a series of amino acid derivatives (**1.34**-**1.38**) in benzene/dimethoxyethylene(DME) mixed solvent because the interaction of the probe with the two enantiomers generated two different diastereomers, which should have different fluorescence intensity. It was found that *ef* values were all higher than 1.7 for these amino acid derivatives. 1.34 exhibited the best result with *ef* = 5.7.

Figure 1.11. Structure of the macrocyclic fluorescent probes **1.31** and **1.32** and substrates

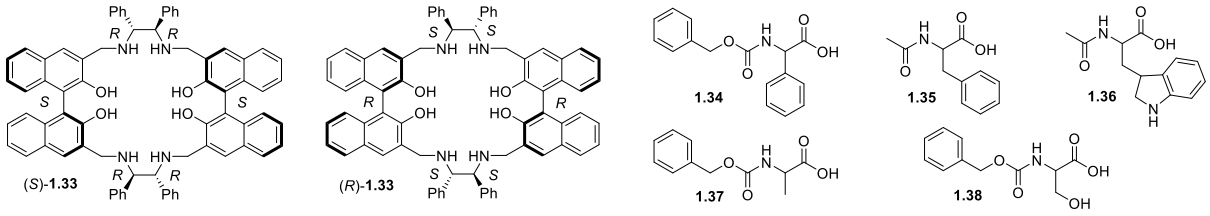

He et al. synthesized fluorescent probes **1.39** containing benzylaminomethyl groups at 3,3'-position of BINOL.[46] The probes showed higher enantioselective fluorescent response toward various *N*-Boc-protected amino acid derivatives (**1.40**-**1.45**). The enantioselective fluorescence enhancement could be due to the suppression of excited state proton transfer process and the formation of two different diastereomers between the probe and the two enantiomers via hydrogen bonding interaction. **1.40** showed the highest enantioselectivity (*ef* = 10.4) for interaction with (*R*,*S*)-**1.39**.

Figure 1.12. Structure of the fluorescent probes **1.39** and substrates

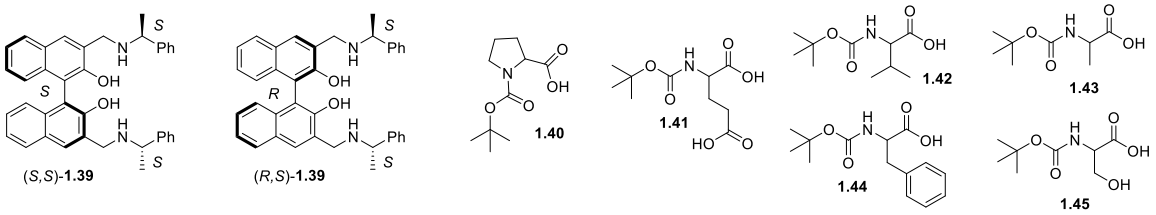

Liu et al. synthesized the BINOL-amino alcohol compound (*S*)-**1.46** (Figure **1.13**) for the enantioselective recognition of various amino acid derivatives (**1.34**, **1.37**, **1.38**, **1.47**-**1.49**).[47] The different hydrogen bonding interaction between the probe and two enantiomers of the substrates led to enantioselective fluorescence enhancement. **1.38** showed the highest enantioselectivity (*ef* = 12.5) at λ = 460 nm.

Figure 1.13. Structure of the fluorescent probes (*S*)-**1.46** and substrates

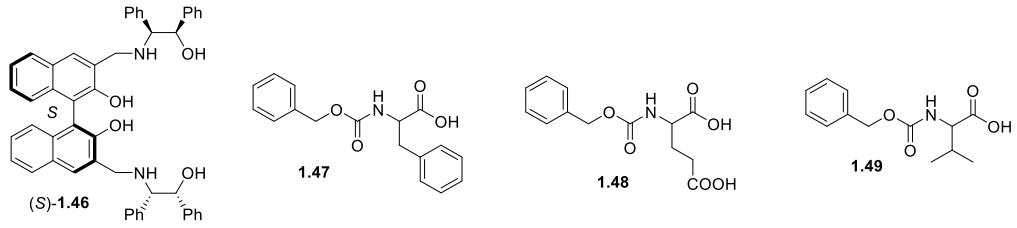

It was found that fluorescent probe **1.17** could be used in the enantioselective recognition of free amino acids in the presence of Zn^{2+} and Bu_4NOH in methanol.[30] It had highly enantioselective fluorescent response toward phenylalanine **1.50** at λ = 515 nm. It also had moderate enantioselectivity after interacting with other amino acids (**1.51**-**1.55**) (Figure **1.14**).

Figure 1.14. Structure of the fluorescent probes (*S*)-**1.17** and amino acid substrates

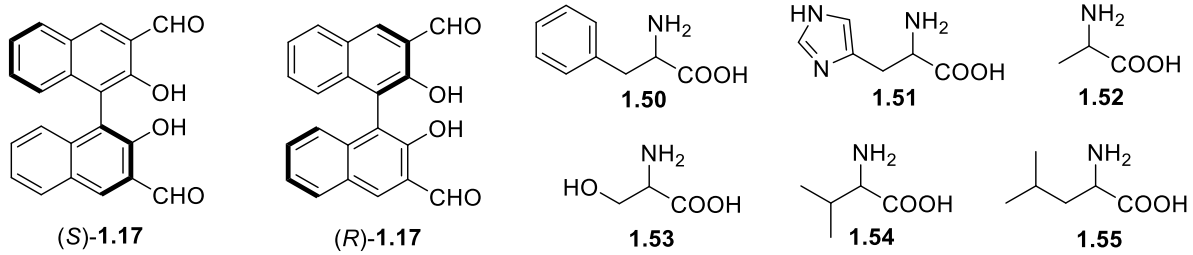

1.3.2. Other fluorescent probes

Cyclodextrins are cyclic oligosaccharides which contain six, seven, and eight D-glucopyranose units, and they are called α-, β-, and γ-cyclodextrins, respectively. These compounds can interact with various organic compounds to bind them inside their hydrophobic cavities in aqueous solutions. Corradini et al. synthesized phenylalanine-based fluorescent β-cyclodextrins **1.56** (Figure **1.15**) for the enantioselective recognition of amino acids.[48] These compounds contained a chiral binding site for Cu(II) derived from phenylalanine and a dansyl fluorophore. These metal complexes had weak fluorescence intensity due to the quenching of Cu(II) toward the dansyl group. After the addition of two enantiomers of amino acids, the fluorescence of the complexes would be enantioselectively enhanced. This is because the formation cyclodextrin-Cu(II)-amino acid complexes had different stabilities for the two enantiomers. In addition, displacement of the dansyl group from Cu(II) by amino acids suppressed the quenching of Cu(II). It was found that proline **1.57** showed the highest enantioselectivity with *ef* = 3.89.

Figure 1.15. Structure of the fluorescent probes **1.56** and amino acid substrate

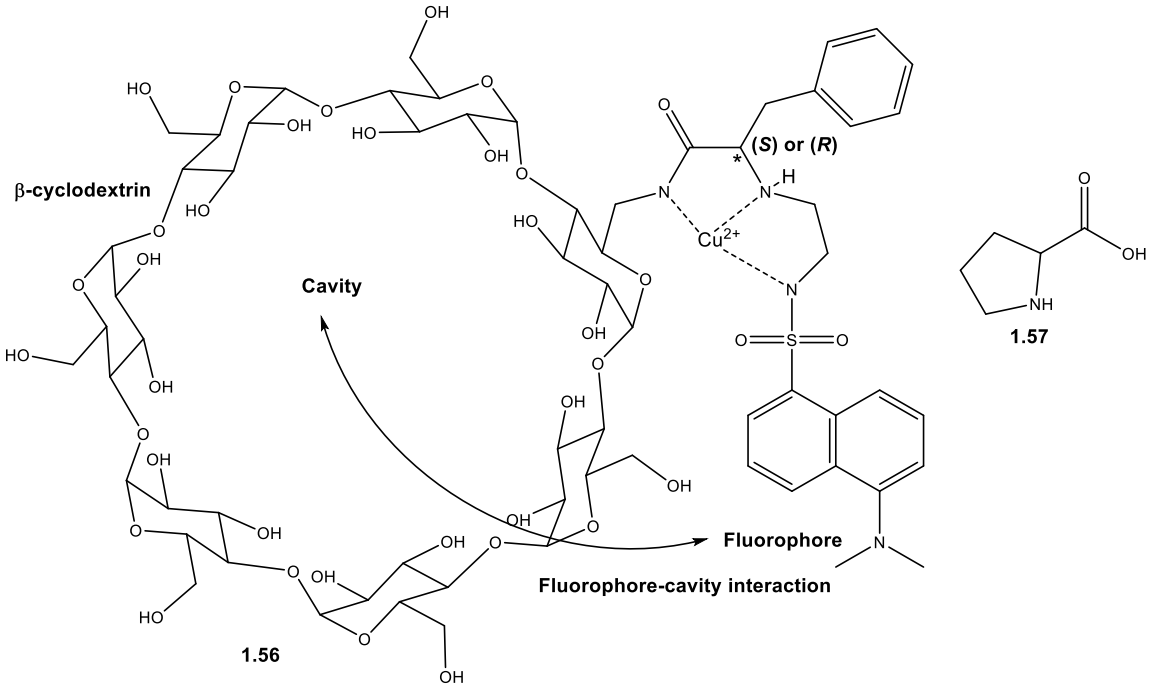

Wong et al. synthesized chiral terpyridine macrocycle containing multiple ether groups as a fluorescent sensor **1.58** (Figure 1.15) for enantioselective recognition of amino acid derivatives in CH_2Cl_2. The fluorescence intensity of the sensor would be quenched after the addition of α-phenylglycine methyl ester hydrochloride (PhEtOMe, **1.59**) due to the chelation between terpyridine and ammonium salt. The enantioselectivity of the probe is around 3.8-fold, which resulted from the difference of binding constant. One enantiomer binds more tightly with the sensor, and the formed two diastereomers led to fluorescence intensity difference.

Figure 1.16. Structure of the fluorescent probes **1.58** and amino acid derivative **1.59**

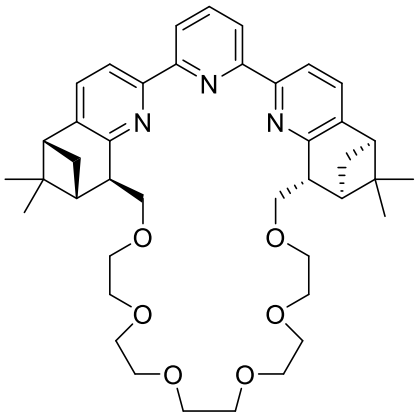

1.58

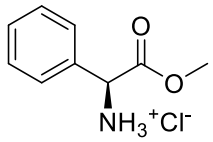

(*S*)-**1.59**

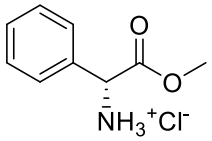

(*R*)-**1.59**

Wolf et al. synthesized a chiral 1,8-diacridylnaphthalene-derived fluorescent sensor **1.60** for enantioselective recognition of *N*-Boc-protect amino acid derivatives (**1.40**, **1.45**, **1.61**-**1.64**).[49] The sensor had weak fluorescence intensity probably due to the photoinduced electron transfer (PET) quenching of nitrogen atom. The hydrogen bonding interaction between the sensor and substrates could suppress the quenching and enhanced fluorescence intensity was observed. The enantioselective fluorescence enhancement could be due to the formation of different diastereomers between sensor and two enantiomers.

Figure 1.17. Structure of the fluorescent probes **1.60** and amino acid derivatives

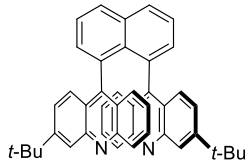

1.60

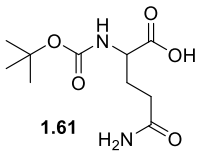

1.61

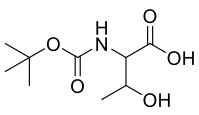

1.62

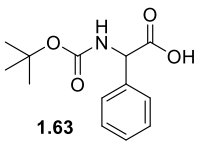

1.63

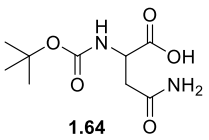

1.64

1.4. Enantioselective fluorescent recognition of other chiral organic molecules

A number of fluorescent sensors had been developed in our laboratory for the enantioselective recognition of α-hydrocarboxylic acids. For example, the chiral bisbinaphthyl molecule **1.65** was designed for the enantioselective recognition of mandelic acid **1.66**.[50] The

sensor had weak fluorescence intensity due to quenching by excited state proton transfer. Hydrogen bonding interaction between **1.65** and **1.66** enhanced the fluorescence intensity because of the suppressed proton transfer process. **1.67** was a proposed complex of **1.65** and (*S*)-**1.66** formed by three hydrogen bonding interaction. The enantioselective fluorescence enhancement was due to the formation of different diastereomeric complexes and the *ef* value was 2.49 in benzene/2%DME solvent. Dendric derivatives **1.68** and **1.69** (Figure **1.18**) were also synthesized to increase the sensitivity of **1.65**.[51] The fluorescence enhancement was much higher after the interaction between **1.68** or **1.69** with **1.66**. The enantioselectivity was also maintained. For **1.68**, the *ef* value is 2.05; for **1.69**, the *ef* value is 1.49.

Figure 1.18. Structure of the fluorescent probes **1.65**, **1.68**, **1.69**

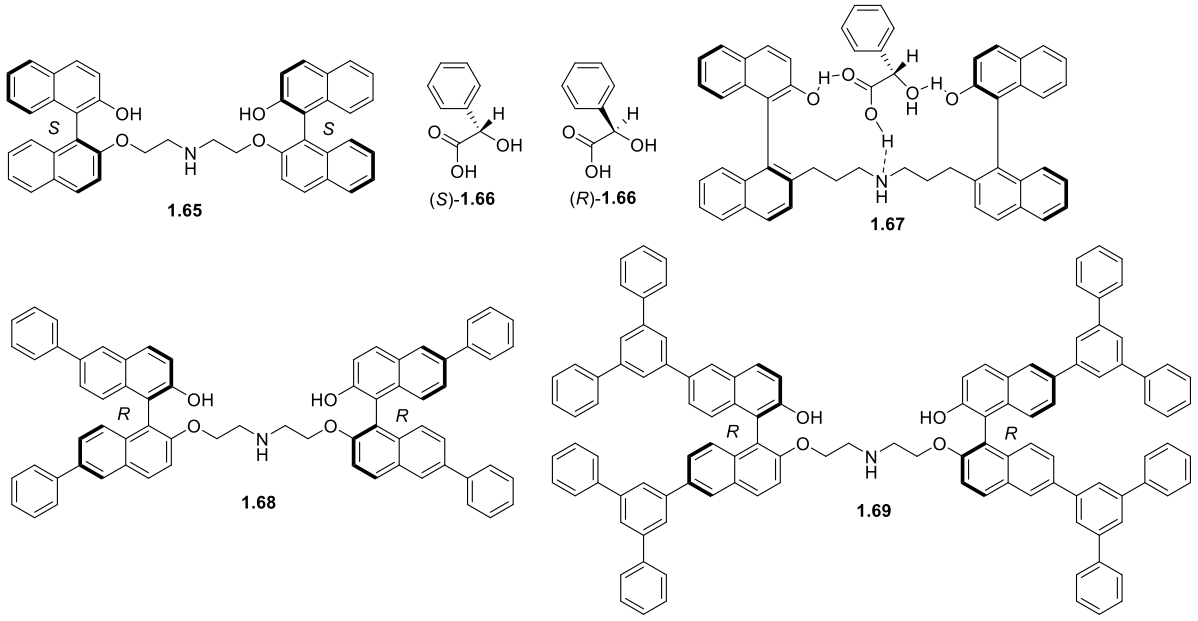

Liu et al. developed the fluorescent sensor **1.70** to expand the substrates of α-hydrocarboxylic acid for enantioselective recognition. 1.70 showed highly enantioselective fluorescent response toward various α-hydrocarboxylic acids (**1.66**, **1.71**-**1.77**).[52] The fluorescence intensity ratio, I_R/I_S ratio, is 11.2 for **1.66**, 25.8 for **1.71** and 22.8 for **1.74**, representing very high enantioselectivity. The high enantioselectivity could be explained by a

two-stage mechanism. As shown in Figure **1.19**, in the first stage, (*S*)-**1.70** and (*R*)-**1.66** formed a relatively stable 1:1 complex **1.78** via hydrogen bonding interaction. **1.78** still had weak fluorescence intensity because there was a second nitrogen atom that was not protonated and could undergo excited state proton transfer to quench the fluorescence of **1.78**. The second stage involved the protonation of the second nitrogen by another **1.66** molecule, which will greatly suppress the proton transfer process, resulting in the fluorescence enhancement. The enantioselectivity was due to the formation of different diastereomeric complexes.

Figure 1.19. Structure of the fluorescent probes **1.70** and substrates

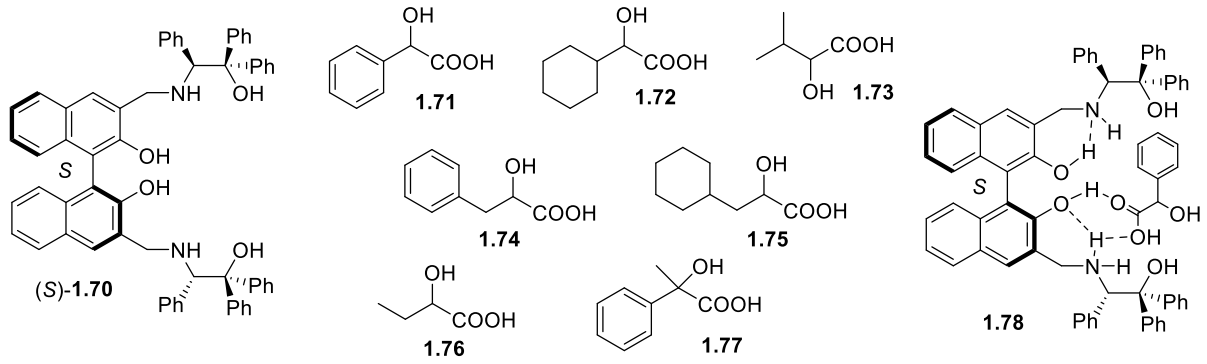

Yu et al. developed pseudoenantiomeric fluorescent sensor pair with 1:1 mixture of (*S*)-**1.70** and (*R*)-**1.79**, an H_8BINOL based-fluorescent sensor (Figure **1.20**), for simultaneous determination of *ee* and concentration of **1.66** in CH_2Cl_2 solution.[53] H_8BINOL is the partial hydrogenation product of BINOL and is less conjugated. (*S*)-**1.70** had high enantioselective fluorescent response toward **1.66** at λ_1 = 374 nm. (*R*)-**1.79** had similar enantioselectivity toward **1.66** but the fluorescent emission wavelength was shifted from λ_1 = 374 nm to λ_2 = 330 nm due to the less conjugated structure. Therefore, the pseudoenantiomeric fluorescent pair had dual emission at 374 nm and 330 nm. The concentration and *ee* of **1.66** can be determined with by one single fluorescence measurement and calculating the sum and difference of the fluorescence intensities at λ_1 and λ_2.

Figure 1.20. Structure of the fluorescent probes **1.79**

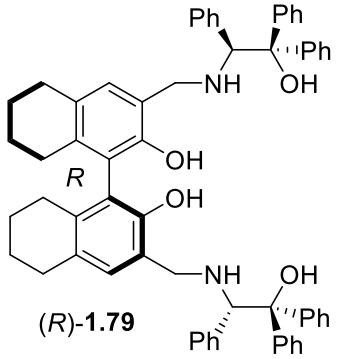

(*R*)-**1.79**

Shinkai et al. synthesized BINOL-based diboronic acids fluorescent probes **1.80** for enantioselective recognition of D- and L-monosaccharide.[54] The fluorescence intensity of the probe greatly enhanced after the addition of monosaccharide in water:methanol (2:1) buffer at pH = 7.77. Cyclic boronate esters **1.81** could be formed as shown in Figure **1.21**, which increased the Lewis acidity of the boronic acids and strengthened the interaction with the adjacent amine group. The fluorescence enhancement was probably due to the increased structural rigidity. The fluorescence enhancement was enantioselective. When using (*R*)-**1.80**, The fluorescence intensity ratio I_D/I_L was 1.47 for fructose (**1.82**), 1.93 for glucose (**1.83**) and 0.82 for galactose (**1.84**).

Figure 1.21. Structure of fluorescent probes **1.80** and substrates

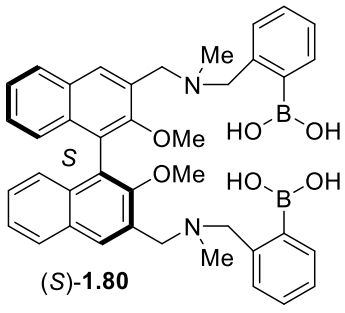

(*S*)-**1.80**

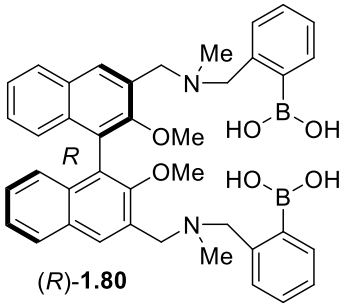

(*R*)-**1.80**

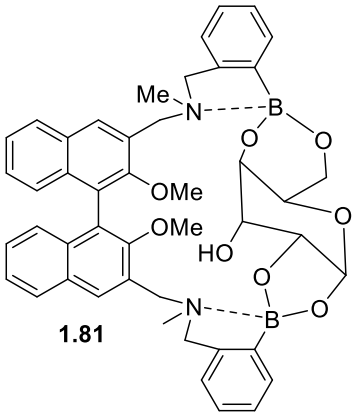

1.81

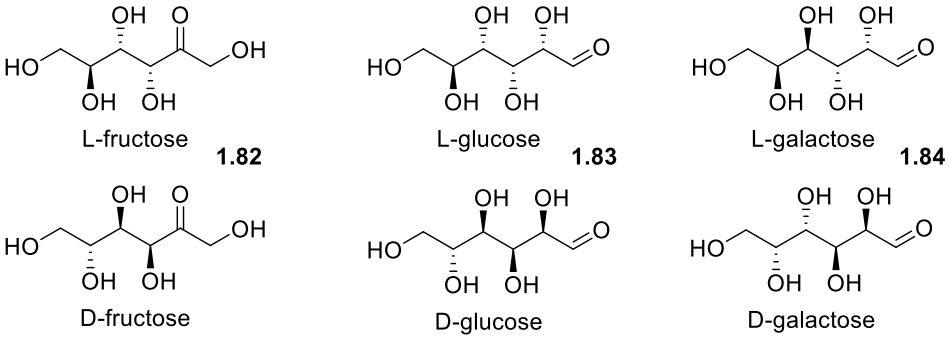

James et al. developed a 3,6-disubstituted carbazole-based bisboronic acid fluorescent sensor **1.85** (Figure **1.22**) for enantioselective recognition of tartaric acid **1.86**. The (*S*,*S*)- and (*R*,*R*)-**1.85** showed highly enantioselective fluorescence enhancement toward **1.86** in pH = 5.6 NaCl ionic buffer (52.1% methanol in water). The fluorescence enhancement could be due to the hydrogen bond interaction and protonation of nitrogen atom in the sensor, which led to suppression of PET quenching.

Figure 1.22. Structure of fluorescent probes **1.85** and substrates

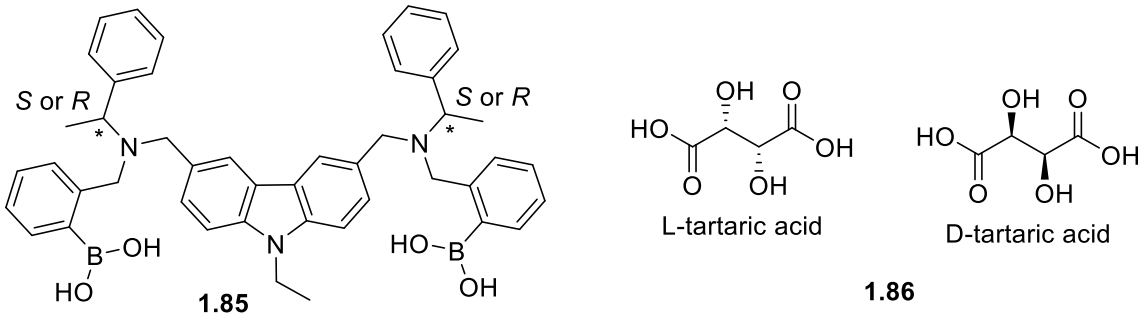

1.5. Application of enantioselective fluorescent probes

Enantioselective fluorescent probes can be used to determine the enantiomeric composition in analytes. Therefore, it is useful in the asymmetric catalyst screening experiment. The *ee* of the products can be determined by using suitable fluorescent probes after reactions, and the asymmetric catalyst which leads to the highest *ee* can be identified. For example, Li et al. reported the application of the bisbinaphthyl macrocycles (*S*)-**1.87** and (*R*)-**1.87** in the chiral

catalyst screening of a mandelic acid derivative (**1.89**) formation reaction (Figure **1.23**).[55] (*S*)-**1** and (*R*)-**1** had enantioselective fluorescent response toward **1.66**[56] and its derivative **1.89** due to different hydrogen bonding interactions between sensor and two enantiomers. **1.89** was not soluble in many common organic solvents but dissolved well in THF. **1.89** can be precipitated out after the reaction and dissolved in THF for fluorescence measurement. It was found that the fluorescence intensity difference, ΔI ($\Delta I = (I_S/I_{S0}) - (I_R/I_{R0})$), had a linear relationship with the *ee* of **1.89**. Therefore, the *ee* of **1.89** can be determined using this curve, and the chiral ligand that led to the highest ee can be found.

Figure 1.23. Catalyst screening by using the fluorescent probe **1.87**, Reprinted (adapted) with permission from (*Org. Lett*. **2005**, 7 (16), 3441–3444). Copyright (2005) American Chemical Society.

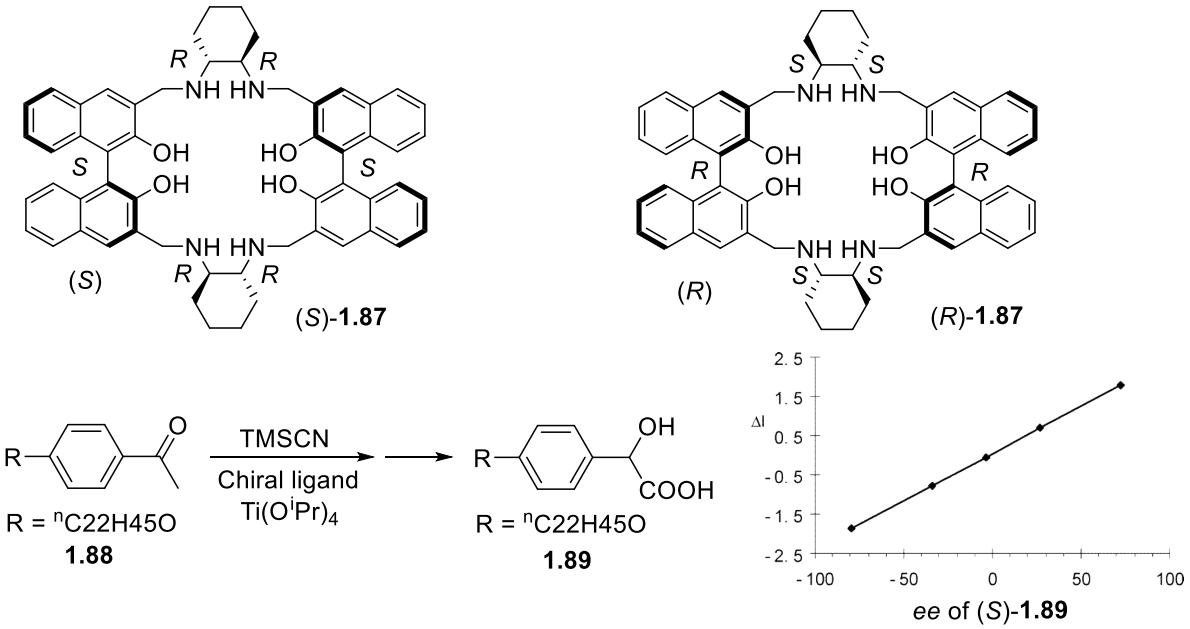

The enantioselective fluorescent probes have the potential to be employed in high throughput screening (HTS), in which numerous experimental samples are simultaneously tested under given conditions. HTS has been utilized in the catalyst screening of organic

reactions as well as dug discovery. As shown in Figure **1.24**, in traditional approach to asymmetric synthesis, a single design-synthesis-testing cycle is designed and tested for reactivity and selectivity.[8] The cycle continues until a system that is found to produce the desired *ee* value. This method is time consuming because the *ee* measurement is relatively slow using traditional method. HTS greatly improves the efficiency of this process by largely multiplying each step and employing new methods for *ee* measurement in short time. Fluorescence method is a good choice due to its high sensitivity and real-time analysis, which significantly decreases the time and efforts in *ee* measurement. However, small molecule fluorescent sensors have their own limitations if applied in HTS process. When a fluorescent probe is added into a chiral catalyst screening reaction mixture, other components in the reaction besides the desired product, including the catalyst, reagent, starting material and side product, could potentially interfere with the fluorescence measurement and reduce the effectiveness of the chiral sensor.[57]

Figure 1.24. Methods for catalyst screening

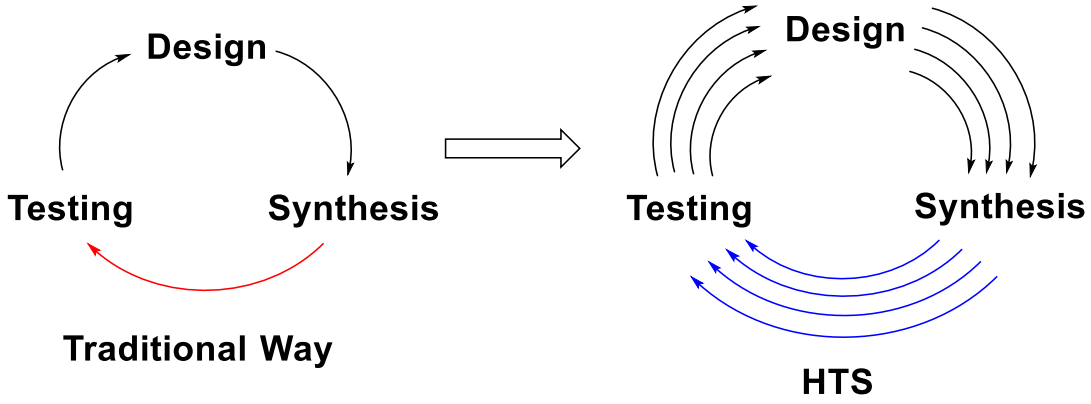

Enantioselective fluorescent probes can also be used in the fluorescent imaging of amino acids in living cells. Zeng et al. reported that 1,1'-Spirobiindane-7,7'-diol (SPINOL)-based chiral aldehydes (*R*)- and (*S*)-**1.90** had highly enantioselective fluorescence enhancement

toward various chiral amino acids (**1.50**, **1.52**, **1.53**, **1.55**, **1.91**, **1.92**) in the presence of Zn^{2+} and Bu_4NOH (Figure **1.25**).[58] The probes could be used in the enantioselective fluorescent imaging of free chiral amino acids in living cells and it is possible to determine the enantiomeric composition of amino acids *in vivo*. However, the sensor is not soluble in aqueous solution, and Bu_4NOH is toxic for cells,[59] which hinders the usage of this probe for further *in vivo* applications.

Figure 1.25. Structure of the fluorescent probes **1.90** and amino acid substrates

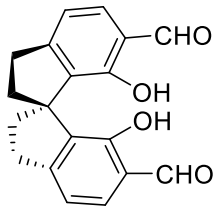

1.90

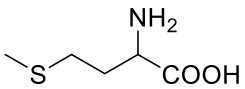

1.91

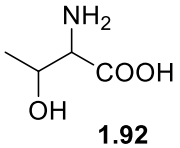

1.92

1.6. Conclusion

Enantioselective fluorescent probes have been widely used in the recognition of various substrates. They have the potential to be used in HTS and fluorescent imaging. However, new probes need to be developed to overcome the shortcomings in practical applications. In this project, we tried to incorporate the BINOL-aldehyde small molecule sensor **1.17** with water-soluble polymers, which could increase the solubility of the polymer-based sensors in aqueous solutions. In addition, polymers have unique solvent properties compared with small molecules, which makes it possible to separate the reaction product from the original mixture and reduce the interference of other components when conducting fluorescence measurements.

Reference

(1) Zhang, X.; Yin, J.; Yoon, J. *Chem. Rev.* **2014**, *114* (9), 4918–4959.

(2) Noguez, C.; Hidalgo, F. *Chirality* **2014**, *26* (9), 553–562.

(3) Weiss-López, B. E.; Azocar, M.; Montecinos, R.; Cassels, B. K.; Araya-Maturana, R. *Langmuir* **2001**, *17* (22), 6910–6914.

(4) Bentley, R. *Chem. Soc. Rev.* **2005**, *34* (7), 609.

(5) Campbell, D. B.; Wilson, K. *Biochem. Soc. Trans.* **1991**, *19* (2), 472–475.

(6) Mohan, S. J.; Mohan, E. C.; Yamsani, M. R. *Int. J. Pharm. Sci. Nanotechnol.* **2009**, *1* (4), 309–316.

(7) Joyce, L. A.; Shabbir, S. H.; Anslyn, E. V. *Chem. Soc. Rev.* **2010**, *39* (10), 3621–3632.

(8) Leung, D.; Kang, S. O.; Anslyn, E. V. *Chem. Soc. Rev.* **2012**, *41* (1), 448–479.

(9) Ilisz, I.; Berkecz, R.; Péter, A. *J. Pharm. Biomed. Anal.* **2008**, *47* (1), 1–15.

(10) Simó, C.; Barbas, C.; Cifuentes, A. *Electrophoresis* **2003**, *24* (15), 2431–2441.

(11) Prokhorova, A. F.; Shapovalova, E. N.; Shpigun, O. A. *J. Pharm. Biomed. Anal.* **2010**, *53* (5), 1170–1179.

(12) Schurig, V. *J. Chromatogr. A* **2002**, *965* (1–2), 315–356.

(13) Evans, M. A.; Morken, J. P. *J. Am. Chem. Soc.* **2002**, *124* (31), 9020–9021.

(14) Reetz, M. T.; Eipper, A.; Tielmann, P.; Mynott, R. *Adv. Synth. Catal.* **2002**, *344* (9), 1008–1016.

(15) Wolf, C. *Chem. Soc. Rev.* **2005**, *34* (7), 595.

(16) Martínez-Máñez, R.; Sancenón, F. *Chem. Rev.* **2003**, *103* (11), 4419–4476.

(17) Kim, J. S.; Quang, D. T. *Chem. Rev.* **2007**, *107* (9), 3780–3799.

(18) Ueno, T.; Nagano, T. *Nat. Methods* **2011**, *8* (8), 642–645.

(19) Pu, L. *Chem. Rev.* **2004**, *104* (3), 1687–1716.

(20) Nugent, T. *Chiral Amine Synthesis: Methods, Developments and Applications*; Wiley, 2010.

(21) Iwanek, W.; Mattay, J. *J. Photochem. Photobiol. A Chem.* **1992**, *67* (2), 209–226.

(22) Pu, L. *1, 1'-binaphthyl-based Chiral Materials: Our Journey.*; World Scientific, 2009.

(23) Pu, L. *Acc. Chem. Res.* **2012**, *45* (2), 150–163.

(24) Pu, L. *Acc. Chem. Res.* **2017**, *50* (4), 1032–1040.

(25) Hu, Q. S.; Pugh, V.; Sabat, M.; Pu, L. *J. Org. Chem.* **1999**, *64* (20), 7528–7536.

(26) Pugh, V. J.; Hu, Q. S.; Zuo, X.; Lewis, F. D.; Pu, L. *J. Org. Chem.* **2001**, *66* (18), 6136–6140.

(27) Pugh, V. J.; Hu, Q.; Pu, L. *Angew. Chem.* **2000**, *20* (112), 3784–3787.

(28) Yu, S.; Plunkett, W.; Kim, M.; Pu, L. *J. Am. Chem. Soc.* **2012**, *134* (50), 20282–20285.

(29) Wang, C.; Wu, E.; Wu, X.; Xu, X.; Zhang, G.; Pu, L. *J. Am. Chem. Soc.* **2015**, *137* (11), 3747–3750.

(30) Huang, Z.; Yu, S.; Wen, K.; Yu, X.; Pu, L. *Chem. Sci.* **2014**, *5* (9), 3457.

(31) Song, T.; Cao, Y.; Zhao, G.; Pu, L. *Inorg. Chem.* **2017**, *56* (8), 4395–4399.

(32) Zhang, X.; Wang, C.; Wang, P.; Du, J.; Zhang, G.; Pu, L. *Chem. Sci.* **2016**, *7* (6), 3614–3620.

(33) Wang, Y.; Hu, L.; Zhao, F.; Yu, S.; Tian, J.; Shi, D.; Wang, X.; Yu, X.; Pu, L. *Chem. - A Eur. J.* **2017**, *23* (70), 17678–17681.

(34) Reetz, M. T.; Sostmann, S. *Tetrahedron* **2001**, *57* (13), 2515–2520.

(35) Liu, S.; Pestano, J. P. C.; Wolf, C. **2008**, *73* (11), 4267–4270.

(36) Xu, Y.; Zheng, L.; Huang, X.; Cheng, Y.; Zhu, C. *Polymer (Guildf).* **2010**, *51* (5), 994–997.

(37) Savelieva, K. V.; Zhao, S.; Pogorelov, V. M.; Rajan, I.; Yang, Q.; Cullinan, E.; Lanthorn, T. H. *PLoS One* **2008**, *3* (10).

(38) Tejero, J.; Biswas, A.; Wang, Z. Q.; Page, R. C.; Haque, M. M.; Hemann, C.; Zweier, J. L.; Misra, S.; Stuehr, D. J. *J. Biol. Chem.* **2008**, *283* (48), 33498–33507.

(39) Errico, F.; Napolitano, F.; Nisticò, R.; Usiello, A. *Amino Acids* **2012**, *43* (5), 1861–1871.

(40) Han, H.; Miyoshi, Y.; Ueno, K.; Okamura, C.; Tojo, Y.; Mita, M.; Lindner, W.; Zaitsu, K.; Hamase, K. *J. Chromatogr. B Anal. Technol. Biomed. Life Sci.* **2011**, *879* (29), 3196–3202.

(41) Billard, J.-M. *Amino Acids* **2012**, *43* (5), 1851–1860.

(42) Simó, C.; Barbas, C.; Cifuentes, A. *Electrophoresis* **2005**, *26* (7–8), 1306–1318.

(43) Kitagawa, F.; Otsuka, K. *J. Chromatogr. B Anal. Technol. Biomed. Life Sci.* **2011**, *879* (29), 3078–3095.

(44) Lin, J.; Li, Z. B.; Zhang, H. C.; Pu, L. *Tetrahedron Lett.* **2004**, *45* (1), 103–106.

(45) Liu, H.-L.; Zhao, Q.-L.; Hou, X.-L.; Pu, L. *Chem. Commun.* **2011**, *47* (12), 3646.

(46) He, X.; Cui, X.; Li, M.; Lin, L.; Liu, X.; Feng, X. *Tetrahedron Lett.* **2009**, *50* (42), 5853–5856.

(47) Liu, H.; Zhu, H.; Hou, X.; Pu, L. *Org. Lett.* **2010**, *12* (18), 4172–4175.

(48) Pagliari, S.; Corradini, R.; Galaverna, G.; Sforza, S.; Dossena, A.; Marchelli, R. *Tetrahedron Lett.* **2000**, *41* (19), 3691–3695.

(49) Wolf, C.; Liu, S.; Reinhardt, B. C. *Chem. Commun.* **2006**, No. 40, 4242.

(50) Lin, J.; Hu, Q. S.; Xu, M. H.; Pu, L. *J. Am. Chem. Soc.* **2002**, *124* (10), 2088–2089.

(51) Xu, M. H.; Lin, J.; Hu, Q. S.; Pu, L. *J. Am. Chem. Soc.* **2002**, *124* (47), 14239–14246.

(52) Liu, H.-L.; Peng, Q.; Wu, Y.-D.; Chen, D.; Hou, X.-L.; Sabat, M.; Pu, L. *Angew. Chemie, Int. Ed.* **2010**, *49* (3), 602–606, S602/1–S602/58.

(53) Yu, S.; Pu, L. *J. Am. Chem. Soc.* **2010**, *132* (50), 17698–17700.

(54) James, T. D.; Samankumara Sandanayake, K. R. A.; Shinkai, S. *Nature*. 1995, pp 345–347.

(55) Li, Z. B.; Lin, J.; Qin, Y. C.; Pu, L. *Org. Lett.* **2005**, *7* (16), 3441–3444.

(56) Li, Z. B.; Lin, J.; Pu, L. *Angew. Chemie - Int. Ed.* **2005**, *44* (11), 1690–1693.

(57) Nian, S.; Pu, L. *Chem. - A Eur. J.* **2017**, *23* (71), 18066–18073.

(58) Zeng, C.; Zhang, X.; Pu, L. *Chem. - A Eur. J.* **2017**, *23* (10), 2432–2438.

(59) Mori, I. C.; Arias-Barreiro, C. R.; Koutsaftis, A.; Ogo, A.; Kawano, T.; Yoshizuka, K.; Inayat-Hussain, S. H.; Aoyama, I. *Chemosphere* **2015**, *120*, 299–304.

Chapter 2. Poly (*N*-isopropylacrylamide): Synthesis, Property and Application

2.1. Introduction

Poly (*N*-isopropylacrylamide) (PNIPAM) is the most extensively studied thermo-responsive polymer which is synthesized by the polymerization of *N*-isopropylacrylamide (NIPAM). It is an amphiphilic polymer and can be dissolved in water and various organic solvents. It is soluble in water at low temperature, and when the temperature rises to a certain degree (around 32 ^{o}C), PNIPAM will precipitate out of the solution abruptly. This temperature is called lower critical solution temperature (LCST). It has shown broad applications in areas such as drug delivery, tissue engineering and biosensing[1,2] based on this unique thermoproperty.

Figure 2.1. Polymerization of NIPAM

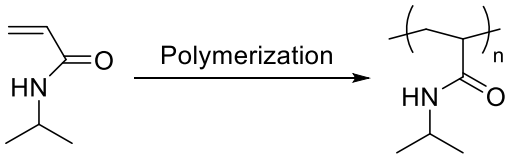

2.2. Synthesis of Poly (*N*-isopropylacrylamide)

2.2.1. Free radical polymerization

PNIPAM was first synthesized in 1956.[2] Since then, numerous methods were developed for the polymerization of *N*-isopropylacrylamide. The most common method is free radical polymerization. This kind of polymerization is initiated by reactive species termed initiator, which can generate radicals and add to monomer molecules by activating its π-bond to form a new radical.[3] This process is repeated as more and more monomers are added to the propagating chain continuously and finally a polymer chain is formed. Free radical polymerization consists of four elementary reactions: initiation, propagation, transfer and termination. Scheme **2.1** shows a general radical polymerization process.

Scheme 2.1. Free radical polymerization process

Initiation

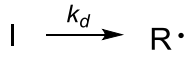

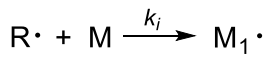

Propagation

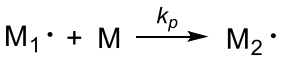

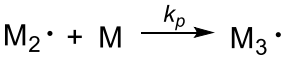

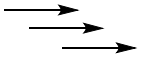

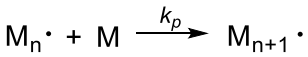

Termination

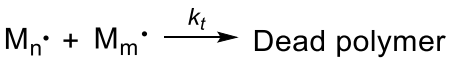

For example, Winnik reported the free radical polymerization of PNIPAM using *tert*-butyl alcohol as solvent. 5.0 g *N*-isopropylacrylamide was dissolved in 25 mL tert-butyl alcohol. Then 30 mg azobisisobutyronitrile (AIBN, **2.1**) in 1 mL *tert*-butyl alcohol was added under nitrogen. The solution was stirred for 15 h at 70 ^{o}C to obtain PNIPAM.[4]

However, in conventional free radical polymerization, the average life time of the propagating polymer chain is about 1 second, which is too short for any synthetic manipulation, chain end group functionalization and molecular weight (MW) control of PNIPAM.[5]

2.2.2. Control/living radical polymerization

In order to control the structural parameters of polymer, a new kind of radical polymerization, termed control/living radical polymerization (CRP), has been developed in the recent two decades.[6] CRP has the properties of fast initiation and absence of termination, which

means the simultaneous propagation of all polymer chains can be realized and the narrow polydispersity index (PDI) can be achieved. Also, because of the absence of termination step, the MW can be easily controlled and numerous block copolymers can be synthesized. In general, the development of CRP greatly expands the synthesis of new polymeric materials and application of polymers.

For the polymerization of NIPAM, the most commonly used CRP methods are reversible addition-fragmentation chain transfer (RAFT) polymerization and atom transfer radical polymerization (ATRP). Scheme **2.2** shows the mechanism of the RAFT process.[7] The propagating radical can add to the reactive carbon sulfur double bond and form an intermediate. The intermediate can either undergo the reversible addition process, or it can release another growing radical to initiate more monomers. In this process, an equilibrium is established between dormant and active species.

Scheme 2.2. Mechanism of RAFT polymerization

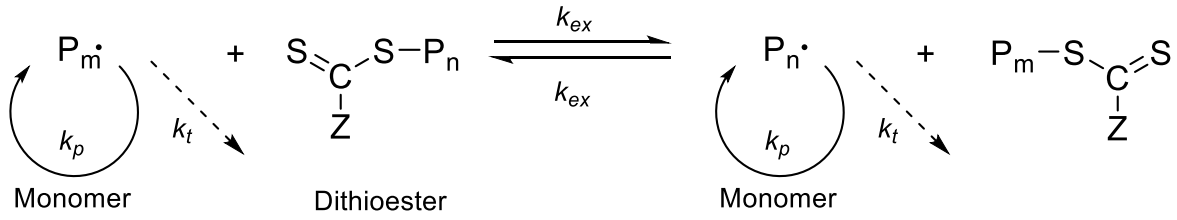

There are many reports detailing the RAFT polymerization of NIPAM. For example, Ganachaud et al. reported the AIBN initiated solution RAFT polymerization of NIPAM using two different chain transfer agents. PNIPAM was obtained by employing benzyl dithiobenzoate (**2.2**) in benzene or by cumyl dithiobenzoate (**2.3**) in 1,4-dioxane at 60 °C and the PDI of PNIPAM is less than 1.2, indicating a good MW control.[8] Schilli et al. also conducted the benzyl (**2.4**) and cumyl 1-pyrrolecarbodithioate (**2.5**)-mediated RAFT polymerization of NIPAM in 1,4-dioxane at 60 °C, and the PDI is also less than 1.21.[9] Convertine et al. reported the use of

2-dodecylsulfanylthiocarbonylsulfanyl- 2-methyl propionic acid (**2.6**), a trithiocarbonate RAFT CTA, in combination with azo initiator 2,2'-azobis(4-methoxy-2,4-dimethylvaleronitrile) (**2.7**) can lead to the RAFT polymerization of NIPAM in DMF at 25 °C, and the PDI is less than 1.1.[10] Figure **2.2** shows the structure of some initiators and chain transfer agents in RAFT.

Figure 2.2. Initiators and chain transfer agents in RAFT

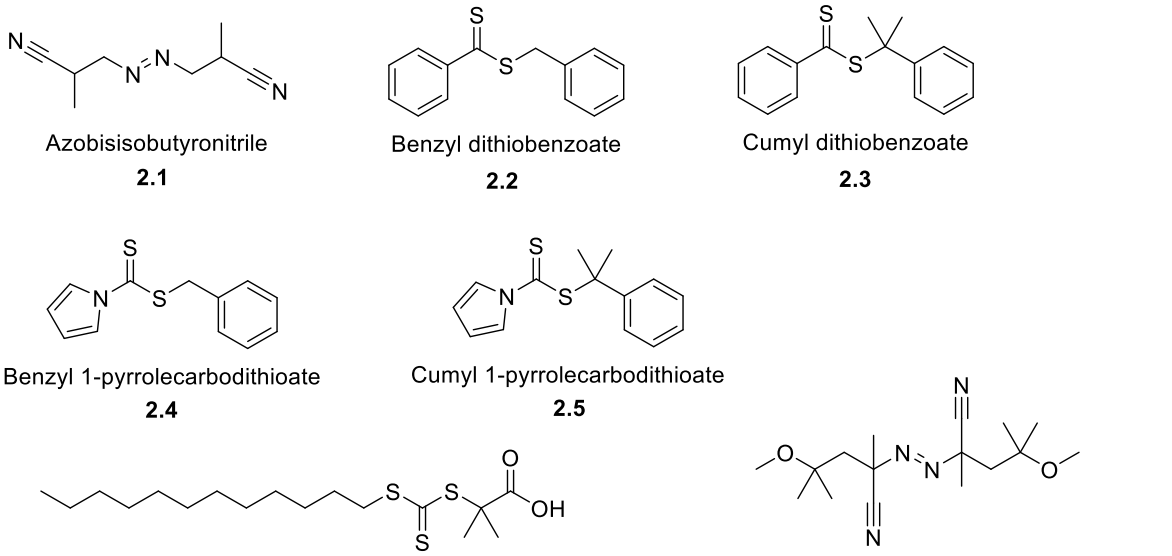

Atom transfer radical polymerization (ATRP) is one of the most widely used CRP. Compare to other CRP process, ATRP has its own advantages. One advantage is that all ATRP reagents (initiators, ligands and transition metals) are commercially available. In addition, the equilibrium between active radicals and dormant species can be properly adjusted in a polymerization system simply by modifying the structure of the complexing ligand. Scheme **2.3** shows the mechanism of ATRP process. The equilibrium is established between propagating radicals and dormant species, usually a polymer chain with a halogen or pseudohalogen atom at the end of the chain. The propagating radicals are generated by a reversible redox process, which is catalyzed by a transition metal complex. The metal complex

can abstract a halogen or pseudohalogen atom from the dormant species and undergo a one electron oxidation process. A homocleavage of carbon halogen bond of the dormant species occurs and the propagating radicals are generated to initiate more monomers and form polymer chains. The transition metal species need to have the ability to expand its coordination site and change its oxidation number in order to achieve the redox process.

Scheme 2.3. Mechanism of ATRP

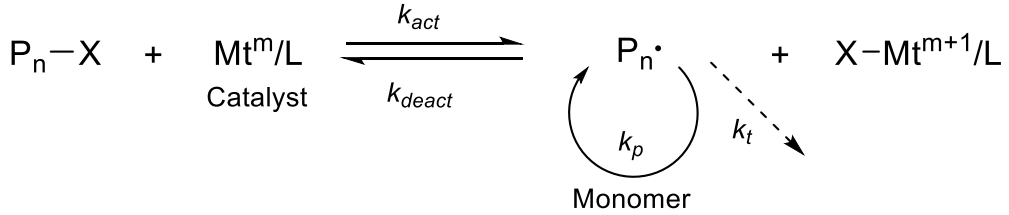

In ATRP, the rate constant of activation, k_{act}, is much smaller than the rate constant of deactivation, k_{deact}. In general, the equilibrium constant K_{ATRP}, which equals to k_{act} /k_{deact}, is in the range of 10^{-9} to 10^{-4}. The very small equilibrium constant ensures that most of the polymer chains are in the dormant state and the propagating radicals are in very low concentration, which greatly reduce the probability of termination between polymer chains.[6] Typically, less than 5% of the polymer chains undergo termination in ATRP process, and the absence of termination makes the propagating radical controllable and the polymerization exhibits a living property.

ATRP has been widely used in the synthesis of PNIPAM. For example, Masci et al. reported the ATRP of NIPAM by using CuCl/Me_6TREN (**2.8**) as the catalyst and ethyl 2-chloropropionate (**2.9**) as the initiator. The reaction was conducted in DMF:water 1:1 (v/v) mixed solvent at 20 ^oC. The controlled MW of PNIPAM was obtained and the PDI was 1.19.[11] Stover et al. reported the ATRP of NIPAM with CuCl/Me_6TREN as the catalyst and methyl 2-chloropropionate (**2.10**) as the initiator in isopropanol at room temperature. The obtained PNIPAM has a PDI less than 1.2.[12] Figure **2.3** shows the ligand and initiators used in ATRP.

Figure 2.3. Ligand and initiators in ATRP

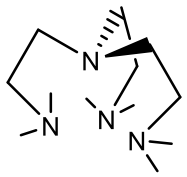

Me6TREN

2.8

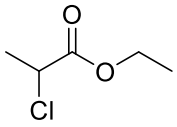

Ethyl 2-chloropropionate

2.9

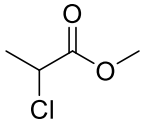

Methyl 2-chloropropionate

2.10

2.3. Solution properties of PNIPAM

2.3.1. Lower critical solution temperature (LCST) property

PNIPAM is soluble in water at low temperature, when the temperature rises to a certain degree, PNIPAM will precipitate out of the solution abruptly. This temperature is called lower critical solution temperature (LCST). At LCST, PNIPAM changes from an expanded random coil hydrophilic polymeric structure in water solution to a globular hydrophobic conformation followed by aggregation to precipitate.[1] The LCST of PNIPAM is between about 30 and 35℃, depending on the microstructure of PNIPAM.

This LCST property can be explained by using Gibbs free energy equation: $\Delta G = \Delta H - T\Delta S$. The dissolution of hydrophilic amide group of PNIPAM in water is an exothermic process due to the formation of hydrogen bonding between water and amid group. Therefore, $\Delta H < 0$. The dissolution of hydrophobic isopropyl groups with a hydrocarbon backbone of PNIPAM in water is also exothermic. Meanwhile, the hydrophobic parts of PNIPAM are surrounded by water molecules, and these water molecules need to reorient their position to forms a solvation shell around PNIPAM.[13] This process is entropy unfavored and $\Delta S < 0$. Therefore, when temperature is low, ΔH dominates the equation, $\Delta G < 0$, and PNIPAM is soluble in water as random coils. When the temperature is high enough, $T\Delta S$ dominates the equation, $\Delta G > 0$, and PNIPAM is insoluble in water, it will form a globular hydrophobic conformation followed by aggregation to precipitate out, and this transition temperature is LCST.

There are several factors that can influence the LCST of PNIPAM. Stover et al. reported the influence of molecular weight on LCST.[14] The PNIPAM was synthesized by using the ATRP method, with Me_6TREN/CuCl as the catalyst and various initiators. The polymers showed an inverted relationship between MW and LCST. For example, the LCST of the PNIPAM initiated by ethyl 2-chloropropionate decreased from 40.6 to 33.3℃ when the MW increased from 3000 to 15200. Kubosaki et al. reported the influence of tacticity on LCST.[15] Tacticity is the regularity of polymer chains. The higher the isotacticity, the higher the regularity of a polymer chain. PNIPAMs with various isotacticity were synthesized by using RAFT polymerization. The study revealed that increase in tacticity will decrease the LCST. For example, the atactic PNIPAM with an isotacticity of 46% had LCST at 33℃. However, when the isotacticity increased to 64%, the LCST decreased to 25℃.

There are several ways to measure the LCST of PNIPAM, such as UV-Vis, dynamic light scattering (DLS) and differential scanning calorimetry (DSC). Schild et al. used 500 nm visible light and spectrophotometer to measure the optical density of NIPAM solution. When the solution reached LCST, the optical density would increase abruptly.[16] Fujishige used DLS method the measure the hydrodynamic radius of PNIPAM in water. The hydrodynamic radius would suddenly decrease at LCST.[17] Shibayama et al. used DSC to monitor the transition of PNIPAM in water. As the temperature increase, the ordered water molecule would gradually dissociate from PNIPAM, which is endothermic. The endothermic peak can be found in DSC curve, which corresponds to LCST.[18]

2.3.2. Cononsolvency property

The term cononsolvency refers to a phenomenon when two solvents can dissolve a polymer well but the mixture of the two solvents is a bad solvent for the same polymer.[19] In the

case of PNIPAM, one solvent is water, and the other solvent is water-soluble organic solvent such as alcohol, acetone, DMSO and THF. PNIPAM is soluble in pure water, after gradually addition of water-soluble organic solvent, PNIPAM will precipitate out of the mixed solvent. When continue adding the organic solvent, PNIPAM will be soluble in the mix solvent again. Therefore, PNIPAM experiences a coil-to-globule-to-coil transition of conformation when the proportion of organic solvent gradually increases. Cononsolvency property is closely related with LCST of PNIPAM. The PNIPAM will precipitate out at room temperature in mixed solvent, this is because the LCST of PNIPAM is much lower than room temperature at that solvent. Figure **2.4** briefly demonstrates this relationship.

Figure 2.4. Relationship between LCST and the fraction of organic solvent in water

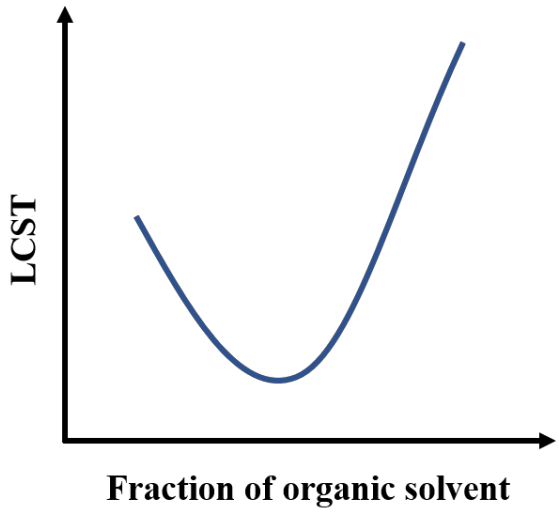

A lot of studies have been carried out to understand the cononsolvency property of PNIPAM. Schild et al. proposed that when methanol was added into water, water preferred to form complex with methanol rather than form hydrogen bonding with PNIPAM, which led to the disruption of PNIPAM coil structure in the mixed solvent.[19] Zhang et al. studied cononsolvency property of PNIPAM in extremely dilute methanol/water solution. They found that the coil to globule conformation change could be attributed to the formation of various

water/methanol complexes, which are poor solvents for PNIPAM.[20] Rodríguez-Ropero et al. found that methanol preferentially binds to the PNIPAM globule and drives polymer collapse. The binding between methanol and PNIPAM results in a significant increase in the globule's configurational entropy, which stabilizes methanol-enriched globular structures.[21]

2.4. Application of PNIPAM

2.4.1. Drug delivery

This LCST of PNIPAM is very close to the temperature of human body, which is around 37℃. Therefore, it has a promising potential in drug delivery applications.[22] The general idea is that drugs are delivered by PNIPAM micelles, which requires the copolymerization of hydrophilic NIPAM with other hydrophobic monomers to form a core-shell structure in aqueous solution. The hydrophobic drugs are carried in the hydrophobic core, surrounded by the hydrophilic PNIAPM shell. Below LCST, the micelles are stable in aqueous environment and the inner drug can be delivered to the desired location of the body. By local heating, the temperature will be above LCST and PNIPAM becomes hydrophobic, leading to the dissociation of the micelles. The drugs can be released consequently.[23] Figure **2.5** shows this process.

Figure 2.5. Temperature modulated drug delivery

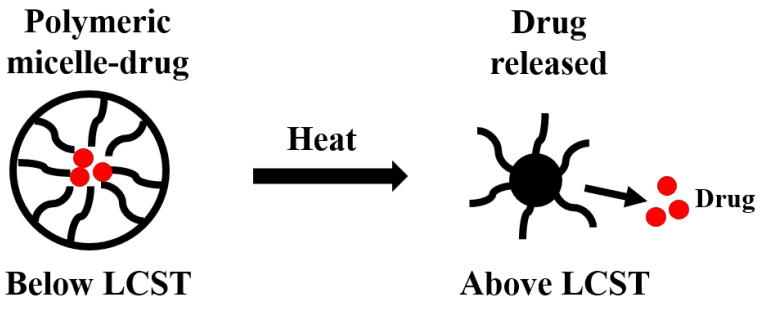

For example, Chung et al. reported the application of poly(N-isopropylacrylamide-*b*-butylmethacrylate) block copolymer as a drug carrier. The polymer had a LCST at 32.5 ^{o}C and was used to deliver doxorubicin, an anti-cancer drug, into cells. The formed micelles showed no cytotoxicity and over 80% of carried drugs could be released within 10 h.[24] Wei et al. used poly(*N*-isopropylacrylamide-*b*-methyl methacrylate), which has a LCST at 33 ^{o}C, for the delivery of prednisone acetate, a drug used for eye treatment. About 90% of the drugs were released within 20 h *in vitro*.[25]

2.4.2. Catalytic Application

PNIPAM hydrogels can incorporate with other catalysts to form a thermosensitive catalyst system. When the temperature is lower than LCST, the reaction occurs in the presence of PNIPAM catalyst. However, when the temperature is above LCST, the PNIPAM hydrogel shrinks and prevents the catalysts from contacting with the reaction substrates, which greatly reduces the reaction rate.

For example, Zhu et al. synthesized PNIPAM/Au nanoparticle composite hydrogels by gamma-radiation-assisted polymerization of *N*-isopropylacrylamide aqueous solution in the presence of $HAuCl_4 \cdot 4H_2O$.[26] The hydrogel had a LCST of 33 ^{o}C, and was used for the reduction of *o*-nitroaniline (**2.11**) to 1,2-benzenediamine (**2.12**) in the presence of $NaBH_4$. It was found that the reaction rate was faster at 30 ^{o}C than at 33 ^{o}C due to the shrink of hydrogel and the reduce speed of diffusion of reactant to Au nanoparticle. Scheme **2.4** describes the reaction.

Scheme 2.4. Reduction of *o*-nitroaniline using PNIPAM/Au nanoparticle hydrogel as catalyst

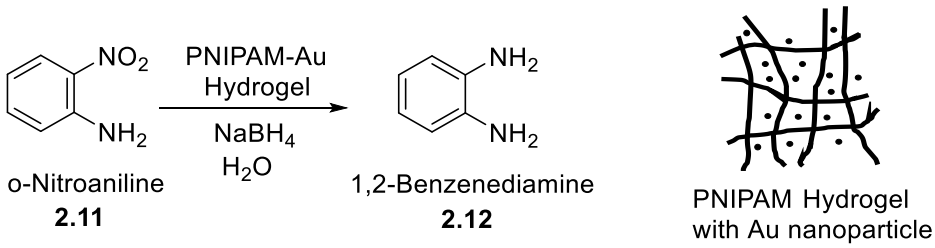

Chen et al. reported the application of PNIPAM based hydrogel containing *N*-aryl phenothiazine photocatalysts on photocontrolled ATRP of various monomers.[27] The hydrogel was able to initiate the ATRP of NIPAM and poly(ethylene glycol) methyl ether acrylate (**2.15**) in water when temperature is lower than LCST. When the temperature of the reaction system was above LCST, the gel would shrink, and the polymerization stopped due to the inefficient initiation of the catalyst. Scheme **2.5** shows the synthesis of PNIPAM hydrogel photocatalyst.

Scheme 2.5. Synthesis of PNIPAM hydrogel photocatalyst

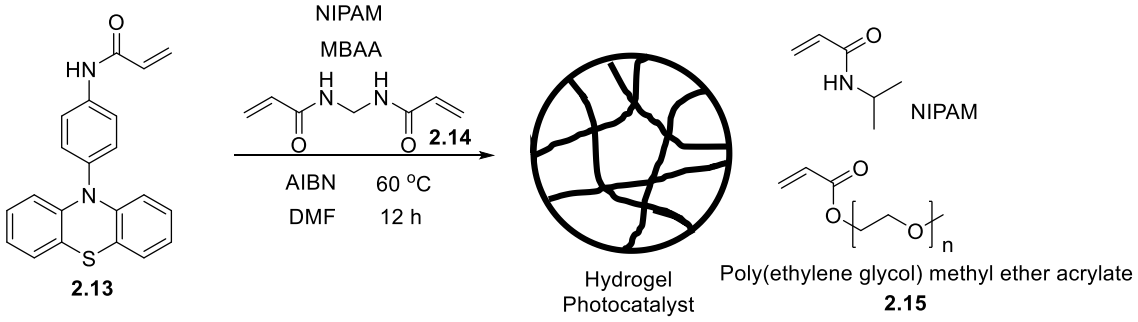

2.4.3. Application in bioengineering

In modern macromolecular engineering systems, the development of novel biocompatible functional polymers that can carry enzyme and gene with no toxic side effects becomes more and more important.[28] Because of the reversible phase-transition behavior of PNIPAM, it has been widely utilized in macromolecular bioengineering and biotechnology such as bioconjugation and separation.

For example, Chen et al. reported the separation of human immunoglobulin using PNIPAM-Protein A conjugate.[29] As Protein A has high affinity toward immunoglobulin,[30] the

conjugate could bind with immunoglobulin to form PNIPAM-Protein A/immunoglobulin complex. The complex can be separated from the solution conveniently by raising the temperature above LCST of PNIPAM. This affinity separation method was rapid and efficient, avoiding the use of column chromatography. Kim et al. developed PNIPAM hydrogel beads which conjugated with a cell adhesive peptide, GRGDY (Gly-Arg-Gly-Asp-Tyr).[31] Chondrocytes, which was used for the treatment of rheumatoid arthritis, could attach on the hydrophobic surface of conjugates when the temperature was above LCST and detach from the hydrophilic surface of conjugates when the temperature was below LCST. Therefore, these conjugated PNIPAM hydrogel beads could be utilized as cell carriers to efficiently detach/attach cells by controlling the environmental temperature.

2.5. Conclusion

PNIPAM has been extensively studied and widely used in many fields. Its unique solvent property and amphiphilicity make it an ideal choice to incorporate with small BINOL-aldehyde sensors to generate amphiphilic polymer sensors. The potential water solubility of the sensors makes it possible for the enantioselective recognition of amino acids in aqueous solution. In addition, the potential thermo-responsive property of the sensor may lead to the separation of the reaction product from the reaction mixture, which is very promising in asymmetric reaction screening experiments. Moreover, the bio-compatibility of PNIPAM makes the polymer sensor feasible in the enantioselective fluorescent imaging of amino acids *in vitro* and *in vivo*.

References

(1) Schild, H. G. *Prog. Polym. Sci.* **1992**, *17* (2), 163–249.

(2) Halperin, A.; Kröger, M.; Winnik, F. M. *Angew. Chemie - Int. Ed.* **2015**, *54* (51), 15342–15367.

(3) Odian, G. *Principles of Polymerization*, 4th ed.; Wiley, 2004.

(4) Winnik, F. M. *Macromolecules* **1990**, *23* (1), 233–242.

(5) Coates, G. W. *Chem. Rev.* **2000**, *100* (4), 1223–1252.

(6) Braunecker, W. A.; Matyjaszewski, K. *Prog. Polym. Sci.* **2007**, *32* (1), 93–146.

(7) Kali, G.; Georgiou, T. K.; Iván, B.; Patrickios, C. S. *J. Polym. Sci. Part a-Polymer Chem* **2009**, *47* (17), 4289–4301.

(8) Ganachaud, F.; Monteiro, M. J.; Gilbert, R. G.; Dourges, M. A.; Thang, S. H.; Rizzardo, E. *Macromolecules* **2000**, *33* (18), 6738–6745.

(9) Schilli, C.; Lanzendörfer, M. G.; Müller, A. H. E. *Macromolecules* **2002**, *35* (18), 6819–6827.

(10) Convertine, A. J.; Ayres, N.; Scales, C. W.; Lowe, A. B.; McCormik, C. L. *Biomacromolecules* **2004**, *5* (4), 1177–1180.

(11) Masci, G.; Giacomelli, L.; Crescenzi, V. *Macromol. Rapid Commun.* **2004**, *25* (4), 559–564.

(12) Xia, Y.; Yin, X.; Burke, N. A. D.; Stöver, H. D. H. *Macromolecules* **2005**, *38* (14), 5937–5943.

(13) Winnik, F. M.; Ottaviani, M. F.; Bossmann, S. H.; Pan, W.; Garcia-Garibay, M.; Turro, N. J. *Macromolecules* **1993**, *26* (17), 4577–4585.

(14) Xia, Y.; Burke, N. A. D.; Stöver, H. D. H. *Macromolecules* **2006**, *39* (6), 2275–2283.

(15) Katsumoto, Y.; Kubosaki, N. *Macromolecules* **2008**, *41* (15), 5955–5956.

(16) Schild, H. G.; Tirrell, D. A. *J. Phys. Chem.* **1990**, *94* (10), 4352–4356.

(17) Fujishige, S.; Kubota, K.; Ando, I. *J. Phys. Chem.* **1989**, *93* (8), 3311–3313.

(18) Shibayama, M.; Suetoh, Y.; Nomura, S. *Macromolecules* **1996**, *29* (21), 6966–6968.

(19) Schild, H. G.; Muthukumar, M.; Tirrell, D. A. *Macromolecules* **1991**, *24* (4), 948–952.

(20) Zhang, G.; Wu, C. *J. Am. Chem. Soc.* **2001**, *123* (7), 1376–1380.

(21) Rodríguez-Ropero, F.; Hajari, T.; Van Der Vegt, N. F. A. *J. Phys. Chem. B* **2015**, *119* (51), 15780–15788.

(22) Ruel-Gariépy, E.; Leroux, J.-C. *Eur. J. Pharm. Biopharm.* **2004**, *58* (2), 409–426.

(23) Wei, H.; Cheng, S.-X.; Zhang, X.-Z.; Zhuo, R.-X. *Prog. Polym. Sci.* **2009**, *34* (9), 893–910.

(24) Chung, J. E.; Yokoyama, M.; Yamato, M.; Aoyagi, T.; Sakurai, Y.; Okano, T. *J. Control. Release* **1999**, *62* (1–2), 115–127.

(25) Wei, H.; Zhang, X. Z.; Zhou, Y.; Cheng, S. X.; Zhuo, R. X. *Biomaterials* **2006**, *27* (9), 2028–2034.

(26) Zhu, C. H.; Hai, Z. Bin; Cui, C. H.; Li, H. H.; Chen, J. F.; Yu, S. H. *Small* **2012**, *8* (6), 930–936.

(27) Chen, M.; Deng, S.; Gu, Y.; Lin, J.; MacLeod, M. J.; Johnson, J. A. *J. Am. Chem. Soc.* **2017**, *139* (6), 2257–2266.

(28) Rzaev, Z. M. O.; Dinçer, S.; Pişkin, E. *Prog. Polym. Sci.* **2007**, *32* (5), 534–595.

(29) Chen, J. P.; Huffman, A. S. *Biomaterials* **1990**, *11* (9), 631–634.

(30) Forsgren, A.; Sjoquist, J. *J. Immunol.* **2012**, *97* (6), 822–827.

(31) Mee, R. K.; Ji, H. J.; Tae, G. P. *Biotechnol. Prog.* **2002**, *18* (3), 495–500.

Chapter 3. Amphiphilic Polymer-Based Fluorescent Probe for Enantioselective Recognition of Amino Acids in Immiscible Water and Organic Phases

3.1. Introduction

Enantioselective fluorescent sensors can potentially provide a fast-analytical tool to determine the enantiomeric composition of chiral molecules. Although significant progress has been made in this area in the past two decades,[1–5] there are still challenges for the direct application of the enantioselective fluorescent sensors in the high throughput screening of asymmetric reactions. For example, when a fluorescent probe is added into a chiral catalyst screening reaction mixture, other components in the reaction besides the desired product, including the catalyst, reagent, starting material and side product, could potentially interfere with the fluorescence measurement and reduce the effectiveness of the chiral sensor. In order to minimize such interferences, we have initiated a project to use the amphiphilic poly(*N*-isopropylacrylamide) (PNIPAM) to construct fluorescent sensors that are capable of conducting enantioselective recognition in phases separated from the original substrate media due to the unique solution properties of PNIPAM.[6,7]

As introduced in Chapter 1, we discovered that the 1,1'-bi-2-naphthol (BINOL)-based chiral aldehyde (*S*)-**1.17** in the presence of Zn^{2+} exhibits enantioselective fluorescent response toward functional chiral amines including diamines, amino alcohols and amino acids.[8] Since (*S*)-**1.17** was not soluble in water, when it was used for the recognition of amino acids, the substrates needed to be treated with tetrabutylammonium hydroxide for fluorescence measurement in methanol. We have incorporated (*S*)-**1.17** into PNIPAM and studied the use of the resulting polymeric receptor for the enantioselective recognition of amino acids.

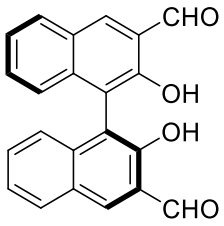

(*S*)-**1.17**

3.2. Results and Discussion

3.2.1. Synthesis and characterization of the polymer-based fluorescent probe

Previously, the atom transfer radical polymerization (ATRP)[9] of NIPAM in the presence of CuCl, tris[2-(dimethylamino)ethyl]amine (Me_6TREN) and an initiator (methyl 2-chloropropionate) was used to generate the linear and narrow-dispersed PNIPAM.[10] In order to synthesize a PNIPAM-supported fluorescent sensor, we have prepared the BINOL-sensor-based initiator to conduct the ATRP of NIPAM.

Scheme 3.1. Synthesis of the initiator (*S*)-**3.8** and polymer (*S*)-**3.9**

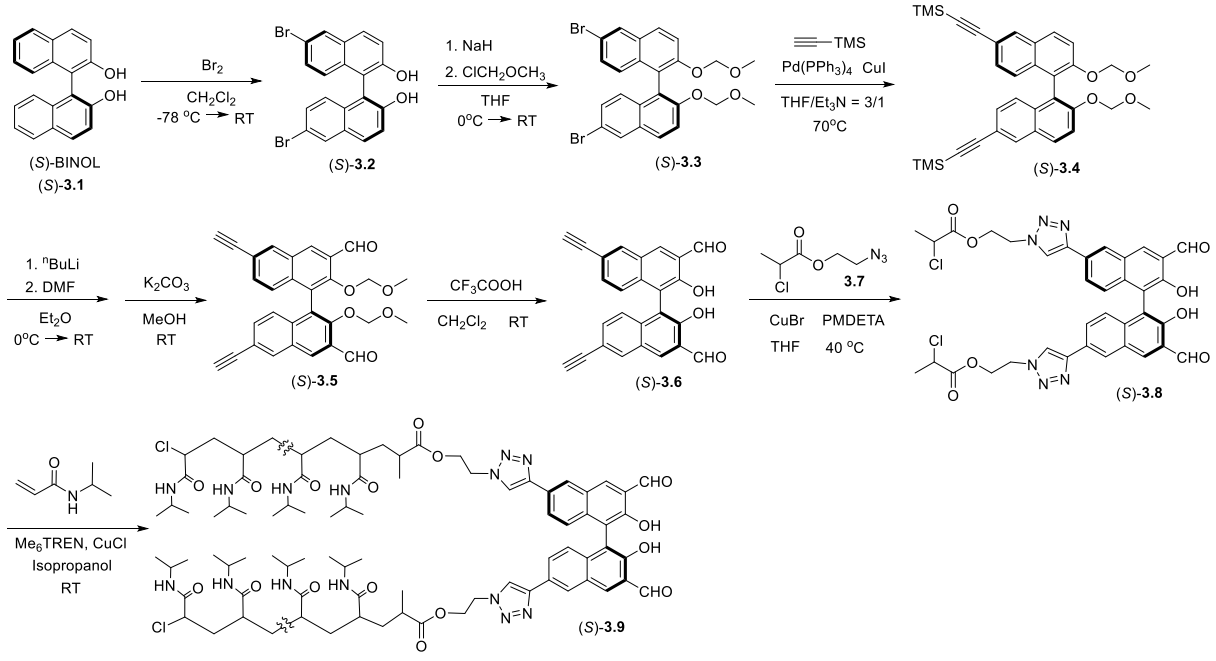

As shown in Scheme **3.1**, Sonogashira coupling of (*S*)-**3.3** with trimethylsilylacetylene gave (*S*)-**3.4**. Orthometalation of (*S*)-**3.4** with *n*-BuLi followed by the addition of *N*,*N*-dimethylformamide and deprotection of trimethylsilyl group with K_2CO_3 gave (*S*)-**3.5**. Removal of the protecting ether group of (*S*)-**3.5** gave (*S*)-**3.6**. Click cycloaddition of (*S*)-**3.6** with 2-azidoethyl 2-chloropropanoate gave (*S*)-**3.8**. This compound was used as a diinitiator for the ATRP of NIPAM.

Polymerization of NIPAM in the presence of (*S*)-**3.8**, Me_6TREN and CuCl was conducted in isopropanol at room temperature. After 48 h, the resulting polymer (*S*)-**3.9** was obtained and purified. This polymer was soluble in water as well as common organic solvents including methanol, isopropanol, THF, acetone, CH_2Cl_2 , chloroform and 1,2-dichloroethane but insoluble in hexane, benzene, toluene and diethyl ether. The ^{1}H NMR spectrum (Figure **3.1**) of (*S*)-**3.9** in $CDCl_3$ gave two signals at δ 10.62 and 10.25 for the hydroxyl and aldehyde protons respectively. The proton signal of the CH group connected to the NH unit of the polymer was observed at δ 4.00. The ratio of the signal at δ 10.25 versus that at δ 4.00 is 1:98 which allows the molecular weight (M_n) of (*S*)-**3.9** to be determined as 22,900. (NMR parameters: Spectra window: 14 to -2 ppm. Digital resolution: 0.13 Hz/pt. S/N ratio: 32. Pulse angle: 45^o. Relaxation delay: 1 s. When the pulse angle was changed to 90^o and the relaxation delay to 5 s and 25 s, no change was observed for the NMR spectrum and the integration ratio). Gel permeation chromatograph (GPC) analysis of (*S*)-**3.9** in THF showed PDI = 1.20. The molecular weight determined by GPC relative to polystyrene standards in THF is M_n = 4300 which is about 5 times smaller than that determined by ^{1}H NMR analysis. That is, using the polystyrene standards greatly underestimates the molecular weight of this polymer. We also prepared the BINOL enantiomer of (*S*)-**3.9**, (*R*)-**3.9**, from the (*R*)-BINOL-based starting

materials. Its molecular weight (M_n) is 23,000 as determined by ^{1}H NMR analysis and is 5900 as determined by GPC analysis. The molecular weight obtained by GPC was used for further study.

Figure 3.1. ^{1}H NMR spectra of (*S*)-**3.9** in $CDCl_3$

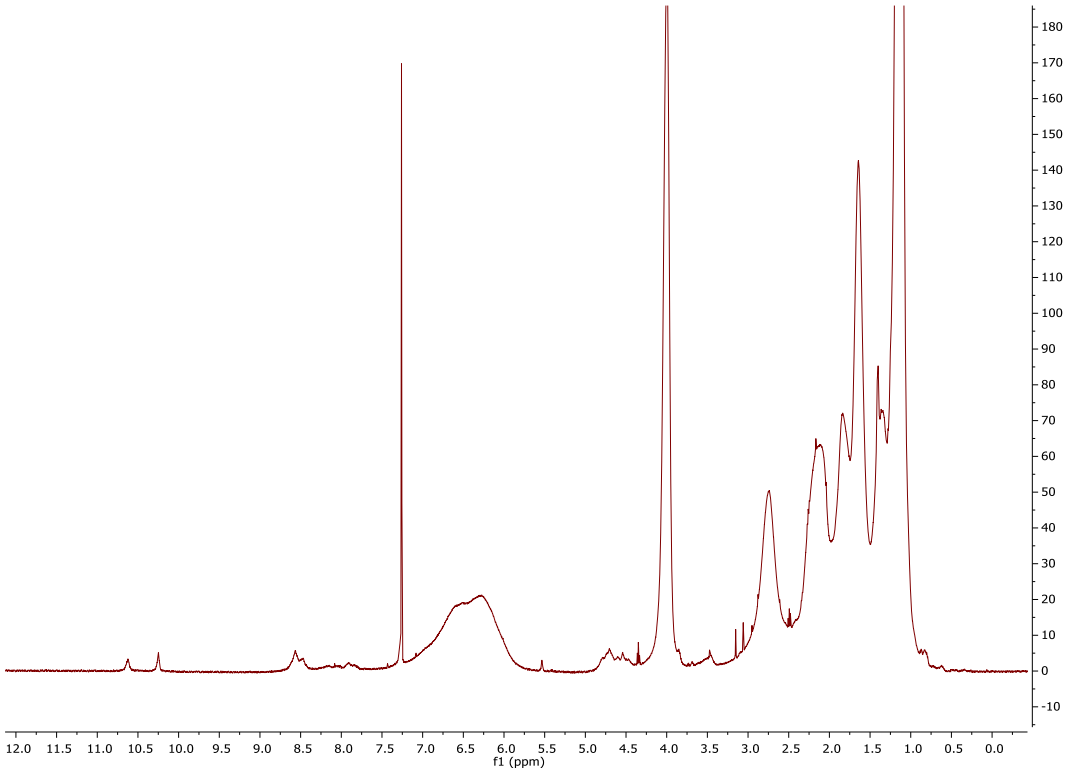

The thermo-response of the aqueous solution of (*S*)-**3.9** was studied. When a water solution of (*S*)-**3.9** (1.0 mM) was heated at a rate of 1 ^{o}C/min, it formed a cloud precipitate at 32 ^{o}C. That is, this polymer-supported BINOL-dialdehyde showed the same LCST as that of PNIPAM. The central BINOL-dialdehyde unit did not change this unique property.

3.2.2. Optimization of conditions for enantioselective recognition of amino acids

The water solubility of (*S*)-**7** allowed us to examine the use of this polymer to recognize amino acids in aqueous solution. This was impossible previously because of the insolubility of (*S*)-**3.1** in water. We measured the fluorescence response of (*S*)-**3.9** toward a chiral amino acid

leucine (**3.10**), in HEPES or BICINE buffer solutions at various pHs in the presence of $Zn(OAc)_2$ to find the optimized condition for enantioselective recognition of amino acids.

Figure 3.2. Structure of buffer molecule and leucine

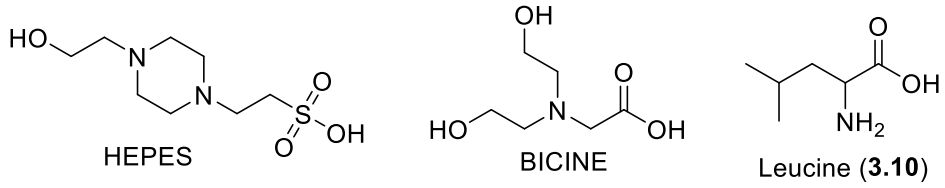

We first tried to use HEPES buffer, which has a pH range between 6.8-8.2. For fluorescence measurement. 25 mM HEPES buffers with pH = 7.60 and 8.10 were freshly prepared. Then 1 mM (*S*)-**3.9** solution in HEPES buffer, 2 mM $Zn(OAc)_2$ solution in water and 4 mM L- or D-**3.10** in HEPES buffer were freshly prepared. Then 50 μL (*S*)-**3.9** solution (1 equiv.), 50 μL $Zn(OAc)_2$ solution (2 equiv.) and various equivalents of L- or D-**3.10** solution were mixed together. The mixtures were allowed to stand at room temperature for 2 h and then diluted to 5 mL using HEPES buffer to make the concentration of sensor as 10 μM.

When using pH =7.60 HEPES buffer, fluorescence measurement revealed that the addition of L-**3.10** showed higher fluorescence enhancement than then addition of D-**3.10** (Figure **3.3**). We further increased the pH of HEPES buffer (25 mM) to 8.10 to investigate the influence of pH to fluorescence intensity and enantioselectivity. However, both the addition of D-**3.10** and L-**3.10** gave high fluorescence enhancement and the enantioselectivity was low (Figure **3.4**). Therefore, we sought for another buffer solution to obtained better enantioselectivity.

Figure 3.3. Fluorescence spectra of (*S*)-**3.9** (1.0 mM) with various equiv of D-**3.10** or L-**3.10** (4.0 mM) in 25 mM HEPES buffer (pH = 7.60) in the presence of 2 equiv of $Zn(OAc)_2$ water solution (2.0 mM). The mixture was allowed to stand at room temperature for 2 h and diluted

to 10^{-5} M by using 25 mM HEPES buffer (pH = 7.60), and the fluorescence spectra were then recorded (λ_{exc} = 320 nm. Slit 5/5 nm). The fluorescence intensity at λ_{em} = 513 nm was used for the equivalent versus fluorescence intensity figure.

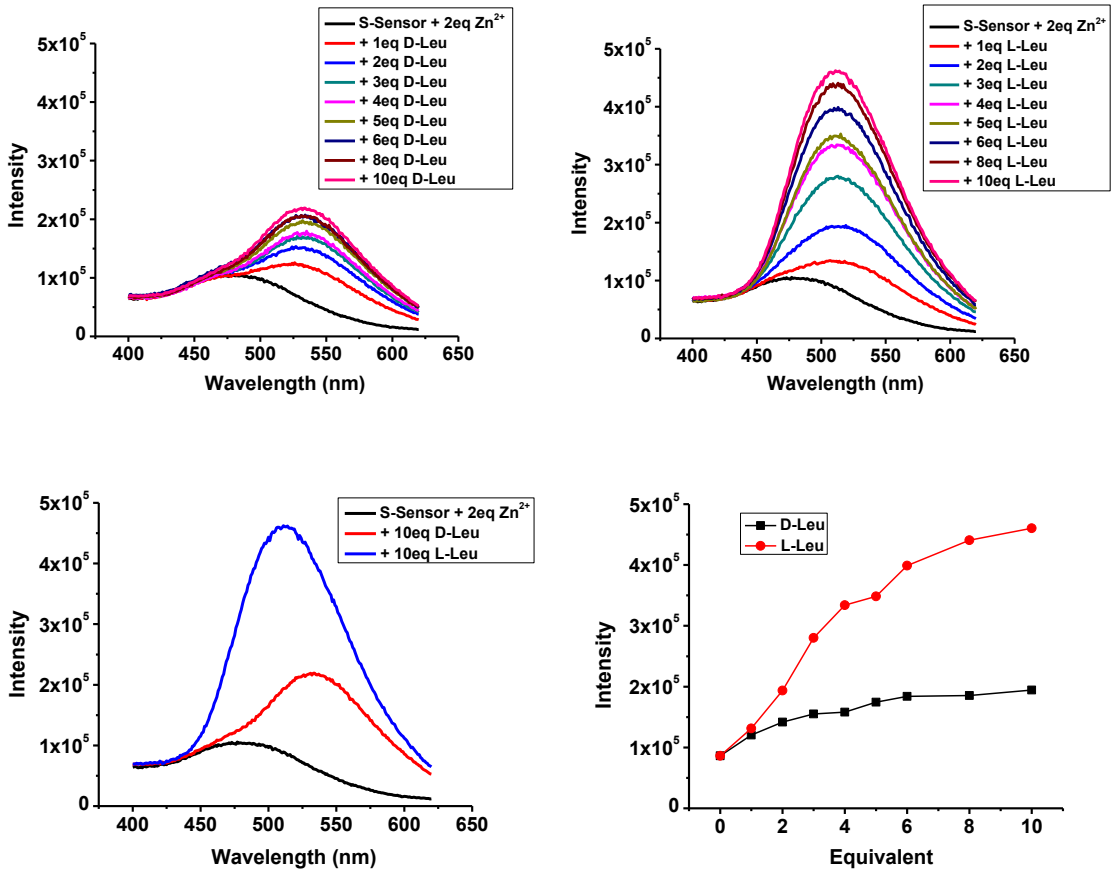

Figure 3.4. Fluorescence spectra of (*S*)-**3.9** (1.0 mM) with various equiv of D-**3.10** or L-**3.10** (4.0 mM) in 25 mM HEPES buffer (pH = 8.10) in the presence of 2.0 equiv of $Zn(OAc)_2$ water solution (2.0 mM). The mixture was allowed to stand at room temperature for 2 h and diluted to 10^{-5} M by using 25 mM HEPES buffer (pH = 8.10), and the fluorescence spectra were then recorded (λ_{exc} = 320 nm. Slit 5/5 nm.). The fluorescence intensity at λ_{em} = 532 nm was used for the equivalent versus fluorescence intensity figure.

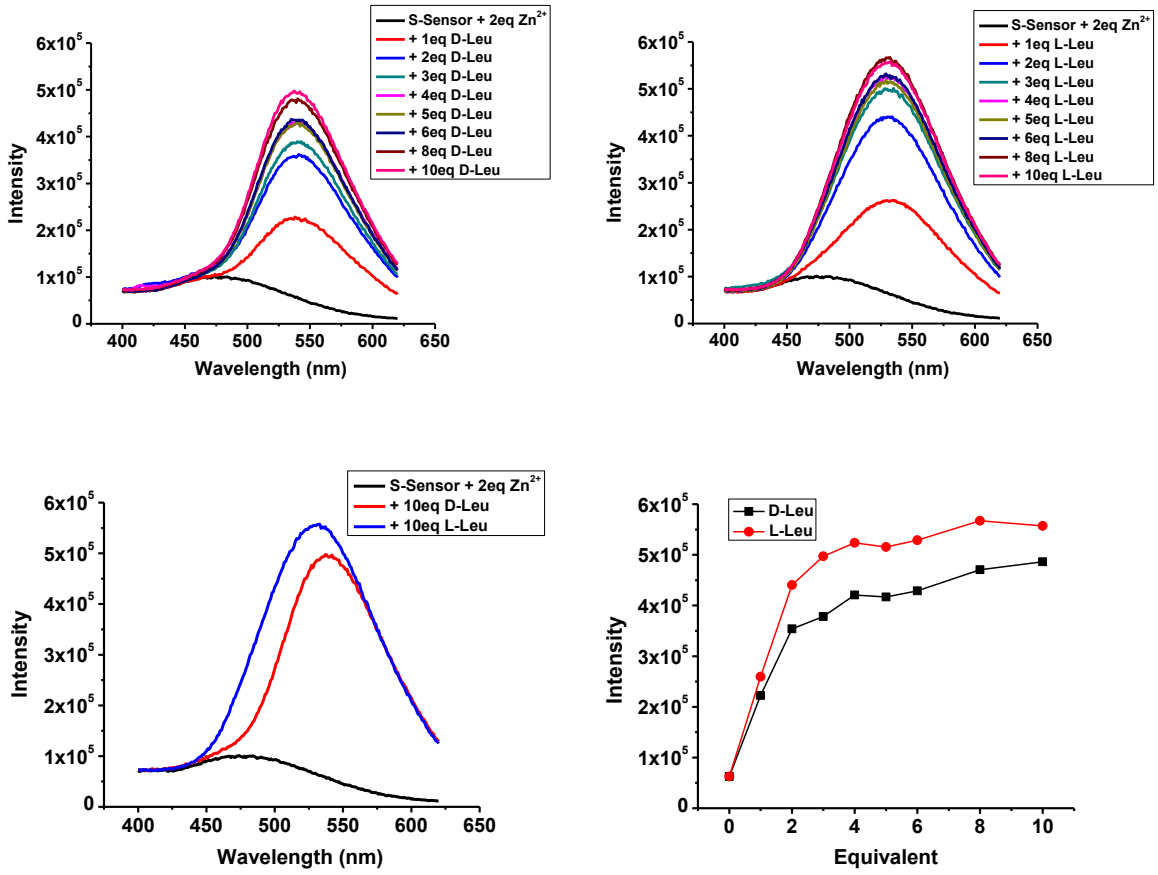

It was found that in BICINE buffer solutions (25 mM), (*S*)-**3.9** showed better enantioselective fluorescent response toward this amino acid. As shown in Figure **3.5**-**3.7**, although D-**3.10** generated little fluorescence response of (*S*)-**3.9**, L-**3.10** greatly enhanced the fluorescence at λ_{em} = 504 nm. When the pH of BICINE buffer increased for 8.10 to 8.80, the enantioselectivity also increased. Thus, BICINE buffer solution (25 mM, pH = 8.80) was used for all the measurements in this work.

Figure 3.5. Fluorescence spectra of (*S*)-**3.9** (1.0 mM) with various equiv of D-**3.10** or L-**3.10** (4.0 mM) in 25 mM BICINE buffer (pH = 8.10) in the presence of 2.0 equiv of $Zn(OAc)_2$ water solution (2.0 mM). The mixture was allowed to stand at room temperature for 2 h and diluted to 10^{-5} M by using 25 mM BICINE buffer (pH = 8.10), and the fluorescence spectra were then

recorded (λ_{exc} = 320 nm. Slit 5/5 nm.). The fluorescence intensity at λ_{em} = 504 nm was used for the equivalent versus fluorescence intensity figure.

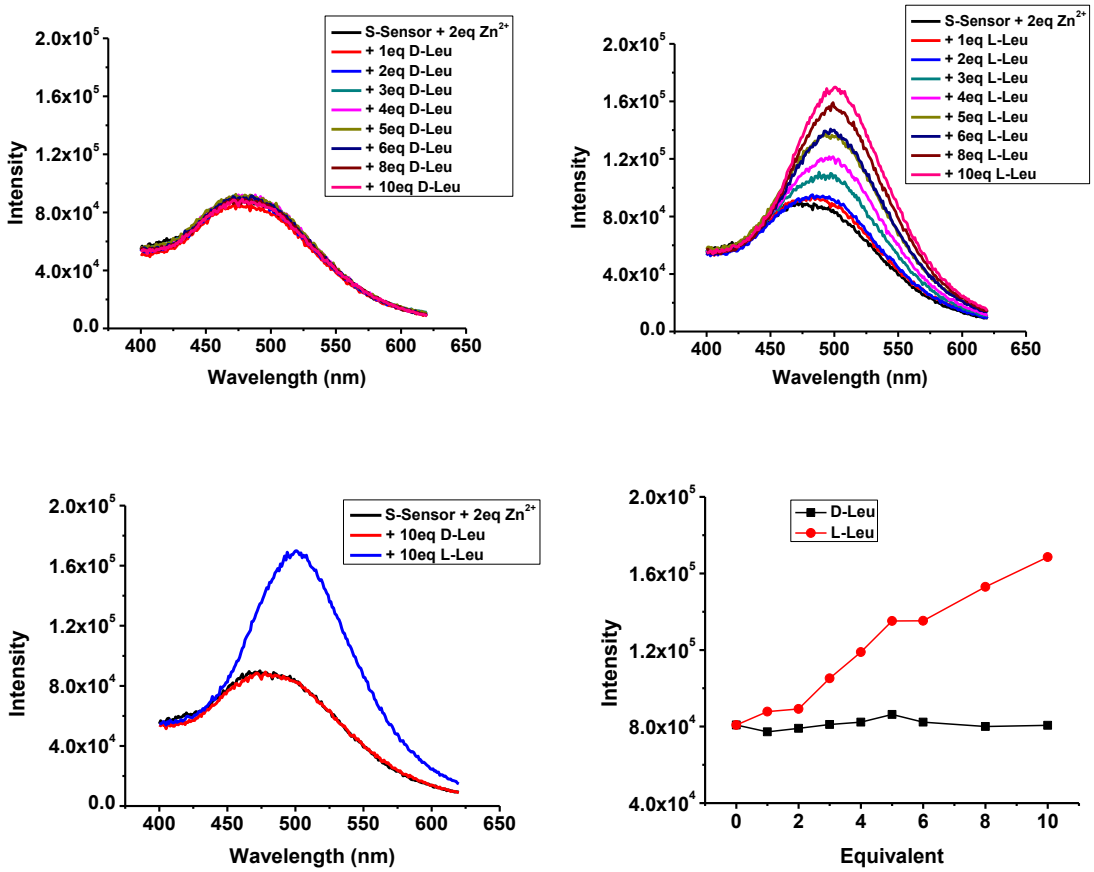

Figure 3.6. Fluorescence spectra of (*S*)-**3.9** (1.0 mM) with various equiv of D-**3.10** or L-**3.10** (4.0 mM) in 25 mM BICINE buffer (pH = 8.50) in the presence of 2.0 equiv of $Zn(OAc)_2$ water solution (2.0 mM). The mixture was allowed to stand at room temperature for 2 h and dilute to 10^{-5} M using 25 mM BICINE buffer (pH = 8.50), and the fluorescence spectra were then recorded (λ_{exc} = 320 nm. Slit 5/5 nm.). The fluorescence intensity at λ_{em} = 504 nm was used for the equivalent versus fluorescence intensity figure.

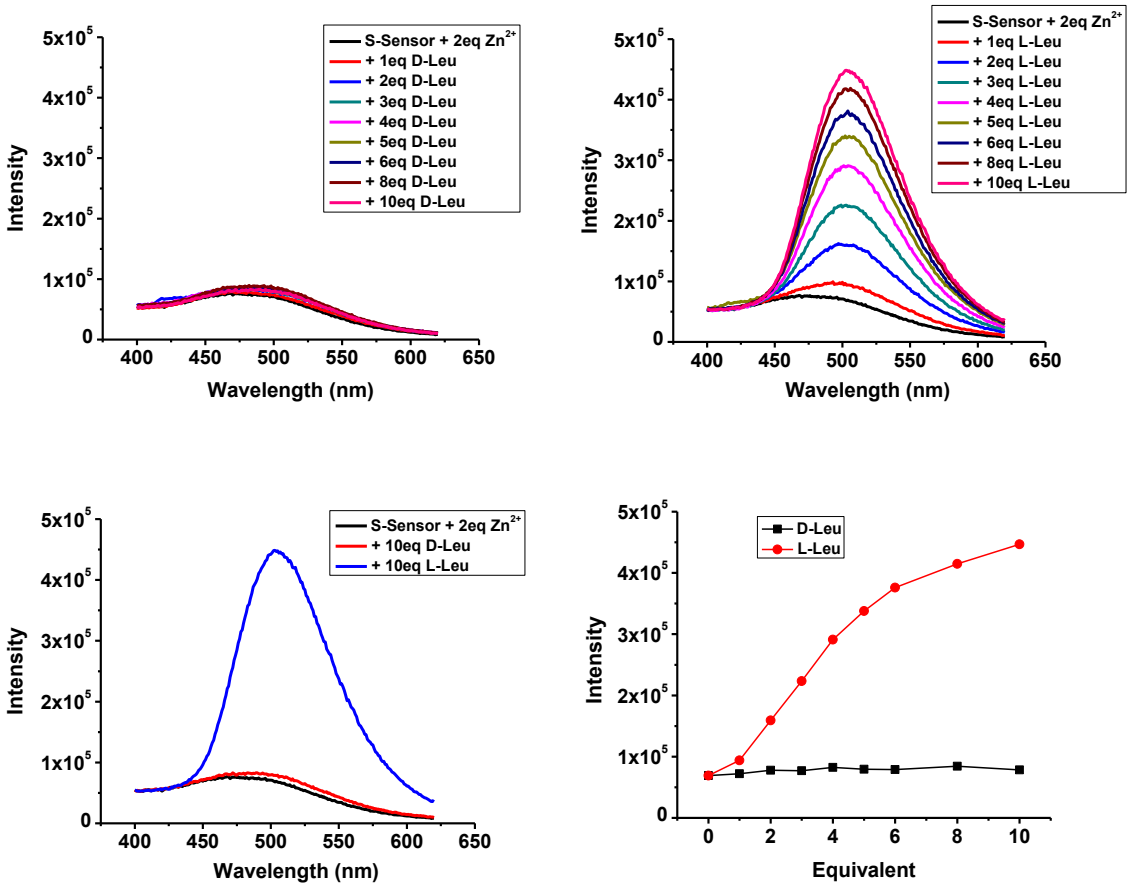

Figure 3.7. Fluorescence spectra of (*S*)-**7** (1.0 mM) with various equiv of D-**8** or L-**8** (4.0 mM) in 25 mM BICINE buffer (pH = 8.80) in the presence of 2.0 equiv of $Zn(OAc)_2$ water solution (2.0 mM). The mixture was allowed to stand at room temperature for 2 h and diluted to 10^{-5} M by using 25 mM BICINE buffer (pH = 8.80), and the fluorescence spectra were then recorded (λ_{exc} = 320 nm. Slit 5/5 nm.). The fluorescence intensity at λ_{em} = 504 nm was used for the equivalent versus fluorescence intensity figure.

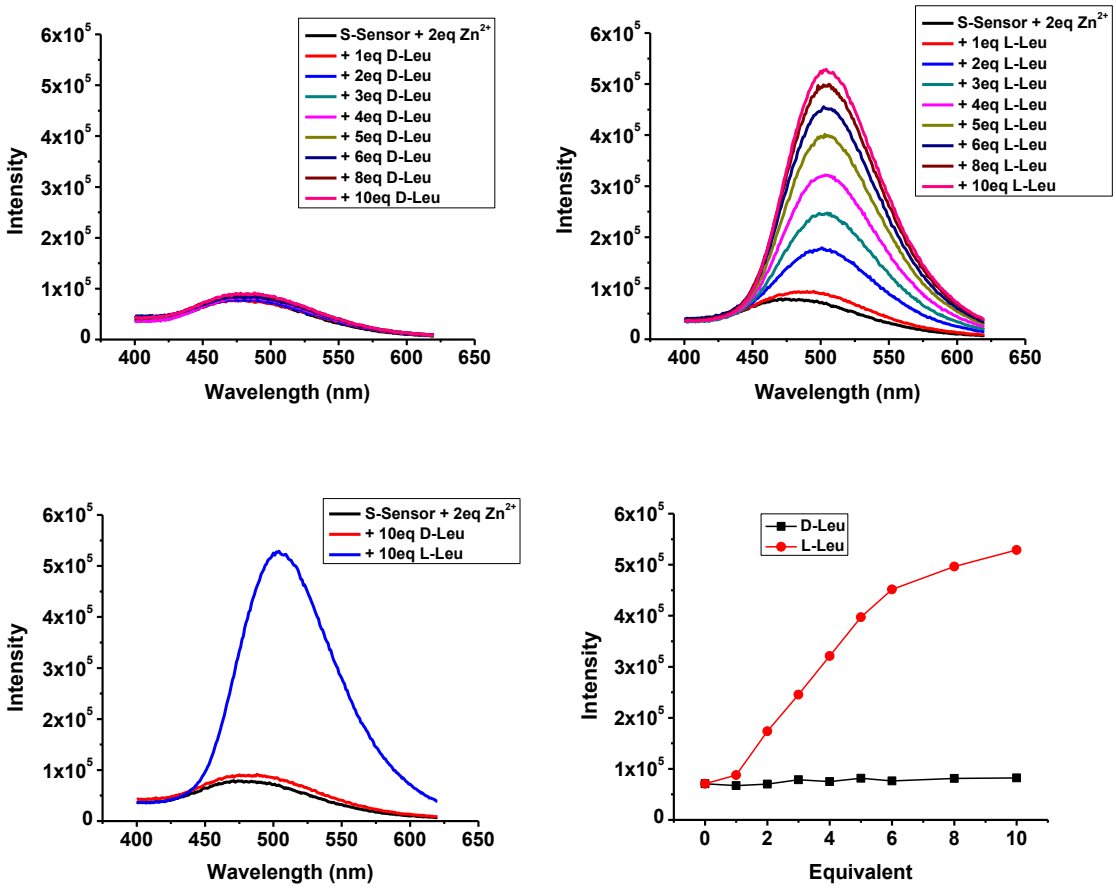

3.2.3. Detailed study on enantioselective fluorescent response of (*S*)-3.9 toward 3.10

We did a more detailed study on the enantioselective fluorescent response toward leucine, **3.10**, and three independent measurements were carried out. As shown in Figure **3.8**, the fluorescence enhancement reached maximum when the concentration of L-**3.10** was greater than 10 equiv. The fluorescence enhancement kept almost stable when the concentration of L-**3.10** is between 10 to 20 equiv. And the fluorescence intensity gradually decreased when more than 20 equiv. of L-**3.10** was added. In contrast, the addition of D-**3.10** led to little fluorescence enhancement when various equiv. of D-**3.10** was added. We used enantiomeric fluorescence enhancement ratio (*ef*) to quantify the enantioselectivity of this probe. $ef = (I_L - I_0)/(I_D - I_0)$, where I_L is the fluorescence intensity after the addition of L-amino acid, I_D is the fluorescence

intensity after the addition of D-amino acid, I_0 is the fluorescence intensity of the background. At 10 equiv of **3.10**, the *ef* value is 45.1, which represents a very high enantioselectivity.

Figure 3.8. Fluorescence titration of (*S*)-**3.9** (1.0 mM, 1 equiv) with (a) D-**3.10** (4.0 mM) and (b) L-**3.10** (4.0 mM) in BICINE in the presence of $Zn(OAc)_2$ (2.0 mM in water, 2 equiv) (Reaction time: 2 h, then diluted 100-fold with BICINE. λ_{exc} = 320 nm. Slit: 5/5 nm). (c) Fluorescence intensity at λ_{em} = 504 nm versus the equivalency of D- and L-**3.10** from three independent measurements.

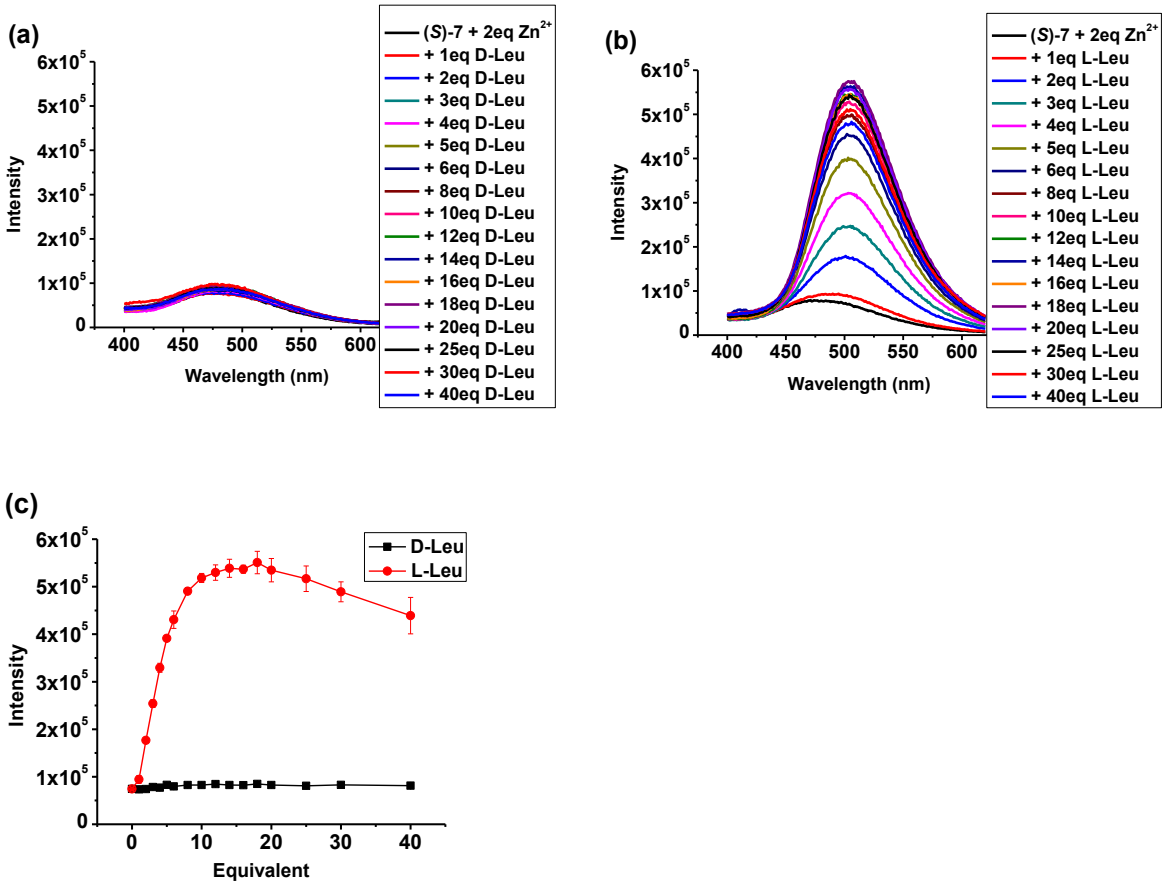

We also examined the use of the enantiomeric sensor (*R*)-**3.9** to interact with the amino acid under the same conditions. It was found that D-**3.10** greatly enhanced the fluorescence of (*R*)-**3.9** but L-**3.10** did not (Figure **3.9**). That is, the fluorescence responses of (*R*)-**3.9** toward

the amino acid are the mirror images of those of (*S*)-**3.9**. This confirms the observed high enantioselectivity of the fluorescent sensor. It also demonstrates that the random steric structure of the PNIPAM chain does not interfere with the chiral recognition of the BINOL core.

Figure 3.9. Fluorescence titration of (*R*)-**3.9** (1.0 mM, 1 equiv) with (a) D-**3.10** (4.0 mM) and (b) L-**3.10** (4.0 mM) in BICINE in the presence of $Zn(OAc)_2$ (2.0 mM in water, 2 equiv) (Reaction time: 2 h, then diluted 100-fold with BICINE. λ_{exc} = 320 nm. Slit: 5/5 nm). (c) Fluorescence intensity at λ_{em} = 504 nm versus the equivalency of D- and L-**3.10**.

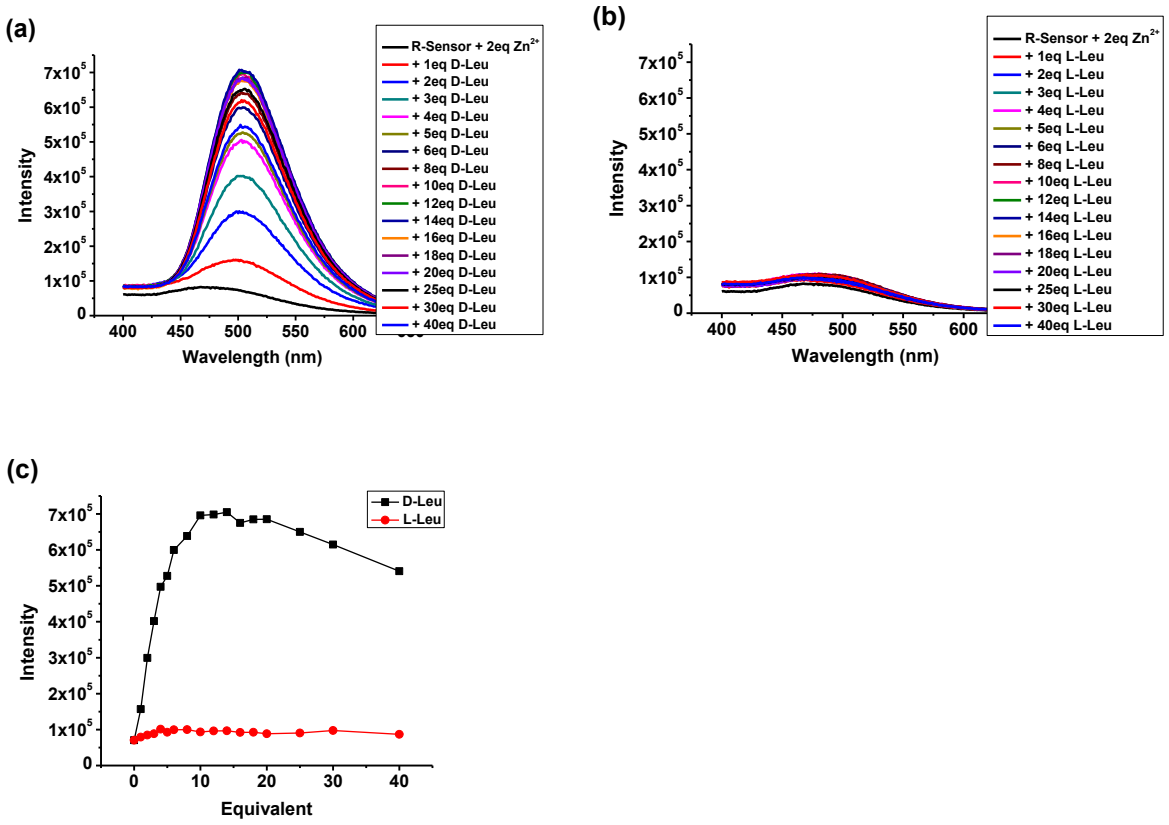

In order to use the polymer-supported fluorescence sensor to determine the enantiomeric composition of the amino acid, we studied the fluorescence response of (*S*)-**3.9** toward **3.10** at various *ee*s [*ee*, enantiomeric excess, = (L-D)/(L+D)]. In the experiment, (*S*)-**3.9** (1.0 mM in BICINE, 50 μL, 1.0 equiv) was mixed with $Zn(OAc)_2$ (2.0 mM in water, 50 μL, 2.0 equiv) and

3.10 (4.0 mM in BICINE, 200 μL, 16 equiv) with various *ee*s for 2 h. Then the mixtures were diluted to 5 mL for fluorescence measurement (Figure **3.10**). As shown in Figure **3.9**, a large nonlinear effect was observed. There is almost no fluorescence enhancement when *ee* < 0, and the fluorescence intensity gradually increase when *ee* > 0. We also examined the use of the enantiomeric sensor (*R*)-**3.9** for *ee* study under the same condition, and an opposite result was observed (Figure **3.11**). These results indicated that the non-fluorescence-enhancing enantiomer can greatly suppress the fluorescence-enhancing effect of its antipode. The simplest explanation for this observation would be the formation of complex structures between the two enantiomers of the amino acid, the fluorescent sensor and the Zn^{2+} which prevent them from reacting with the fluorescent sensor. Only when the fluorescence enhancing enantiomer is in excess, can it turn on the fluorescence of the sensor.

Figure 3.10. Fluorescence responses of (*S*)-**3.9** (1.0 mM) toward 16 equiv of **3.10** (4.0 mM) at various *ee* (*ee* = (L − D)/(L + D)) in 25 mM BICINE buffer (pH = 8.80) in the presence of 2.0 equiv of $Zn(OAc)_2$ water solution (2 mM). The mixture was allowed to stand at room temperature for 2 h and diluted to 10^{-5} M by using 25 mM BICINE buffer (pH = 8.80), and the fluorescence spectra were then recorded (λ_{exc} = 320 nm. Slit 5/5 nm. The fluorescence intensity at λ_{em} = 504 nm was used for each data points).

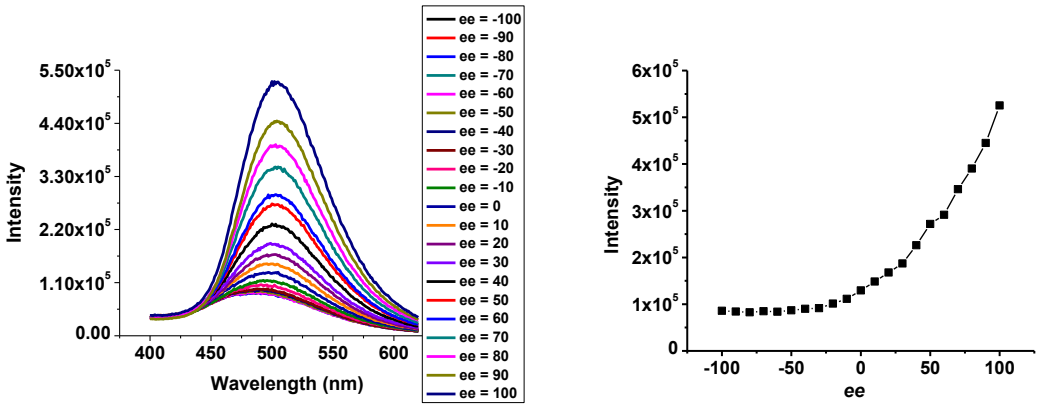

Figure 3.11. Fluorescence responses of (*R*)-**3.9** (1.0 mM) toward 16 equiv of **3.10** (4.0 mM) at various *ee* (*ee* = (L − D)/(L + D)) in 25 mM BICINE buffer (pH = 8.80) in the presence of 2.0 equiv of $Zn(OAc)_2$ water solution (2 mM). The mixture was allowed to stand at room temperature for 2 h and diluted to 10^{-5} M by using 25 mM BICINE buffer (pH = 8.80), and the fluorescence spectra were then recorded (λ_{exc} = 320 nm. Slit 5/5 nm. The fluorescence intensity at λ_{em} = 504 nm was used for each data points).

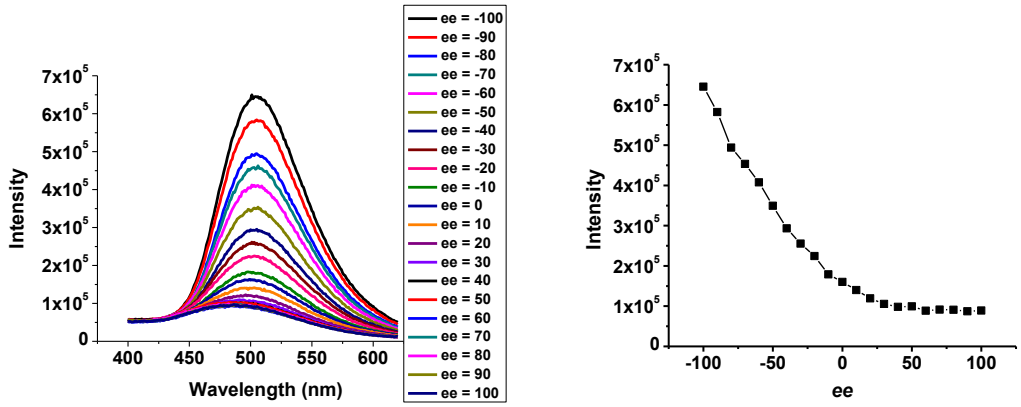

3.2.4. Application of the polymer sensors based on amphiphilic property

The sensors are amphiphilic and the fluorescence measurements are in buffer aqueous solution. Therefore, it is possible to extract the product out from the aqueous mixture to the organic layer after the reaction. We studied the extraction of the aqueous sensor-substrate solution with the water immiscible chloroform. A solution of (*R*)-**3.9** (1.0 equiv in BICINE) was mixed with $Zn(OAc)_2$ (2.0 equiv in water) and L- or D-**3.10** (4.0 equiv in BICINE) for 2 h at room temperature. Then, chloroform was added to extract with vigorous mixing and the fluorescence of the separated organic phase was measured. As shown in Figure **3.12**, similar to those observed in the aqueous solution, L-**3.10** greatly enhanced the fluorescence of (*R*)-**3.9** but D-**3.10** did not. This chloroform extraction experiment demonstrates that the amphiphilic

property of PNIPAM allows the fluorescent recognition to be conducted in two separated phases with retention of the high enantioselectivity.

Figure 3.12. Fluorescence spectra of the following chloroform extracts after they were diluted 10-fold: Chloroform (3.0 mL) was used to extract the reaction mixture of (*R*)-**3.9** (1.0 mM in BICINE, 1.0 mL, 1.0 equiv), $Zn(OAc)_2$ (2.0 mM in water, 1.0 mL, 2.0 equiv) and D- or L-**3.10** (4.0 mM in BICINE, 1.0 mL, 4.0 equiv). (reaction time: 2 h. λ_{exc} = 320 nm. Slit: 5/5 nm).

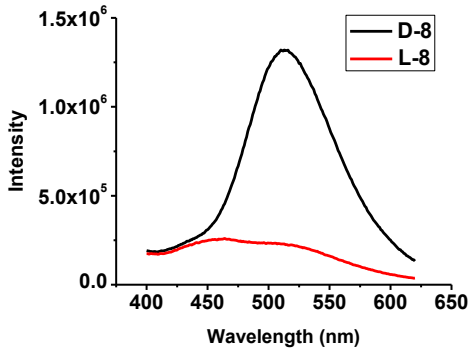

We studied the fluorescence response of (*S*)-**3.9** toward **3.10** at various *ee*s in both aqueous and chloroform phases. In the experiment, (*S*)-**3.9** (1.0 mM in BICINE, 0.5 mL, 1.0 equiv) was mixed with $Zn(OAc)_2$ (2.0 mM in water, 0.5 mL, 2.0 equiv) and **3.10** (4.0 mM in BICINE, 2 mL, 16 equiv) with various *ee*s for 2 h. Then 30 μL of the mixture was taken out and diluted to 3 mL by using the BICINE buffer to measure fluorescence (Figure **3.14**). To the remaining aqueous solution, $CHCl_3$ (3.0 mL) was added and vigorously mixed. After 30 min, the fluorescence of the $CHCl_3$ solution was measured. Figure **3.13** and **3.14** demonstrate that when (*S*)-**3.9** is used, the enantiomeric composition of the amino acid at *ee* > 0, that is L-**3.10** in excess, can be determined in both aqueous and organic phases because of the significant fluorescence enhancement of (*S*)-**3.9** by L-**3.10**. In order to determine the enantiomeric composition of the samples when D-**3.10** is in excess (*ee* < 0), the enantiomeric sensor (*R*)-**3.9** can be used.

Figure 3.13. Fluorescent response of 1.0 mM (*S*)-**3.9** toward 16 equiv of 4.0 mM **3.10** at various *ee* in 25 mM BICINE buffer (pH = 8.80) in the presence of 2.0 equiv of 2.0 mM $Zn(OAc)_2$ water solution. The mixture was allowed to stand at room temperature for 2 h, and then diluted to 10^{-5} M by using 25 mM BICINE buffer (pH = 8.80). (λ_{exc} = 320 nm. Slit: 5/5 nm. Data points at λ_{em} = 504 nm were used for the *ee* versus fluorescence intensity figure)

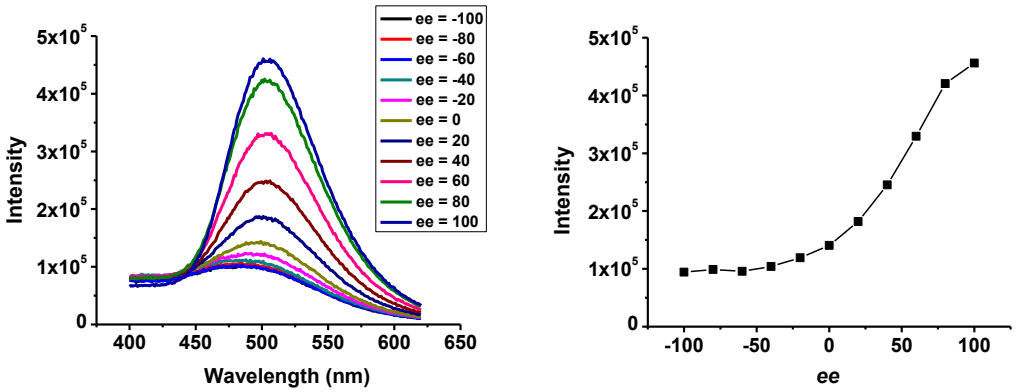

Figure 3.14. Fluorescent spectra of the diluted chloroform solution after extraction with various *ee* value (left) and fluorescence response at λ_{em} = 506 nm after the aqueous solutions were extracted with chloroform (3.0 mL) and diluted 5-fold (right). (λ_{exc} = 320 nm. Slit: 5/5 nm.)

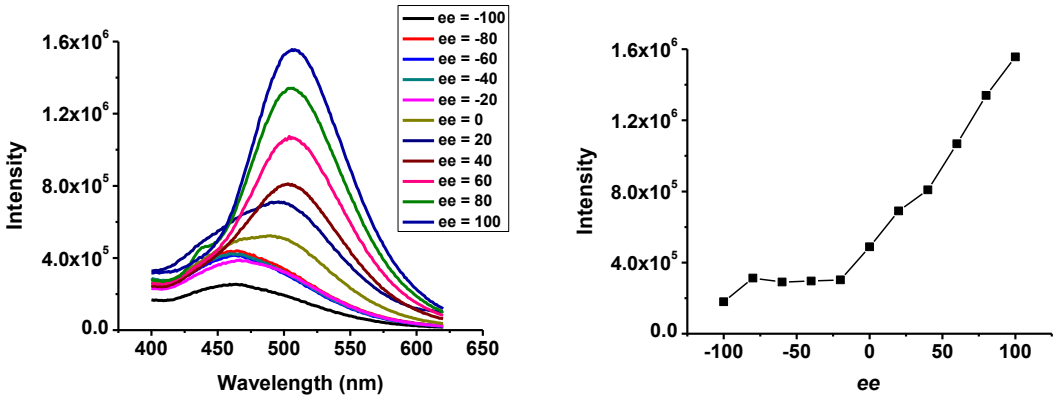

The ability of the polymeric sensor (*S*)-**3.9** to determine the enantiomeric composition in both aqueous solution and chloroform extract is very attractive. For example, when the amino acid substrate is generated in aqueous media from enzyme catalysis or other aqueous

asymmetric reaction processes, fluorescence measurement by chloroform extraction in the presence of the polymer-based sensor should minimize the interference by the water-soluble components and facilitate the determination of the enantiomeric composition of the amino acids.

3.2.5. Application of the polymer sensors based on LCST property

We studied the thermo-response of (*S*)-**3.9** in BICINE. A solution of (*S*)-**3.9** (1.0 mM) in BICINE was heated at 1 ^{o}C per minute which became cloud at 34 ^{o}C. That is, the LCST of (*S*)-**3.9** in BICINE buffer is only 2 ^{o}C above it in pure water. The LCST of the mixture of 1.0 equiv of (*S*)-**3.9** with 2.0 equiv of $Zn(OAc)_2$ and 4.0 equiv. of L-**3.10** or D-**3.10** was measured. After the mixture was allowed to stand at room temperature for 2 h, the LCSTs of both of the L-**3.10** and D-**3.10** solutions were found to be 34 ^{o}C. That is, the addition of $Zn(OAc)_2$ and amino acids had no effect on the polymer LCST.

We used the LCST property of (*S*)-**3.9** to separate the sensor-amino acid adduct for fluorescence measurement. Stock solutions of (*S*)-**7** (1.0 mM) in BICINE, D-**3.10** and L-**3.10** (4.0 mM) in BICINE and $Zn(OAc)_2$ (2.0 mM) in water were freshly prepared. (*S*)-**3.9** (1.0 equiv) was mixed with $Zn(OAc)_2$ (2.0 equiv) and D-**3.10** or L-**3.10** (4.0 equiv) in test tubes for 2 h at room temperature. When two test tubes containing D-**3.10** and L-**3.10** respectively were heated at 45 ^{o}C in a water bath for 5 min, cloudy precipitates formed in both cases (Figure **3.15**, only one test tube is shown). Then, the precipitate was separated by centrifugation while the sample test tube was kept warm. Both the precipitates from L-**3.10** and D-**3.10** were redissolved in BICINE and the fluorescence spectra of the solutions were obtained. As shown in Figure **3.16**, the solution from L-**3.10** gives strong fluorescence signal at λ = 504 nm while that from D-**3.10** gives a very weak signal. Thus, enantioselective fluorescence response of (*S*)-**3.9** toward

the amino acid was maintained in the precipitates generated above the LCST of the polymer. This LCST property of (*S*)-**7** provides a new way to separate the fluorescence measurement from the original substrate solution, which should be useful when the enantioselective fluorescent sensor is used in asymmetric reaction screening since it can minimize the interference by other reaction components on the fluorescence measurement.

Figure 3.15. Photos for the mixture of (*S*)-**3.9** (1.0 mM, 1.0 equiv) with L-**3.10** (4.0 mM, 4.0 equiv) in BICINE in the presence of $Zn(OAc)_2$ (2.0 mM in water, 2.0 equiv) at room temperature for 2 h (left), and then heated at 45 ^oC for 5 min (right).

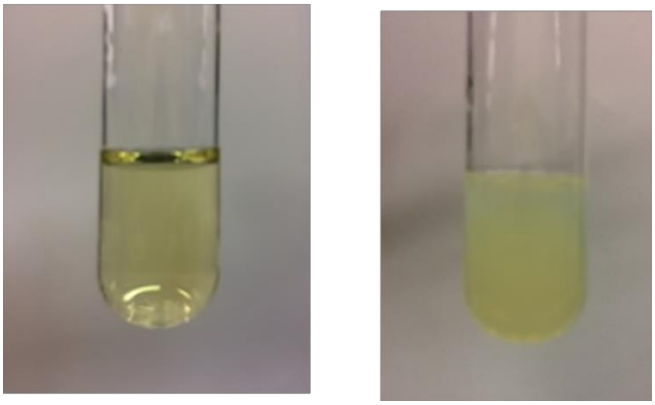

Figure 3.16. Fluorescence spectra of the redissolved precipitates (5 mL, BICINE) isolated from the reaction of (*S*)-**3.9** (1.0 mM, 1.0 equiv) with D- or L-**3.10** (4.0 mM, 4.0 equiv) in BICINE in the presence of $Zn(OAc)_2$ (2.0 mM in water, 2.0 equiv) at room temperature for 2 h then heated at 45 ^oC for 5 min (λ_{exc} = 320 nm. Slit 5/5 nm).

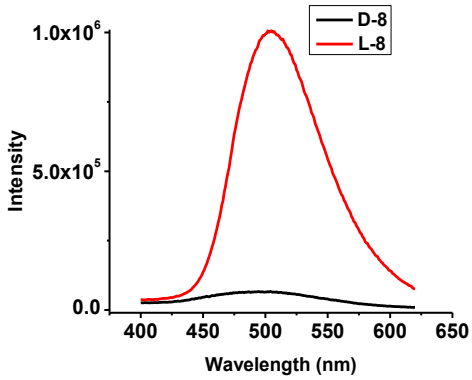

3.2.6. Enantioselective fluorescent response of (*S*)-3.9 toward other amino acids

Besides leucine, we also studied the fluorescence response of (*S*)-**3.9** toward 17 common amino acids (Figure **3.17**) in BICINE in the presence of $Zn(OAc)_2$. Highly enantioselective fluorescence enhancements were observed for histidine, glutamine, threonine and arginine. As shown in Figure **3.18-3.22**, while the L enantiomers of these amino acids greatly enhance the fluorescence of (*S*)-**3.9** at above 500 nm, the corresponding D-enantiomers did not cause much change on the fluorescence. In Figure **3.18**, very high *ef* values of (*S*)-**3.9** in the presence of these amino acids are observed with 32.9 for histidine, 35.2 for glutamine, 73.7 for threonine and 55.0 for arginine respectively. Under the same conditions, (*S*)-**3.9** also showed good enantioselective fluorescent response toward phenylalanine, tyrosine, serine, asparagine, and valine (Figure **3.23**–**3.27**), and moderate enantioselectivity toward tryptophan, cysteine and methionine (Figure **3.28**–**3.30**), but little fluorescence response toward proline, alanine, lysine, aspartic acid and glutamic acid (Figure **3.31**–**3.35**).

Figure 3.17. Structure of amino acids

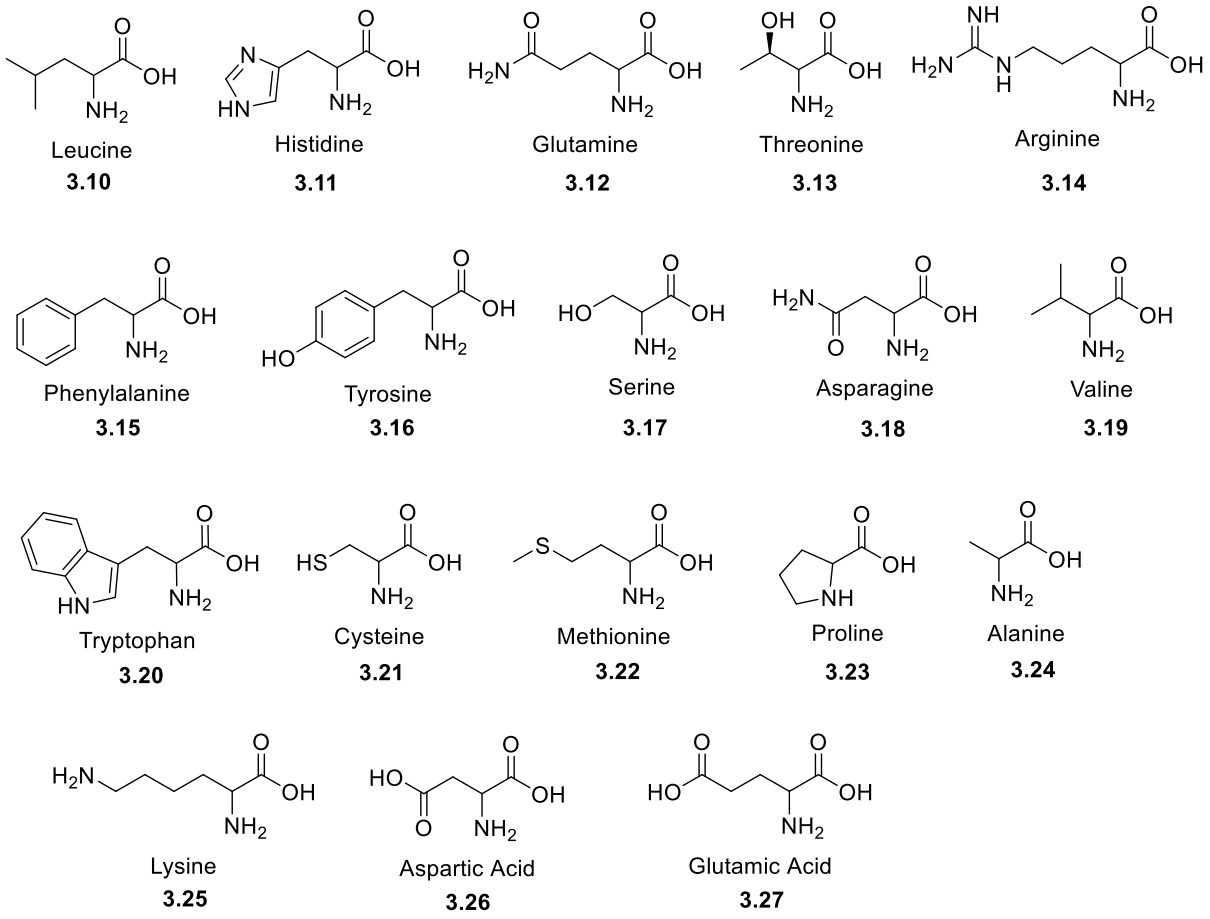

Figure 3.18. Fluorescence spectra of (*S*)-**3.9** (1.0 mM in BICINE, 1.0 equiv) in the presence of 2 equiv 2 mM $Zn(OAc)_2$ (2.0 mM in water, 2.0 equiv) with amino acids in BICINE: (a) histidine (4.0 mM, 10.0 equiv), (b) glutamine (4.0 mM, 10.0 equiv), (c) threonine (4.0 mM, 8.0 equiv), and (d) arginine (4.0 mM, 10.0 equiv) (reaction time: 2 h, then diluted 100 fold using BICINE. λ_{exc} = 320 nm. Slit: 5/5 nm).

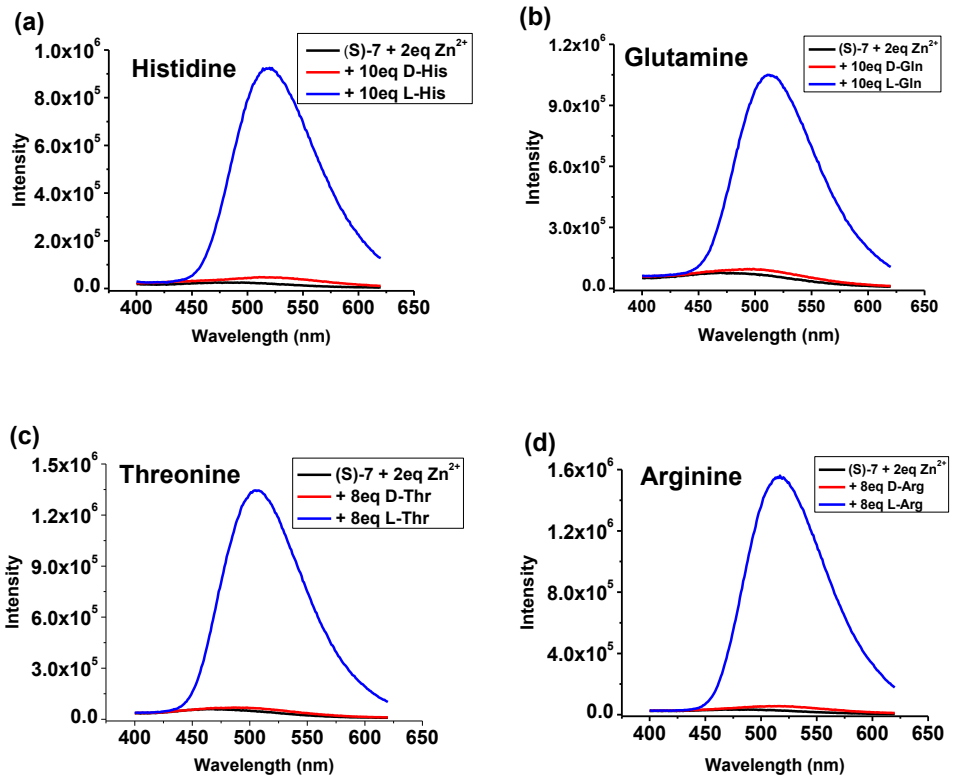

Figure 3.19. Fluorescence spectra of (*S*)-**3.9** (1.0 mM) with various equiv of histidine, D-**3.11** or L-**3.11** (4.0 mM) in 25 mM BICINE buffer (pH = 8.80) in the presence of 2.0 equiv of $Zn(OAc)_2$ water solution (2.0 mM). Reaction time: 2 h, then diluted 100-fold using BICINE. (λ_{exc}=320 nm. Slit 5/5 nm. Fluorescence intensity at λ_{em} = 520 nm was used for each data point).

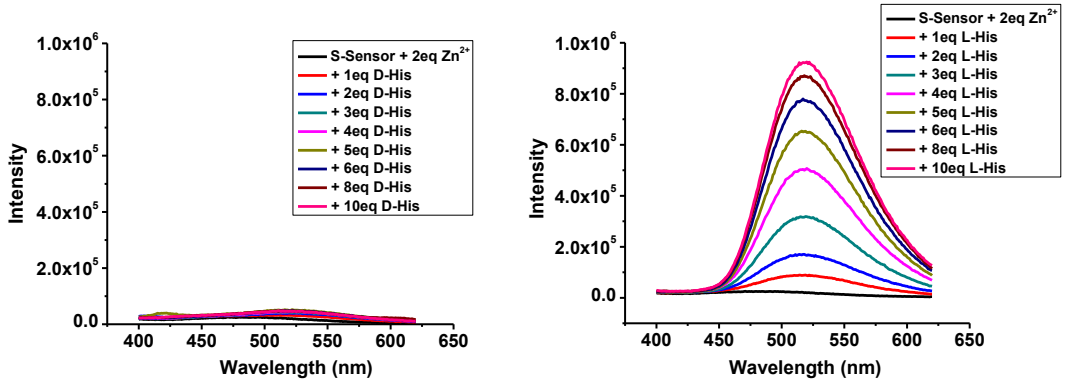

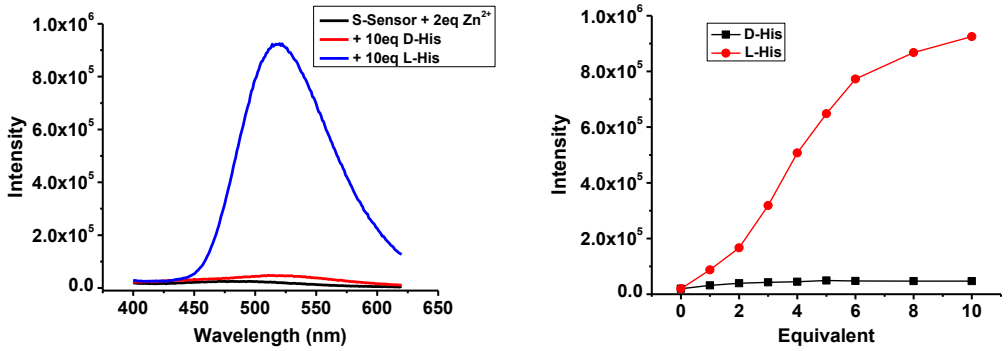

Figure 3.20. Fluorescence spectra of (*S*)-**3.9** (1.0 mM) with various equiv of glutamine, D-**3.12** or L-**3.12** (4.0 mM) in 25 mM BICINE buffer (pH = 8.80) in the presence of 2.0 equiv of $Zn(OAc)_2$ water solution (2.0 mM). Reaction time: 2 h, then diluted 100-fold using BICINE. (λ_{exc}=320 nm. Slit 5/5 nm. Fluorescence intensity at λ_{em} = 513 nm was used for each data point).

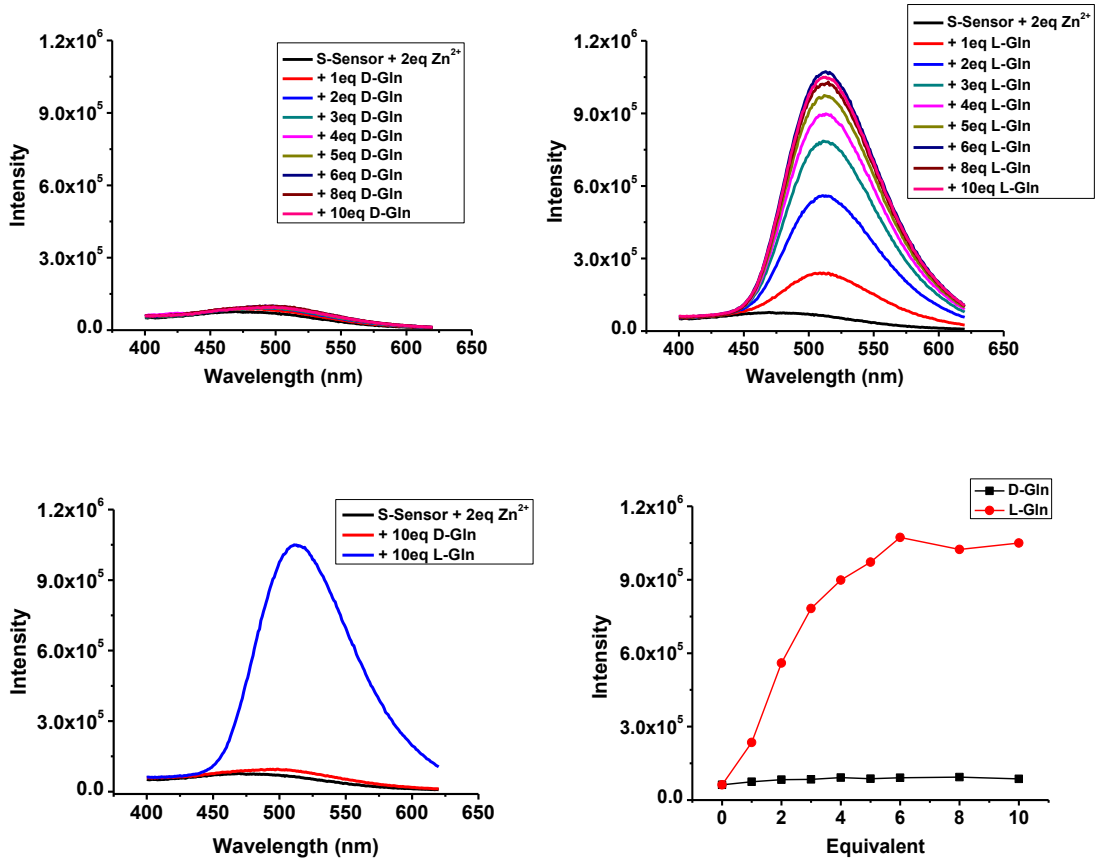

Figure 3.21. Fluorescence spectra of (*S*)-**3.9** (1.0 mM) with various equiv of threonine, D-**3.13** or L-**3.13** (4.0 mM) in 25 mM BICINE buffer (pH = 8.80) in the presence of 2.0 equiv of $Zn(OAc)_2$ water solution (2.0 mM). Reaction time: 2 h, then diluted 100-fold using BICINE. (λ_{exc}=320 nm. Slit 5/5 nm. Fluorescence intensity at λ_{em} = 506 nm was used for each data point).

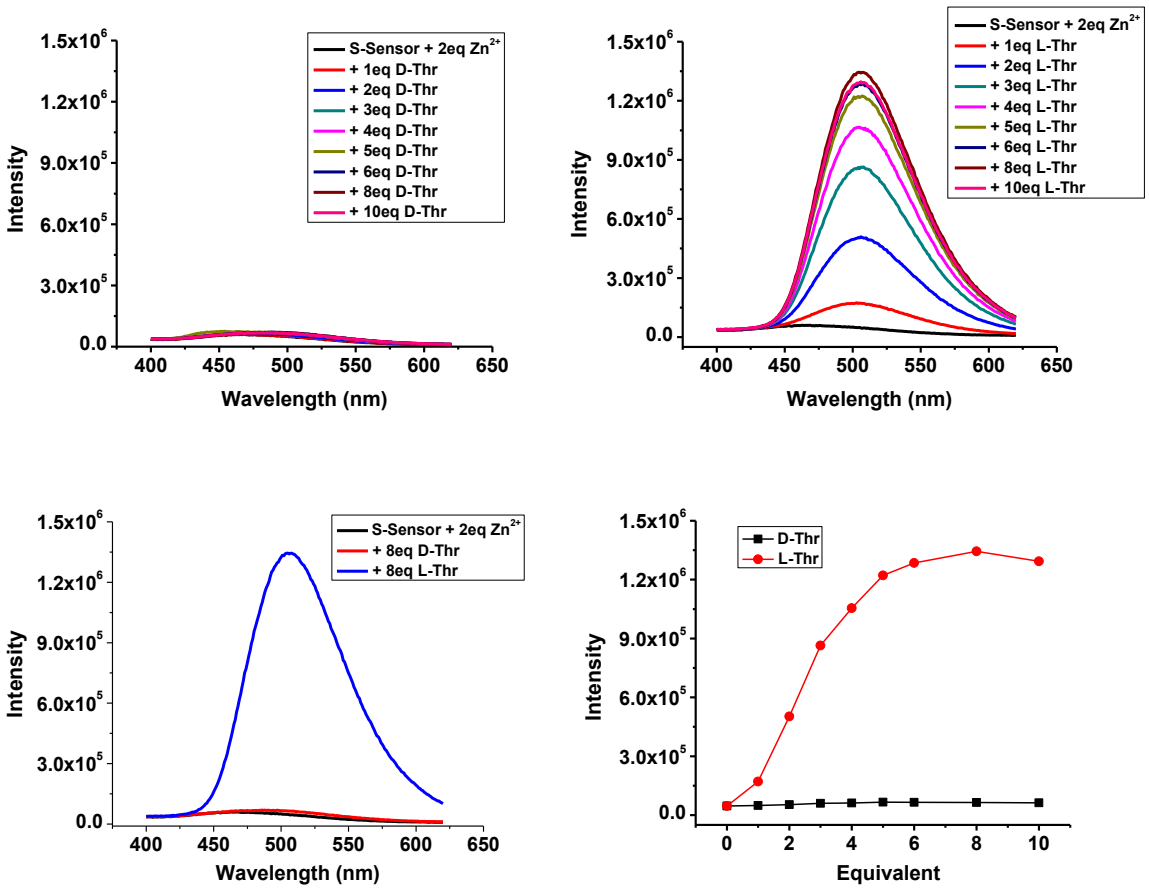

Figure 3.22. Fluorescence spectra of (*S*)-**3.9** (1.0 mM) with various equiv of arginine, D-**3.14** or L-**3.14** (4.0 mM) in 25 mM BICINE buffer (pH = 8.80) in the presence of 2.0 equiv of $Zn(OAc)_2$ water solution (2.0 mM). Reaction time: 2 h, then diluted 100-fold using BICINE. (λ_{exc}=320 nm. Slit 5/5 nm. Fluorescence intensity at λ_{em} = 517 nm was used for each data point).

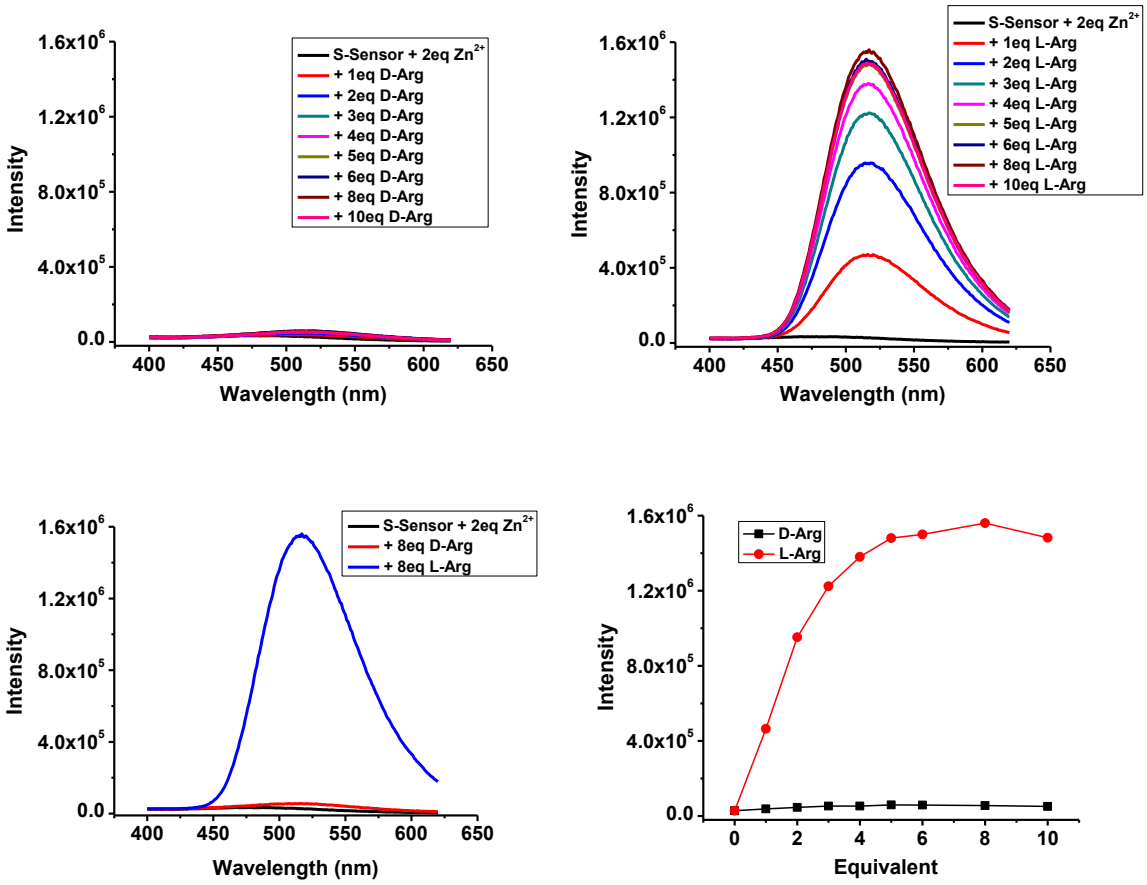

Figure 3.23. Fluorescence spectra of (*S*)-**3.9** (1.0 mM) with various equiv. of phenylalanine, D-**3.15** or L-**3.15** (4.0 mM) in 25 mM BICINE buffer (pH = 8.80) in the presence of 2.0 equiv. of $Zn(OAc)_2$ water solution (2.0 mM). Reaction time: 2 h, then diluted 100-fold using BICINE. (λ_{exc}=320 nm. Slit 5/5 nm. Fluorescence intensity at λ_{em} = 509 nm was used for each data point).

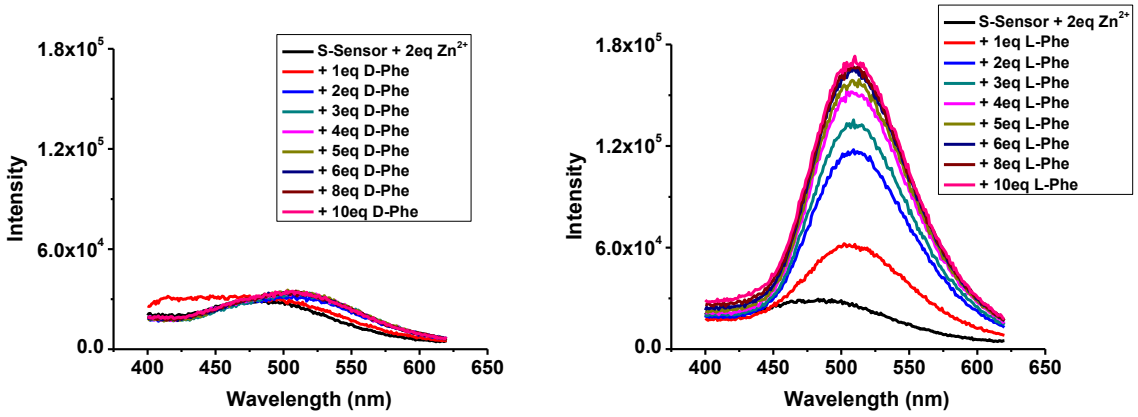

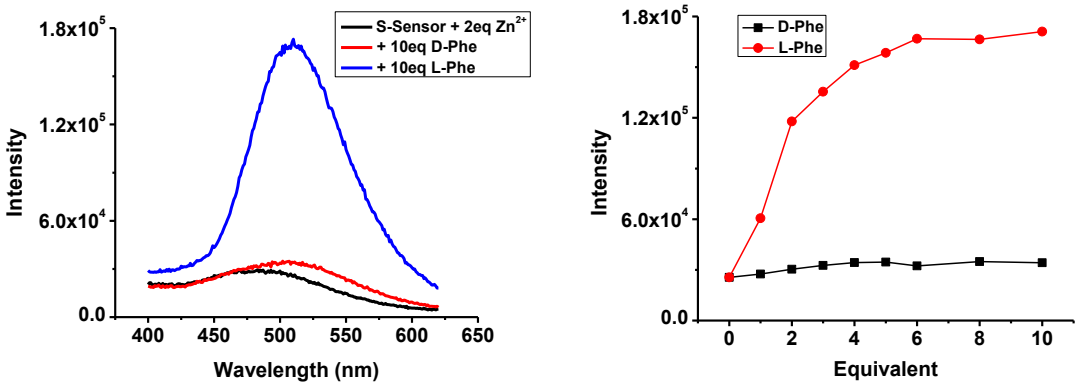

Figure 3.24. Fluorescence spectra of (*S*)-**3.9** (1.0 mM) with various equiv of tyrosine, D-**3.16** or L-**3.16** (2.0 mM) in 25 mM BICINE buffer (pH = 8.80) in the presence of 2.0 equiv of $Zn(OAc)_2$ water solution (2.0 mM). Reaction time: 2 h, then diluted 100-fold using BICINE. (λ_{exc}=320 nm. Slit 5/5 nm. Fluorescence intensity at λ_{em} = 513 nm was used for each data point).

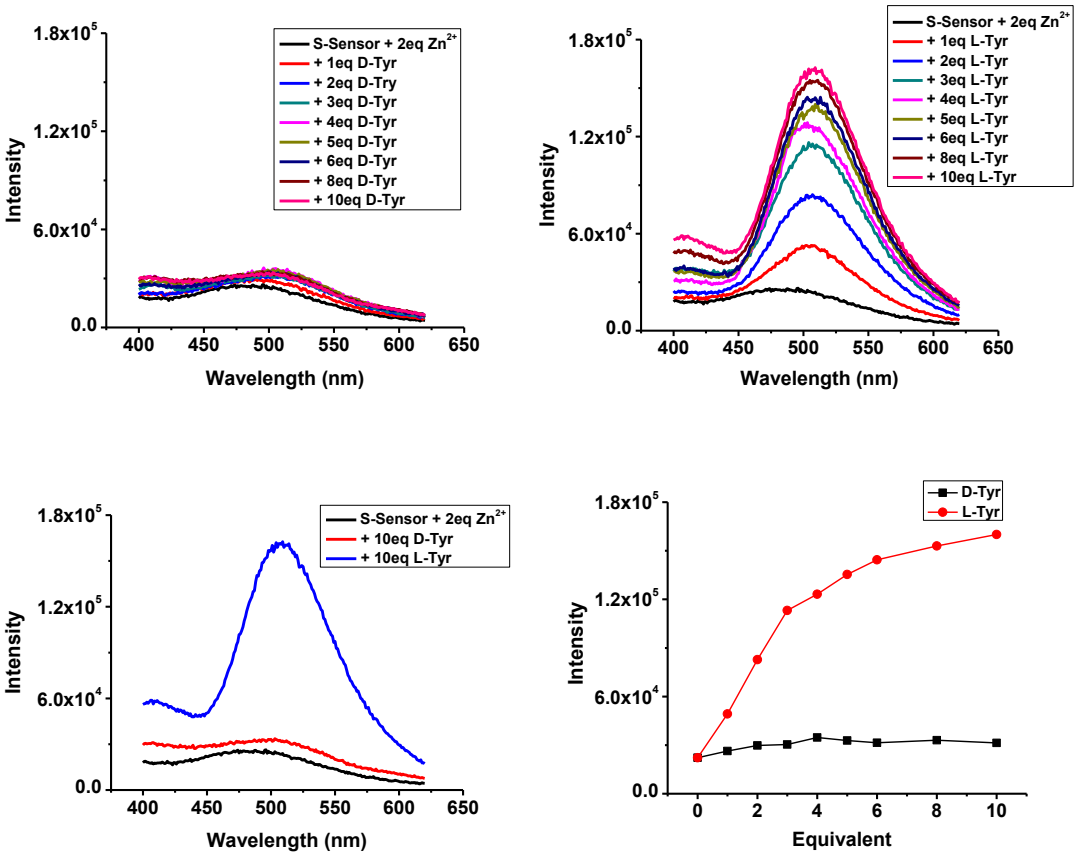

Figure 3.25. Fluorescence spectra of (*S*)-**3.9** (1.0 mM) with various equiv of serine, D-**3.17** or L-**3.17** (4.0 mM) in 25 mM BICINE buffer (pH = 8.80) in the presence of 2.0 equiv of $Zn(OAc)_2$ water solution (2.0 mM). Reaction time: 2 h, then diluted 100-fold using BICINE. (λ_{exc} = 320 nm. Slit 5/5 nm. The fluorescence intensity at λ_{em} = 513 nm was used for each data point).

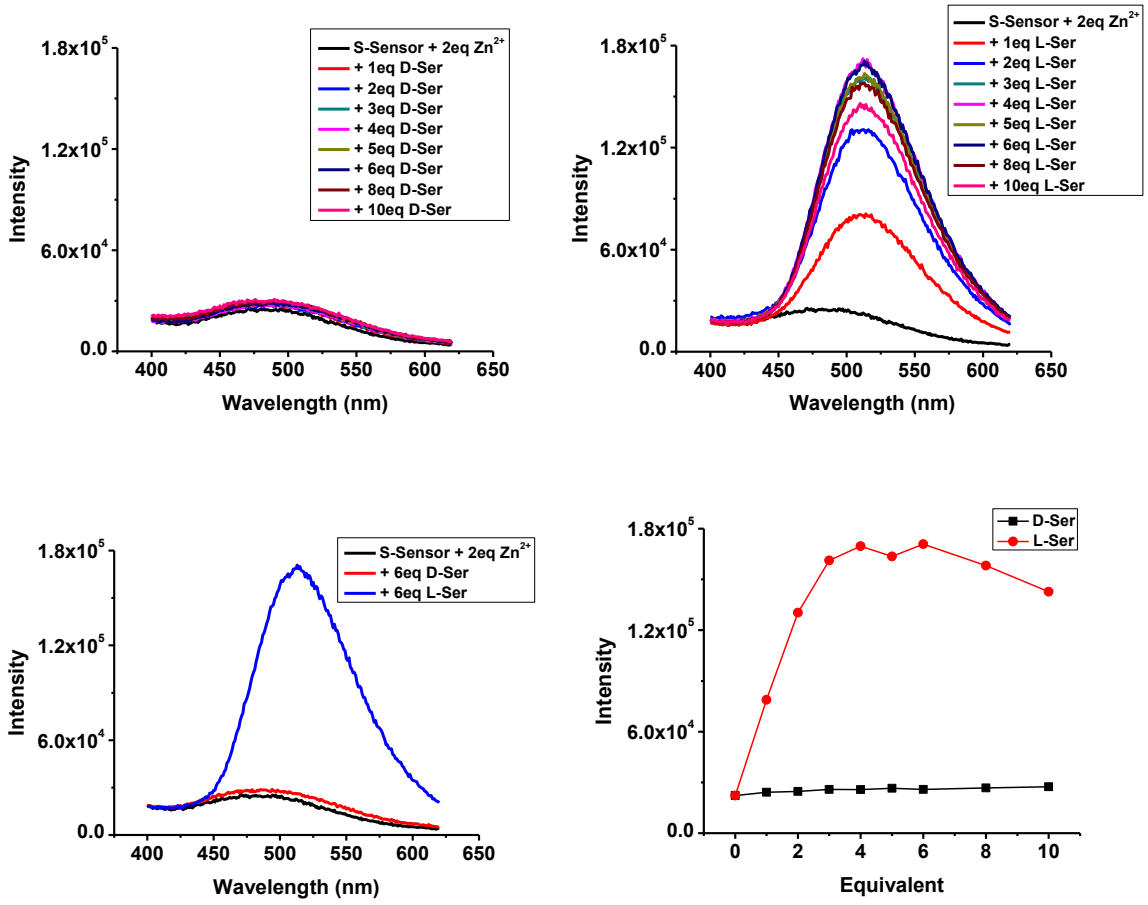

Figure 3.26. Fluorescence spectra of (*S*)-**3.9** (1.0 mM) with various equiv of asparagine, D-**3.18** or L-**3.18** (4.0 mM) in 25 mM BICINE buffer (pH = 8.80) in the presence of 2.0 equiv of $Zn(OAc)_2$ water solution (2.0 mM). Reaction time: 2 h, then diluted 100-fold using BICINE. (λ_{exc}=320 nm. Slit 5/5 nm. Fluorescence intensity at λ_{em} = 513 nm was used for each data point).

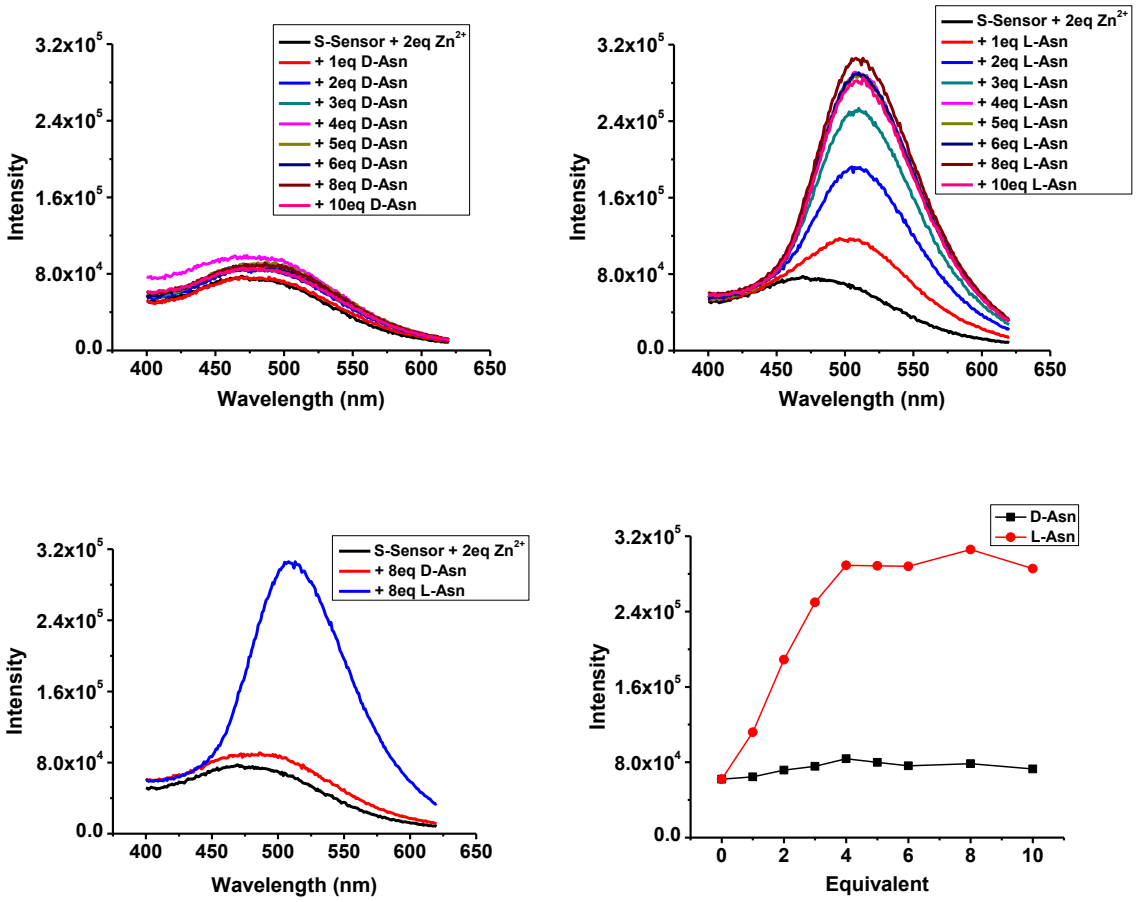

Figure 3.27. Fluorescence spectra of (*S*)-**3.9** (1.0 mM) with various equiv of valine, D-**3.19** or L-**3.19** (4.0 mM) in 25 mM BICINE buffer (pH = 8.80) in the presence of 2.0 equiv of $Zn(OAc)_2$ water solution (2.0 mM). Reaction time: 2 h, then diluted 100-fold using BICINE. (λ_{exc} = 320 nm. Slit 5/5 nm. The fluorescence intensity at λ_{em} = 502 nm was used for each data point).

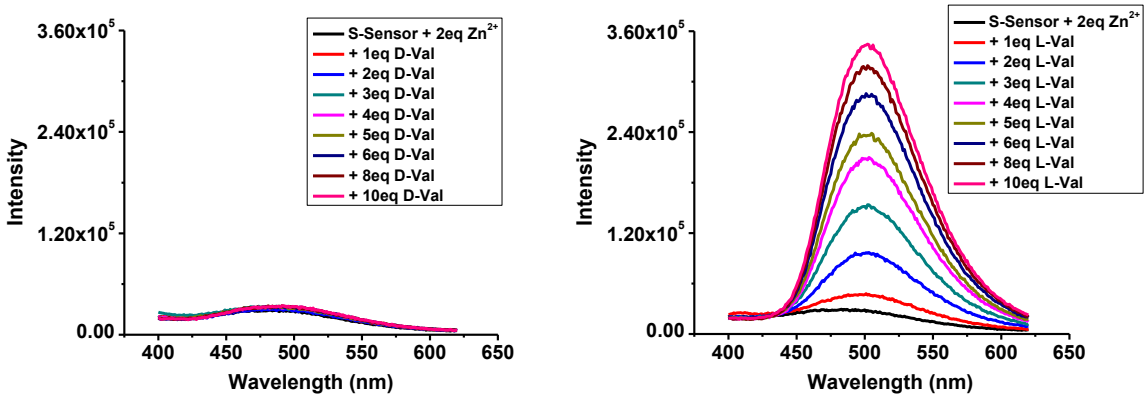

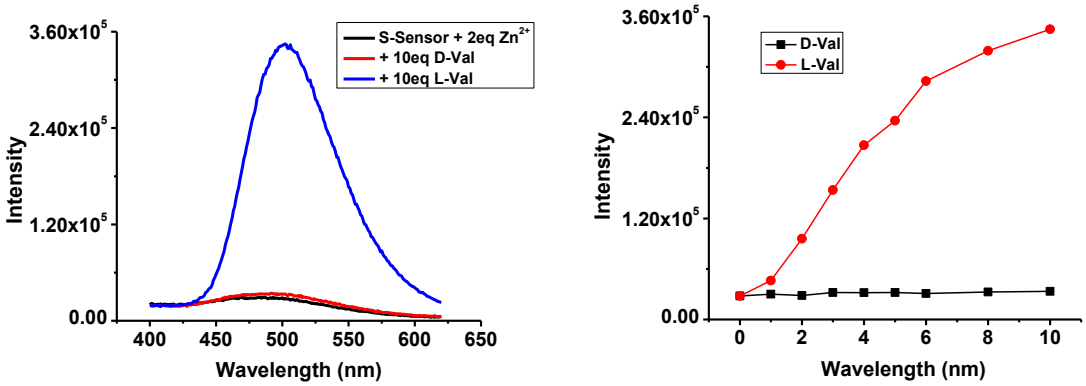

Figure 3.28. Fluorescence spectra of (*S*)-**3.9** (1.0 mM) with various equiv of tryptophan, D-**3.20** or L-**3.20** (4.0 mM) in 25 mM BICINE buffer (pH = 8.80) in the presence of 2.0 equiv of $Zn(OAc)_2$ water solution (2.0 mM). Reaction time: 2 h, then diluted 100-fold using BICINE. (λ_{exc}=320 nm. Slit 5/5 nm. Fluorescence intensity at λ_{em} = 513 nm was used for each data point).

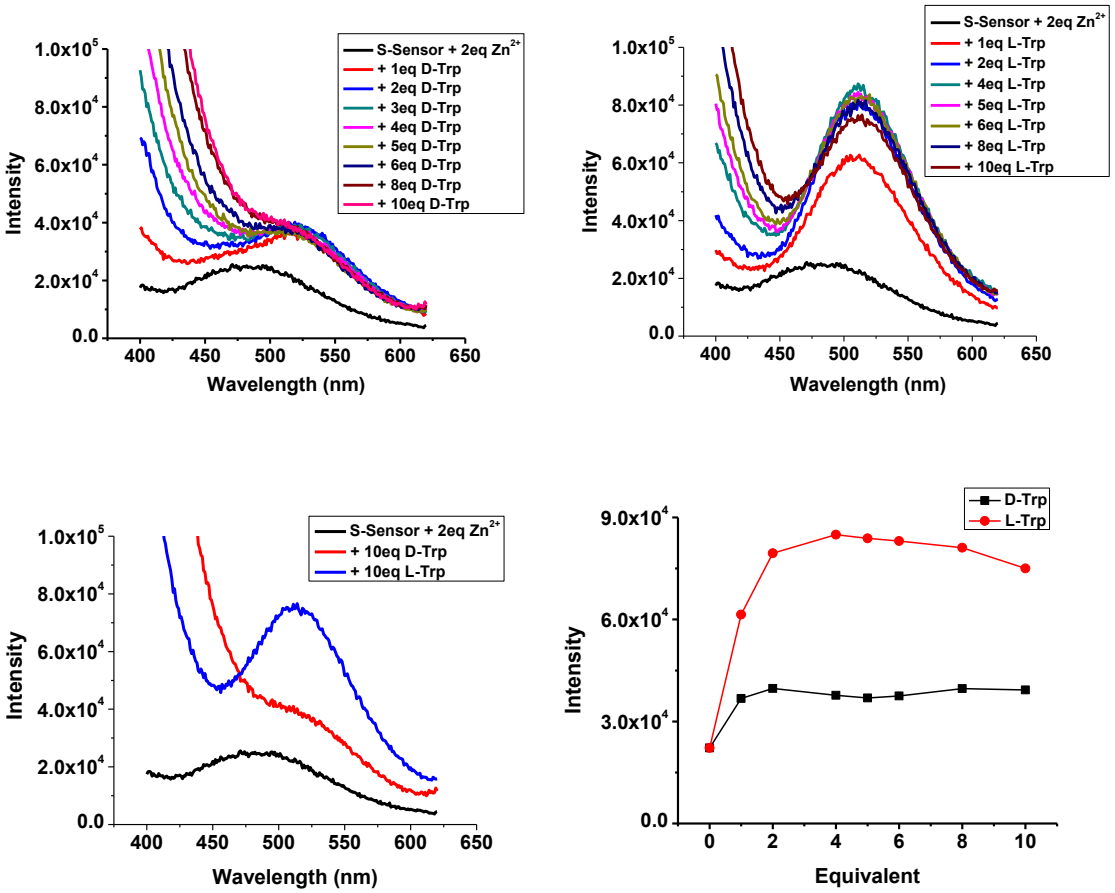

Figure 3.29. Fluorescence spectra of (*S*)-**3.9** (1.0 mM) with various equiv of cysteine, D-**3.21** or L-**3.21** (4.0 mM) in 25 mM BICINE buffer (pH = 8.80) in the presence of 2.0 equiv of $Zn(OAc)_2$ water solution (2.0 mM). Reaction time: 2 h, then diluted 100-fold using BICINE. (λ_{exc}=320 nm. Slit 5/5 nm. Fluorescence intensity at λ_{em} = 513 nm was used for each data point).

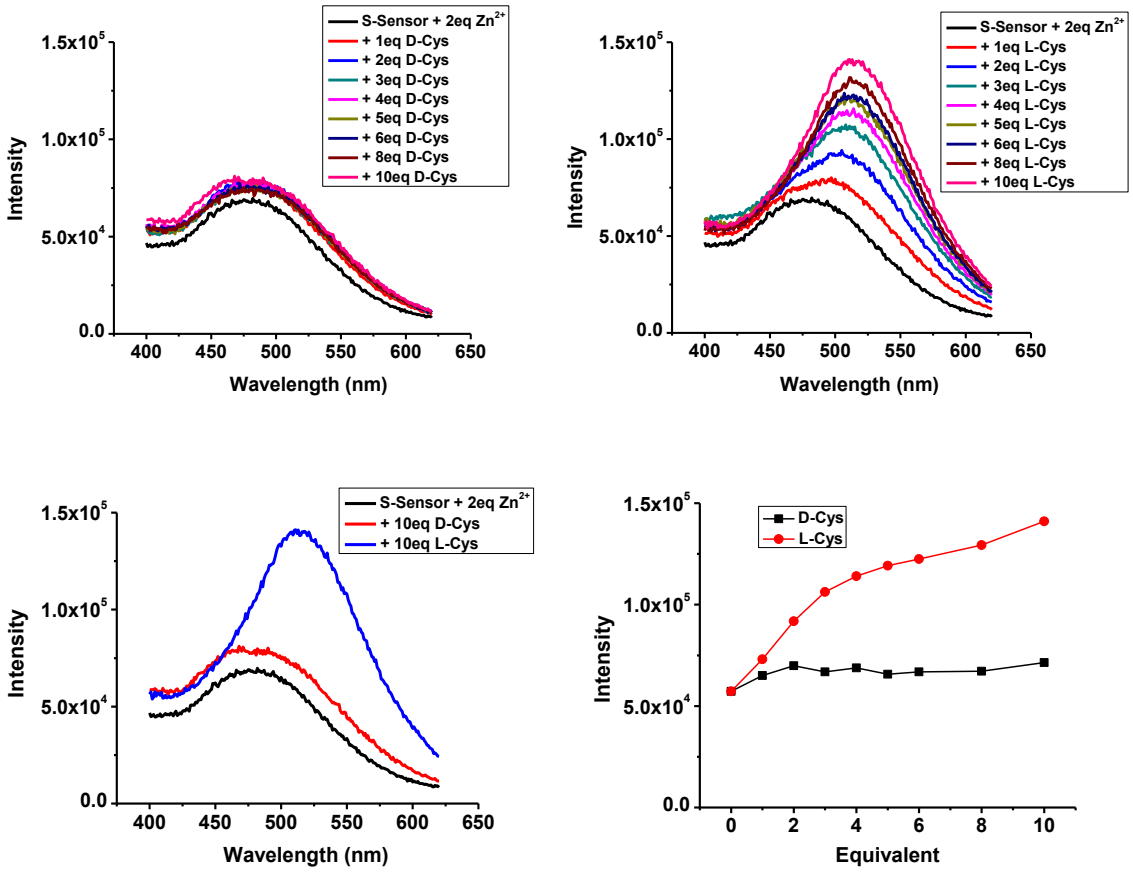

Figure 3.30. Fluorescence spectra of (*S*)-**3.9** (1.0 mM) with various equiv of methionine, D-**3.22** or L-**3.22** (4.0 mM) in 25 mM BICINE buffer (pH = 8.80) in the presence of 2.0 equiv of $Zn(OAc)_2$ water solution (2.0 mM). Reaction time: 2 h, then diluted 100-fold using BICINE. (λ_{exc}=320 nm. Slit 5/5 nm. Fluorescence intensity at λ_{em} = 509 nm was used for each data point).

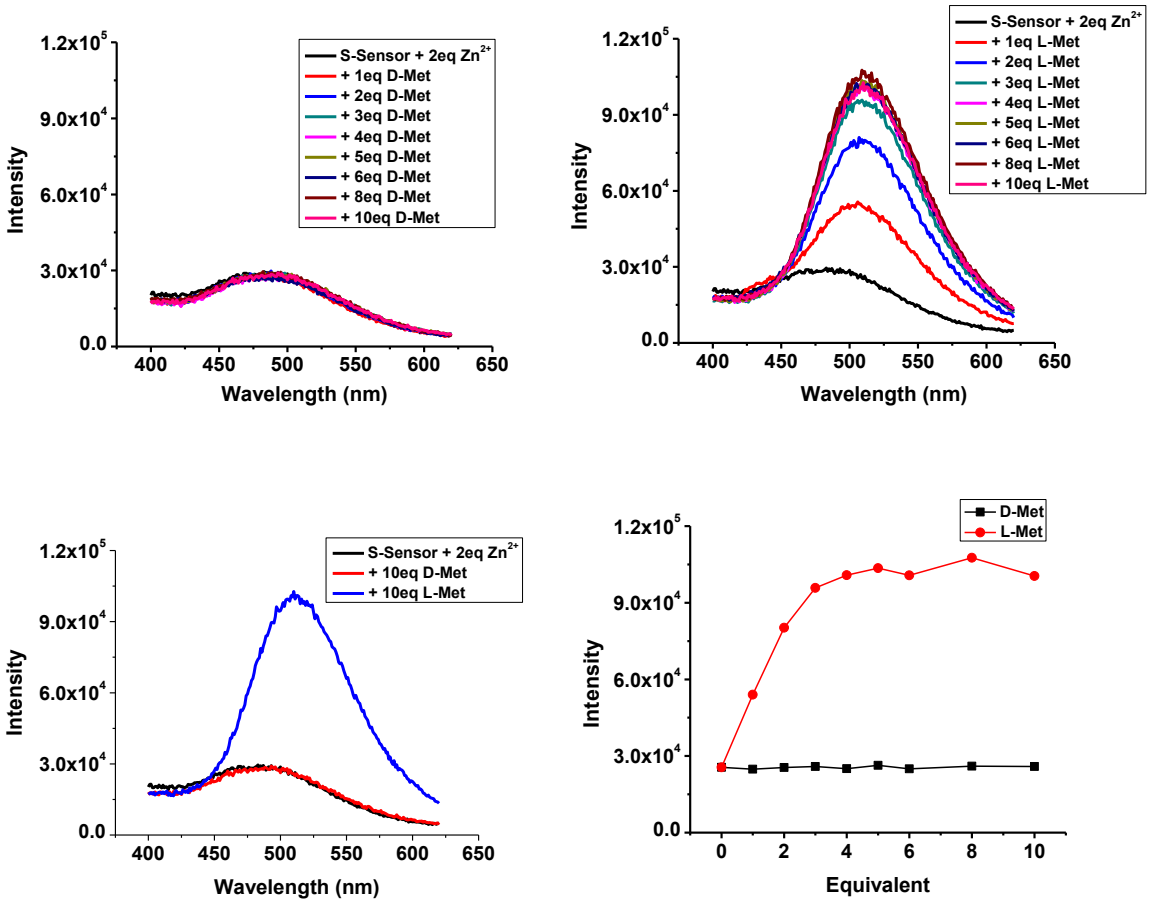

Figure 3.31. Fluorescence spectra of (*S*)-**3.9** (1.0 mM) with various equiv of proline, D-**3.23** or L-**3.23** (4.0 mM) in 25 mM BICINE buffer (pH = 8.80) in the presence of 2.0 equiv of $Zn(OAc)_2$ water solution (2.0 mM). Reaction time: 2 h, then diluted 100-fold using BICINE. (λ_{exc} = 320 nm. Slit 5/5 nm. The fluorescence intensity at λ_{em} = 475 nm was used for each data point).

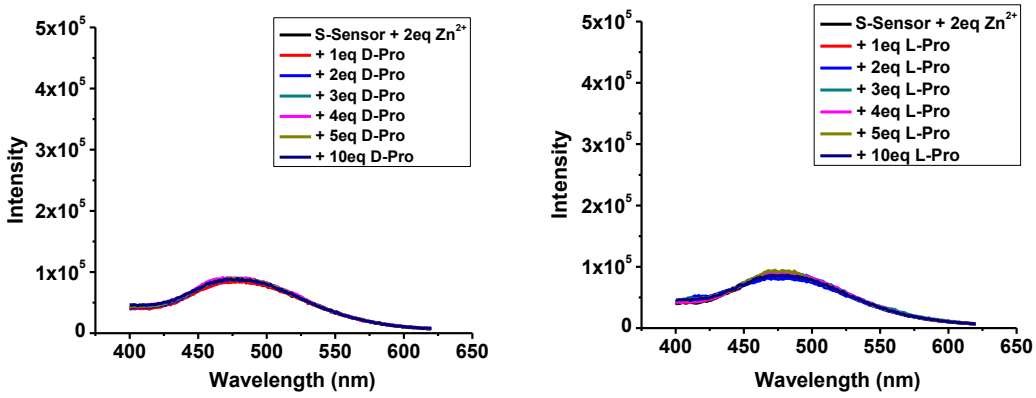

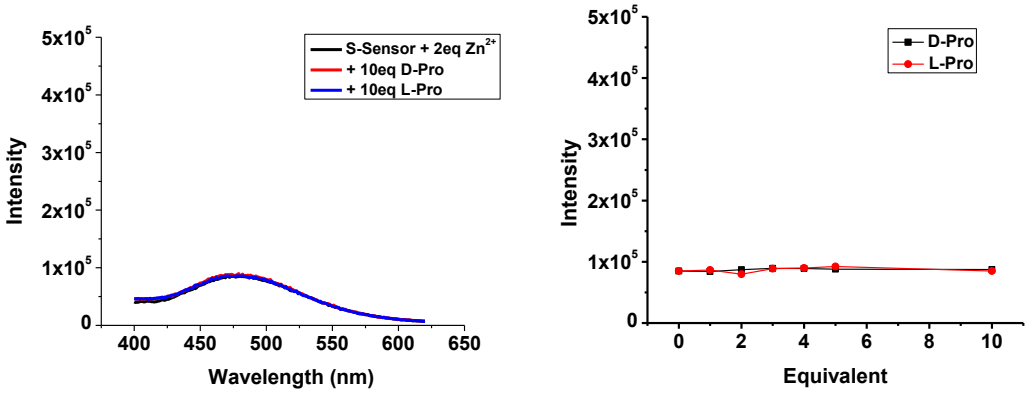

Figure 3.32. Fluorescence spectra of (*S*)-**3.9** (1.0 mM) with various equiv of alanine, D-**3.24** or L-**3.24** (4.0 mM) in 25 mM BICINE buffer (pH = 8.80) in the presence of 2.0 equiv of $Zn(OAc)_2$ water solution (2.0 mM). Reaction time: 2 h, then diluted 100-fold using BICINE. (λ_{exc} = 320 nm. Slit 5/5 nm. The fluorescence intensity at λ_{em} = 475 nm was used for each data point).

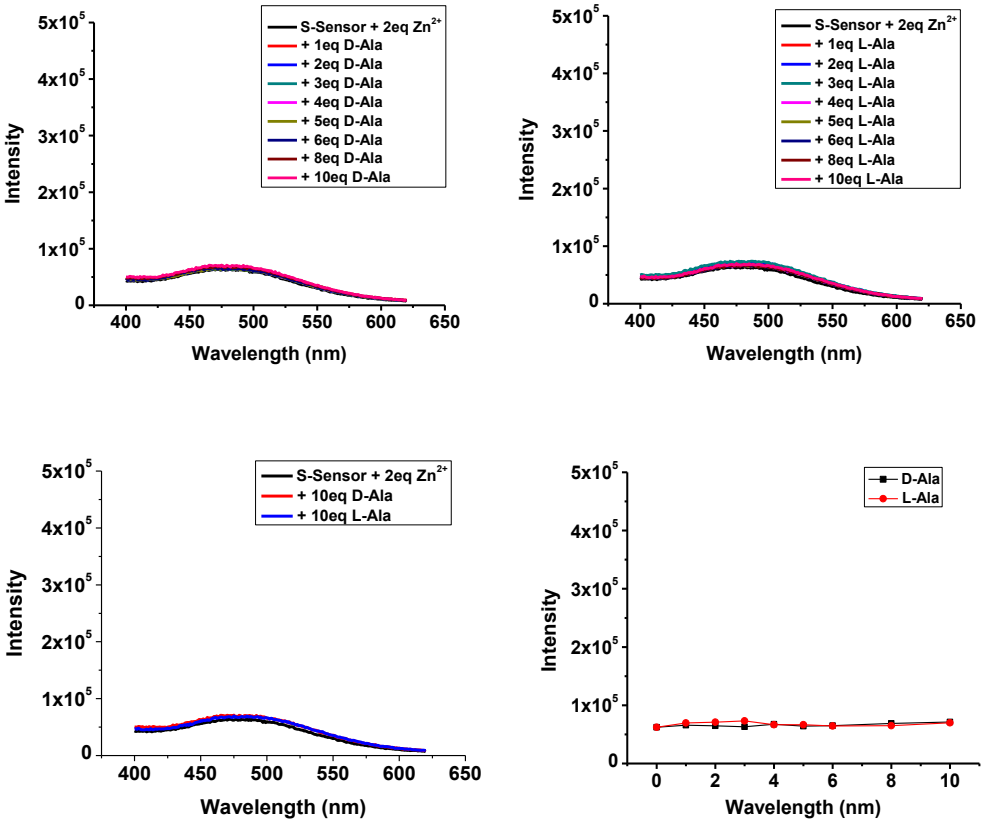

Figure 3.33. Fluorescence spectra of (*S*)-**3.9** (1.0 mM) with various equiv of lysine, D-**3.25** or L-**3.25** (4.0 mM) in 25 mM BICINE buffer (pH = 8.80) in the presence of 2.0 equiv of $Zn(OAc)_2$ water solution (2.0 mM). Reaction time: 2 h, then diluted 100-fold using BICINE. (λ_{exc} = 320 nm. Slit 5/5 nm. The fluorescence intensity at λ_{em} = 475 nm was used for each data point).

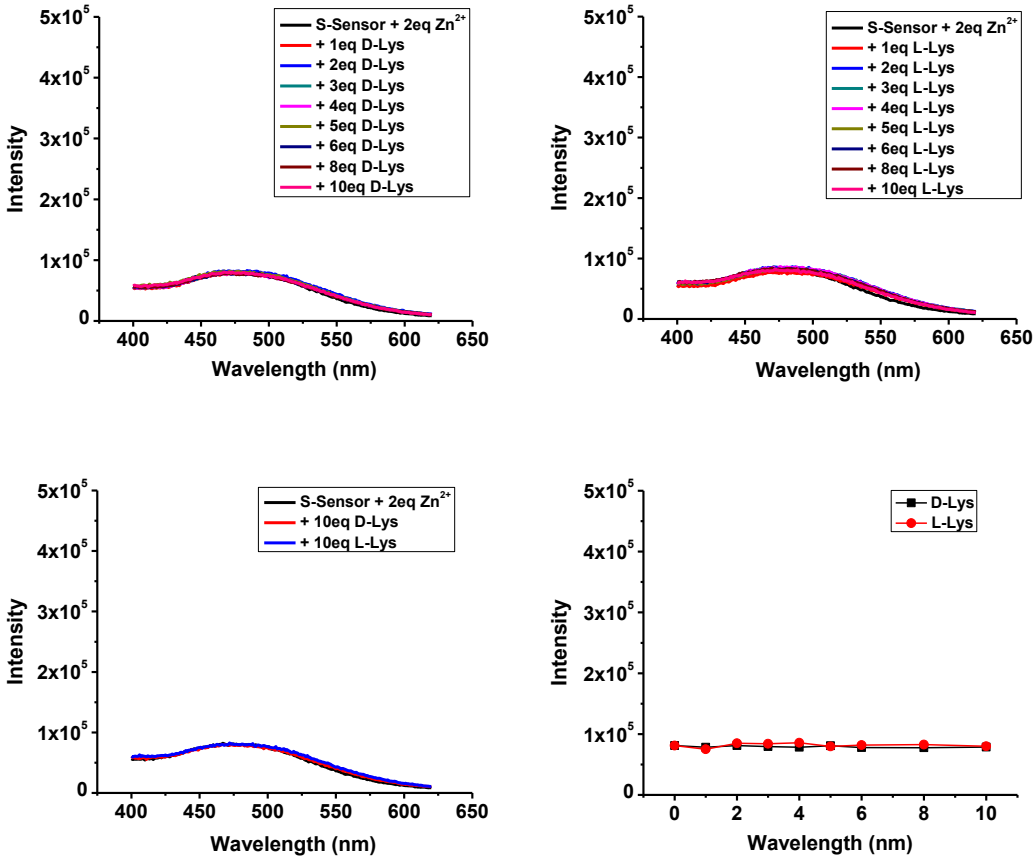

Figure 3.34. Fluorescence spectra of (*S*)-**3.9** (1.0 mM) with various equiv of aspartic acid, D-**3.26** or L-**3.26** (4.0 mM) in 25 mM BICINE buffer (pH = 8.80) in the presence of 2.0 equiv of $Zn(OAc)_2$ water solution (2.0 mM). Reaction time: 2 h, then diluted 100-fold using BICINE. (λ_{exc}=320 nm. Slit 5/5 nm. Fluorescence intensity at λ_{em} = 475 nm was used for each data point).

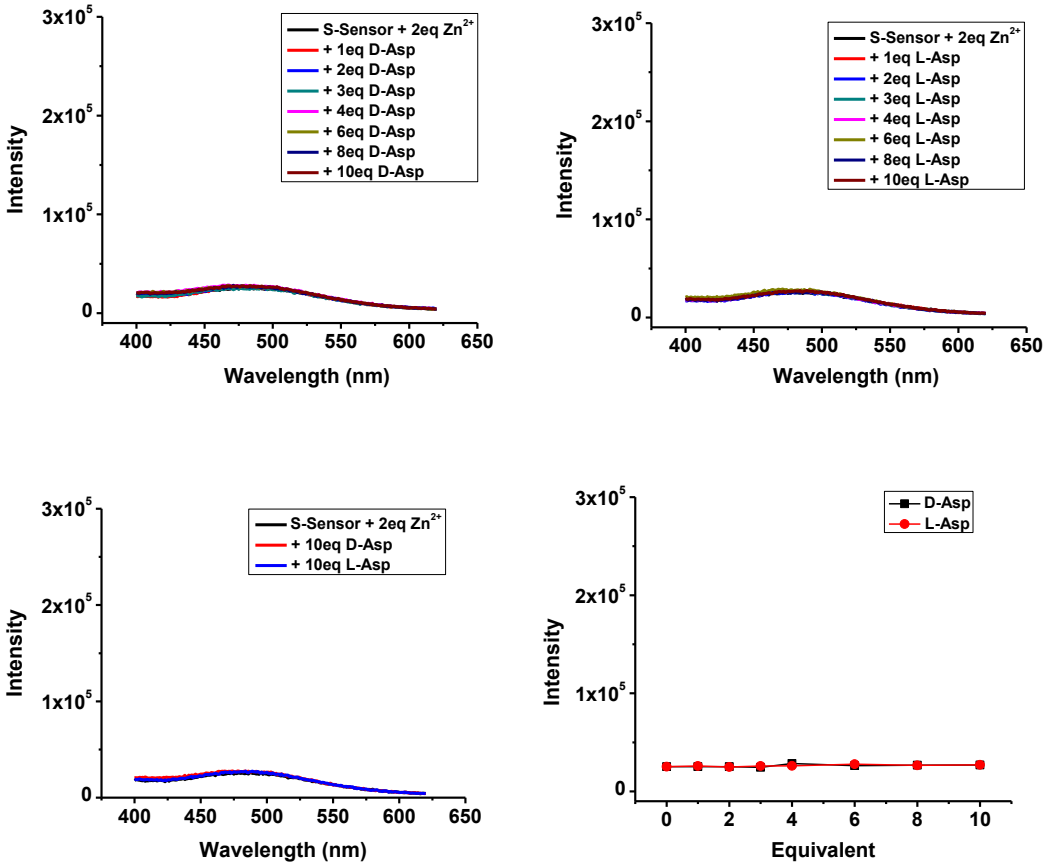

Figure 3.35. Fluorescence spectra of (*S*)-**3.9** (1.0 mM) with various equiv of glutamic acid, D-**3.27** or L-**3.27** (4.0 mM) in 25 mM BICINE buffer (pH = 8.80) in the presence of 2.0 equiv of $Zn(OAc)_2$ water solution (2.0 mM). Reaction time: 2 h, then diluted 100-fold using BICINE. (λ_{exc}=320 nm. Slit 5/5 nm. Fluorescence intensity at λ_{em} = 475 nm was used for each data point).

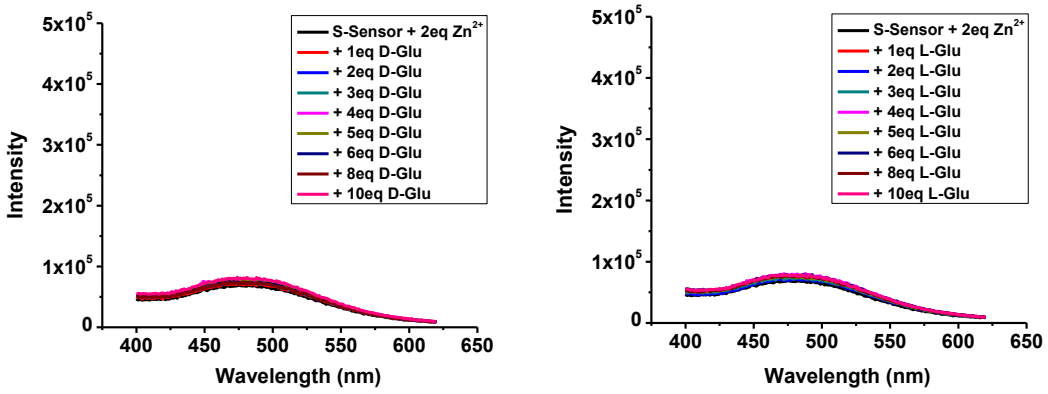

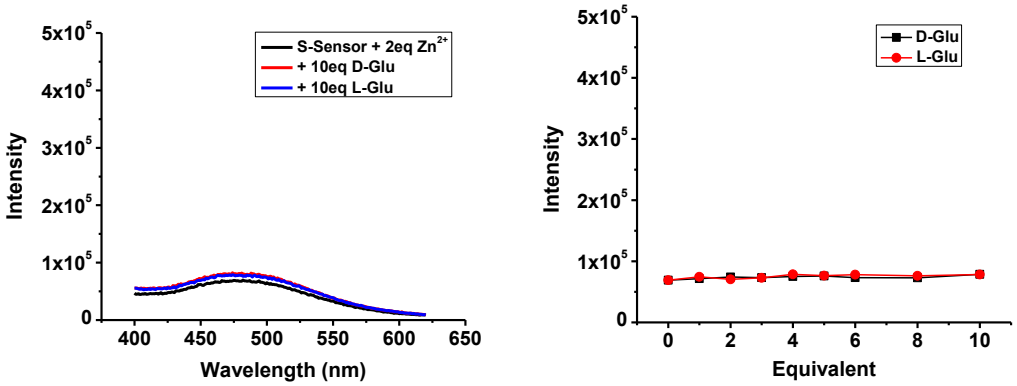

3.2.7. ^{1}H NMR spectroscopy study on the enantioselective recognition mechanism

In order to gain a better understanding on the enantioselective fluorescent response of (*S*)-**3.9** toward the amino acids, we conducted a ^{1}H NMR spectroscopy study. In this study, the BICINE buffer (pH = 8.80, 25 mM) was prepared by using D_2O as the solvent. As shown in Figure **3.36**, the aldehyde and aromatic signals of (*S*)-**3.9** in the aqueous buffer solution are very broad. This could be attributed to hydrophobicity of the central BINOL unit in the polymer chain which slows down its tumbling in the water solution and greatly broaden the NMR signals. When the BICINE solution of (*S*)-**3.9** (1.0 equiv) was mixed with $Zn(OAc)_2$ (2.0 equiv) and L-**3.10** (2 equiv), new broad signals at δ -0.20 to 0.38 appeared. Such high field signals were not observed when D-**3.10** was used (Figure **3.37**).

Figure 3.36. ^{1}H NMR spectra of the reaction mixture of (*S*)-**3.9** (20.0 mM in BICINE, 1.0 equiv) with L-**3.10** (40.0 mM in BICINE, 2.0 equiv) and $Zn(OAc)_2$ (40 mM in D_2O, 2.0 equiv) at various reaction time (BICINE buffer: 25 mM at pH = 8.80 made with D_2O. The intense signals of the PNIPAM backbone and BICINE at δ = 1 – 6 are removed for clarity).

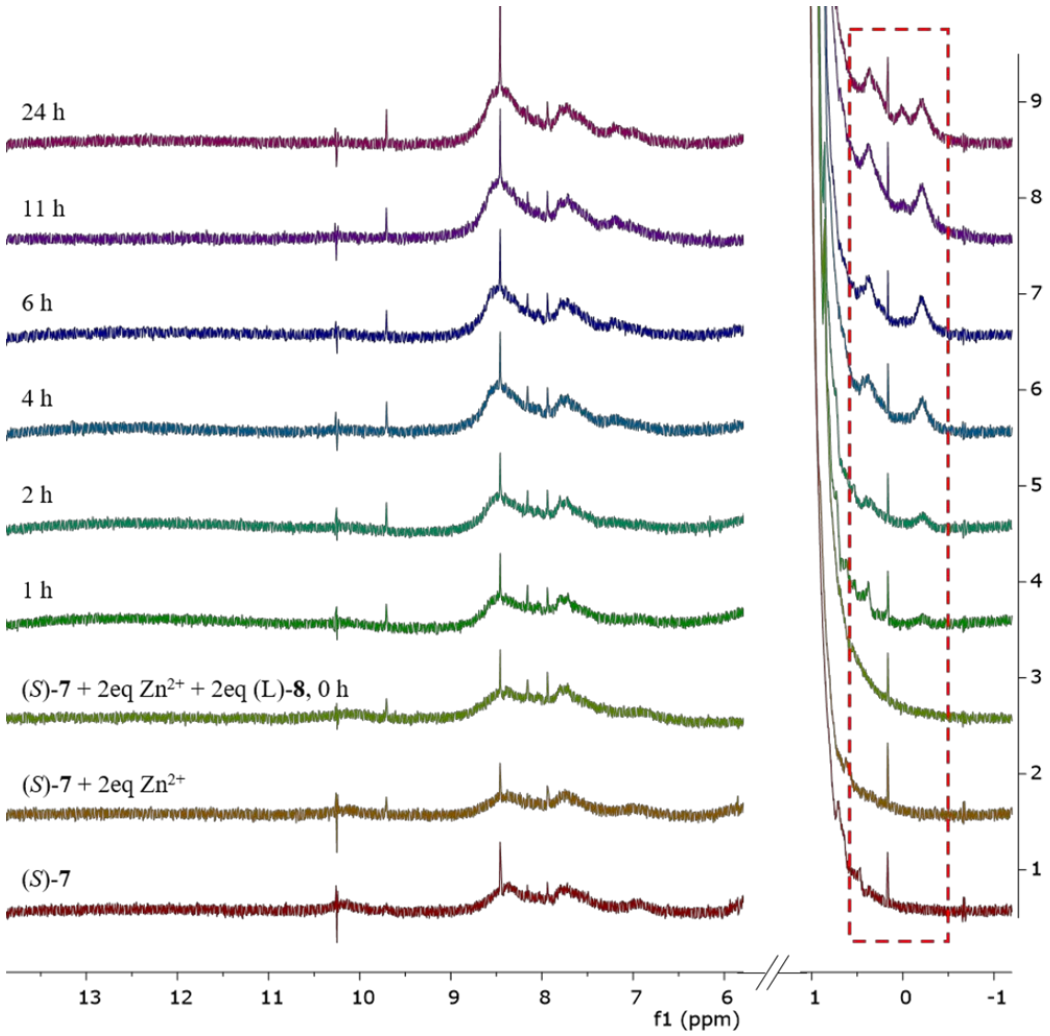

Figure 3.37. ^{1}H NMR spectra of the reaction mixture of (*S*)-**3.9** (20.0 mM in BICINE, 1.0 equiv) with D-**3.10** (40.0 mM in BICINE, 2.0 equiv) and $Zn(OAc)_2$ (40 mM in D_2O, 2.0 equiv) at various reaction time (BICINE buffer: 25 mM at pH = 8.80 made with D_2O. The intense signals of the PNIPAM backbone and BICINE at δ = 1 – 6 are removed for clarity).

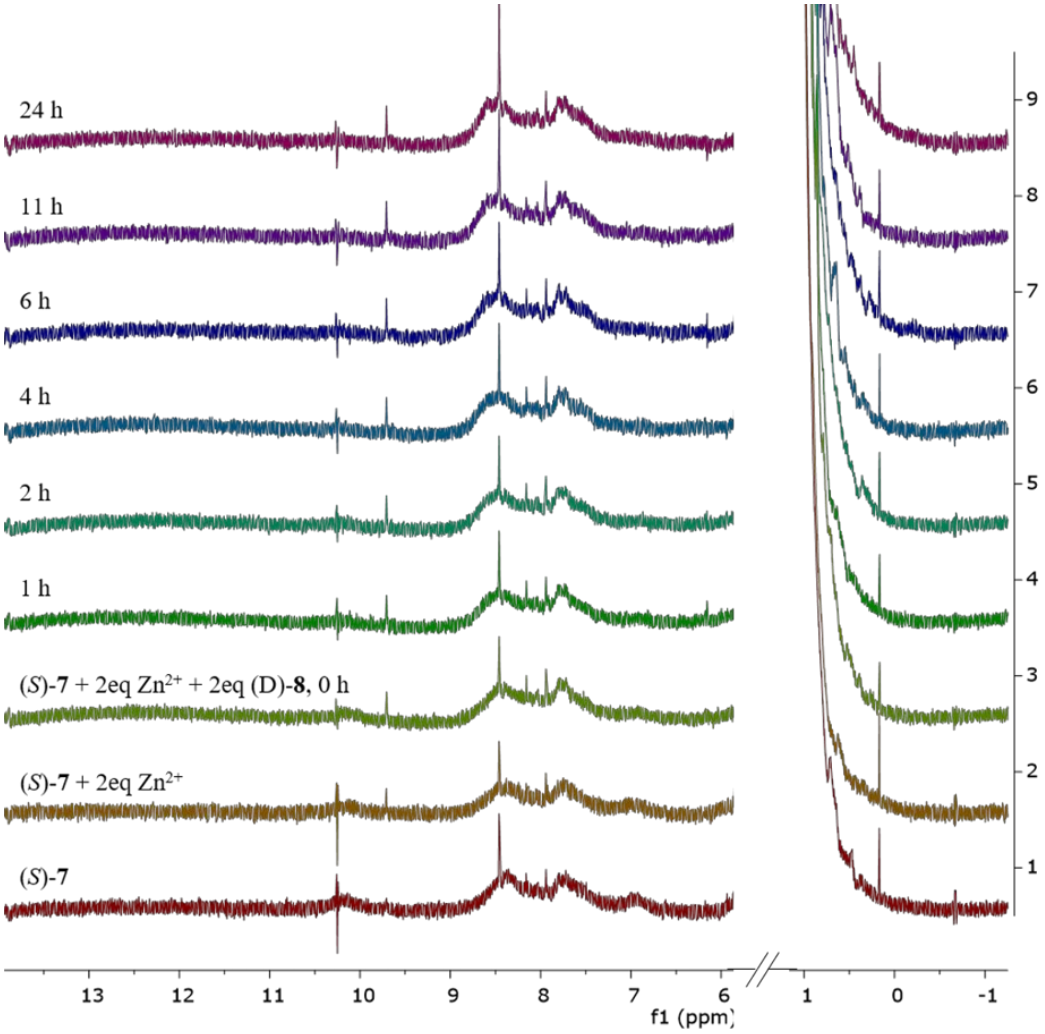

We then found that when acetone-d_6 was added as the cosolvent better resolved ^{1}H NMR spectra were obtained for the interaction of (*S*)-**3.9** with L- and D-**3.10** in the presence of Zn^{2+}. As shown in Figure **3.38**, the ^{1}H NMR spectrum of (*S*)-**3.9** in a 1:1 BICINE-D_2O buffer and acetone-d_6 gives much sharper signals for the aldehyde and aromatic protons because the BINOL core should be better solubilized by acetone-d_6. Addition of Zn^{2+} and L-**3.10** led to decrease for the aldehyde signal at δ 10.59 while several upfield signals at δ 0 to 0.7 were growing. Figure **3.39** gives the ^{1}H NMR spectra for the reaction of (*S*)-**3.9** with D-**3.10** under the same conditions which showed little reaction of D-**3.10** with the sensor system.

Figure 3.38. ^{1}H NMR spectra of the solutions (200 μL) withdrawn at various reaction time from the mixture of (*S*)-**3.9** (20.0 mM in BICINE, 1.0 equiv) with L-**3.10** (40.0 mM in BICINE, 2.0 equiv) and $Zn(OAc)_2$ (40.0 mM in D_2O, 2.0 equiv) and mixed with acetone-d_6 (200 μL). (BICINE buffer: 25 mM at pH = 8.80 made with D_2O. The intense signals of the PNIPAM backbone and BICINE at δ = 1 – 6 are removed for clarity).

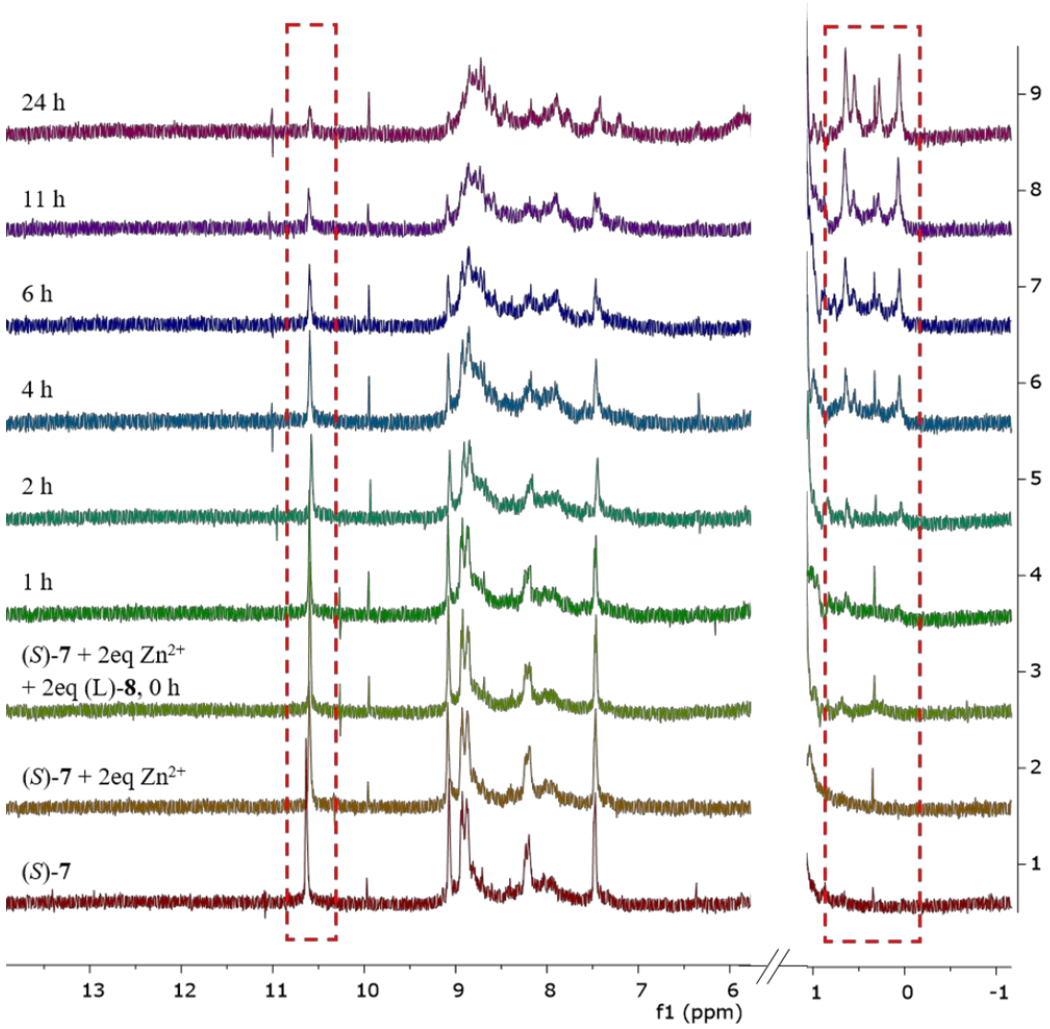

Figure 3.39. ^{1}H NMR spectra of the solutions (200 μL) withdrawn at various reaction time from the mixture of (*S*)-**3.9** (20.0 mM in BICINE, 1.0 equiv) with L-**3.10** (40.0 mM in BICINE, 2.0 equiv) and $Zn(OAc)_2$ (40.0 mM in D_2O, 2.0 equiv) and mixed with acetone-d_6 (200 μL).

(BICINE buffer: 25 mM at pH = 8.80 made with D_2O. The intense signals of the PNIPAM backbone and BICINE at δ = 1 – 6 are removed for clarity).

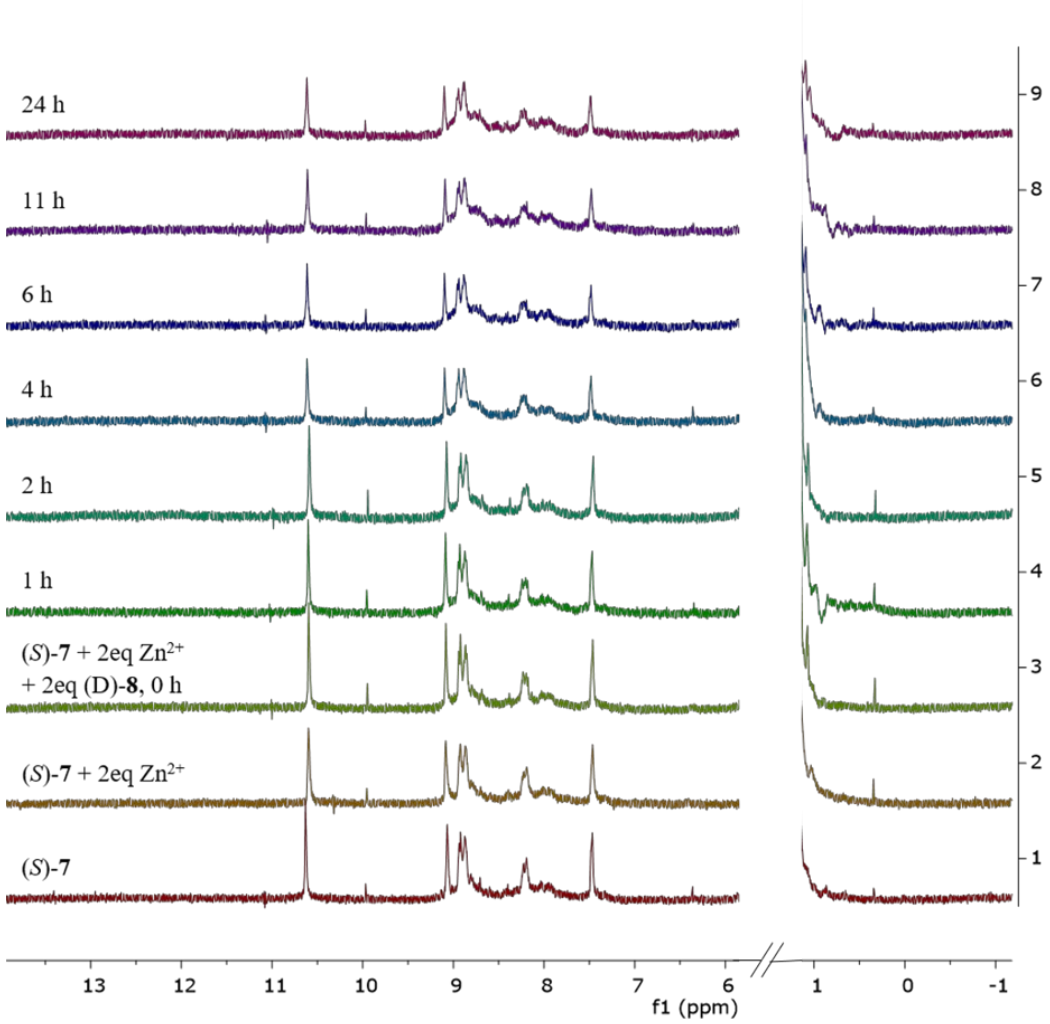

When (*S*)-**3.9** in the mixed solvent of BICINE-D_2O buffer and acetone-d_6 was treated with L-**3.10** in the absence of Zn^{2+}, no change in the ^1H NMR spectrum was observed with no fluorescence enhancement either. That is, addition of Zn^{2+} is necessary for the reaction of (*S*)-**3.9** with L-**3.10** to generate the greatly enhanced fluorescence.

Previously, we studied the ^1H NMR spectrum of the BINOL-based imine compound **3.28** in the presence of Zn^{2+}.[11] It was found that when **3.28** was treated with $Zn(OAc)_2$ in $CDCl_3/CD_3OD$ (4:1, v) solution, an unusual upfield signal at δ 0.57 was observed (Figure **3.40**).

Evidence was obtained for the formation of $2+nZn^{2+}$ ($n \geq 2$) complexes by coordination of two molecules of **3.28** with two or more Zn^{2+} centers as shown in Figure **3.40**. In these complexes such as **3.29**, the Me groups of **3.28** are placed in the shielding region of the aromatic rings of the BINOL units, giving rise to the significantly upfield-shifted ^1H NMR signal.

Figure 3.40. Structure of **3.28** and **3.29**. ^1H NMR spectra of **3.28** (10 mM) titrated with $Zn(AcO)_2 \cdot 2H_2O$ (0−2 equiv) in $CDCl_3/CD_3OD$ (4:1, v/v). (The ^1H NMR spectra were taken after the solution was allowed to stand at room temperature for 3 h.)

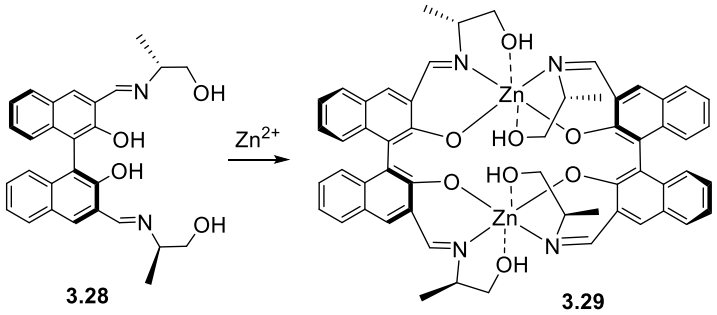

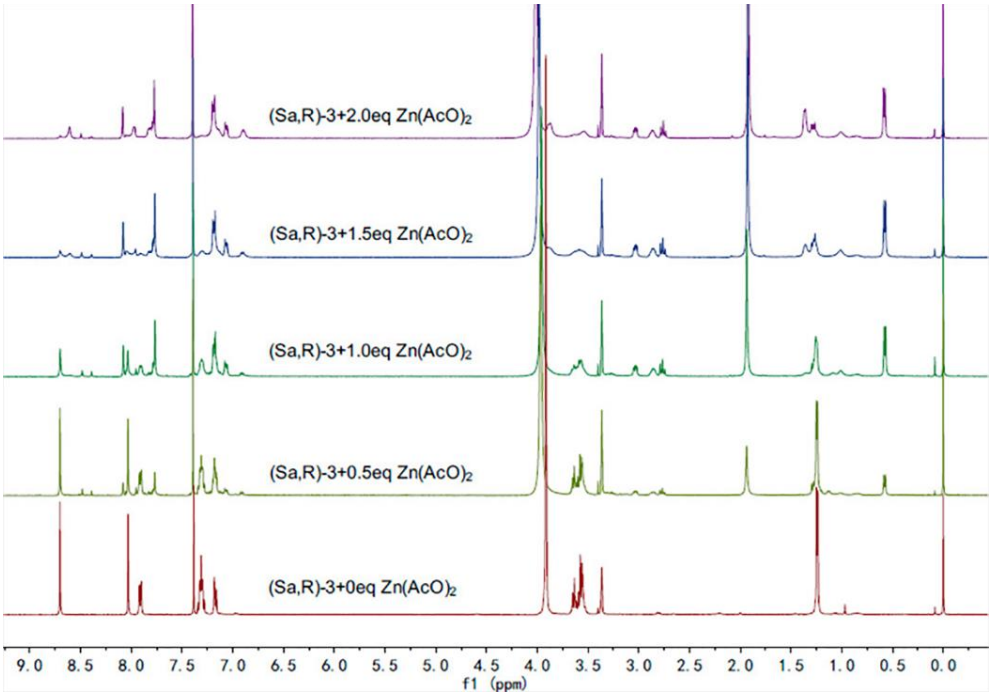

Thus, the observed upfield signals for the reaction of (*S*)-**3.9** with L-**3.10** and Zn^{2+} at δ = -0.20 to 0.38 in D_2O (at δ = 0 to 0.7 in 1:1 D_2O:acetone-d_6) could also be attributed to the

formation of multiple BINOL core+nZn^{2+}+nL-**3.10** complexes in which the isopropyl groups of L-**3.10** can be placed in the shielding region of the aromatic rings of the BINOL core to give the high field ^{1}H NMR signals in Figures **3.36** and **3.38**. We therefore propose that the large fluorescence enhancement of (*S*)-**3.9** in the presence of L-**3.10** could be due to the formation of such structurally rigid complexes **3.30** similar to that observed for the reaction of **3.28** with Zn^{2+} as shown in Figure **3.41**. In addition, the product could form a stable micelle structure in aqueous solution. The rigid complexes are hydrophobic and can form a core at the center, which is surrounded by the amphiphilic PNIPAMs. The polymer forms a shell which inhibits the water to approach the core and prevents the hydrolysis of imine bonds in the complexes. Since the interaction of D-**3.10** with (*S*)-**3.9** and Zn^{2+} did not give the high field NMR signals as shown in Figures **3.36** and **3.38**, it indicates that D-**3.10** could not generate similar structurally rigid complexes with (*S*)-**3.9** and Zn^{2+} due to the chirality mismatch, resulting in little fluorescence response.

Figure 3.41. Proposed structure of product for reaction between (*S*)-**3.9** and L-**3.10** in the presence of Zn^{2+}

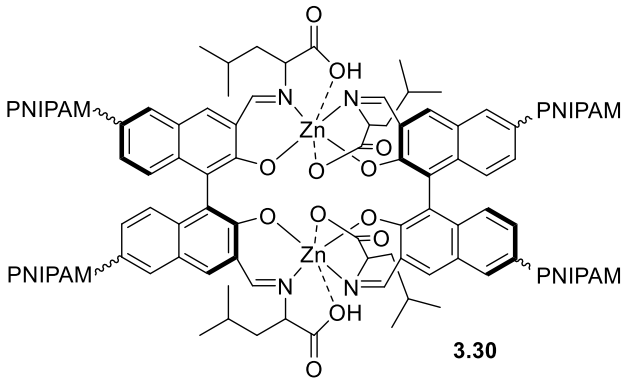

3.30

3.3. Conclusion

A new class of fluorescent sensor has been constructed by using the amphiphilic polymer PNIPAM for the enantioselective recognition of amino acids. Using a BINOL-based

diinitiator (*S*)-**3.8**, we conducted the ATRP of NIPAM to generate the PNIPAM (*S*)-**3.9** which is found to be soluble in both water and common organic solvents. It shows LCST at 32 ^{o}C in water solution the same as the unmodified PNIPAM. Its CH_2Cl_2 solution can undergo an unprecedented water-induced phase transition to form undissolved aggregates although this polymer is soluble in both CH_2Cl_2 and water. This cononsolvency of PNIPAM by using two immiscible solvents may lead to interesting new applications for this class of polymer.

Polymer (*S*)-**3.9** in combination with Zn^{2+} in aqueous buffer solution is found to exhibit highly enantioselective fluorescence enhancement when treated with a number of amino acids. It allows direct recognition of amino acids in water. We found that chloroform can be used to extract out the sensor-amino acid adduct for fluorescence measurement away from the original amino acid water solution while the high enantioselectivity and sensitivity were maintained. This provides a new method to use fluorescence to determine the enantiomeric composition of a chiral compound in a phase separated from the original substrate solution. This technique could be useful in the high throughput screening of asymmetric reactions since it could greatly reduce the interference by other reaction components on the fluorescence measurement.

We have further demonstrated that the LCST of the polymer allows the sensor-substrate adduct to precipitate out at $\geq$ 34 ^{o}C in water and the highly enantioselective fluorescence response is preserved in the precipitates when they are redissoved in the aqueous buffer solution. This provides an additional method to conduct the fluorescence measurement away from the original substrate solution which could be useful for asymmetric reaction screening. On the basis of ^{1}H NMR analyses, it is proposed that the chirality matched sensor and amino acid interaction might lead to the formation of structurally rigid higher ordered products to give

the observed large fluorescence enhancement. Whereas, the chirality mismatched sensor and substrate cannot generate those products with little fluorescence response.

In summary, this work has provided a new strategy to address one important challenge in the field of enantioselective fluorescent sensing. The unique properties exhibited by the polymer-based enantioselective fluorescent sensor make it very promising for practical applications.

3.4. Experimental Part

3.4.1. General information

All reactions were carried out under N_2 unless otherwise noted. All chemicals were purchased from Sigma Aldrich, Alfa Aesar or Thermo Fisher Scientific. Optical rotations were measured on a Jasco P-2000 digital polarimeter. NMR spectra were recorded on Varian-600 MHz spectrometer. Chemical shifts for ^{1}H NMR spectra were reported in parts per million relative to a singlet at 7.26 ppm for deuterated chloroform, and a singlet at 4.79 ppm for D_2O. Chemical shifts for ^{13}C NMR were reported relative to the centerline of a triplet at 77.16 ppm for deuterated chloroform. Steady-state fluorescence emission spectra were recorded on Horiba FluoroMax-4 spectrofluorometer. High-resolution mass spectra were obtained from the University of Illinois at Urbana-Champaign (UIUC) Mass Spectrometry Facility. Gel permeation chromatography (GPC) measurements were performed on an Agilent 1260 (LC) system with two Agilent PLgel 5 μm MIXED-C GPC columns in series at 40 °C and a flow rate of 1 mL/min. HPLC grade tetrahydrofuran (THF) stabilized with BHT (anhydrous, purchased from Thermo Fisher Scientific) was used as the eluent. An Agilent Infinity II refractive index detector was set at 40 °C for polymer analysis. pH measurements were performed on a Fisher Scientific Accumet AB15 pH meter.

3.4.2. Synthesis and Characterization of Compounds

(*S*)-((2,2'-bis(methoxymethoxy)-[1,1'-binaphthalene]-6,6'-diyl)bis(ethyne-2,1-diyl))bis(trimethylsilane), (*S*)-3.4

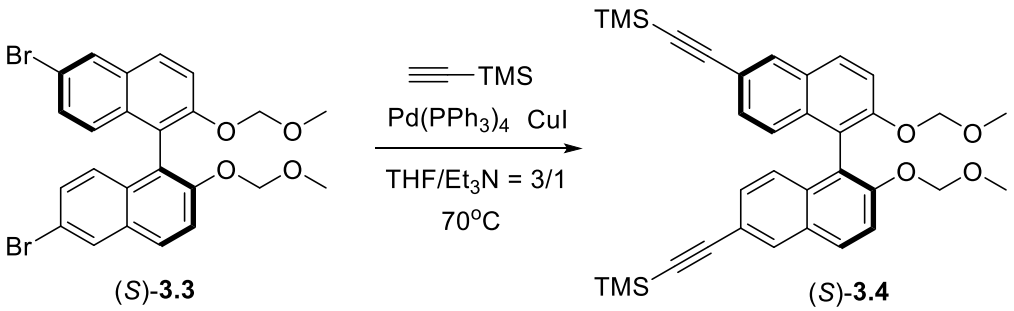

(*S*)-**3.3** (*S*)-**3.4**

Under nitrogen, (*S*)-6,6'-dibromo-2,2'-bis(methoxymethoxy)-1,1'-binaphthalene, (*S*)-**3.3**[12] (1.5 mmol, 798.3 mg) was dissolved in 15 mL THF/Et_3N (v/v = 3/1) mixed solvent. Then, trimethylsilylacetylene (3.75 mmol, 519 μL), $Pd(PPh_3)_4$ (0.15 mmol, 173.3 mg) and CuI (0.15 mmol, 28.6 mg) were added sequentially. The reaction mixture was stirred at 70 ºC for 16 h and then cooled down to room temperature. Then, then mixture was filtered by vacuum filtration to obtain yellow solution. The solution was diluted by 30 mL ethyl acetate and then extracted with water (3 × 30 mL). The combined aqueous layer was extracted with ethyl acetate (30 mL). Then, the combined organic layer was washed with brine (50 mL) and dried over anhydrous Na_2SO_4. After the evaporation of solvent, the residue was purified by column chromatography on silica gel eluted with hexane/ethyl acetate (15/1) to afford compound (*S*)-**3.4** as a white solid in 88% yield[13]. ^{1}H NMR (600 MHz, $CDCl_3$) δ 8.04 (s, 2H), 7.89 (d, *J* = 9.1 Hz, 1H), 7.57 (d, *J* = 9.1 Hz, 1H), 7.24 (d, *J* = 8.8 Hz, 1H), 7.04 (d, *J* = 8.8 Hz, 1H), 5.10 (d, *J* = 6.9 Hz, 1H), 4.96 (d, *J* = 6.9 Hz, 1H), 3.13 (s, 6H), 0.26 (s, 18H). ^{13}C NMR (151 MHz, $cdcl_3$) δ 153.54, 133.62, 132.26, 129.61, 129.34, 129.18, 125.51, 120.83, 118.69, 117.60, 105.66, 95.01, 94.27, 56.06, 0.18. HRMS Calcd for $C_{34}H_{39}O_4Si_2$ (MH^+): 567.2387. Found: 567.2374.

(*R*)-((2,2'-bis(methoxymethoxy)-[1,1'-binaphthalene]-6,6'-diyl)bis(ethyne-2,1-diyl))bis(trimethylsilane), (*R*)-3.4

Compound (*R*)-**3.4**, the enantiomer of (*S*)-**3.4**, was synthesized as a white solid in 86% yield using the same protocol described above but starting with (*R*)-6,6'-dibromo-2,2'-bis(methoxymethoxy)-1,1'-binaphthalene, (*R*)-**3.3**. ^{1}H NMR (600 MHz, $CDCl_3$) δ 8.03 (s, 2H), 7.89 (d, *J* = 9.1 Hz, 2H), 7.57 (d, *J* = 9.1 Hz, 2H), 7.24 (d, *J* = 8.8 Hz, 2H), 7.04 (d, *J* = 8.8 Hz, 2H), 5.10 (d, *J* = 6.9 Hz, 2H), 4.96 (d, *J* = 6.9 Hz, 2H), 3.13 (s, 6H), 0.26 (s, 18H). ^{13}C NMR (151 MHz, $CDCl_3$) δ 153.54, 133.63, 132.26, 129.61, 129.35, 129.19, 125.51, 120.83, 118.70, 117.60, 105.67, 95.02, 94.27, 56.06, 0.19.

(*S*)-6,6'-diethynyl-2,2'-bis(methoxymethoxy)-[1,1'-binaphthalene]-3,3'-dicarbaldehyde, (*S*)-3.5

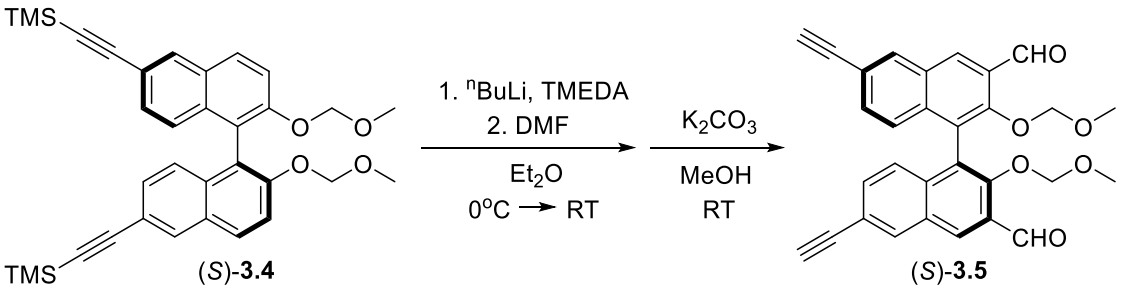

Under nitrogen, (*S*)-**3.4** (1 mmol, 566.2 mg) was dissolved in 30 mL diethyl ether following the addition of tetramethylethylenediamine (TMEDA) (4 mmol, 596 µL). The solution was cooled to 0 °C, and n-BuLi (2.5 M in hexane, 4 mmol, 1.6 mL) was added dropwise. The reaction mixture was stirred at room temperature for 4 h and then cooled to 0 °C, and dimethylformamide (DMF) (5 mmol, 386 µL) was added dropwise. The reaction mixture was further stirred at room temperature for 6 h. Saturated NH_4Cl aqueous solution (10 mL) was added to quench the reaction. The organic layer was separated, and the aqueous layer was extracted with ethyl acetate (3 × 20 mL). The combined organic layer was washed with brine and dried over anhydrous Na_2SO_4.[14] After the evaporation of solvent, the residue was diluted with 60 mL

methanol, and K_2CO_3 (6 mmol, 829 mg) was added. The reaction mixture was stirred at room temperature under nitrogen for 5 h and then neutralized by adding 1 N HCl. The mixture was evaporated to removed methanol following the addition of 30 mL ethyl acetate. The organic layer was separated, and the aqueous layer was extracted with ethyl acetate (3 × 20 mL). The combined organic layer was washed with brine and dried over anhydrous Na_2SO_4. After the evaporation of solvent, the residue was purified by column chromatography on silica gel eluted with hexane/ethyl acetate (11/1) to afford compound (*S*)-**3.5** as a pale-yellow solid in 35% yield.[15] ^{1}H NMR (600 MHz, $CDCl_3$) δ 10.51 (s, 2H), 8.56 (s, 2H), 8.23 (s, 2H), 7.46 (d, *J* = 8.8 Hz, 2H), 7.15 (d, *J* = 8.8 Hz, 2H), 4.75 (d, *J* = 6.3 Hz, 2H), 4.68 (d, *J* = 6.3 Hz, 2H), 3.20 (s, 2H), 2.86 (s, 6H). ^{13}C NMR (151 MHz, $CDCl_3$) δ 190.31, 155.04, 136.18, 134.37, 132.43, 132.40, 129.73, 129.67, 126.28, 125.93, 120.42, 100.87, 82.89, 79.10, 57.19. HRMS Calcd for $C_{30}H_{22}O_6Na$ (MNa^+): 501.1314. Found: 501.1318.

(*R*)-6,6'-diethynyl-2,2'-bis(methoxymethoxy)-[1,1'-binaphthalene]-3,3'-dicarbaldehyde, (*R*)-3.5

Compound (*R*)-**3.5**, the enantiomer of (*S*)-**3.5**, was synthesized as a pale-yellow solid in 30% yield using the same protocol described above but starting with (*R*)-**3.4**. ^{1}H NMR (600 MHz, $CDCl_3$) δ 10.51 (s, 2H), 8.55 (s, 2H), 8.23 (s, 2H), 7.45 (d, *J* = 8.8 Hz, 2H), 7.14 (d, *J* = 8.8 Hz, 2H), 4.75 (d, *J* = 6.3 Hz, 2H), 4.68 (d, *J* = 6.3 Hz, 2H), 3.19 (s, 2H), 2.85 (s, 6H). ^{13}C NMR (151 MHz, $CDCl_3$) δ 190.31, 155.03, 136.18, 134.36, 132.43, 132.39, 129.73, 129.66, 126.28, 125.92, 120.42, 100.87, 82.89, 79.10, 57.19.

(S)-6,6'-diethynyl-2,2'-dihydroxy-[1,1'-binaphthalene]-3,3'-dicarbaldehyde, (*S*)-3.6

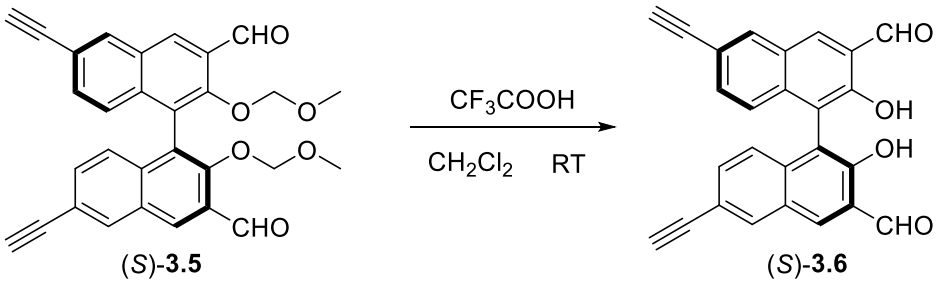

(*S*)-**3.5** (*S*)-**3.6**

Under nitrogen, (*S*)-**3.5** (0.3 mmol, 143.6 mg) was dissolved in 5 mL CH_2Cl_2, the reaction mixture was cooled to 0 ^oC, and trifluoracetic acid (3.9 mmol, 0.3 mL) was added slowly. The reaction was stirred at room temperature for 30 min. Saturated $NaHCO_3$ aqueous solution was added to quench the reaction. The organic layer was separated, and the aqueous layer was extracted with CH_2Cl_2 (3 × 20 mL). The combined organic layer was washed with brine and dried over anhydrous Na_2SO_4. After the evaporation of solvent, the solid was washed with methanol to removed small amount of impurities and afford compound (*S*)-**3.6** as a yellow solid in 80% yield. ^1H NMR (600 MHz, $CDCl_3$) δ 10.66 (s, 2H), 10.19 (s, 2H), 8.30 (s, 2H), 8.16 (s, 2H), 7.45 (d, *J* = 8.4 Hz, 2H), 7.12 (d, *J* = 8.4 Hz, 2H), 3.15 (s, 2H). ^{13}C NMR (151 MHz, $CDCl_3$) δ 196.77, 154.76, 138.35, 136.98, 134.21, 133.34, 127.21, 125.07, 122.70, 118.51, 116.54, 83.20, 78.31. HRMS Calcd for $C_{26}H_{15}O_4$ (MH^+): 391.0970. Found: 391.0964.

(*R*)-6,6'-diethynyl-2,2'-dihydroxy-[1,1'-binaphthalene]-3,3'-dicarbaldehyde, (*R*)-3.6

Compound (*R*)-**3.6**, the enantiomer of (*S*)-**3.6**, was synthesized as a pale-yellow solid in 30% yield using the same protocol described above but starting with (*R*)-**3.5**. ^1H NMR (600 MHz, $CDCl_3$) δ 10.66 (s, 2H), 10.19 (s, 2H), 8.30 (s, 2H), 8.16 (s, 2H), 7.45 (d, *J* = 8.8 Hz, 2H), 7.12 (d, *J* = 8.8 Hz, 2H), 3.15 (s, 2H). ^{13}C NMR (151 MHz, cdcl$_3$) δ 196.77, 154.76, 138.35, 136.98, 134.21, 133.34, 127.21, 125.08, 122.70, 118.52, 116.54, 83.20, 78.31.

2-azidoethyl 2-chloropropanoate, 3.7

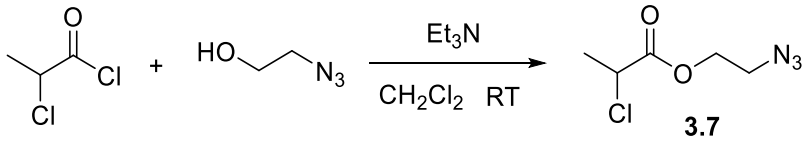

Under nitrogen, 2-azidoethan-1-ol[16] (3 mmol, 261.2 mg) was dissolved in 15 mL CH_2Cl_2 following the addition of Et_3N (6 mmol, 838 μL). The solution was cooled to 0 °C , and 2-chloropropanoyl chloride (3 mmol, 291 μL) was added dropwise. The reaction mixture was stirred at room temperature for 8 h, and the mixture was extracted with 1 N HCl (3 × 20 mL) to remove excess Et_3N. The organic layer was further washed with brine and dried over anhydrous Na_2SO_4. After the evaporation of solvent, the residue was purified by column chromatography on silica gel eluted with hexane/ethyl acetate (10/1) to afford pure 2-azidoethyl 2-chloropropanoate as transparent liquid in 80% yield. ^{1}H NMR (600 MHz, $CDCl_3$) δ 4.43 (q, *J* = 6.9 Hz, 1H), 4.32 (t, *J* = 4.7 Hz, 2H), 3.51 (t, *J* = 4.7 Hz, 2H), 1.70 (d, *J* = 6.9 Hz, 3H). ^{13}C NMR (151 MHz, $CDCl_3$) δ 169.88, 64.51, 52.27, 49.62, 21.46. HRMS Calcd for $C_5H_9O_2N_3Cl$ (MH^+): 178.03833. Found: 178.03832.

(((*S*)-3,3'-diformyl-2,2'-dihydroxy-[1,1'-binaphthalene]-6,6'-diyl)bis(1H-1,2,3-triazole-4,1-diyl))bis(ethane-2,1-diyl) bis(2-chloropropanoate), (*S*)-3.8

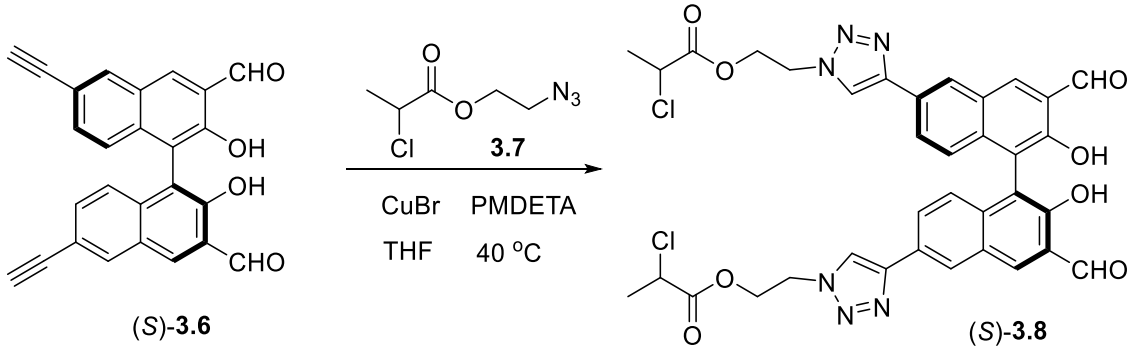

Under nitrogen, (*S*)-**2** (0.3 mmol, 117.1 mg) was dissolved in 20 mL THF. 2-azidoethyl 2-chloropropanoate (0.66 mmol, 117.2 mg), CuBr (0.3 mmol, 43 mg) and N,N,N',N'',N''-pentamethyldiethylenetriamine (PMDETA) (0.3 mmol, 62.6 μL) was added. The reaction mixture was stirred at 40 ^{o}C for 12 h. 20 mL ethyl acetate was added, and the mixture was extracted with water (3 × 50 mL). The organic layer was washed with brine and dried over anhydrous Na_2SO_4. After the evaporation of solvent, the residue was purified by column chromatography on silica gel eluted with hexane/ethyl acetate (1/1) to afford compound (*S*)-**4** as a yellow solid in 50% yield.[17] ^{1}H NMR (600 MHz, $CDCl_3$) δ 10.66 (s, 2H), 10.21 (s, 2H), 8.53 (s, 2H), 8.39 (s, 2H), 7.95 (s, 2H), 7.79 (d, *J* = 8.8 Hz, 2H), 7.28 (d, *J* = 8.9 Hz, 2H), 4.74 (t, *J* = 4.8 Hz, 4H), 4.61 (m, 2H), 4.41 (q, *J* = 6.9 Hz, 4H), 1.66 (d, *J* = 6.8 Hz, 6H). ^{13}C NMR (151 MHz, $CDCl_3$) δ 196.93, 169.55, 154.22, 147.49, 138.84, 137.17, 128.73, 127.91, 126.78, 126.48, 125.73, 122.72, 120.79, 116.69, 63.92, 52.21, 49.11, 21.40. HRMS Calcd for $C_{36}H_{31}N_6O_8Cl_2$ (MH^+): 745.1580. Found: 745.1572. $[\alpha]_D$ = -95.8 (c = 0.37, CH_2Cl_2).

(((*R*)-3,3'-diformyl-2,2'-dihydroxy-[1,1'-binaphthalene]-6,6'-diyl)bis(1H-1,2,3-triazole-4,1-diyl))bis(ethane-2,1-diyl) bis(2-chloropropanoate), (*R*)-3.8

Compound (*R*)-**3.8**, the enantiomer of (*S*)-**3.8**, was synthesized as a pale-yellow solid in 48% yield using the same protocol described above but starting with (*R*)-**3.6**. ^{1}H NMR (600 MHz, $CDCl_3$) δ 10.66 (s, 2H), 10.17 (s, 2H), 8.47 (s, 2H), 8.34 (s, 2H), 7.93 (s, 2H), 7.79 (d, *J* = 8.0 Hz, 2H), 7.27 (d, *J* = 8.0 Hz, 2H), 4.72 (t, *J* = 5.2 Hz, 4H), 4.62 (m, 2H), 4.41 (q, *J* = 7.0 Hz, 4H), 1.65 (d, *J* = 7.0 Hz, 6H). ^{13}C NMR (151 MHz, $CDCl_3$) δ 196.95, 169.54, 154.16, 147.39, 138.82, 137.10, 128.68, 127.88, 126.75, 126.40, 125.69, 122.66, 120.81, 116.63, 63.89, 52.20, 49.07, 21.39. $[\alpha]_D$ = 93.7 (c = 0.37, CH_2Cl_2).

Atom transfer radical polymerization of *N*-isopropylacrylamide using (*S*)-3.8 as initiator

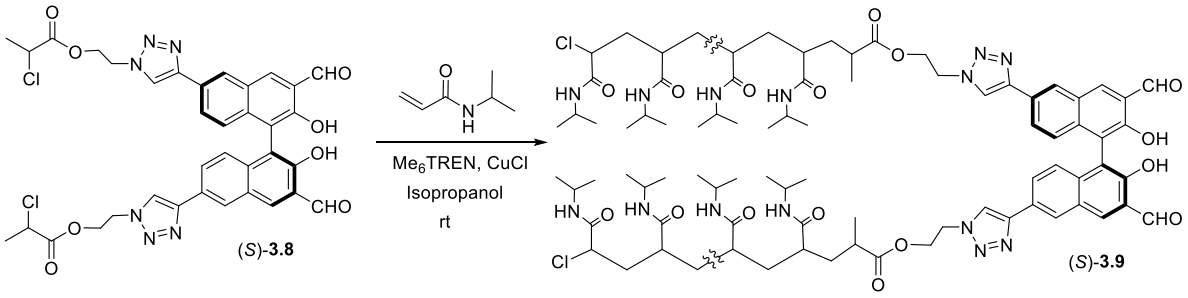

N-isopropylacrylamide (2 mmol, 226.3 mg) was dissolved in 500 μL isopropanol. Tris[2-(dimethylamino)ethyl]amine (Me_6TREN) (0.04 mmol, 10.7 μL) was added. The mixture was degassed by three freeze-pump-thaw cycles. Under nitrogen, CuCl (0.04 mmol, 4 mg) was added and the mixture was stirred for 15 min. Then, (*S*)-**3.8** (0.02 mmol, 14.9 mg) was added. And the reaction mixture was stirred under nitrogen at room temperature for 48 h. The reaction mixture was exposed to air, diluted by THF and passed through a short neutral alumina column to remove the catalyst. The collected eluent was concentrated and added to 100mL diethyl ether dropwise to isolate poly (*N*-isopropylacrylamide) (*S*)-**3.9** by precipitation and centrifugation. The polymer was further dissolved in THF and precipitated in diethyl ether for another two times to fully remove trace amount of monomers. Isolated yield: 30%. GPC data: M_n = 4291, M_w = 5150, PDI = 1.20. $[\alpha]_D$ = -2.8 (c = 0.40, CH_2Cl_2).

(*R*)-**3.8** was also used as initiator for the ATRP of NIPAM to synthesize (*R*)-**3.9** using the same protocol described above. Isolated yield: 42%. GPC data: M_n = 5942, M_w = 7084, PDI = 1.19. $[\alpha]_D$ = 2.9 (c = 0.40, CH_2Cl_2).

3.4.3. Sample preparation

Samples preparation for fluorescence measurements

Polymer (*S*)-**3.9** and (*R*)-**3.9** was dried under vacuum and stored under nitrogen. The enantiomers of amino acids were purchased from Sigma Aldrich or Alfa Aesar and used without further purification. Stock solution of 1 mM polymer sensor (*S*)-**3.9** or (*R*)-**3.9** and 4 mM amino acids in BICINE buffer (pH = 8.80, 25mM) were freshly prepared. Stock solution of 2 mM $Zn(OAc)_2$ in water was freshly prepared. In the fluorescence enhancement study, a 50 μL solution of (*S*)-**3.9** or (*R*)-**3.9** (1 equiv.) was mix with 50 μL $Zn(OAc)_2$ solution (2 equiv.) and various equivalent of amino acids in 5 mL volumetric flasks. The resulting solution was allowed to stand at room temperature for 2 h before diluting to desired concentration (0.01 mM). All the measurements were taken within 1 h.

Samples preparation for ^{1}H NMR study

Stock solution of 20 mM (*S*)-**3.9** or (*R*)-**3.9** in BICINE buffer (pH = 8.80, 25mM), 40 mM L- or D-**3.10** in BICINE buffer and 40 mM $Zn(OAc)_2$ in D_2O were freshly prepared. Then 1 equiv. of (*S*)-**3.9** was mixed with 2 equiv. of $Zn(OAc)_2$ and 2 equiv. of L- or D-**3.10** for NMR study. NMR spectra were recorded at certain time point.

References

(1) Pu, L. *Chem. Rev.* **2004**, *104* (3), 1687–1716.

(2) Zhou, Y.; Yoon, J. *Chem. Soc. Rev.* **2012**, *41* (1), 52–67.

(3) Leung, D.; Kang, S. O.; Anslyn, E. V. *Chem. Soc. Rev.* **2012**, *41* (1), 448–479.

(4) Pu, L. *Acc. Chem. Res.* **2012**, *45* (2), 150–163.

(5) Pu, L. *Acc. Chem. Res.* **2017**, *50* (4), 1032–1040.

(6) Scarpa, J. S.; Mueller, D. D.; Klotz, I. M. *J. Am. Chem. Soc.* **1967**, *89* (24), 6024–6030.

(7) Schild, H. G. *Prog. Polym. Sci.* **1992**, *17* (2), 163–249.

(8) Huang, Z.; Yu, S.; Wen, K.; Yu, X.; Pu, L. *Chem. Sci.* **2014**, *5* (9), 3457.

(9) Matyjaszewski, K.; Tsarevsky, N. V. *J. Am. Chem. Soc.* **2014**, *136* (18), 6513–6533.

(10) Xia, Y.; Yin, X.; Burke, N. A. D.; Stöver, H. D. H. *Macromolecules* **2005**, *38* (14), 5937–5943.

(11) Song, T.; Cao, Y.; Zhao, G.; Pu, L. *Inorg. Chem.* **2017**, *56* (8), 4395–4399.

(12) Hu, Q.; Zheng, X.; Pu, L. *J. Org. Chem.* **1996**, *6* (6), 5200–5201.

(13) Sasai, H.; Tokunaga, T.; Watanabe, S.; Suzuki, T.; Itoh, N.; Shibasaki, M. *J. Org. Chem.* **1995**, *60* (23), 7388–7389.

(14) Zhang, H.; Huang, W.; Pu, L. *J. Org. Chem.* **2001**, *66* (2), 481–487.

(15) Fazio, M. A.; Lee, O. P.; Schuster, D. I. *Org. Lett.* **2008**, *10* (21), 4979–4982.

(16) Yu, S. S.; Lau, C. M.; Barham, W. J.; Onishko, H. M.; Nelson, C. E.; Li, H.; Smith, C. A.; Yull, F. E.; Duvall, C. L.; Giorgio, T. D. *Mol. Pharm.* **2013**, *10* (3), 975–987.

(17) Zheng, Y.; Wang, L.; Zheng, S.; Si, S. O. *Eur. Polym. J.* **2012**, *48* (5), 945–955.

(18) Song, T.; Cao, Y.; Zhao, G.; Pu, L. *Inorg. Chem.* **2017**, *56* (8), 4395–4399.

(19) Zhang, H. C.; Huang, W. S.; Pu, L. *J. Org. Chem.* **2001**, *66* (2), 481–487.

Chapter 4. Amphiphilic Polymer-Based Fluorescent Probe for Enantioselective Recognition of Amino Alcohols

4.1. Introduction

Chiral amino alcohols are important building blocks for making a variety of biologically active molecules or as ligands for stereoselective catalysts. Due to their broad application in pharmaceutical and biological fields, there have been many reports on enantioselective recognition of chiral amino alcohols.[1,2]

BINOL-based fluorescent probes have shown high enantioselective fluorescence response toward various amino alcohols.[3] However, no fluorescence measurement was achieved in aqueous solutions due to the lack of solubility of probes and fast hydrolysis of imine bond in water. Amino alcohols have high solubility in water, therefore, the asymmetric synthesis of amino alcohols can be achieved in aqueous solution[4] or the amino alcohol products can be extracted to aqueous phase. Thus, it is useful for enantioselective recognition of amino alcohols in aqueous solutions because of the potential asymmetric catalyst screening application. The polymer-based fluorescent probe **3.9** was soluble in aqueous solution and has the potential for enantioselective recognition of amino alcohol since it had shown highly enantioselective fluorescence response toward various amino acids in BICINE buffer. In addition, a unique solution property, named cononsolvency, was observed for fluorescent probe **3.9**. We also tried to use this property for enantioselective recognition of amino alcohols.

Figure 4.1. Structure of fluorescent probes **3.9** and amino alcohol substrates

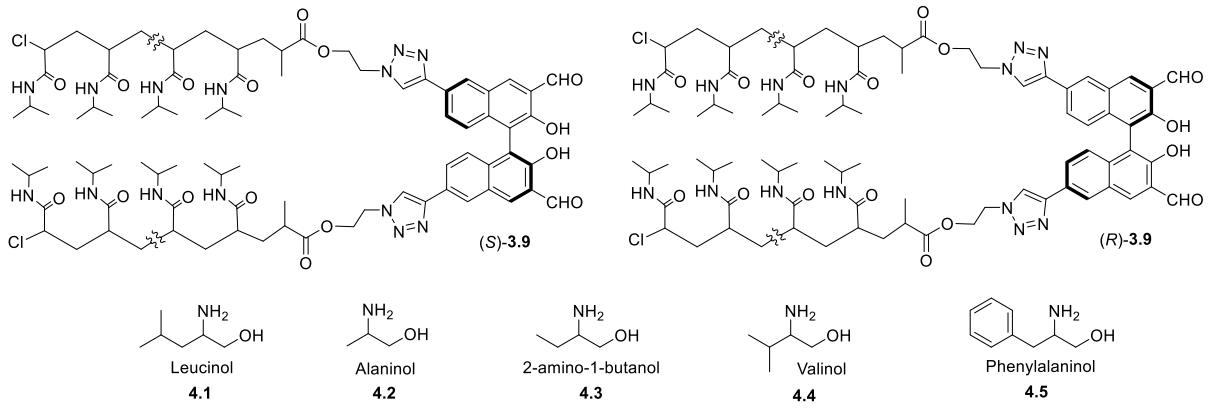

4.2. Results and Discussion

4.2.1. Enantioselective fluorescent recognition of amino alcohols in aqueous and organic solvents

We first studied fluorescent recognition of amino alcohols in BICINE buffer (25 mM, pH = 8.80). (*S*)-**3.9** (50 μL, 1 equiv., 1 mM in BICINE buffer) and $Zn(OAc)_2$ (50 μL, 2 equiv., 2 mM in water) were mixed with various volume of leucinol **4.1** (4 mM in BICINE buffer). The mixture was allowed to stand at room temperature for 2h then diluted to 5 mL using BICINE buffer for fluorescence measurement. However, no fluorescence response was observed (Figure **4.2**). We then change the solvent to water. (*S*)-**3.9** (50 μL, 1 equiv., 1 mM in water) and $Zn(OAc)_2$ (50 μL, 2 equiv., 2 mM in water) were mixed with various volume of leucinol **4.1** (4 mM in water). The mixture was allowed to stand at room temperature for 2h then diluted to 5 mL using water for fluorescence measurement. This time, highly enantioselective fluorescence response was observed (Figure **4.3**). Therefore, by simply using pure water as solvent, the polymer probe **3.9** can be used for enantioselective recognition of leucinol.

Figure 4.2. Fluorescence titration of (*S*)-**3.9** (1.0 mM, 1 equiv) with (a) (*S*)-**4.1** (4.0 mM) and (b) (*R*)-**4.1** (4.0 mM) in BICINE in the presence of $Zn(OAc)_2$ (2.0 mM in water, 2 equiv) (Reaction time: 2 h, then diluted 100-fold with BICINE. λ_{exc} = 320 nm. Slit: 5/5 nm).

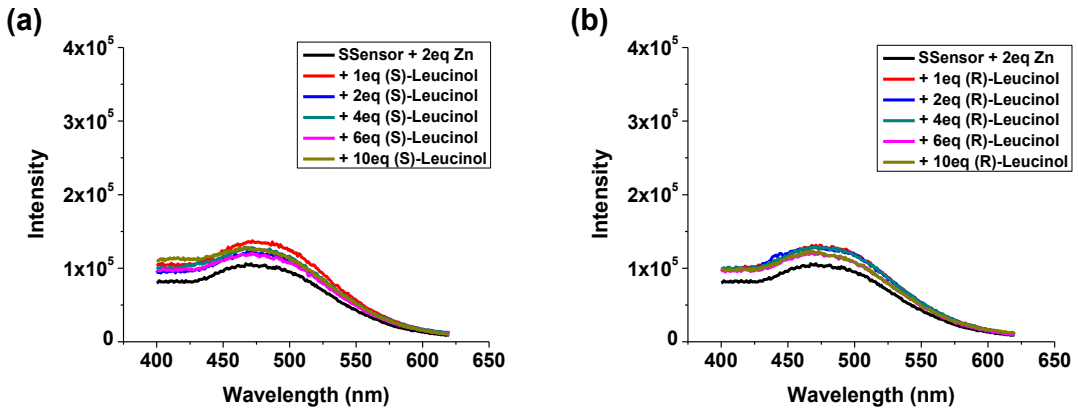

Figure 4.3. Fluorescence titration of (*S*)-**3.9** (1.0 mM, 1 equiv) with (*S*)-**4.1** (4.0 mM) or (*R*)-**4.1** (4.0 mM) in water in the presence of $Zn(OAc)_2$ (2.0 mM in water, 2 equiv) (Reaction time: 2 h, then diluted 100-fold with water. λ_{exc} = 320 nm. Slit: 5/5 nm). Fluorescence intensity at λ_{em} = 530 nm was used for the equivalent versus fluorescence intensity figure.

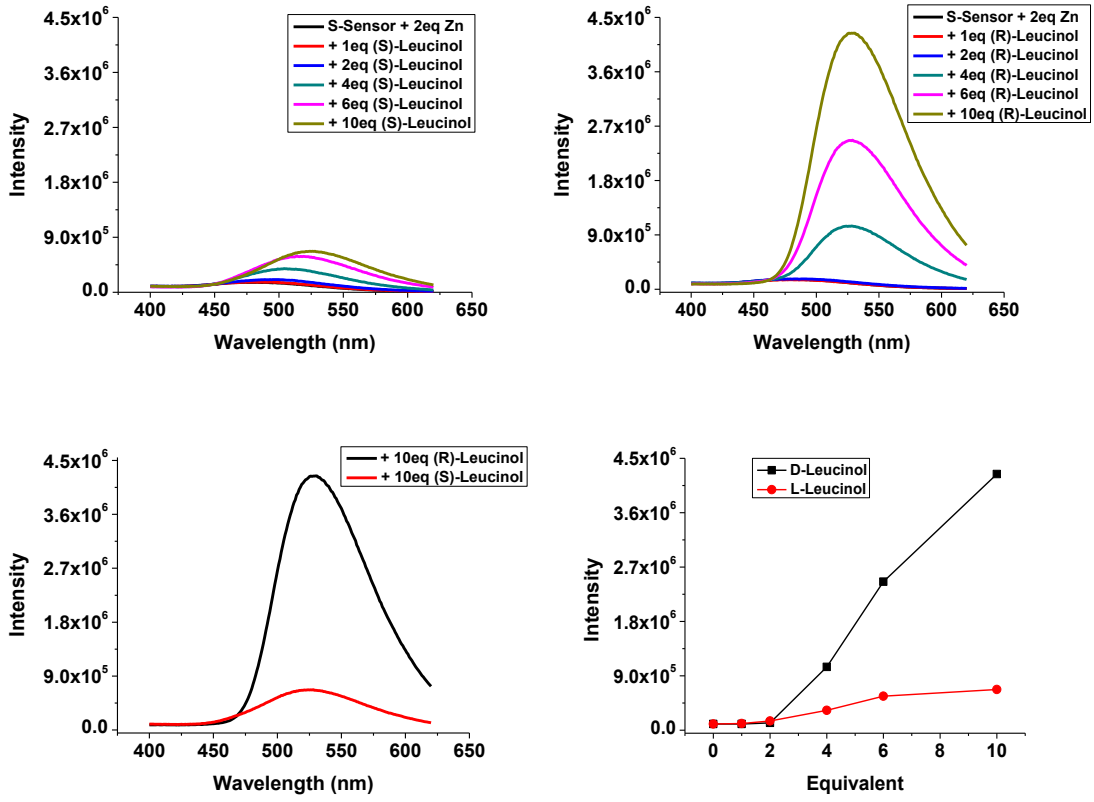

We also studied enantioselective recognition of other amino alcohols (**4.2**-**4.5**) using (*S*)-**3.9**. Highly enantioselective fluorescence response was observed for all these amino alcohols (Figure **4.4**-**4.7**). Interestingly, when **4.2** and **4.3** was used, *R* enantiomer led to much higher fluorescence enhancement than *S* enantiomer. For **4.4** and **4.5**, the enantioselectivity was reversed. This indicates that the fluorescence of the probe is very sensitive to the structure of the amino alcohol substrates.

Figure 4.4. Fluorescence titration of (*S*)-**3.9** (1.0 mM, 1 equiv) with (*S*)-**4.2** (4.0 mM) or (*R*)-**4.2** (4.0 mM) in water in the presence of $Zn(OAc)_2$ (2.0 mM in water, 2 equiv) (Reaction time: 2 h, then diluted 100-fold with water. λ_{exc} = 320 nm. Slit: 5/5 nm). Fluorescence intensity at λ_{em} = 531 was used for the equivalent versus fluorescence intensity figure.

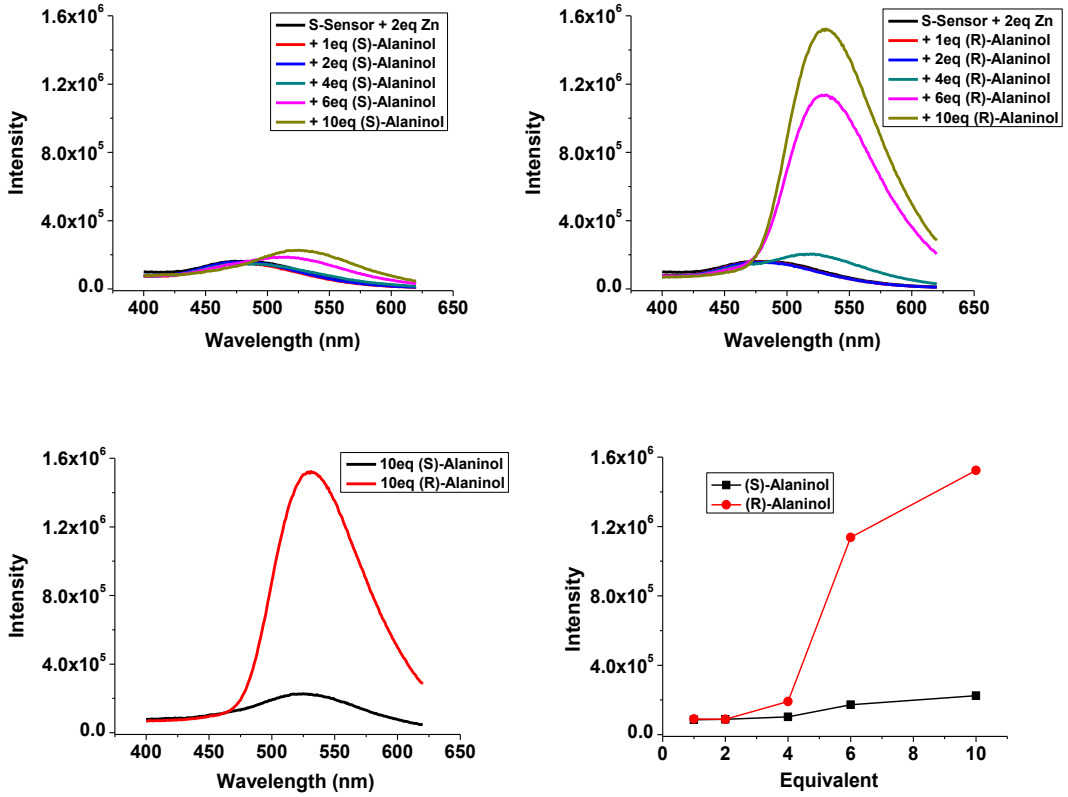

Figure 4.5. Fluorescence titration of (*S*)-**3.9** (1.0 mM, 1 equiv) with (*S*)-**4.3** (4.0 mM) or (*R*)-**4.3** (4.0 mM) in water in the presence of $Zn(OAc)_2$ (2.0 mM in water, 2 equiv) (Reaction time: 2 h, then diluted 100-fold with water. λ_{exc} = 320 nm. Slit: 5/5 nm). Fluorescence intensity at λ_{em} = 527 nm was used for the equivalent versus fluorescence intensity figure.

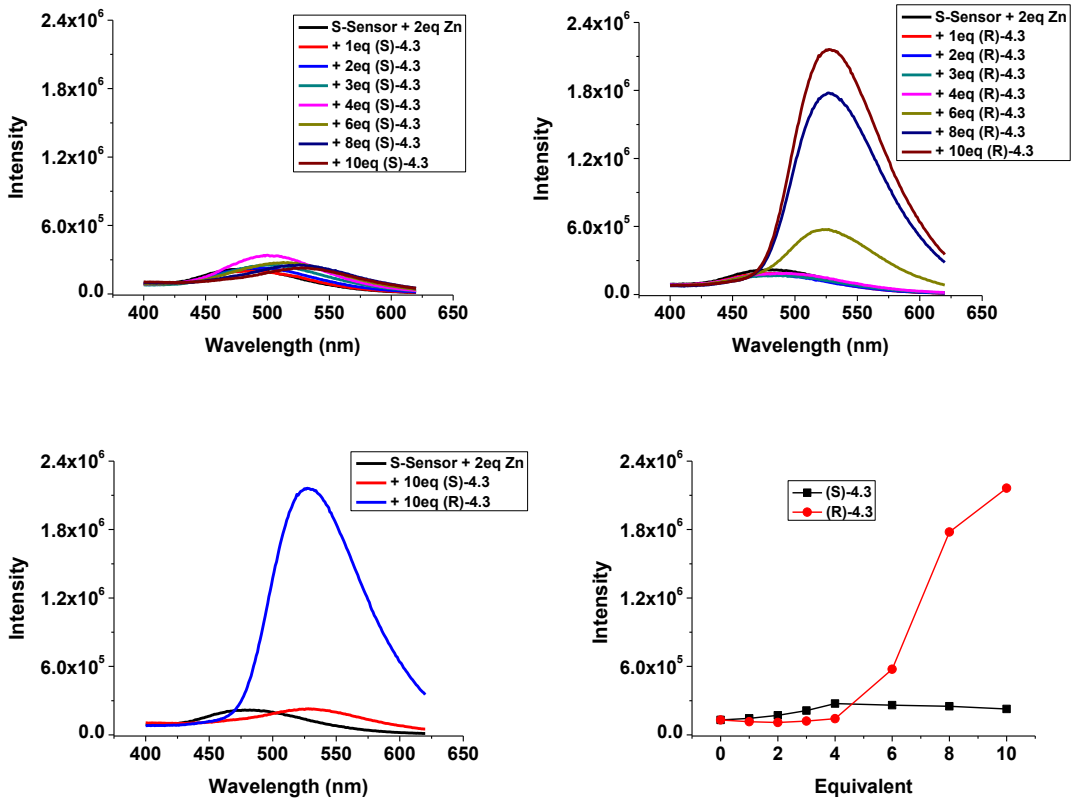

Figure 4.6. Fluorescence titration of (*S*)-**3.9** (1.0 mM, 1 equiv) with (*S*)-**4.4** (4.0 mM) or (*R*)-**4.4** (4.0 mM) in water in the presence of $Zn(OAc)_2$ (2.0 mM in water, 2 equiv) (Reaction time: 2 h, then diluted 100-fold with water. λ_{exc} = 320 nm. Slit: 5/5 nm). Fluorescence intensity at λ_{em} = 506 nm was used for the equivalent versus fluorescence intensity figure.

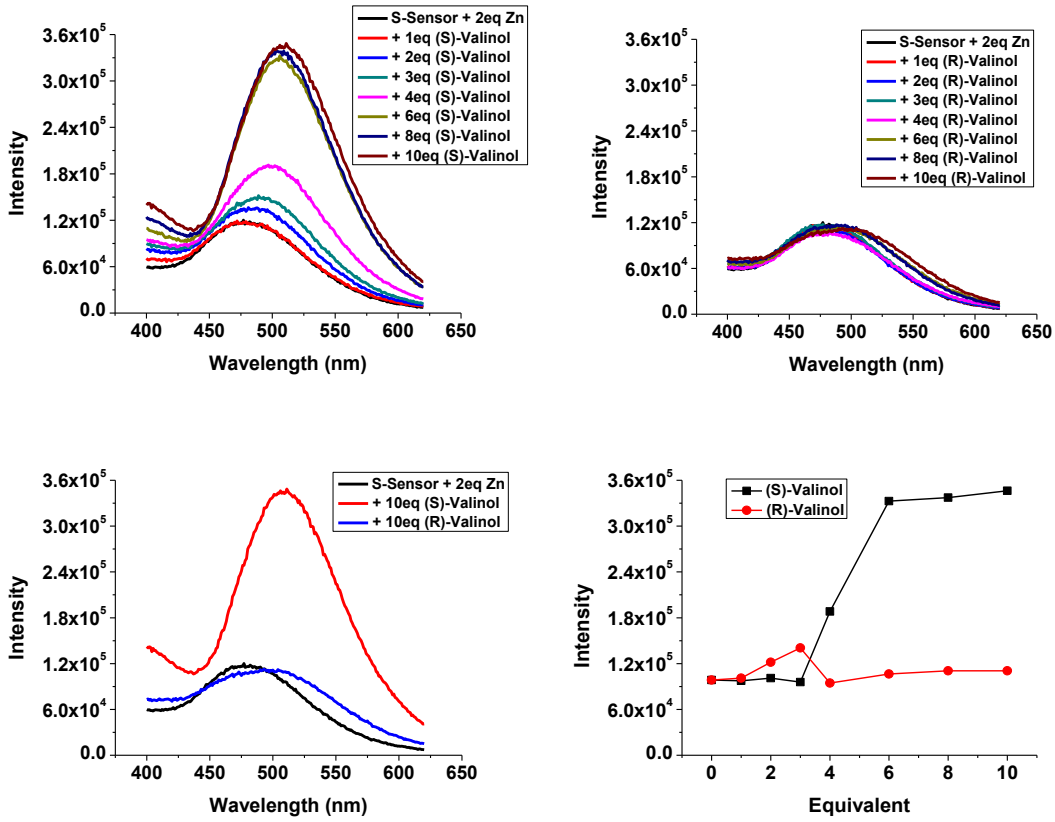

Figure 4.7. Fluorescence titration of (*S*)-**3.9** (1.0 mM, 1 equiv) with (*S*)-**4.5** (4.0 mM) or (*R*)-**4.5** (4.0 mM) in water in the presence of $Zn(OAc)_2$ (2.0 mM in water, 2 equiv) (Reaction time: 2 h, then diluted 100-fold with water. λ_{exc} = 320 nm. Slit: 5/5 nm). Fluorescence intensity at λ_{em} = 506 nm was used for the equivalent versus fluorescence intensity figure.

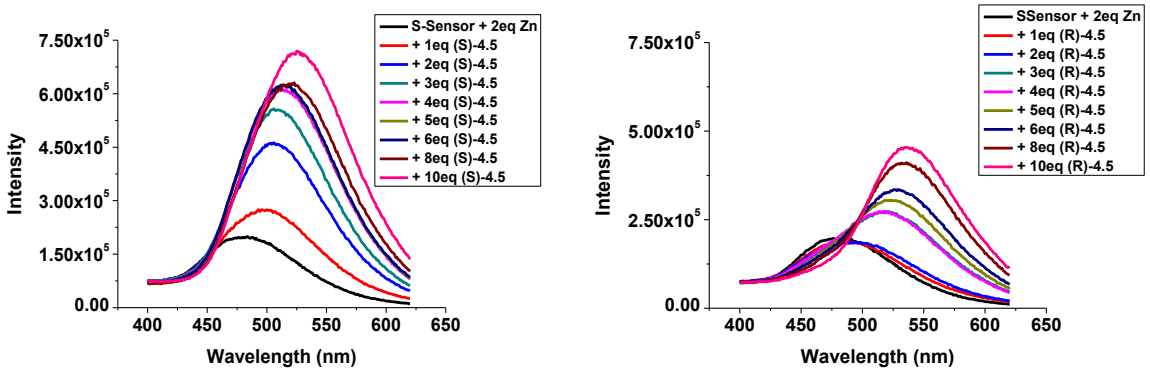

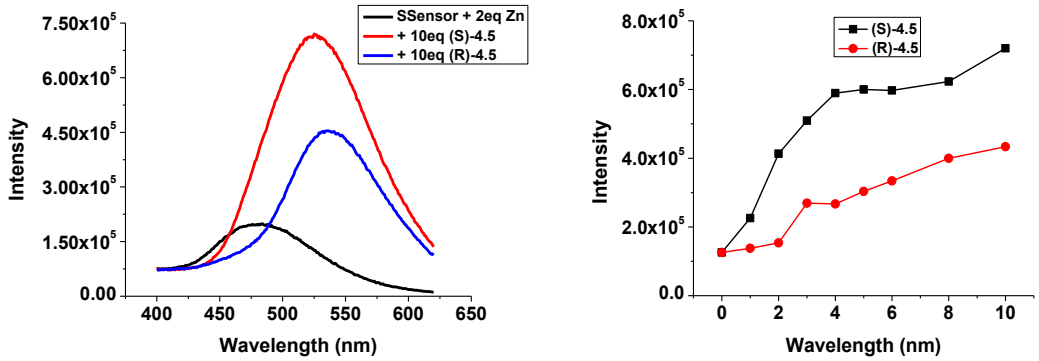

We then studied the enantioselective recognition of leucinol **4.1** in detail. (*R*)-**3.9** (40 μL, 1 equiv., 1 mM in water) and $Zn(OAc)_2$ (40 μL, 2 equiv., 2 mM in water) were mixed with various volume of **4.1** (20 mM in water). Various volume of water was added for each mixture to make the total volume equal to 280 μL. After 2 h, the mixtures were diluted to 4 mL for fluorescence measurement. As shown in Figure **4.8**, addition of (*S*)-**4.1** led to much higher fluorescence enhancement than (*R*)-**4.1**, the fluorescence intensity almost did not change when more than 40 equiv. of **4.1** was added. The results were also opposite to the data obtained by using (*S*)-**3.9**, confirming the high enantioselectivity of the probe.

Figure 4.8. Fluorescence titration of (*R*)-**3.9** (1.0 mM, 1 equiv) with (*S*)-**4.1** (20.0 mM) or (*R*)-**4.1** (20.0 mM) in water in the presence of $Zn(OAc)_2$ (2.0 mM in water, 2 equiv) (Reaction time: 2 h; reaction volume: 280 μL, then diluted 100-fold with water. λ_{exc} = 320 nm. Slit: 5/5 nm). Fluorescence intensity at λ_{em}=529 nm was used for the equiv. vs. fluorescence intensity figure.

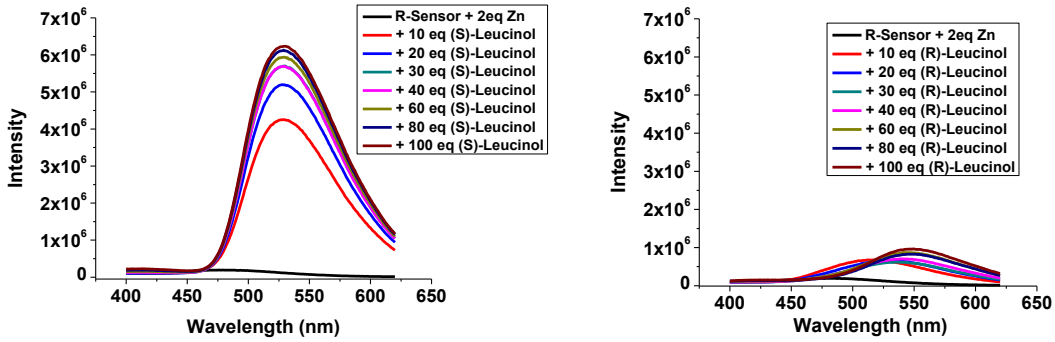

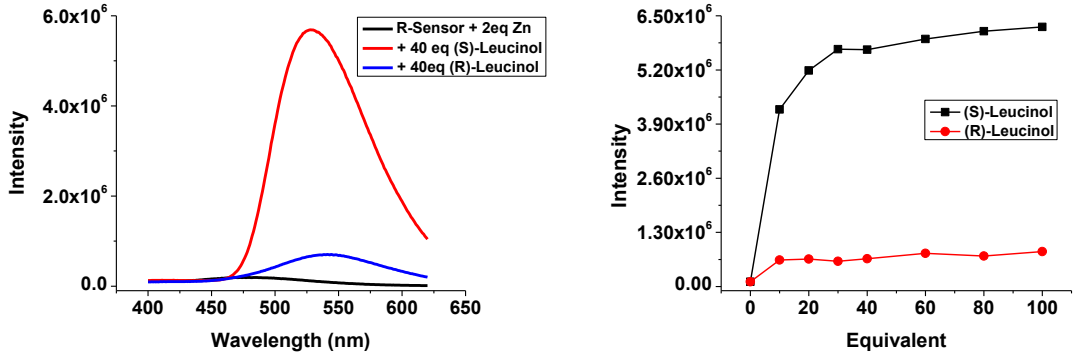

The stability of fluorescence after dilution of reaction mixture was investigated. The fluorescence intensities were measured at 0, 90 and 180 min after dilution. (*R*)-**3.9** was used and the reaction condition and fluorescence measurement procedure was the same as described above. As we can see in Figure **4.9**, the fluorescence intensity kept decreasing at various equiv. after dilution. This might be due to the gradual hydrolysis of imine bonds of products.

Figure 4.9. Fluorescent stability study. Fluorescence titration of (*R*)-**3.9** (1.0 mM, 1 equiv) with (*S*)-**4.1** or (*R*)-**4.1** (20.0mM, 20, 30, 60, 100 equiv.) in water in the presence of $Zn(OAc)_2$ (2.0 mM in water, 2 equiv) (Reaction time: 2 h; reaction volume: 280 μL, then diluted 100-fold with water. λ_{exc} = 320 nm. Slit: 5/5 nm). Fluorescence intensities at λ_{em} = 529 were recorded after dilution at various time points.

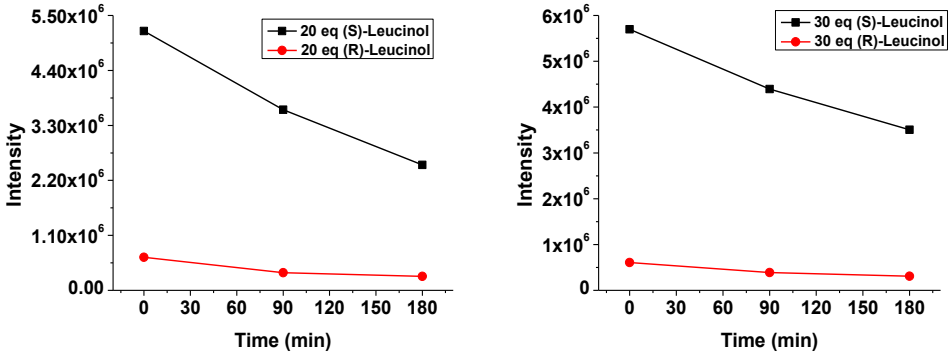

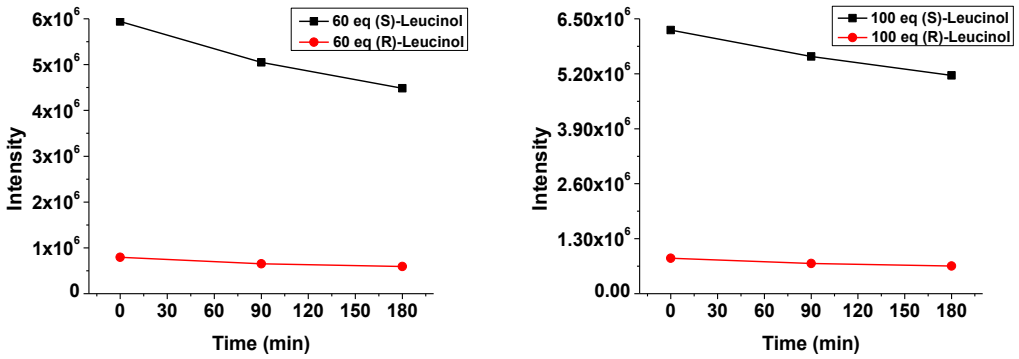

Thus, we sought for another solvent for dilution after the reaction between probe and substrates in water. Five water-soluble solvents, DMSO, DMF, methanol, THF and acetonitrile were tested. (*R*)-**3.9** (40 μL, 1 equiv., 1 mM in water) and $Zn(OAc)_2$ (40 μL, 2 equiv., 2 mM in water) were mixed with leucinol **4.1** (80 μL, 40 equiv., 20 mM in water), then 120 μL of water was added to make the total volume to 280 μL. After 2 h, five different solvents were used to dilute the mixture to 4 mL. Fluorescence of the diluted samples were measured and the stability of fluorescence was also investigated.

It was found that utilization of DMSO, DMF and methanol led to highly enantioselective fluorescence response. Dilution by THF and acetonitrile did not give good enantioselectivity of the probe (Figure **4.10**). Study on the stability of fluorescence revealed that fluorescence intensity kept decreasing in DMF solution and stayed stable in methanol and DMSO solutions (Figure **4.11**). Dilution by DMSO led to higher enantioselectivity of the probe. Therefore, DMSO was chosen to dilute the aqueous reaction mixture.

Figure 4.10. Fluorescence titration of (*R*)-**3.9** (1.0 mM, 1 equiv) with (*S*)-**4.1** or (*R*)-**4.1** (20.0mM, 40 equiv.) in water in the presence of $Zn(OAc)_2$ (2.0 mM in water, 2 equiv) (Reaction time: 2 h; reaction volume: 280 μL, then diluted 100-fold with different solvents. λ_{exc} = 320 nm. Slit: 5/5 nm).

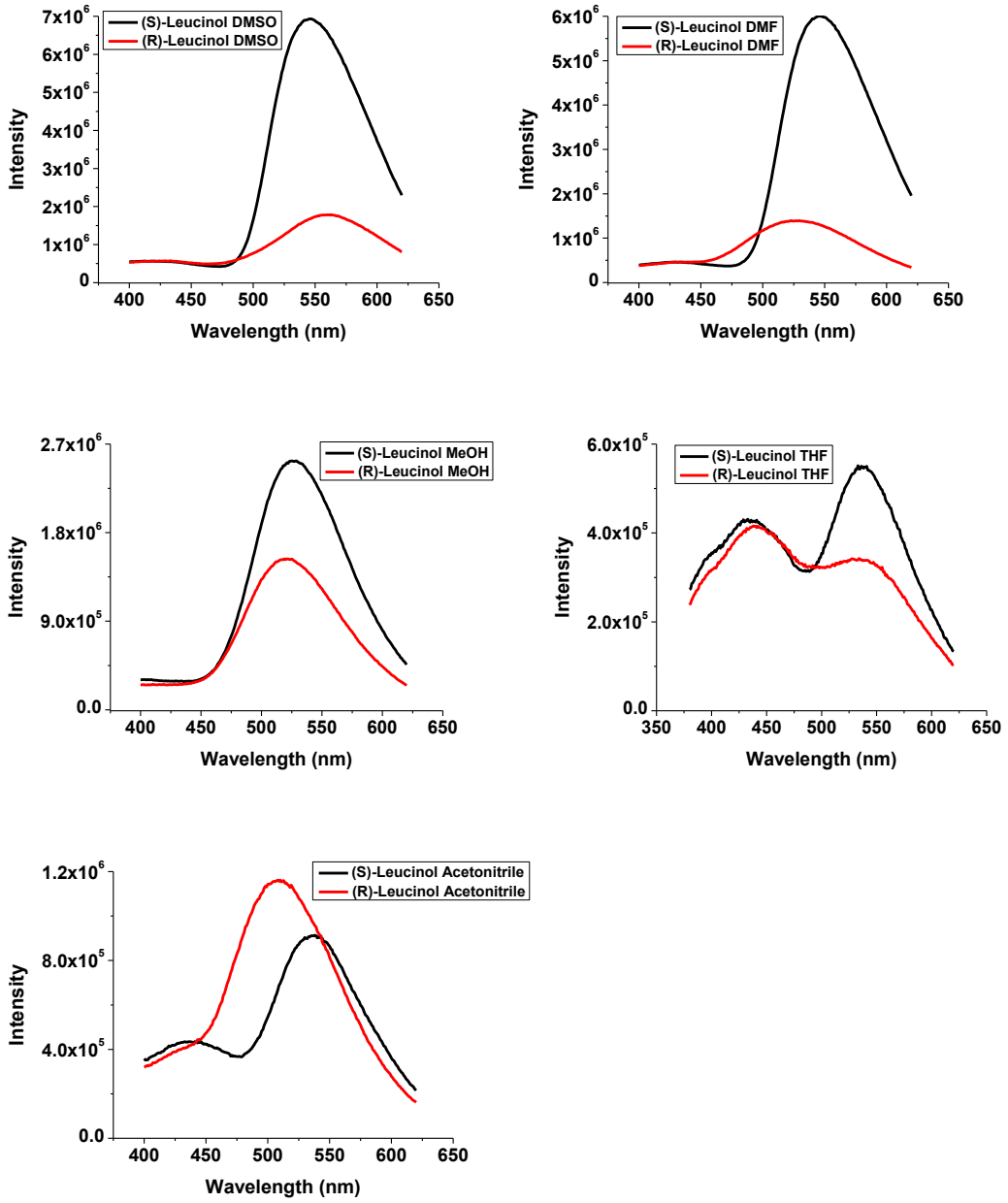

Figure 4.11. Fluorescent stability study. Fluorescence titration of (*R*)-**3.9** (1.0 mM, 1 equiv) with (*S*)-**4.1** or (*R*)-**4.1** (20.0mM, 40 equiv.) in water in the presence of $Zn(OAc)_2$ (2.0 mM in water, 2 equiv) (Reaction time: 2 h; reaction volume: 280 μL, then diluted 100-fold with different solvents. λ_{exc} = 320 nm. Slit: 5/5 nm). Fluorescence intensities (for DMSO, at λ_{em} = 547 nm; for DMF, at λ_{em} = 546 nm; for methanol, at λ_{em} = 529 nm) were recorded after dilution at various time points.

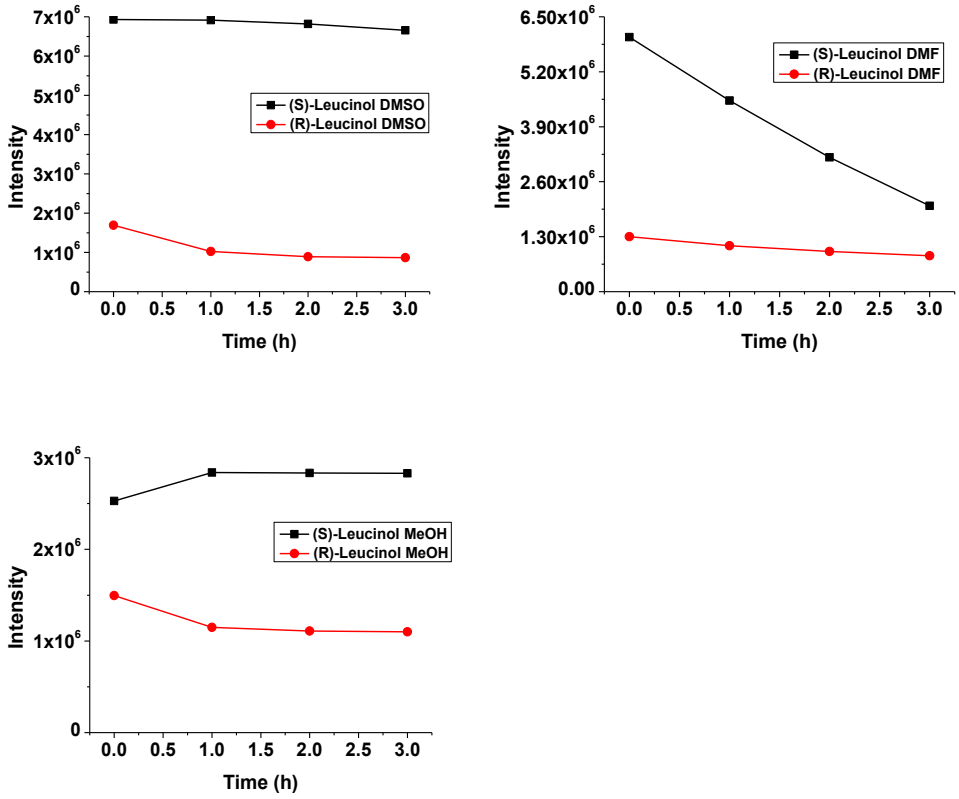

The fluorescence response of (*S*)-**3.9** toward five different amino alcohols by DMSO dilution were studied. (*S*)-**3.9** (40 μL, 1 equiv., 1 mM in water) and $Zn(OAc)_2$ (40 μL, 2 equiv., 2 mM in water) were mixed with various volume of amino alcohols (40 mM in water), then various volume of water was added to make the total volume to 120 μL. After 2 h, the reaction mixtures were diluted to 4 mL using DMSO for fluorescence measurement. Figure **4.12-4.16** showed the fluorescence measurement results. Highly enantioselective fluorescence responses were observed for each amino alcohol.

Figure 4.12. Fluorescence titration of (*S*)-**3.9** (1.0 mM, 1 equiv) with (*S*)-**4.1** (20.0 mM) or (*R*)-**4.1** (40.0 mM) in water in the presence of $Zn(OAc)_2$ (2.0 mM in water, 2 equiv) (Reaction time: 2 h; reaction volume: 120 μL, then diluted 100-fold with DMSO. λ_{exc} = 320 nm. Slit: 5/5 nm). Fluorescence intensity at λ_{em} = 546 nm was used for the equiv. vs. fluorescence intensity figure.

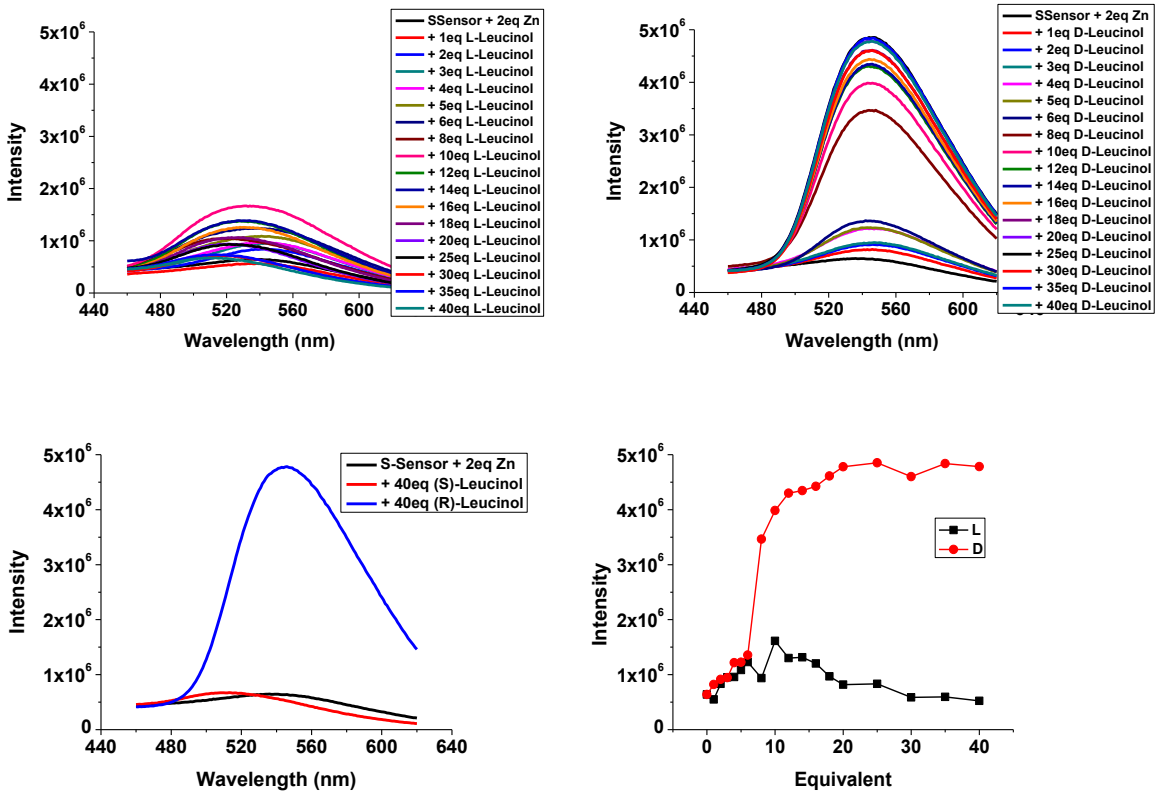

Figure 4.13. Fluorescence titration of (*S*)-**3.9** (1.0 mM, 1 equiv) with (*S*)-**4.2** (20.0 mM) or (*R*)-**4.2** (40.0 mM) in water in the presence of $Zn(OAc)_2$ (2.0 mM in water, 2 equiv) (Reaction time: 2 h; reaction volume: 120 μL, then diluted 100-fold with DMSO. λ_{exc} = 320 nm. Slit: 5/5 nm). Fluorescence intensity at λ_{em}=551 nm was used for the equiv. vs. fluorescence intensity figure.

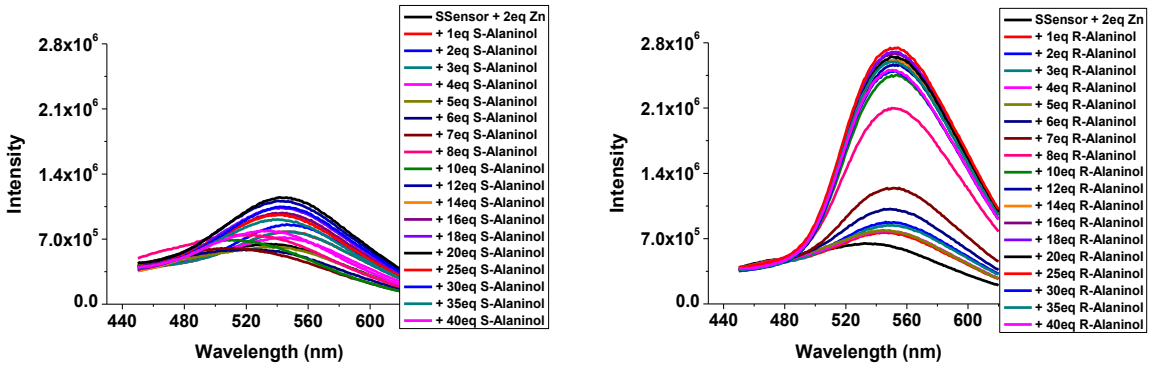

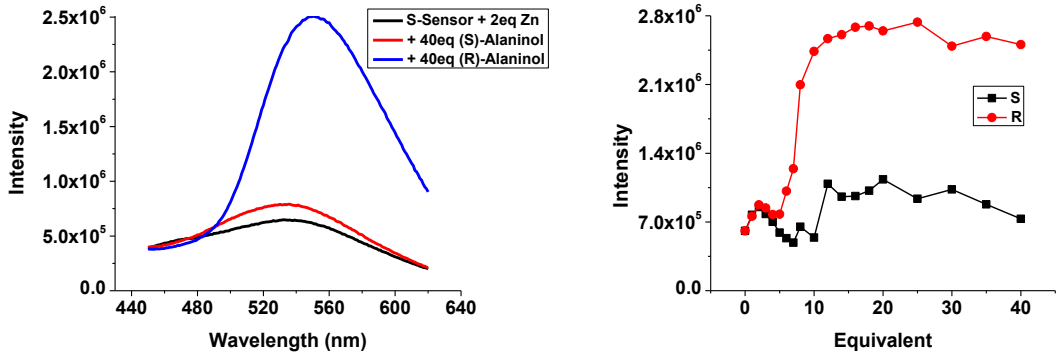

Figure 4.14. Fluorescence titration of (*S*)-**3.9** (1.0 mM, 1 equiv) with (*S*)-**4.3** (20.0 mM) or (*R*)-**4.3** (40.0 mM) in water in the presence of $Zn(OAc)_2$ (2.0 mM in water, 2 equiv) (Reaction time: 2 h; reaction volume: 120 μL, then diluted 100-fold with DMSO. λ_{exc} = 320 nm. Slit: 5/5 nm). Fluorescence intensity at λ_{em} = 547 nm was used for the equiv. vs. fluorescence intensity figure.

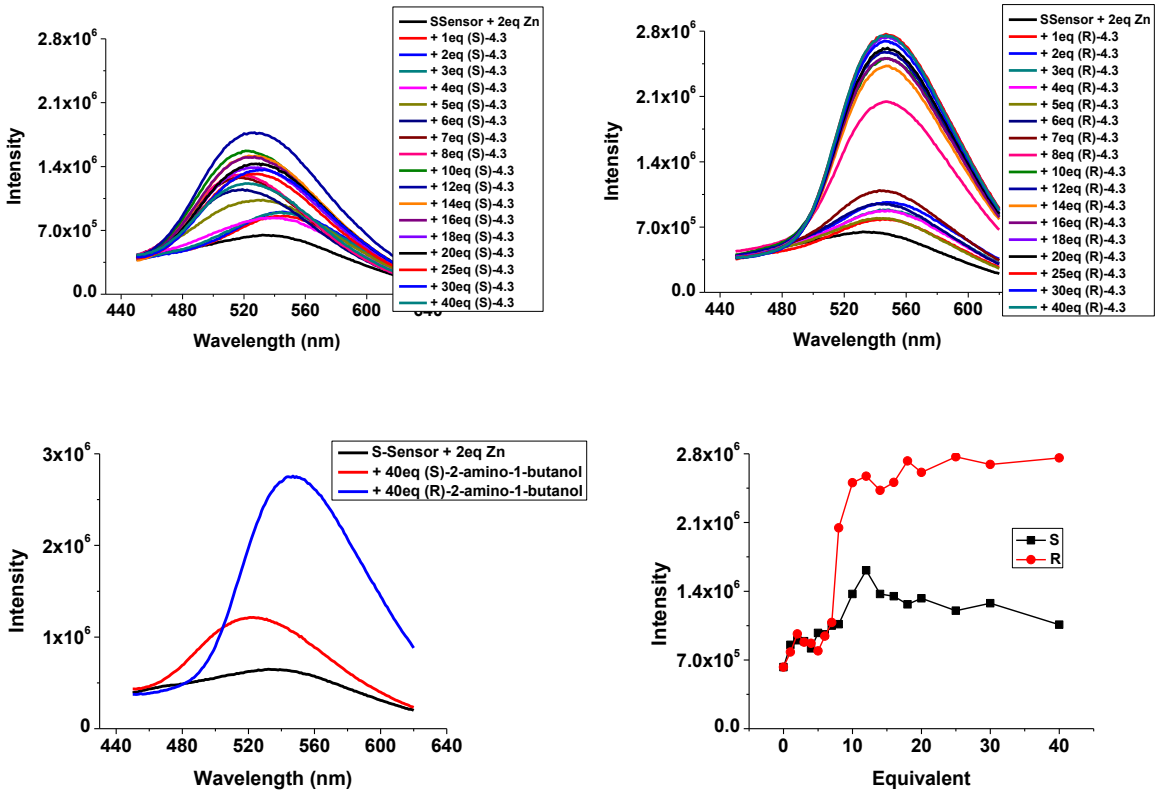

Figure 4.15. Fluorescence titration of (*S*)-**3.9** (1.0 mM, 1 equiv) with (*S*)-**4.4** (20.0 mM) or (*R*)-**4.4** (40.0 mM) in water in the presence of $Zn(OAc)_2$ (2.0 mM in water, 2 equiv) (Reaction time:

2 h; reaction volume: 120 μL, then diluted 100-fold with DMSO. λ_{exc} = 320 nm. Slit: 5/5 nm). Fluorescence intensity at λ_{em} = 515 nm was used for the equiv. vs. fluorescence intensity figure.

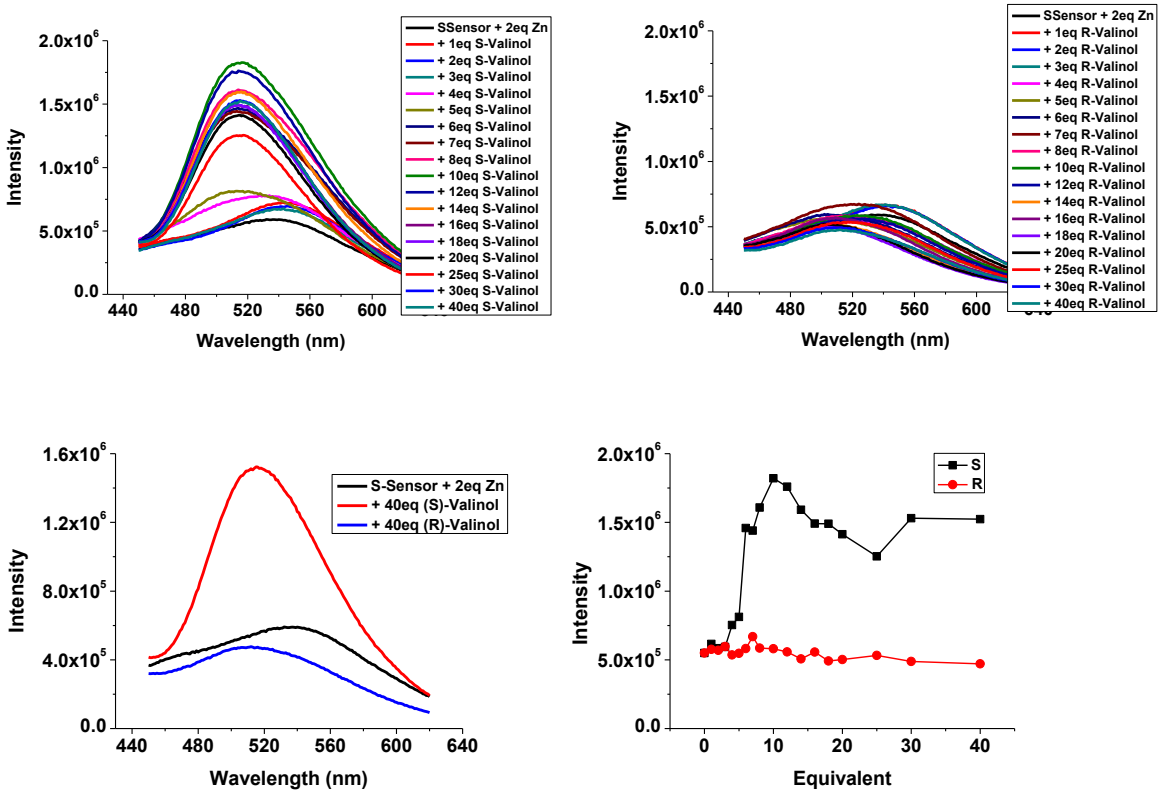

Figure 4.16. Fluorescence titration of (*S*)-**3.9** (1.0 mM, 1 equiv) with (*S*)-**4.5** (20.0 mM) or (*R*)-**4.5** (40.0 mM) in water in the presence of $Zn(OAc)_2$ (2.0 mM in water, 2 equiv) (Reaction time: 2 h; reaction volume: 120 μL, then diluted 100-fold with DMSO. λ_{exc} = 320 nm. Slit: 5/5 nm). Fluorescence intensity at λ_{em} = 525 nm was used for the equiv. vs. fluorescence intensity figure.

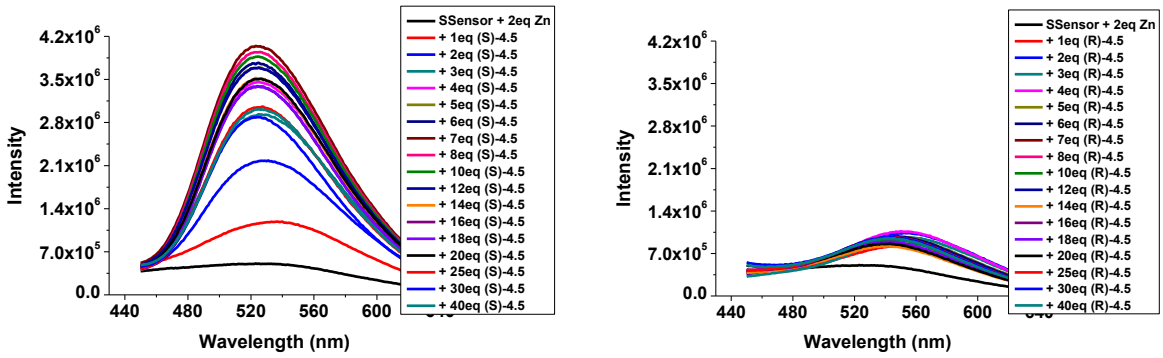

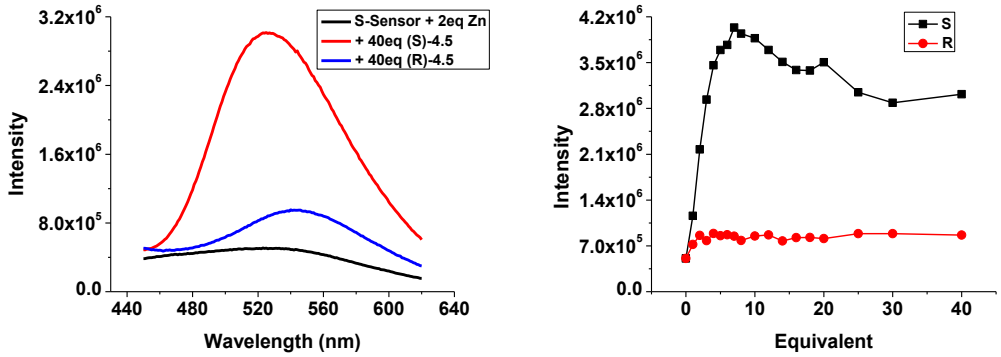

We also studied enantioselective recognition of **4.1** in DMSO, DMF and methanol. (*S*)-**3.9** (40 μL, 1 equiv., 1 mM in solvent) and $Zn(OAc)_2$ (40 μL, 2 equiv., 2 mM in solvent) were mixed with various volume of **4.1** (20 mM in solvent), then various volume of solvent was added to make the total volume to 280 μL. After 2 h, the reaction mixtures were diluted to 4 mL using corresponding solvent for fluorescence measurement. Interestingly, when DMSO and DMF were used, no enantioselectivity was observed. The enantioselectivity was much lower in pure methanol than using previous method (Figure **4.17**-**4.19**). Therefore, conducting reactions in water then diluting using DMSO gave both high enantioselectivity and fluorescent stability.

Figure 4.17. Fluorescence titration of (*S*)-**3.9** (1.0 mM, 1 equiv.) with (*S*)-**4.1** (20.0 mM) or (*R*)-**4.1** (40.0 mM) in DMSO in the presence of $Zn(OAc)_2$ (2.0 mM in DMSO, 2 equiv.) (Reaction time: 2 h; reaction volume: 280 μL, then diluted 100-fold with DMSO. λ_{exc} = 320 nm. Slit: 5/5 nm). Fluorescence intensity at λ_{em} = 550 nm was used for the equiv. vs. fluorescence intensity figure.

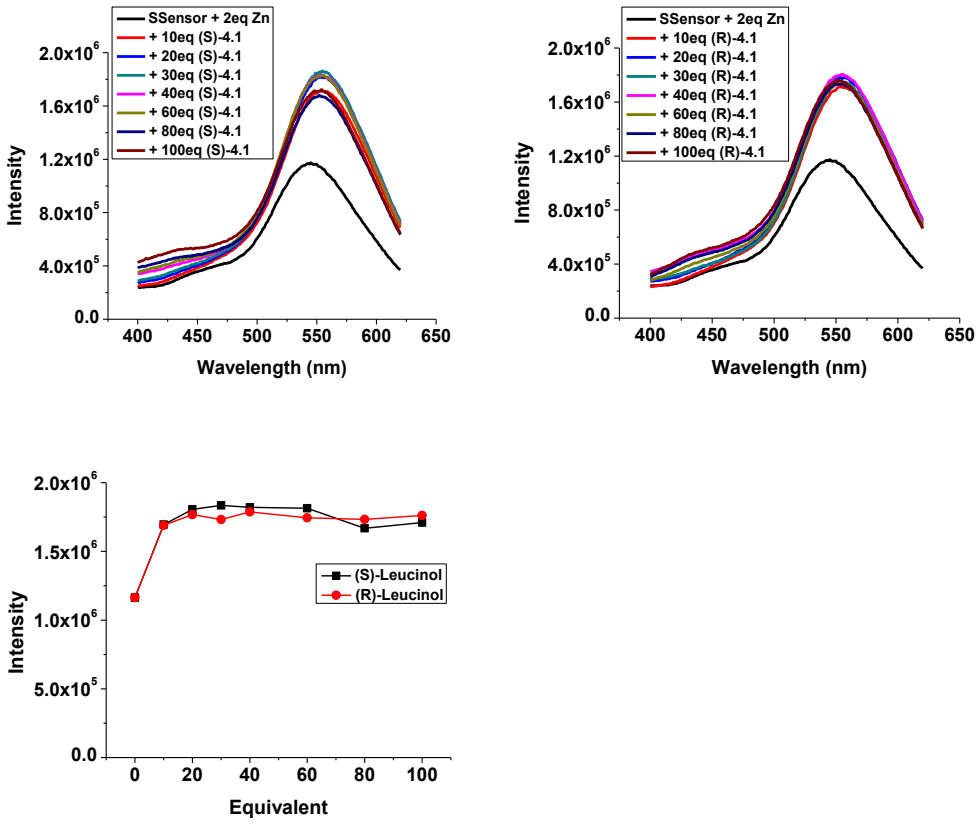

Figure 4.18. Fluorescence titration of (*S*)-**3.9** (1.0 mM, 1 equiv) with (*S*)-**4.1** (20.0 mM) or (*R*)-**4.1** (40.0 mM) in DMF in the presence of $Zn(OAc)_2$ (2.0 mM in DMF, 2 equiv) (Reaction time: 2 h; reaction volume: 280 μL, then diluted 100-fold with DMF. λ_{exc} = 320 nm. Slit: 5/5 nm). Fluorescence intensity at λ_{em} = 543 nm was used for the equiv. vs. fluorescence intensity figure.

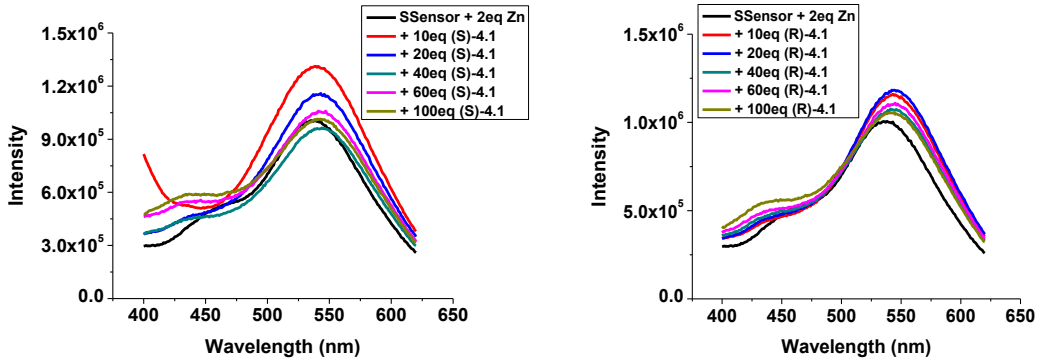

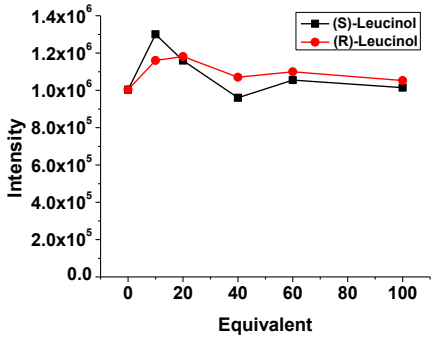

Figure 4.19. Fluorescence titration of (*S*)-**3.9** (1.0 mM, 1 equiv) with (*S*)-**4.1** (20.0 mM) or (*R*)-**4.1** (40.0 mM) in MeOH in the presence of $Zn(OAc)_2$ (2.0 mM in MeOH, 2 equiv) (Reaction time: 2 h; reaction volume: 280 μL, then diluted 100-fold with MeOH. λ_{exc} = 320 nm. Slit: 5/5 nm). Fluorescence intensity at λ_{em} = 543 nm was used for the equivalent vs. fluorescence intensity figure.

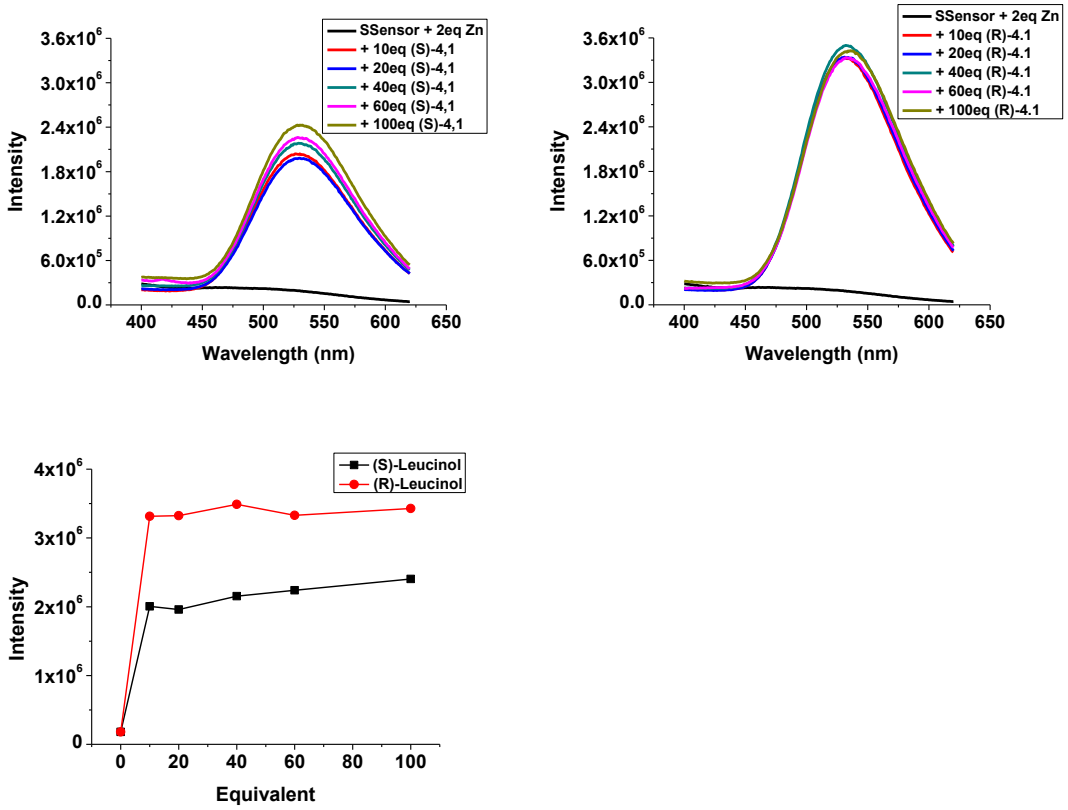

We conducted ^{1}H-NMR study to figure out the mechanism of enantioselectivity. (*S*)-**3.9** (150 μL, 20 mM in D_2O), $Zn(OAc)_2$ (150 μL, 40 mM in D_2O), and (*S*)- or (*R*)-**4.1** (150 μL, 160 mM in D_2O) were mixed together to acquired ^{1}H-NMR spectra at different time. No obvious change was observed for (*S*)- or (*R*)-**4.1** derived ^{1}H-NMR spectra because of the hydrophobicity of BINOL core. After 6 h, 200 μL mixtures were taken out to mix with 200 μL acetone-d_6 for ^{1}H-NMR acquisition. More resolved spectra were obtained. Compared with ^{1}H-NMR spectra of (*S*)-**3.9**, aldehyde peak disappeared for both (*S*)- or (*R*)-**4.1** derived ^{1}H-NMR spectra (Figure **4.20**), indicating the reaction between aldehyde and amine group. For (*S*)-**4.1** derived ^{1}H-NMR spectra, a doublet peak between 0.5-0 ppm appeared. Such peak was not found in (*R*)-**4.1** derived ^{1}H-NMR spectra, revealing the structural difference between products that were derived from the reaction of (*S*)- or (*R*)-**4.1** with (*S*)-**3.9**.

Figure 4.20. ^{1}H NMR spectra of the solutions (200 μL) withdrawn at 6 h from the mixture of (*S*)-**3.9** (20.0 mM in D_2O, 1.0 equiv) with (*S*)- or (*R*)-**4.1** (160.0 mM in D_2O, 8.0 equiv) and $Zn(OAc)_2$ (40.0 mM in D_2O, 2.0 equiv) and mixed with acetone-d_6 (200 μL).

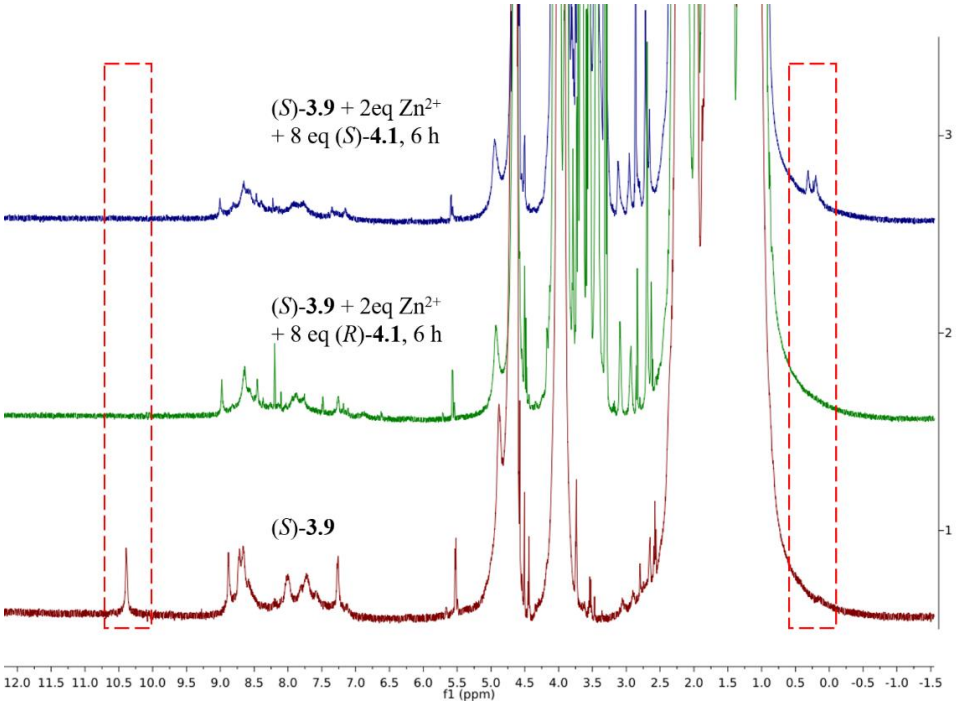

^{1}H-NMR study of valinol **4.4**, which led to opposite enantioselectivity compared with **4.1**, was also conducted. The procedure was the same as described above. As shown in Figure **4.21**, after reacting for 6 h, for (*S*)-**4.4** derived ^{1}H-NMR spectra in D2O: acetone-d_6 1:1 solvent, a doublet peak between 0.5-0 ppm also appeared. Such peak was not found in (*R*)-**4.4** derived ^{1}H-NMR spectra. Aldehyde peak also disappeared for both (*S*)- or (*R*)-**4.1** derived ^{1}H-NMR spectra. From these data, it could be concluded that the difference in structure may lead to the high enantioselectivity of the probe.

Figure 4.21. ^{1}H NMR spectra of the solutions (200 μL) withdrawn at 6 h from the mixture of (*S*)-**3.9** (20.0 mM in D_2O, 1.0 equiv) with (*S*)- or (*R*)-**4.4** (160.0 mM in D_2O, 8.0 equiv) and $Zn(OAc)_2$ (40.0 mM in D_2O, 2.0 equiv) and mixed with acetone-d_6 (200 μL).

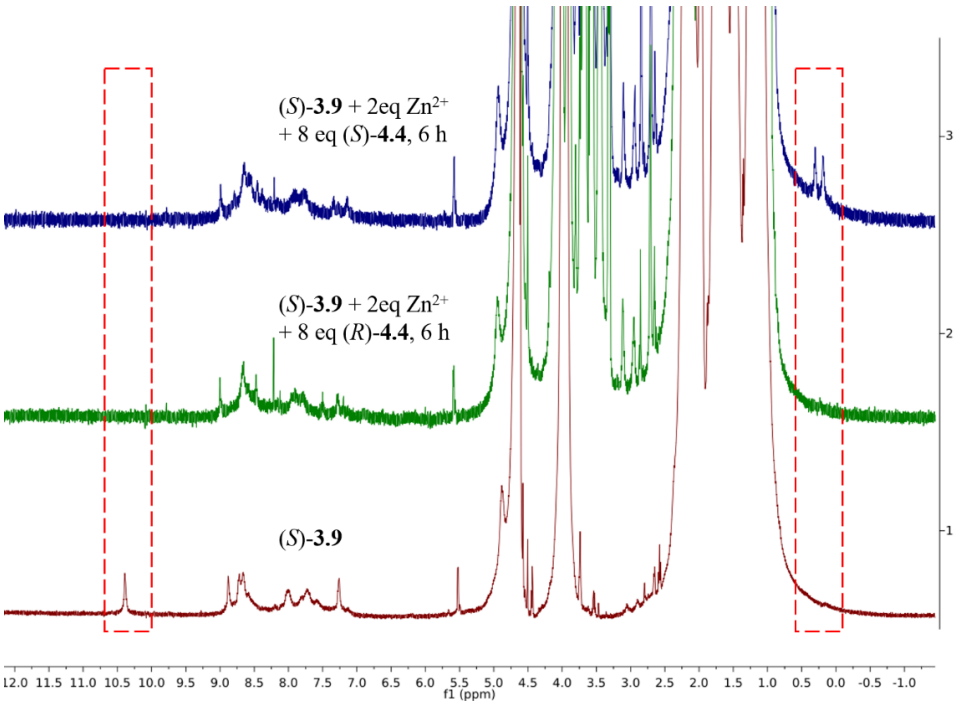

4.2.2. Enantioselective fluorescent recognition of amino alcohols using cononsolvency property of the probe

Polymer probe (*S*)-**3.9** contains PNIPAM chain, which has unique solution properties. An unusual solution behavior of (*S*)-**3.9** was observed. As shown in Figure **4.22**, (*S*)-**3.9** was

first dissolved in CH_2Cl_2 (1.0 mM) and an immiscible water layer was added on top. After the bilayer mixture was shaken vigorously and then set for 6 h at room temperature, a solid polymer film formed at the interface of CH_2Cl_2 and water. After the solvents were decanted, the polymer film can be isolated which was found to be still soluble in both water and CH_2Cl_2. This represents a new type of reversible phase transition for PNIPAM when treated with two immiscible solvents. Although the cononsolvency of PNIPAM in the mixture of water and a water-miscible solvent such as methanol, THF and dioxane has been studied extensively,[5–13] no work was reported when two solvents are immiscible. In order to explain this observation, it is proposed that when water is added to the CH_2Cl_2 solution of (*S*)-**3.9**, the hydrophilic amide groups of the polymer would prefer to interact with water through hydrogen bonding. This should allow the conformation of the polymer in CH_2Cl_2 to change in the presence of water. That is, there is a competitive interaction in which the hydrophilic parts of the polymer interact with water and the hydrophobic parts interact with CH_2Cl_2, leading to the separation of the polymer from both phases.

Figure 4.22. Photos of (*S*)-**3.9** in CH_2Cl_2 (1.0 mM, 800 μL) topped with an immiscible water layer (800 μL) (left), and after mixing and setting at room temperature for 6 h (right).

However, when we treated the water solution of (*S*)-**3.9** with CH_2Cl_2, no polymer film was generated and the polymer was still dissolved in water. This indicates that the conformation

of this polymer in water should be more stable that in CH_2Cl_2 which allows the phase transition to occur from its CH_2Cl_2 solution but not from its water solution when mixing the two solvents.

We tried to use this cononsolvency property of **3.9** for the enantioselective recognition of amino acids and amino alcohols. For the study on amino acid, (*S*)-**3.9** (200 μL, 1 equiv., 1 mM in CH_2Cl_2) was mixed with $Zn(OAc)_2$ (200 μL, 2 mM in water) and (*S*) or (*R*)-leucine (500 μL, 10 equiv. 4 mM in BICINE buffer). After 6 h, polymer films were generated at the interface. Then the polymer films were separated and dissolved in BICINE to make concentration to 10 μM for fluorescence measurement. For the study on amino alcohol, (*S*)-**3.9** (200 μL, 1 equiv., 1 mM in CH_2Cl_2) was mixed with $Zn(OAc)_2$ (200 μL, 2 mM in water) and (*S*) or (*R*)-alaninol (500 μL, 10 equiv. 4 mM in water). After 6 h, polymer films were generated at the interface. Then the polymer films were separated and dissolved in water to make concentration to 10 μM for fluorescence measurement. No fluorescence enhancement was observed for all the measurements, indicating that the probe may not react with leucine or alaninol, and the polymer films were the probe itself.

Since the water solution of (*S*)-**3.9** cannot produce a polymer film upon treatment with CH_2Cl_2, we studied the interaction of the water solution of (*S*)-**3.9** with a chiral amino alcohol leucinol (**4.1**) in CH_2Cl_2 in the presence of $Zn(OAc)_2$. It is our hypothesis that if there is no reaction between (*S*)-**3.9** and the amino alcohol and $Zn(OAc)_2$, there should not be polymer film formation at the interface of these two immiscible solvents. We vigorously mixed a water solution of (*S*)-**3.9** (1.0 mM, 200 μL) and that of $Zn(OAc)_2$ (2.0 mM, 200 μL) with a CH_2Cl_2 solution of (*S*)-**4.1** (4.0 mM, 500 μL). After the mixture was allowed to set at room temperature for 6 h, a polymer film was generated at the interface of the two immiscible solvents as shown in Figure **4.23**. After the solvent was decanted, the polymer film was obtained which was found

to be still soluble in water and CH_2Cl_2 respectively. That is, the reaction product of (*S*)-**1** with the amino alcohol in the presence of $Zn(OAc)_2$ exhibits cononsolvency in water and CH_2Cl_2. We also conducted the same experiment in the absence of $Zn(OAc)_2$ and found no polymer film formation. That is, (*S*)-**3.9** reacts with both the amino alcohol and $Zn(OAc)_2$ to generate the polymer film.

Figure 4.23. Photos of (*S*)-**4.1** in CH_2Cl_2 (4.0 mM, 500 μL) topped with the immiscible water solution of (*S*)-**3.9** (1.0 mM, 200 μL) and $Zn(OAc)_2$ (2.0 mM, 200 μL) (left), and after vigorously mixed and set at room temperature for 6 h (right).

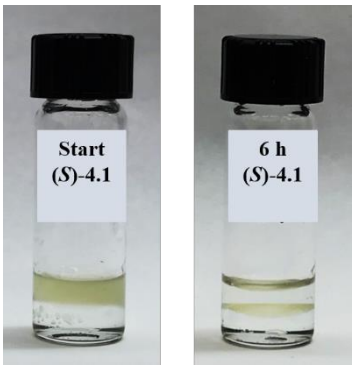

The polymer film isolated from the reaction of (*S*)-**3.9** +$Zn(OAc)_2$ with (*S*)-**4.1** as described above was dissolved in DMSO and the fluorescence spectrum of the solution was obtained. It gives a weak fluorescence signal at λ = 536 nm as shown in Figure **4.24**. We also used the enantiomer of the amino alcohol (*R*)-**4.1** to react with (*S*)-**3.9** and $Zn(OAc)_2$ under the same conditions. A polymer film was generated at the interface of water and CH_2Cl_2 in the same way as that from (*S*)-**4.1** and the fluorescence spectrum of the DMSO solution of the polymer film was obtained. As shown in Figure **4.24**, the polymer film formed from (*R*)-**4.1** shows much greater fluorescence enhancement at λ = 545 nm. Polymer (*S*)-**3.9** alone is nonfluorescent in DMSO. Thus, the precipitate generated due to the cononsolvency of the polymer exhibits highly enantioselective fluorescence response.

Figure 4.24. Fluorescence spectra of (*S*)-**3.9** and the isolated polymer films dissolved in DMSO. Concentration: 10 μM. Two polymer films were obtained from the reaction (*S*)- and (*R*)-**4.1** respectively. (λ_{exc} = 320 nm. Excitation/Emission slit width: 5/5 nm)

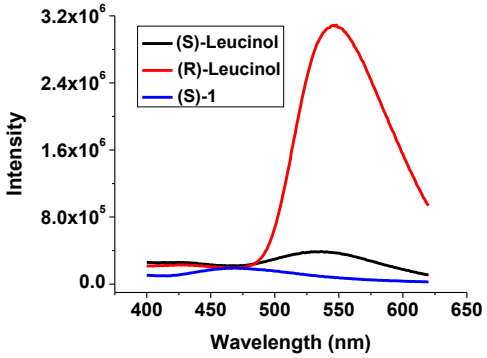

The effect of the concentration of the amino alcohol **4.1** on the fluorescence response of the polymeric probe was studied. The CH_2Cl_2 solutions (500 μL) of (*S*)- or (*R*)-**4.1** at various concentrations were mixed with the water solutions of $Zn(OAc)_2$ (2.0 mM, 200 μL) and (*S*)-**3.9** (1.0 mM, 200 μL). The mixtures were vigorously shaken and allowed to stand at room temperature for 6 h. As shown in Figure **4.25**, polymer films were generated at the interface of the two solvents. After the solvents of these samples were decanted, the polymer films were isolated and dissolved in DMSO (1 mL). These polymer solutions were then diluted to 10 μM with the addition of DMSO and their fluorescence spectra were obtained. As shown in Figure **4.26**, although (*S*)-**4.1** caused little change on the fluorescence of the polymer at various concentrations, (*R*)-**4.1** greatly enhanced the fluorescence of (*S*)-**3.9** when its concentration increased from 4 to 6 equiv. After the concentration of (*R*)-**4.1** was increased to over 6 equiv., the fluorescence enhancement reached a plateau. Thus, Figure **4.26** shows the highly enantioselective fluorescence response of (*S*)-**3.9** toward the chiral amino alcohol at various concentrations.

Figure 4.25. Photos of (*S*)-**4.1** (top) and (*R*)-**4.1** (bottom) in CH_2Cl_2 (various concentration, 500 μL) after they were vigorously mixed with immiscible water solution of (*S*)-**3.9** (1.0 mM, 200 μL) and $Zn(OAc)_2$ (2.0 mM, 200 μL) and set at room temperature for 6 h.

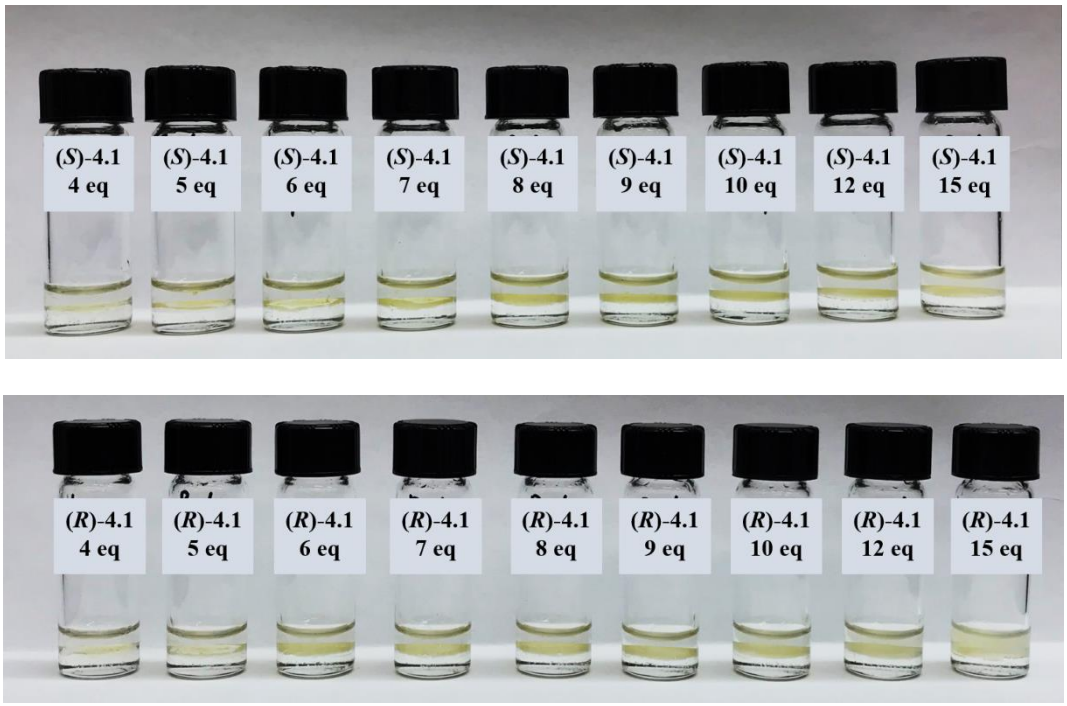

Figure 4.26. Fluorescence spectra of the polymer films in DMSO (10 μM) obtained from the reaction of (*S*)-**3.9** (1.0 mM in water, 200 μL, 1 equiv) and $Zn(OAc)_2$ (2.0 mM in water, 200 μL, 2 equiv) with the CH_2Cl_2 solution (500 μL, various equivalent) of (a) (*S*)-**4.1** and (b) (*R*)-**4.1** (λ_{exc} = 320 nm. Excitation/Emission slit width: 5/5 nm). (c) Fluorescence intensity at λ_{em} = 545 nm versus the equivalency of (*S*)- and (*R*)-**4.1**.

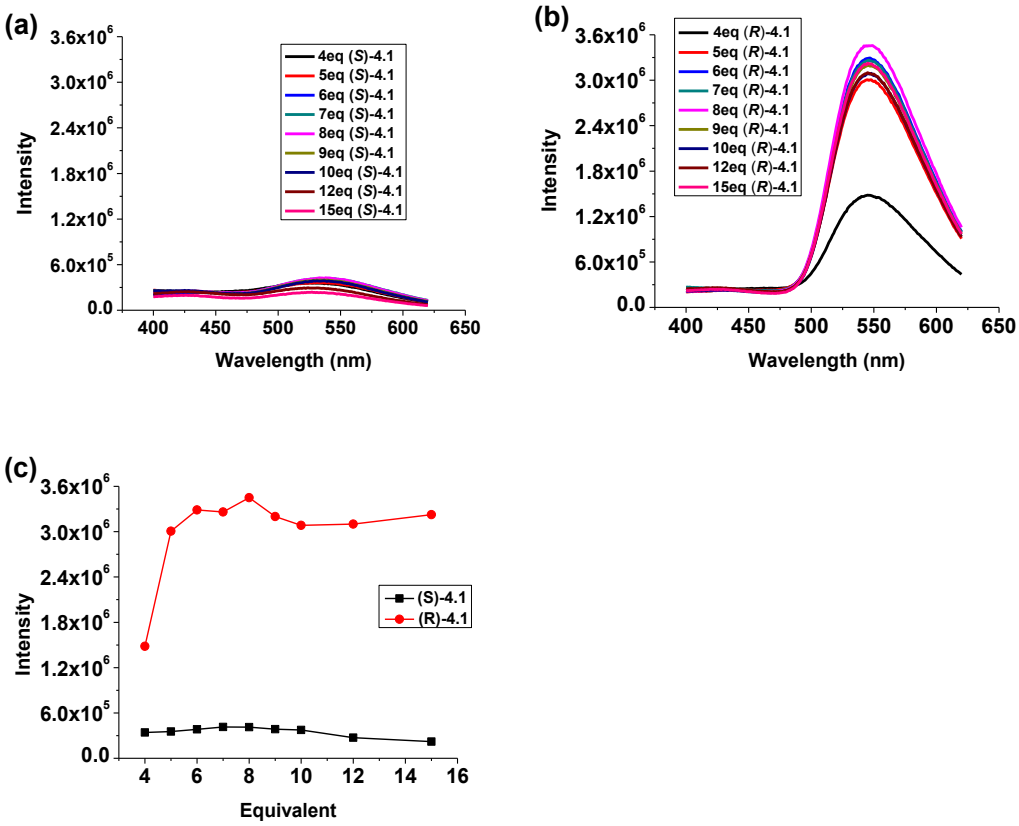

In order to ascertain that the observed fluorescence response of (*S*)-**3.9** toward (*S*)- and (*R*)-**4.1** was due to inherent chiral recognition, we prepared the enantiomer of the polymer, (*R*)-**3.9**, and studied the use of (*R*)-**3.9** to interact with the amino alcohol enantiomers under the same conditions. Polymer films also generated at the interface (Figure **4.27**). It was found that the DMSO solutions of the polymer films derived from the reaction of (*R*)-**3.9** with the amino alcohol (*S*)-**4.1** gave much higher fluorescence enhancement than those with (*R*)-**4.1**. That is, the fluorescence responses of (*R*)-**3.9** toward **4.1** are the mirror images of those of (*S*)-**2** (Figure **4.28**). This confirms the highly enantioselective nature of the polymer sensor in the fluorescent recognition of the amino alcohol.

Figure 4.27. Photos of (*S*)-**4.1** (top) and (*R*)-**4.1** (bottom) in CH_2Cl_2 (various concentration, 500 μL) after they were vigorously mixed with immiscible water solution of (*R*)-**3.9** (1.0 mM, 200 μL) and $Zn(OAc)_2$ (2.0 mM, 200 μL) and set at room temperature for 6 h.

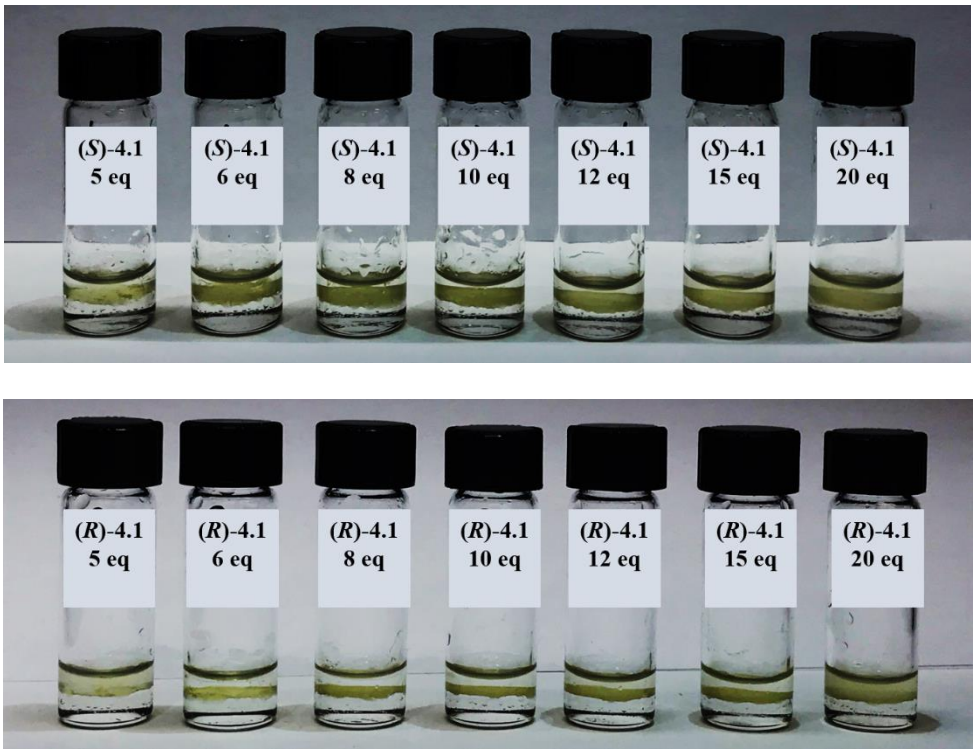

Figure 4.28. Fluorescence spectra of the DMSO solutions of polymer films obtained by mixing (*R*)-**3.9** (1.0 mM in water, 200 μL, 1 equiv.) and $Zn(OAc)_2$ (2.0 mM in water, 200 μL 2 equiv.) with the CH_2Cl_2 solutions (500 μL, various equivalency) of (*S*)-**4.1** or (*R*)-**4.1** (The mixtures were allowed to stand at room temperature for 6 h before the polymer films were separated. λ_{exc} = 320 nm. Excitation/Emission slit width: 5/5 nm). Fluorescence intensity at λ_{em} = 545 nm was used for equivalent versus fluorescence intensity figure.

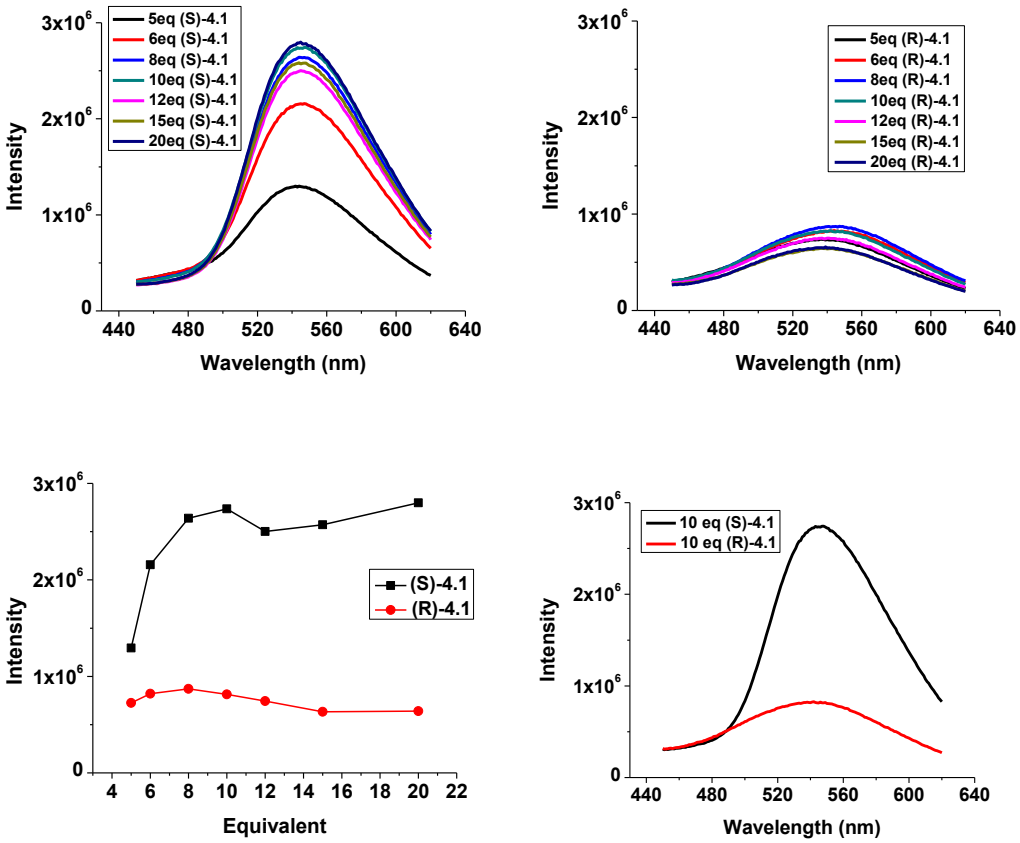

We then investigated the effect of the enantiomeric composition of the amino alcohol on the fluorescence response. The CH_2Cl_2 solutions of **4.1** (4.0 mM, 10 equiv, 500 μL) with various enantiomeric excess [*ee* = (*S*-*R*)/(*S*+*R*)] were mixed with the water solutions of $Zn(OAc)_2$ (2.0 mM, 200 μL) and (*S*)-**3.9** (1.0 mM, 200 μL). The mixtures were vigorously shaken and allowed to stand at room temperature for 6 h. The resulting polymer films at the solvent interface were then separated and dissolved in DMSO for fluorescence measurement. As shown in Figure **4.29**, when (*R*)-**4.1** is in excess in solution (*ee* < 0), the fluorescence intensity of the corresponding polymer film solution increases with the increased composition of the *R* enantiomer. However, when (*S*)-**4.1** is in excess (*ee* >0), little fluorescence enhancement was observed. Thus, there is a large nonlinear effect for the fluorescence response of the polymer toward the enantiomeric composition of the amino alcohol. We also studied the

use of the enantiomeric polymer (*R*)-**3.9** to interact with the amino alcohol at various *ee*s. As shown in Figure **4.30**, when the (*S*)-**4.1** is in excess in solution (*ee* > 0), the fluorescence intensity increases with the *ee* but there is little change in fluorescence intensity when (*R*)-**4.1** is in excess (*ee* < 0). Therefore, polymer (*S*)-**3.9** can be used to determine the *ee* of the amino alcohol when the (*R*)-amino alcohol is in excess, and (*R*)-**3.9** can be used to determine the *ee* when the (S)-amino alcohol is in excess.

Figure 4.29. (a) Fluorescence response of polymer films in DMSO (10 μM) that were derived from (*S*)-**3.9** (1.0 mM in water, 200 μL, 1 equiv) and $Zn(OAc)_2$ (2.0 mM in water, 200 μL, 2 equiv) mixing with **4.1** (4.0 mM in CH_2Cl_2, 500 μL, 10 eq) at various *ee* (The mixtures were allowed to stand at room temperature for 6 h and then separated. λ_{exc} = 320 nm. Excitation/Emission slit width: 5/5 nm). (b) Fluorescence intensity at λ_{em} = 545 nm versus various *ee*.

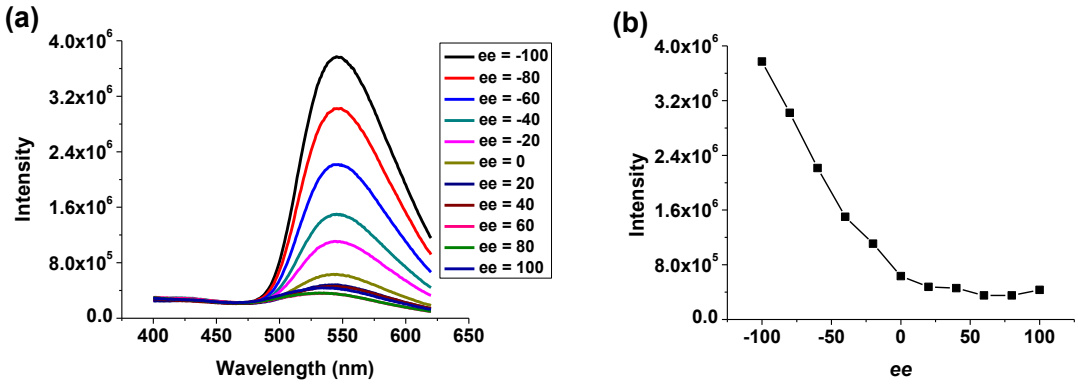

Figure 4.30. (a) Fluorescence response of polymer films in DMSO (10 μM) that were derived from (*R*)-**3.9** (1.0 mM in water, 200 μL, 1 equiv) and $Zn(OAc)_2$ (2.0 mM in water, 200 μL, 2 equiv) mixing with **4.1** (4.0 mM in CH_2Cl_2, 500 μL, 10 eq) at various *ee* (The mixtures were allowed to stand at room temperature for 6 h and then separated. λ_{exc} = 320 nm.

Excitation/Emission slit width: 5/5 nm). (b) Fluorescence intensity at λ_{em} = 545 nm versus various *ee*.

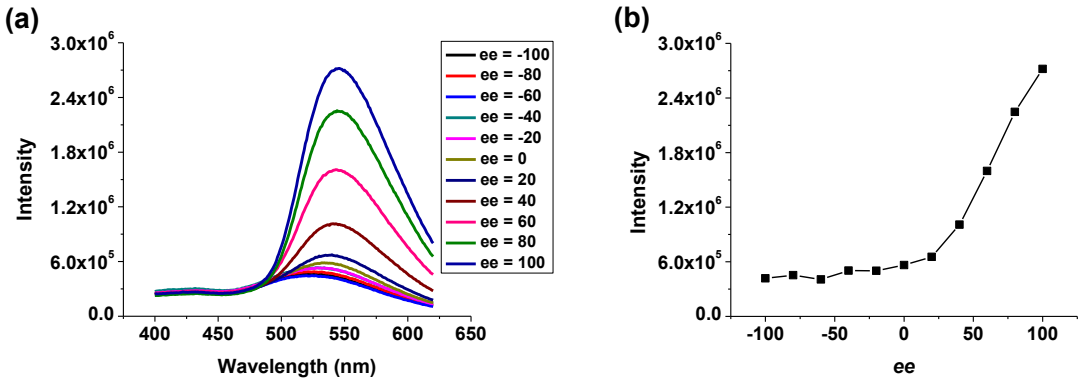

As demonstrated above, the cononsolvency of the PNIPAM-based BINOL sensor allows the sensor-substrate adduct to be readily separated from the original solution which should greatly reduce the interference of other components on the fluorescence measurement when the substrate is produced from a catalyst screening experiment.

Besides the amino alcohol **4.1**, we also studied the fluorescence response of (*S*)-**1** toward other amino alcohols including alaninol (**4.2**), 2-amino-1-butanol (**4.3**), valinol (**4.4**) and phenylalaninol (**4.5**). By using the same method described above, the mixtures with various amino alcohols could also produce polymer films at the interface. In addition, the polymer films derived from (*S*)- or (*R*)-amino alcohols all showed highly enantioselective fluorescence response in DMSO solutions (Figure **4.31**-**4.34**). Interestingly, the polymer solutions derived from valinol and phenylalaninol showed the opposite enantioselectivity in comparison with those derived from leucinol, alaninol and 2-amino-1-butanol. This demonstrates that the fluorescence of the probe is very sensitive to the structure of the amino alcohol substrates.

Figure 4.31. Fluorescence spectra of the DMSO solutions of polymer films obtained by mixing (*S*)-**3.9** (1.0 mM in water, 200 μL, 1 equiv.) and $Zn(OAc)_2$ (2.0 mM in water, 200 μL 2 equiv.)

with the CH_2Cl_2 solutions (500 μL, various equivalency) of (*S*)-**4.2** or (*R*)-**4.2** (The mixtures were allowed to stand at room temperature for 6 h before the polymer films were separated. λ_{exc} = 320 nm. Excitation/Emission slit width: 5/5 nm). Fluorescence intensity at λ_{em} = 549 nm was used for equivalent versus fluorescence intensity figure.

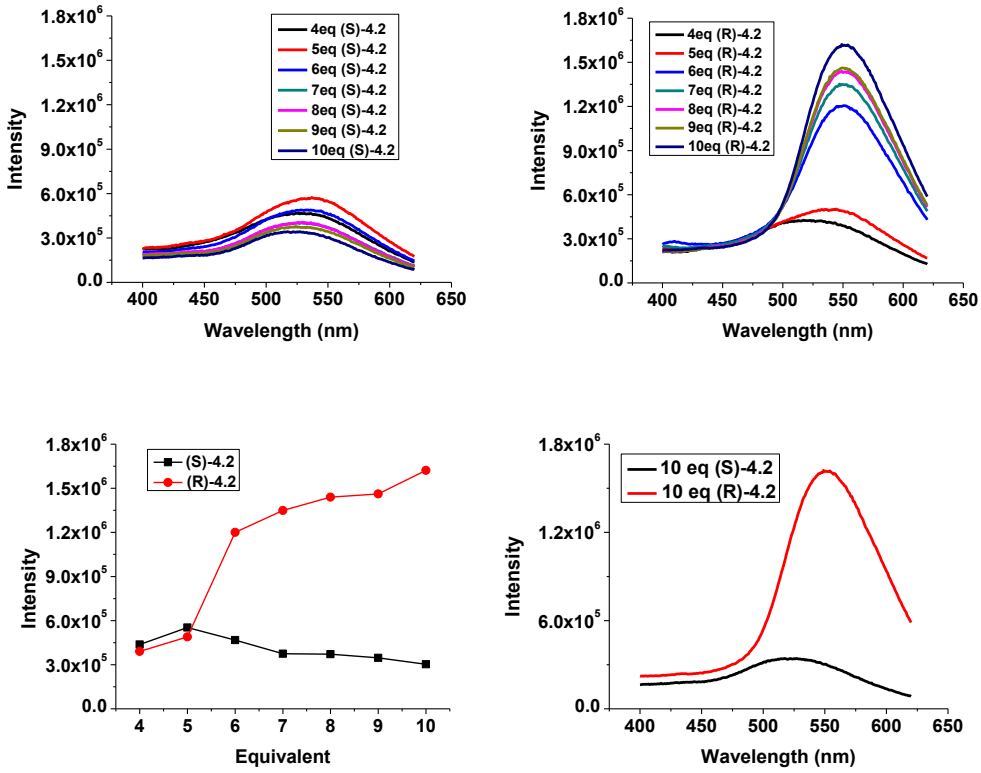

Figure 4.32. Fluorescence spectra of the DMSO solutions of polymer films obtained by mixing (*S*)-**3.9** (1.0 mM in water, 200 μL, 1 equiv.) and $Zn(OAc)_2$ (2.0 mM in water, 200 μL 2 equiv.) with the CH_2Cl_2 solutions (500 μL, various equivalency) of (*S*)-**4.3** or (*R*)-**4.3** (The mixtures were allowed to stand at room temperature for 6 h before the polymer films were separated. λ_{exc} = 320 nm. Excitation/Emission slit width: 5/5 nm). Fluorescence intensity at λ_{em} = 548 nm was used for equivalent versus fluorescence intensity figure.

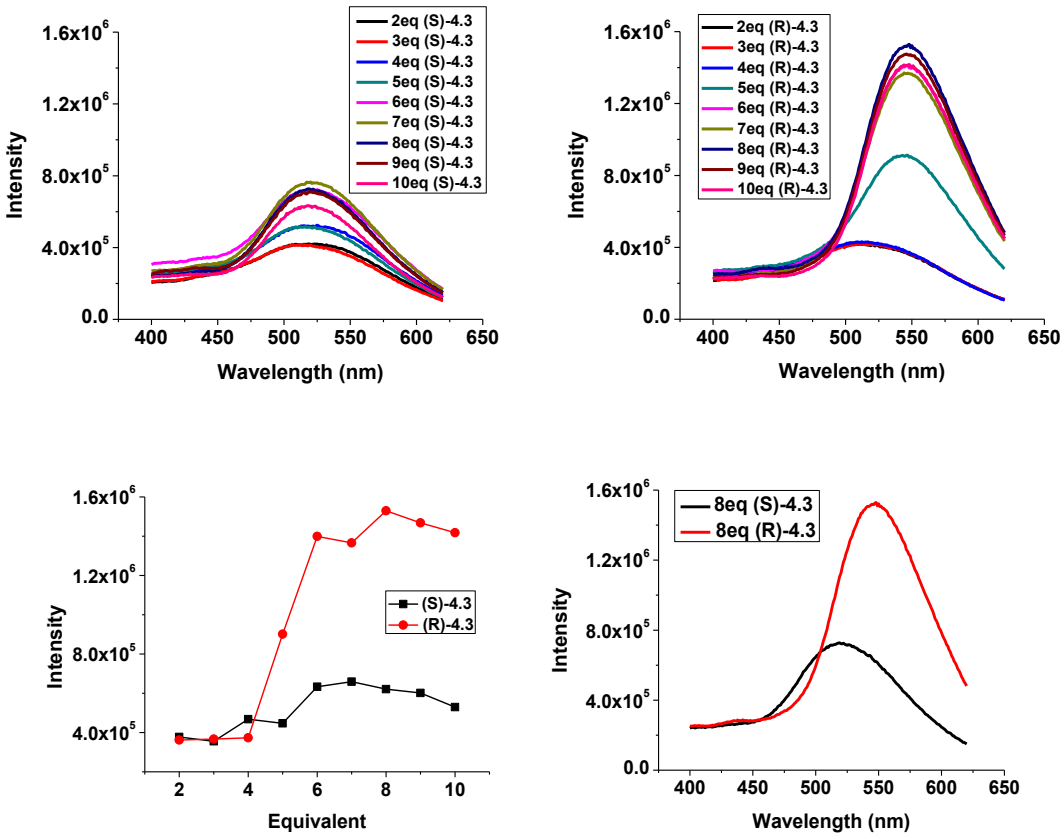

Figure 4.33. Fluorescence spectra of the DMSO solutions of polymer films obtained by mixing (*S*)-**3.9** (1.0 mM in water, 200 μL, 1 equiv.) and $Zn(OAc)_2$ (2.0 mM in water, 200 μL 2 equiv.) with the CH_2Cl_2 solutions (500 μL, various equivalency) of (*S*)-**4.4** or (*R*)-**4.4** (The mixtures were allowed to stand at room temperature for 6 h before the polymer films were separated. λ_{exc} = 320 nm. Excitation/Emission slit width: 5/5 nm). Fluorescence intensity at λ_{em} = 516 nm was used for equivalent versus fluorescence intensity figure.

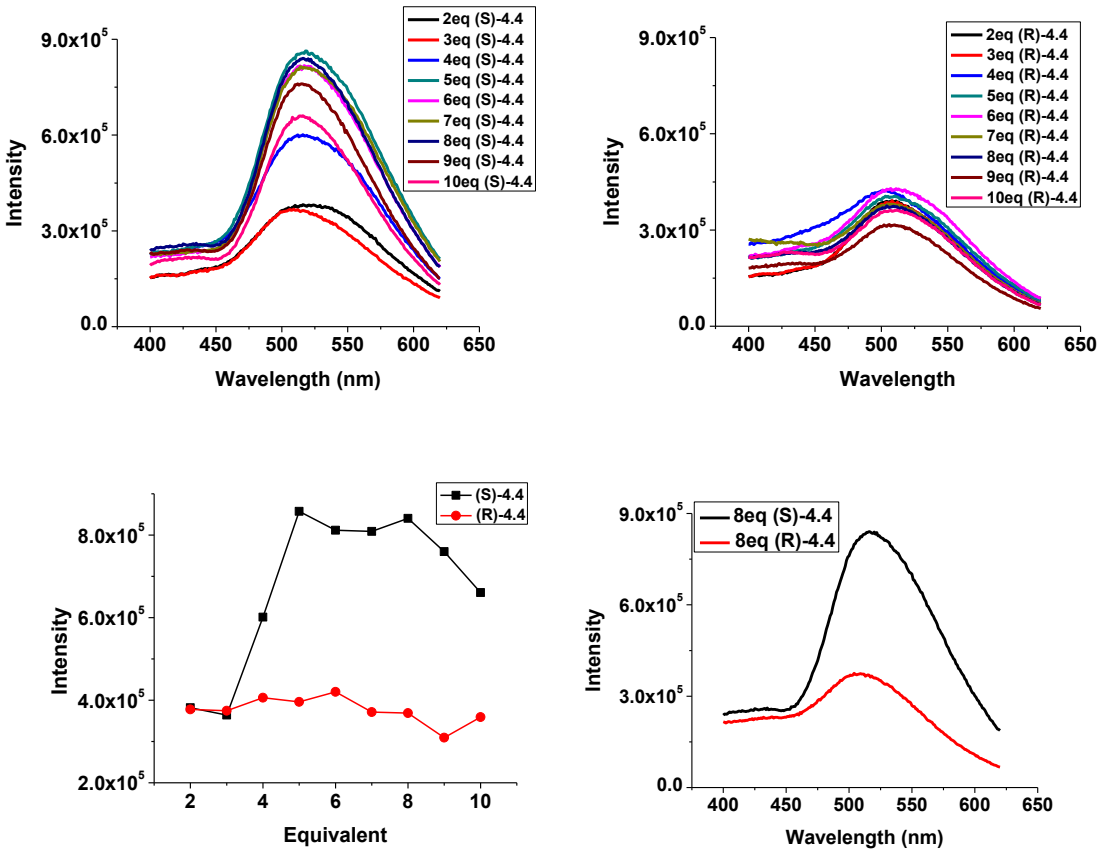

Figure 4.34. Fluorescence spectra of the DMSO solutions of polymer films obtained by mixing (*S*)-**3.9** (1.0 mM in water, 200 μL, 1 equiv.) and $Zn(OAc)_2$ (2.0 mM in water, 200 μL 2 equiv.) with the CH_2Cl_2 solutions (500 μL, various equivalency) of (*S*)-**4.5** or (*R*)-**4.5** (The mixtures were allowed to stand at room temperature for 6 h before the polymer films were separated. λ_{exc} = 320 nm. Excitation/Emission slit width: 5/5 nm). Fluorescence intensity at λ_{em} = 525 nm was used for equivalent versus fluorescence intensity figure.

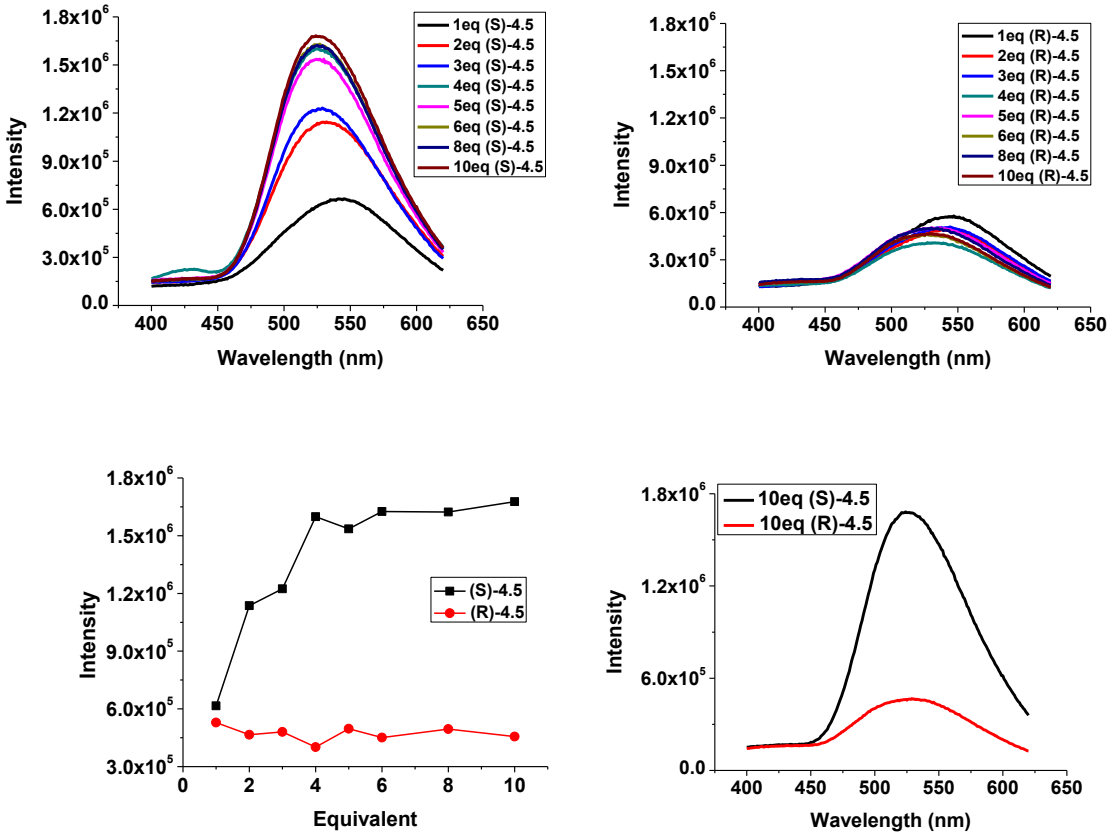

4.2.3. Determination of *ee* of leucinol using *Racemic* polymer probe

In the search of a sensitive as well as enantioselective fluorescent sensor, an enantiomerically pure molecular receptor (S_{Host} or R_{Host}) is generally designed and synthesized to interact with the enantiomers of the targeted chiral substrates (R_{Guest} or S_{Guest}). For example, when S_{Host} shows much greater fluorescence enhancement with R_{Guest} than with S_{Guest} because of the different fluorescence properties of the two diastereomeric interactions, S_{Host} will be identified as an enantioselective fluorescent probe for the guest molecule. It is also expected that when R_{Host} is used, S_{Guest} will generate much greater fluorescence enhancement than R_{guest} due to the mirror image relationship of the chiral materials. Thus, S_{Host} and R_{Host} can be used to determine the *ee* of a given guest sample. The racemic mixture of a fluorescent sensor was

never used to determine the *ee* of a chiral substrate since it is generally believed that a racemic host should be similar to an achiral host and its fluorescence could be sensitive to the total concentration of the substrate ($[R_{Guest}]+[S_{Guest}]$) but not to its enantiomeric composition.[4]

The unusual nonlinear fluorescence response in Figure **4.29** for the interaction of (*S*)-**3.9**+$Zn(OAc)_2$ with the amino alcohol at various *ee*s demonstrates that the fluorescence of (*S*)-**3.9** cannot be turned on by the racemic amino alcohol. Only when (*R*)-**4.1** is in excess of (*S*)-**4.1**, can there be fluorescence enhancement. On the basis of this discovery, we proposed that when the racemic probe *Rac*-**3.9**+$Zn(OAc)_2$ is used to interact with the amino alcohol under the same conditions, there should be fluorescence enhancement only when either (*R*)- or (*S*)-**4.1** is in excess. The racemic amino alcohol, *Rac*-**4.1**, will not be able to turn on the fluorescence of *Rac*-**3.9**.

In order to test the above hypothesis, we synthesized the racemic polymer **3.9**, *Rac*-**3.9** (Figure **4.35**), by using the racemic compound *Rac*-**3.9** ($[\alpha]_D$ = 0.0 in CH_2Cl_2, c = 0.40) to initiate the ATRP of *N*-isopropylacrylamide in the presence of Me_6TREN and CuCl in isopropanol at room temperature. GPC analysis shows the molecular weight of this polymer as M_n = 4000 and M_w = 5000, PDI = 1.25. $[\alpha]_D$ = 0.0 (c = 0.40, CH_2Cl_2). The solubility of this racemic polymer is similar to that of (*S*)-**3.9**.

Figure 4.35. Structure of *Racemic* **3.9**

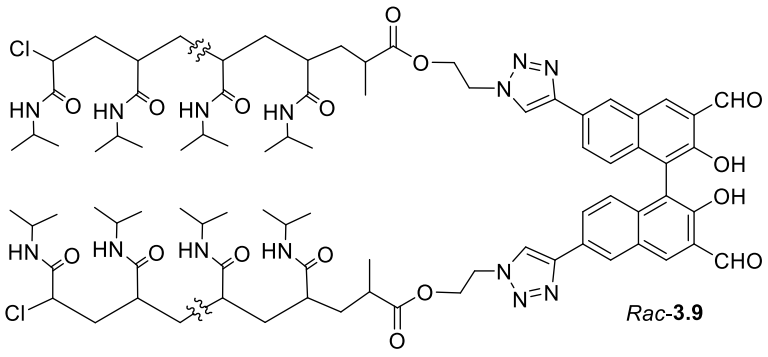

Fluorescence response of *Rac*-**3.9** toward the amino alcohol **4.1** with various *ee* values was investigated. Polymer films were obtained by mixing *Rac*-**3.9** (1.0 mM in water, 200 μL, 1 equiv) and $Zn(OAc)_2$ (2.0 mM in water, 200 μL, 2 equiv) with (*S*)-**4.1** or (*R*)-**4.1** or various mixtures of (*S*)-**4.1** and (*R*)-**4.1** in CH_2Cl_2. The fluorescence intensity of the isolated polymer films at λ_{em} = 545 nm in DMSO solution is plotted against the concentration of (*S*)-**4.1** or (*R*)-**4.1** in Figure **4.36a**. As expected, *Rac*-**3.9** shows the same fluorescence enhancement with the two enantiomers of the amino alcohol. However, when mixtures of (*S*)-**4.1** and (*R*)-**4.1** with various *ee*s [concentration of (*S*)-**4.1** + (*R*)-**4.1**: 10 equiv] were used, the fluorescence intensity of the racemic polymer-based films was found to be linearly related with the *ee*s as shown in Figure 6b-d. The racemic amino alcohol (*ee* = 0) cannot turn on the fluorescence. Figure **4.36b** gives a V shaped plot for the fluorescence intensity of *Rac*-**3.9**+$Zn(OAc)_2$ versus the ± *ee* of the amino alcohol.

Figure 4.36. Fluorescence intensity at λ_{em} = 545 nm for the polymer films in DMSO (10 μM) obtained from the reaction of *Rac*-**3.9** (1.0 mM in water, 200 μL, 1 equiv) and $Zn(OAc)_2$ (2.0 mM in water, 200 μL, 2 equiv) (a) with 500 μL (*S*)-**4.1** or (*R*)-**4.1** in CH_2Cl_2 versus their equivalency; (b) with **4.1** versus its *ee*s (c) Fluorescence intensity versus the *ee* of **4.1** [(*R*)-**4.1** in excess]. Linear fit curve: Y = 821143 + 16747X, R^2 = 0.9892. (d) Fluorescence intensity versus the *ee* of **4.1** [(*S*)-**4.1** in excess]. Linear fit curve: Y = 758894 + 18689X, R^2 = 0.9793. (The error bars are obtained from three independent measurement)

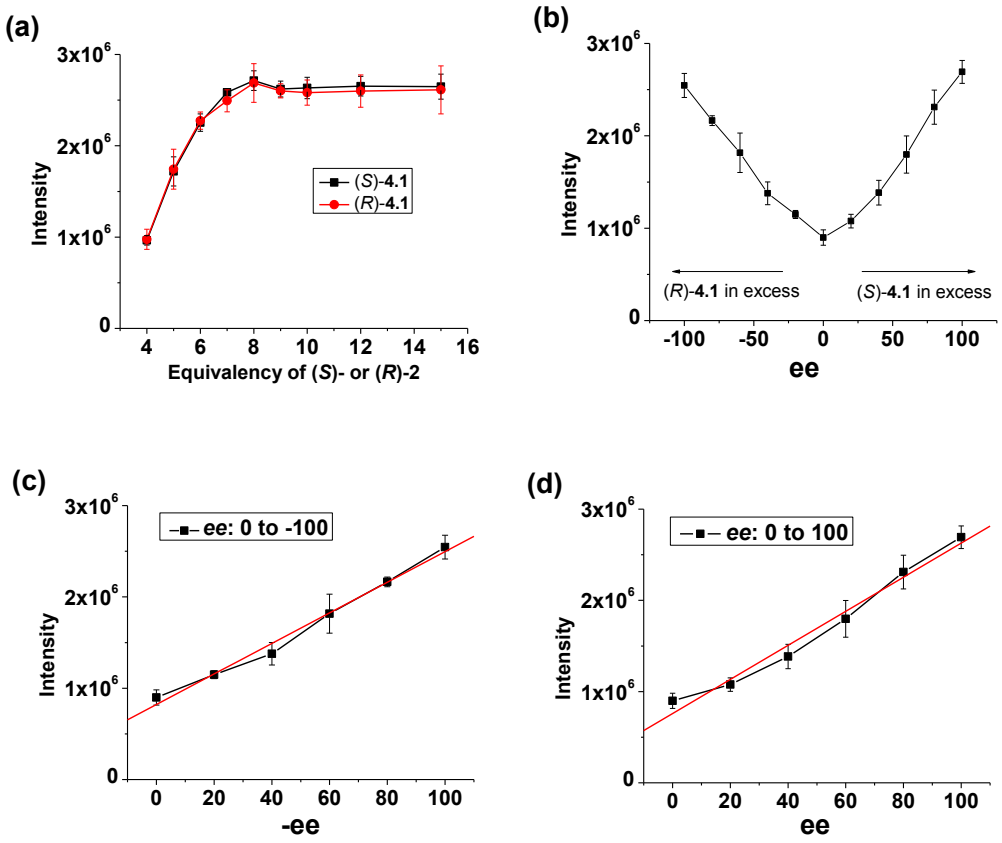

In order to demonstrate the application of this method, we used *Rac*-**3.9** (1.0 mM in water, 200 μL, 1 equiv) in combination with $Zn(OAc)_2$ (2.0 mM in water, 200 μL, 2 equiv) to measure the *ee*s of 6 samples of the amino alcohol **4.1** (500 μL, concentration of (*S*)-**4.1** + (*R*)-**4.1**: 10 equiv). As shown in Table **4.1**, by using Figure **4.36c,d**, the *ee*s of these samples are determined. The measured data are very close to the actual value of the absolute *ee*s. Thus, using the racemic fluorescent probe *Rac*-**1**, we can determine the *ee* of the amino alcohol.

Table 4.1. Determination of absolute *ee* value of test samples by using Figure **4.36c** and **4.36d**

Sample *ee* (%)	-90	-70	-30	15	50	85
Determined by using Figure 6c (%)	92	75	33	16	53	92
Error	2%	7%	10%	7%	6%	8%
Determined by using Figure 6d (%)	86	70	33	18	51	86
Error	4%	0	10%	20%	2%	1%

Reaction and fluorescence measurement condition: *Rac*-**3.9** (1.0 mM in water, 200 μL, 1 equiv) and $Zn(OAc)_2$ (2.0 mM in water, 200 μL, 2 equiv) were mixed with amino alcohol **4.1** (500 μL, concentration of (*S*)-**4.1** + (*R*)-**4.1**: 10 equiv) (Reaction time: 2 h, then polymer films were dissolved in DMSO to 10 μM for fluorescence measurement. λ_{exc} = 320 nm. Excitation/Emission slit width: 5/5 nm).

We used the UV-vis absorption of the polymer to quantify the amount of the polymer aggregated at the interface of water and CH_2Cl_2. *Rac*-**3.9** (1.0 mM in water, 2 mL, 1 equiv.) and $Zn(OAc)_2$ (2.0 mM in water, 2 mL, 2 equiv.) were mixed with (*S*)-**4.1** (4.0 mM in CH_2Cl_2, 5 mL, 10 equiv.). After the polymer film was formed in 6 h, the water and CH_2Cl_2 layers were separated for UV-vis measurement. The concentrations of the remaining polymer in water and CH_2Cl_2 layers were determined to be 0.030 mM and 0.050 mM, respectively by comparing with the UV-vis spectra of the polymer in these solvents (Figure **4.37** and **4.38**). This demonstrates that about 92% of the polymer aggregated at the interface, indicating the high efficiency of the cononsolvency-based separation.

Figure 4.37. UV-Vis spectra of *Rac*-**3.9** in CH_2Cl_2 with different concentration (0.1 mM and 0.01 mM) and CH_2Cl_2 layer after the formation of polymer film.

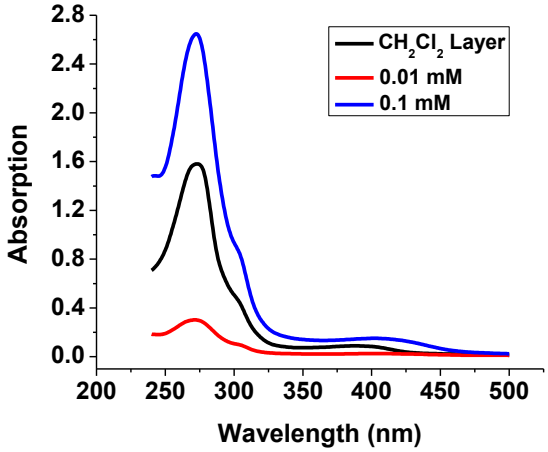

Figure 4.38. UV-Vis spectra of *Rac*-**3.9** in water with different concentration (0.1 mM and 0.01 mM) and water layer after the formation of polymer film.

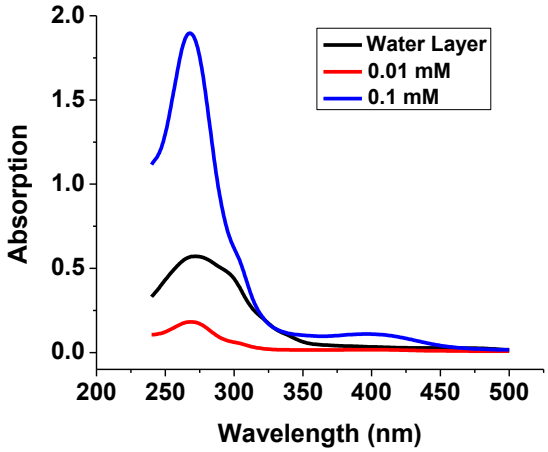

4.2.4. ^{1}H-NMR study on fluorescent recognition mechanism

To better elucidate the structure of the polymer films, we synthesized four salicylaldimines **4.6-4.9** (Scheme **4.1**) and conducted ^{1}H-NMR study on both salicylaldimines+Zn^{2+} and the corresponding polymer films.

Scheme 4.1. Synthesis of the BINOL-Based diastereomeric salicylaldimines **4.6-4.9**

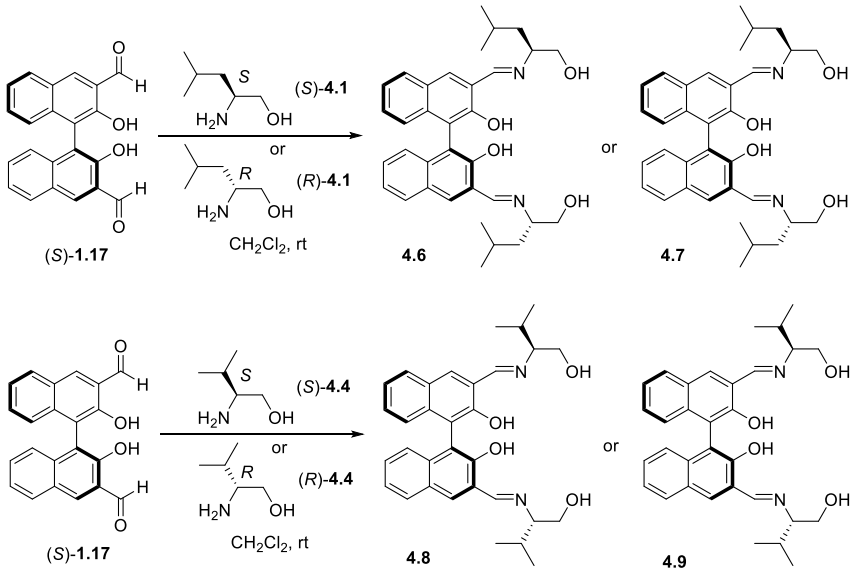

For NMR study of salicylaldimines, **4.6**-**4.9** (200 μL, 20 mM in DMSO-d_6) was mix with $Zn(OAc)_2$ (200 μL, 40 mM in DMSO-d_6). Then ^{1}H-NMR spectra were acquired after 2 h. For NMR study of polymer films, (*S*)-**3.9** (4 mL, 1 mM in water, 1 equiv.) was mixed with Zn $(OAc)_2$ (4 mL, 2 mM in water, 2 equiv.) and (*S*)- or (*R*)-**4.1** or **4.4** (10 mL, 4 mM in CH_2Cl_2, 10 equiv.). The mixture was allowed to stand at room temperature for 6 h, and the polymer films at the interface were separated and dried under vacuum. Then the polymer films were dissolved in 400 μL DMSO-d_6 to make 10 mM solution and NMR spectra were acquired.

From NMR spectra, the difference between polymer films and the similarity between the salicylaldimine-Zn^{2+} adduct and the corresponding polymer films were revealed between -1 to 1 ppm region. In **4.6**-Zn^{2+} spectra, a doublet at 0.22 ppm was appeared after adding Zn^{2+}. Similarly, (*S*)-**4.1** polymer film spectra showed two peaks at 0.34 and 0 ppm (Figure **4.39**). The **4.7**-Zn^{2+} and (*R*)-**4.1** polymer film spectra both showed peaks at around 0.65 ppm and 0.85 ppm, respectively (Figure **4.40**). For **4.8**-Zn^{2+} and (*S*)-**4.4** polymer film, multiple peaks between -1.00 to 0.50 ppm appeared on both spectra (Figure **4.41**). In **4.9**-Zn^{2+} spectra, there is a single peak at 0.32 ppm. In (*R*)-**4.4** polymer film spectra, there is also a single peak at -0.75 ppm

(Figure **4.42**). In addition, the peak at around 13.50 ppm in polymer film NMR spectra corresponds to the proton in the hydroxy group of BINOL core. The large chemical shift was due to the hydrogen bonding between the hydrogen and the nitrogen, indicating the formation of imine bond. This peak can also be found in small molecule-Zn^{2+} spectra at around 13.05 ppm. Figure **4.43** was the comparison of (*S*)- and (*R*)-**4.1** polymer films, Figure **4.44** was the comparison of (*S*)- and (*R*)-**4.4** polymer films. The difference between the polymer films were obvious between -1 to 1 ppm.

Figure 4.39. ^{1}H NMR spectra of 10 mM **4.6** mixed with 2 eq $Zn(OAc)_2$ in DMSO-d_6 after 2 h and 10 mM (*S*)-**4.1** polymer film in DMSO-d_6.

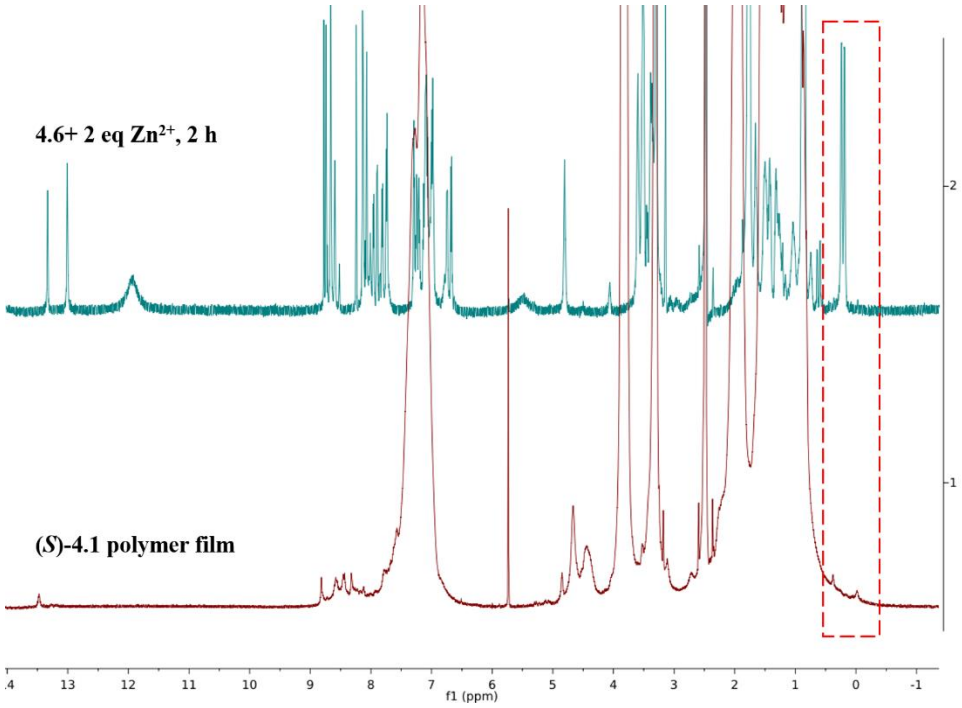

Figure 4.40. ^{1}H NMR spectra of 10 mM **4.7** mixed with 2 eq $Zn(OAc)_2$ in DMSO-d_6 after 2 h and 10 mM (*R*)-**4.1** polymer film in DMSO-d_6.

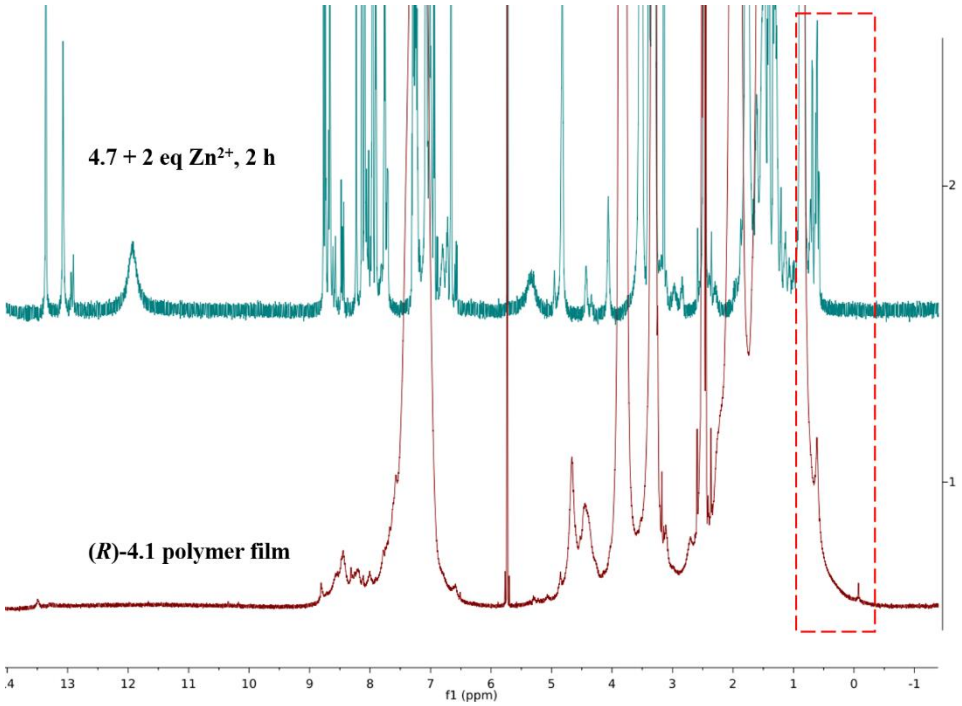

Figure 4.41. ^{1}H NMR spectra of 10 mM **4.8** mixed with 2 eq $Zn(OAc)_2$ in DMSO-d_6 after 2 h and 10 mM (*S*)-**4.4** polymer film in DMSO-d_6.

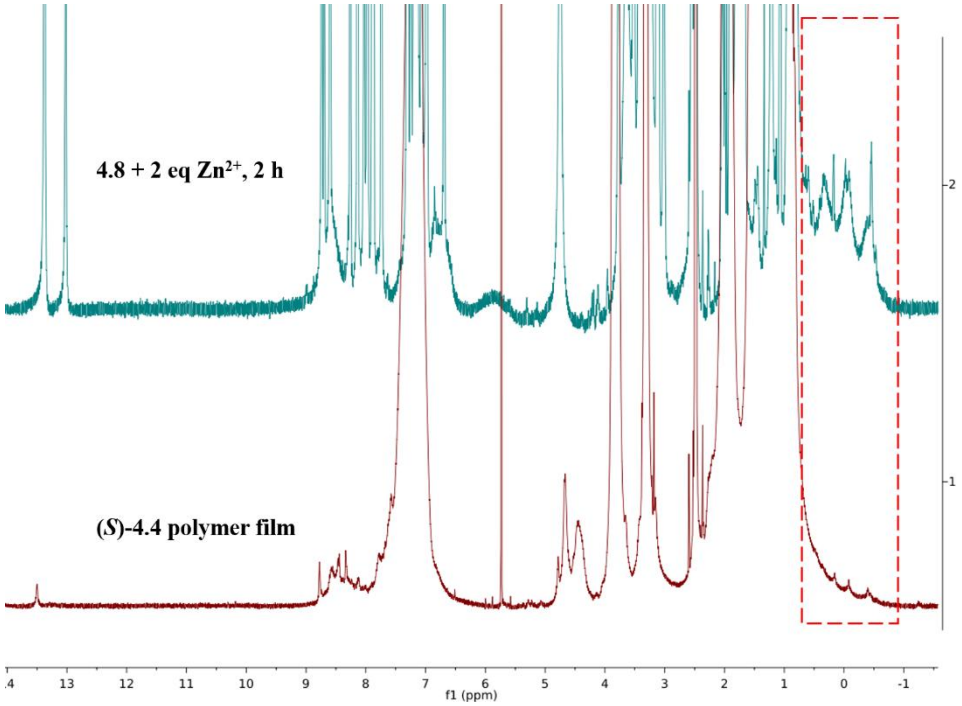

Figure 4.42. ^{1}H NMR spectra of 10 mM **4.9** mixed with 2 eq $Zn(OAc)_2$ in DMSO-d_6 after 2 h and 10 mM (*R*)-**4.4** polymer film in DMSO-d_6.

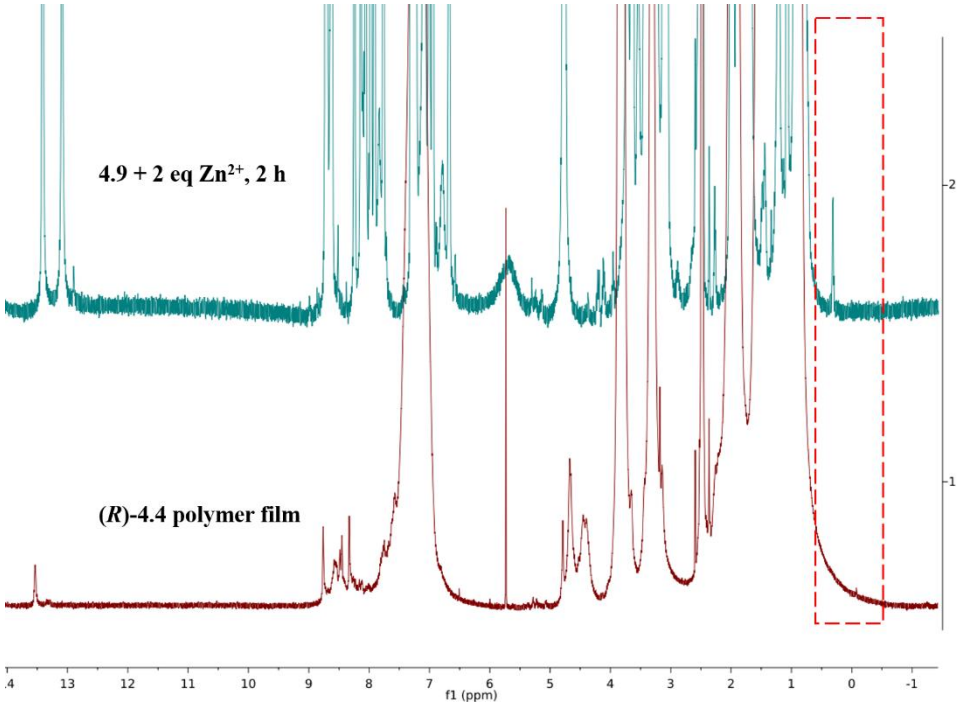

Figure 4.43. ^{1}H NMR spectra of (*S*)-**3.9** and two polymer films that were derived from (*S*)-**4.1** or (*R*)-**4.1** (Solvent: DMSO-d_6. Concentration: 10 mM. The intense signals of the PNIPAM backbone at δ = 1–6 are removed for clarity).

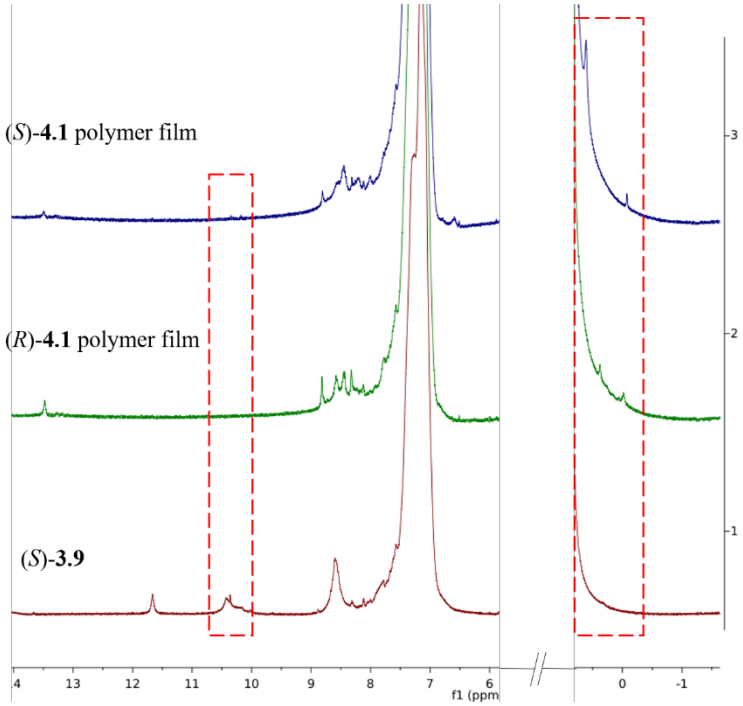

Figure 4.44. ^{1}H NMR spectra of (*S*)-**3.9** and two polymer films that were derived from (*S*)-**4.4** or (*R*)-**4.4** (Solvent: DMSO-d_6. Concentration: 10 mM. The intense signals of the PNIPAM backbone at δ = 1–6 are removed for clarity).

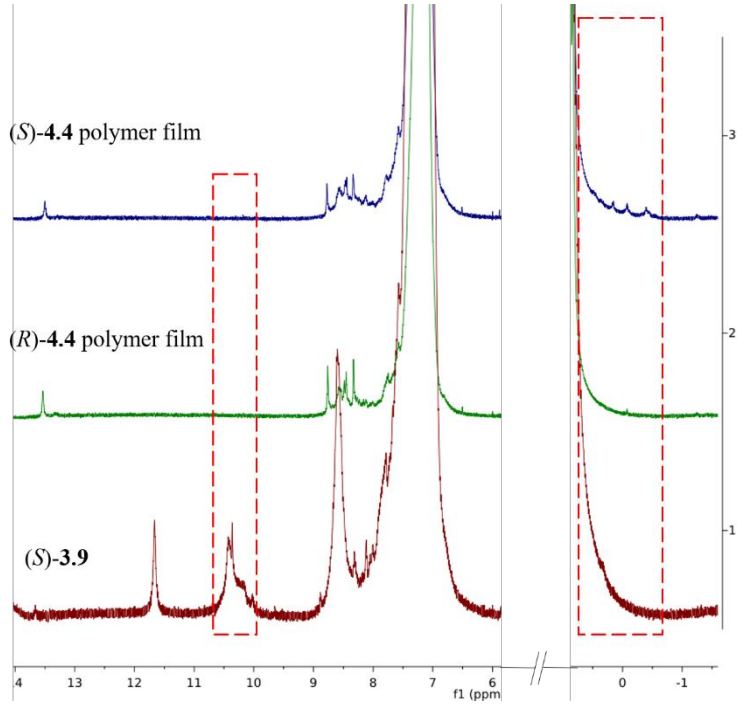

In Chapter 3, we introduced that the salicyaldimine compound **3.28** can coordinate with Zn(II) to form the structurally rigid [2+2] complex **3.29** and the further Zn(II) coordinated **3.29**+Zn(II) [2+3] complex, giving greatly enhanced fluorescence (Figure **4.45**).[12] On the basis of this observation and NMR spectra, we concluded that the condensation of the aldehyde groups of the polymer with the amino alcohols formed the corresponding salicyaldimine compound but the structure of the Zn(II) complex cannot be determined.

We also proposed that the observed large nonlinear effect for the fluorescence response of the polymeric sensor with the *ee* of the amino alcohol could be attributed to the selective formation of the dimeric structures like **3.29** and **3.29**+Zn(II) complexes. When the chirality of the amino alcohol unit matches that of the BINOL unit, large fluorescence enhancement can be observed due to the formation of these structurally rigid complexes.

Figure 4.45. Structure of 3.28 and 3.29

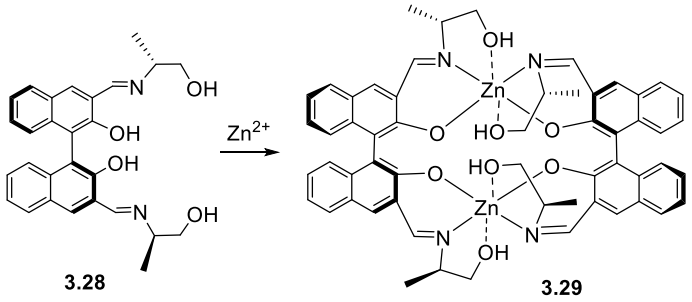

3.28 3.29

Thus, when *Rac*-**3.9** is used, only when one of the enantiomers of **4.1** is in excess, can it react with the chirality matched enantiomer of the polymer in the racemic mixture to form the structurally rigid and higher ordered complexes with Zn^{2+} to give enhanced fluorescence. When the racemic amino alcohol is used to interact with the racemic probe, formation of the chirality mismatched and structurally flexible complexes may be more favorable to give little fluorescence enhancement.

4.3. Conclusion

Fluorescent recognition of various amino alcohols was achieved in water and organic solvents with high enantioselectivity by using the PNIPAM-BINOL-based probes. In addition, contrary to the common intuition, we have demonstrated that a racemic fluorescent probe can be used to determine the *ee* of a chiral substrate. This is made possible because of a large nonlinear effect between the fluorescence response of the probe and the *ee* of the chiral substrate. We found that the poly(*N*-isopropylacrylamide)-based BINOL aldehyde can react with amino alcohols and Zn(II) and the resulting product forms polymeric films at the interface of the two immiscible solvents of water and CH_2Cl_2 due to a highly efficient cononsolvency effect. This allows the polymeric product to be easily separated which shows highly enantioselective fluorescence enhancement in DMSO solution. No fluorescence enhancement was observed unless one enantiomer of the amino alcohol substrate is in excess of another enantiomer. The easy separation of the substrate from its original solution by using the cononsolvency of the polymer-based sensor described here makes this method potentially useful in reaction screening since it can minimize the interference of other reaction components on the fluorescent analysis of the product.

4.4. Experimental part

4.4.1. General Information

All reactions were carried out under N_2 unless otherwise noted. All chemicals were purchased from Sigma Aldrich, Alfa Aesar or Thermo Fisher Scientific. Optical rotations were measured on a Jasco P-2000 digital polarimeter. NMR spectra were recorded on Varian-600 MHz spectrometer. Chemical shifts for ^{1}H NMR spectra were reported in parts per million relative to a singlet at 7.26 ppm for deuterated chloroform, and a singlet at 2.50 ppm for deuterated DMSO. Chemical shifts for ^{13}C NMR were reported relative to the centerline of a triplet at 77.16 ppm for deuterated chloroform. Steady-state fluorescence emission spectra were recorded on Horiba FluoroMax-4 spectrofluorometer. High-resolution mass spectra were obtained from the University of Illinois at Urbana-Champaign (UIUC) Mass Spectrometry Facility. Gel permeation chromatography (GPC) measurements were performed on an Agilent 1260 (LC) system with two Agilent PLgel 5 μm MIXED-C GPC columns in series at 40 °C and a flow rate of 1 mL/min. HPLC grade tetrahydrofuran (THF) stabilized with BHT (anhydrous, purchased from Thermo Fisher Scientific) was used as the eluent. An Agilent Infinity II refractive index detector was set at 40 °C for polymer analysis. pH measurements were performed on a Fisher Scientific accumet AB15 pH meter. Lower critical solution temperature (LCST) was measured using J-KEM Scientific Model Apollo temperature controller system. UV-Vis spectra were measured by Shimadzu UV-2600 UV-Vis spectrometer.

4.4.2. Synthesis and characterization of compounds

Atom transfer radical polymerization of *N*-isopropylacrylamide initiated by *Rac*-3.8. *N*-Isopropylacrylamide (2.0 mmol, 226.3 mg) was dissolved in 500 μL isopropanol. Tris[2-

(dimethylamino)ethyl]amine (Me_6TREN) (0.040 mmol, 10.7 μL) was added. The mixture was degassed by three freeze-pump-thaw cycles. Under nitrogen, CuCl (0.040 mmol, 4.0 mg) was added and the mixture was stirred for 15 min. Then, *Rac*-**3.8** (0.020 mmol, 14.9 mg) was added. And the reaction mixture was stirred under nitrogen at room temperature for 48 h. The reaction mixture was exposed to air, diluted by THF and passed through a short neutral alumina column to remove the catalyst. The collected eluent was concentrated and added to diethyl ether (100 mL) dropwise to precipitate out the poly(*N*-isopropylacrylamide) *Rac*-**3.9** which was isolated by centrifugation. The polymer was further dissolved in THF and precipitated in diethyl ether for two more times to fully remove trace amount of monomers. Isolated yield: 30%. GPC data: M_n = 4000, M_w = 5000, PDI = 1.25. $[\alpha]_D$ = 0 (c = 0.40, CH_2Cl_2).

(*S*)-3,3'-bis((*E*)-(((*S*)-1-hydroxy-4-methylpentan-2-yl)imino)methyl)-[1,1'-binaphthalene]-2,2'-diol, 4.6

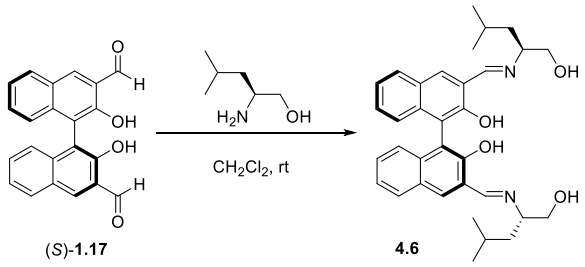

(*S*)-**1.17** **4.6**

Compound **4.6** was synthesized by modifying the reported procedure.[14] (*S*)-**1.17**[15] (58.7 mg, 0.17 mmol) and (*S*)-leucinol (44.2 mg, 0.38 mmol) were dissolved in 10 mL dry dichloromethane (CH_2Cl_2) under nitrogen, and the mixture was stirred at room temperature overnight. After evaporation of the solvent, the crude product was purified by recrystallization in methanol, which gave orange bulk crystals upon slow cooling. The crystals were filtered and

washed with a minimum amount of methanol. After drying under vacuum, **4.6** was obtained in 65% yield (60.1 mg). ^{1}H NMR (600 MHz, $CDCl_3$) δ 13.05 (s, 2H), 8.67 (s, 2H), 8.00 (s, 2H), 7.88 (m, 2H), 7.32-7.30 (m, 4H), 7.23-7.21 (m, 2H), 3.72-3.69 (m, 2H), 3.64-3.61 (m, 2H), 3.49-3.46 (m, 2H), 1.63-1.58 (m, 4H), 1.54-1.49 (m, 2H), 1.32-1.26 (m, 2H), 0.88 (d, J = 6.6 Hz, 12H). ^{13}C NMR (151 MHz, $CDCl_3$) δ 165.91, 154.69, 135.40, 133.78, 129.05, 128.61, 127.73, 124.92, 123.60, 120.93, 116.69, 70.28, 66.53, 40.95, 24.42, 23.57, 21.63. HRMS Calcd for $C_{34}H_{41}N_2O_4$ (MH^+): 541.3066. Found: 541.3063.

(*S*)-3,3'-bis((*E*)-(((*R*)-1-hydroxy-4-methylpentan-2-yl)imino)methyl)-[1,1'-binaphthalene]-2,2'-diol, 4.7

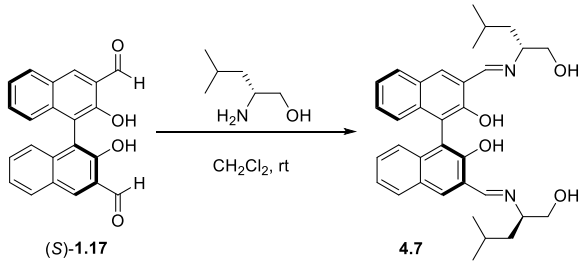

(*S*)-**1.17** **4.7**

The procedure was similar to the preparation of **4.6**, but (*R*)-leucinol (instead of (*S*)-leucinol) was used. After evaporation of the solvent, the crude product was purified by recrystallization in methanol, which gave yellow bulk crystals upon slow cooling. The crystals were filtered and washed with a minimum amount of methanol. After drying under vacuum, **4.7** was obtained in 50% yield (46.2 mg). ^{1}H NMR (600 MHz, $CDCl_3$) δ 13.42 (s, 2H), 8.67 (s, 2H), 7.98 (s, 2H), 7.88-7.86 (m, 2H), 7.31-7.29 (m, 4H), 7.20-7.18 (m, 2H), 3.62-3.58 (m, 4H), 3.47-3.44 (m, 2H), 2.90 (s, 2H), 1.56-1.54 (m, 2H), 1.48-1.46 (m, 2H), 1.27-1.24 (m, 2H), 0.86 (dd, J = 13.3, 6.6 Hz, 12H). ^{13}C NMR (151 MHz, $CDCl_3$) δ 165.78, 154.78, 135.31, 133.51, 129.05, 128.46,

127.74, 125.01, 123.51, 120.89, 116.69, 70.06, 66.36, 40.91, 24.52, 23.58, 21.65. HRMS Calcd for $C_{34}H_{41}N_2O_4$ (MH^+): 541.3066. Found: 541.3080.

(*S*)-3,3'-bis((*E*)-(((*S*)-1-hydroxy-3-methylbutan-2-yl)imino)methyl)-[1,1'-binaphthalene]-2,2'-diol, 4.8

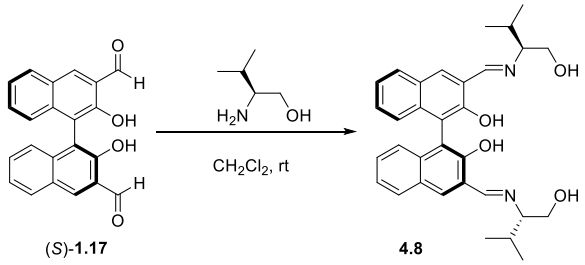

(*S*)-**1.17** 4.8

(*S*)-**1.17** (53.8 mg, 0.16 mmol) and (*S*)-valinol (35.7 mg, 0.35 mmol) were dissolved in 10 mL dry dichloromethane (CH_2Cl_2) under nitrogen, and the mixture was stirred at room temperature overnight. After evaporation of the solvent, the crude product was dissolved in 20 mL toluene and extracted with water (3 × 20 mL) to removed unreacted valinol. The organic layer was washed with brine and dried over anhydrous Na_2SO_4. After the evaporation of solvent, **4.8** was obtained as orange solid in 80% yield (64.4 mg). ^{1}H NMR (600 MHz, $CDCl_3$) δ 12.99 (s, 2H), 8.63 (s, 2H), 8.00 (s, 2H), 7.90-7.88 (m, 2H), 7.32-7.30 (m, 4H), 7.23-7.21 (m, 2H), 3.81-3.79 (m, 2H), 3.72-3.69 (m, 2H), 3.11-3.09 (m, 2H), 1.93-1.87 (m, 2H), 1.68 (s, 2H), 0.93 (dd, J = 20.6, 6.7 Hz, 12H). ^{13}C NMR (151 MHz, $CDCl_3$) δ 166.21, 154.77, 135.35, 133.85, 129.03, 128.54, 127.69, 124.88, 123.52, 120.94, 116.63, 78.32, 64.43, 30.25, 19.74, 18.96. HRMS Calcd for $C_{32}H_{37}N_2O_4$ (MH^+): 513.2753. Found: 513.2762.

(*S*)-3,3'-bis((*E*)-(((*R*)-1-hydroxy-3-methylbutan-2-yl)imino)methyl)-[1,1'-binaphthalene]-2,2'-diol, 4.9

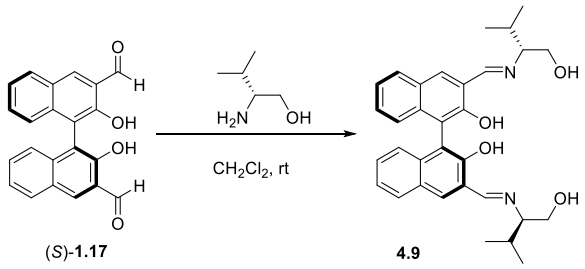

(*S*)-**1.17** **4.9**

The procedure was similar to the preparation of **4.8**, but (*R*)-valinol (instead of (*S*)-valinol) was used. **4.9** was obtained as orange solid in 78% yield (62.4 mg). ^{1}H NMR (600 MHz, $CDCl_3$) δ 13.36 (s, 2H), 8.64 (s, 2H), 7.97 (s, 2H), 7.87-7.85 (m, 2H), 7.30-7.28 (m, 4H), 7.19-7.17 (m, 2H), 3.75-3.67 (m, 4H), 3.12-3.09 (m, 2H), 2.92 (s, 2H), 1.85-1.82 (m, 2H), 0.89 (dd, J = 22.6, 6.8 Hz, 12H). ^{13}C NMR (151 MHz, $CDCl_3$) δ 166.14, 154.82, 135.32, 133.56, 129.01, 128.33, 127.72, 125.09, 123.43, 120.92, 116.67, 78.04, 64.36, 30.22, 19.82, 19.06. HRMS Calcd for $C_{32}H_{37}N_2O_4$ (MH^+): 513.2753. Found: 513.2763.

4.4.3. Preparation of Samples for Fluorescence Measurements.

Polymer (*S*)-**3.9**, (*R*)-**3.9** and *Rac*-**3.9** were dried under vacuum and stored under nitrogen. The enantiomers of amino alcohols were purchased from Sigma Aldrich and used without further purification. Stock solution of 1 mM polymer sensor (*S*)-**3.9,** (*R*)-**3.9** or *Rac*-**3.9** and 2 mM $Zn(OAc)_2$ in water were freshly prepared. Amino alcohols in CH_2Cl_2 with various concentrations were freshly prepared. Polymer films were prepared as followed: 500 μL CH_2Cl_2 solution of amino alcohols (various concentration) was mixed with 200 μL water solution of $Zn(OAc)_2$ (2.0 mM) and 200 μL water solution of (*S*)-**3.9,** (*R*)-**3.9** or *Rac*-**3.9** (1.0 mM). After

the mixtures were vigorously shaken and then set for 6 h, the polymer films were formed at the interface of water and CH_2Cl_2 phases which were isolated after the solvents were decanted. The polymer films were then dissolved in DMSO and diluted to 10 μM for fluorescence measurement.

4.4.4. NMR Study of Polymer Films and Salicylaldimines

Preparation of samples for NMR study of polymer films:

Stock solution of 1 mM polymer sensor (*S*)-**3.9** and 2 mM $Zn(OAc)_2$ in water were freshly prepared. Stock solutions of 4 mM amino alcohols in CH_2Cl_2 were freshly prepared. Polymer films were prepared as followed: 10 mL CH_2Cl_2 solution of amino alcohols was mixed with 4 mL water solution of $Zn(OAc)_2$ and 4 mL water solution of (*S*)-**3.9**, after vigorously shaking and waiting for 6 h, polymer films were formed at the interface of water and CH_2Cl_2 phases. After the solvents were decanted, the polymer film can be isolated and dried under vacuum. Then the polymer films were dissolved in DMSO-d_6 for NMR study.

Preparation of samples for NMR study of Salicylaldimines:

Stock solution of 20 mM salicyaldimines and 40 mM $Zn(OAc)_2$ in DMSO-d_6 were freshly prepared. To an NMR tube, 200 μL salicyaldimines solution and 200 μL $Zn(OAc)_2$ were added to obtain 1:2 molar ration of salicyaldimine:Zn^{2+}. And the final concentration of salicylaldimine was 10 mM. The resulting solutions were used for NMR study.

References

(1) Kwan, M. K.; Park, H.; Kim, H. J.; Chin, J.; Nam, W. *Org. Lett.* **2005**, *7* (16), 3525–3527.

(2) Qing, G. yan; Sun, T. lei; He, Y. bing; Wang, F.; Chen, Z. hong. *Tetrahedron Asymmetry* **2009**, *20* (5), 575–583.

(3) Pu, L. *Acc. Chem. Res.* **2012**, *45* (2), 150–163.

(4) Ingram, C. U.; Bommer, M.; Smith, M.; Dalby, P.; Ward, J.; Hailes, H.; Lye, G. *Biotechnol. Bioeng.* **2007**, *96* (3), 559–569.

(5) Schild, H. G.; Tirrell, D. A. *J. Phys. Chem.* **1990**, *94* (10), 4352–4356.

(6) Schild, H. G.; Muthukumar, M.; Tirrell, D. A. *Macromolecules* **1991**, *24* (4), 948–952.

(7) Winnik, F. M.; Ottaviani, M. F.; Boßmann, S. H.; Pan, W.; Garcia-Garibay, M.; Turro, N. J. *Macromolecules* **1993**, *26* (17), 4577–4585.

(8) Zhang, G.; Wu, C. *J. Am. Chem. Soc.* **2001**, *123* (7), 1376–1380.

(9) Mukherji, D.; Marques, C. M.; Stuehn, T.; Kremer, K. *J. Chem. Phys.* **2015**, *142* (11), 114903.

(10) Rodríguez-Ropero, F.; Hajari, T.; Van Der Vegt, N. F. A. *J. Phys. Chem. B* **2015**, *119* (51), 15780–15788.

(11) Pica, A.; Graziano, G. *Phys. Chem. Chem. Phys.* **2016**, *18* (36), 25601–25608.

(12) Scherzinger, C.; Schwarz, A.; Bardow, A.; Leonhard, K.; Richtering, W. *Curr. Opin. Colloid Interface Sci.* **2014**, *19* (2), 84–94.

(13) Mukherji, D.; Marques, C. M.; Kremer, K. *Nat. Commun.* **2014**, *5* (May), 4882.

(14) Song, T.; Cao, Y.; Zhao, G.; Pu, L. *Inorg. Chem.* **2017**, *56* (8), 4395–4399.

(15) Zhang, H. C.; Huang, W. S.; Pu, L. *J. Org. Chem.* **2001**, *66* (2), 481–487.

Chapter 5. Attempted Research: Asymmetric Catalyst Screening of Reactions and Enantioselective Fluorescent Imaging of Amino Acids *in vivo*

5.1. Asymmetric catalyst screening of amino alcohols and amino acids synthesis

5.1.1. Introduction

There have been numerous catalysts used for the asymmetric synthesis of common amino acids, such as phase transfer catalysts[1], chiral metal complexes[2], chiral organic molecules[3,4] and enzymes[5,6]. Chiral amino alcohols can be synthesized by reduction of corresponding amino acids[7] or by the use of various chiral metal complexes[8,9]. However, the synthesis of these catalysts is sometimes difficult and time consuming, and the enzymes need to be separated from bacteria. Therefore, we tried to develop a simple chiral catalyst system for the asymmetric synthesis of amino acids and amino alcohols. Instead of using HPLC to determine the *ee* of the product, we intended to use the polymer-based fluorescent probes to determine the enantiomeric composition due to the fast response and real-time analysis of fluorescent method. Both enantiomers of the probe would be used to measure the fluorescent response toward the same sample. The difference of fluorescence intensity between the two enantiomers could roughly tell us the *ee* of the sample.

5.1.2. Results and Discussion

5.1.2.1. Asymmetric catalyst screening for the synthesis of amino acids

Ratner et al. reported the synthesis of α-amino acids by the reaction of α-keto acids with ammonia then reduction by palladium catalyzed hydrogenation in methanol:water (50:50) solution.[10] Ogo et al. developed reductive amination of α-keto acids with ammonium formate by Iridium complex in water.[11] Inspired by the two reactions, we tried to synthesize α-amino acids using reductive amination α-keto acids with ammonium formate by palladium on carbon

(Pd/C) catalyst (Scheme **5.1**) because this reaction avoids the use of dangerous hydrogen gas and palladium on carbon catalyst is commercially available and relatively stable in air. We also attempted to add chiral alcohols with Lewis acids to synergically affect the chirality of products.

Scheme 5.1. Reductive amination of α-keto acids with ammonium formate by Pd/C

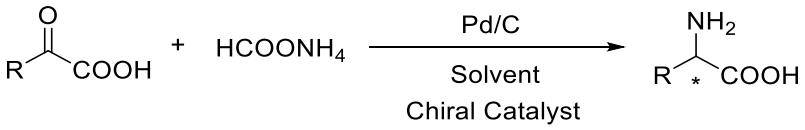

We chose 4-methyl-2-oxovaleric acid **5.1** as the α-keto acid for the synthesis of leucine (Figure **5.1**) because polymer-based probe (*S*)- and (*R*)-**3.9** (Figure **5.2**) had highly enantioselective fluorescent response toward leucine in BICINE buffer.

Figure 5.1. Synthesis of leucine

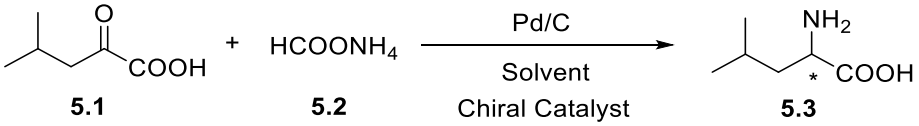

Figure 5.2. Polymer-based fluorescent sensors (*S*)- and (*R*)-**3.9**

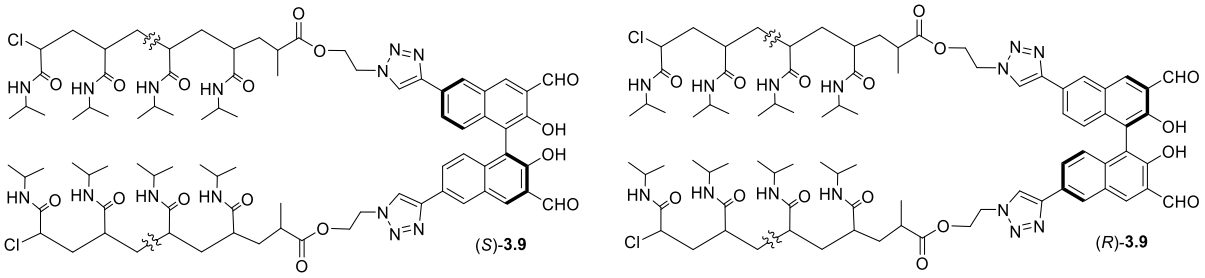

We found that when methanol:water (9:1) was used as solvent, good results were obtained The reaction condition was as followed. 4-methyl-2-oxovaleric acid (39 mg, 0.3 mmol, 1 equiv.) and ammonium formate (132.4 mg, 2.1 mmol, 7 equiv.) were added to 50 mL methanol:water (9:1) solution. 32 mg Pd/C was then added to the mixture. The reaction mixture was stirred at room temperature for 20 h, then the solvent was evaporated and the crude product was taken ^{1}H-NMR in D_2O. As we can see from the ^{1}H-NMR (Figure **5.3**), the product was

clean and the yield was almost 100%. The reaction was tolerant to air, which was easier for operation and catalyst screening. We decreased the scale of the reaction to 1 mL total volume. 4-methyl-2-oxovaleric acid (0.78 mg, 0.006 mmol, 1 equiv.) and ammonium formate (2.6 mg, 0.042 mmol, 7 equiv.) were added to 1 mL methanol:water (9:1) solution in a vial. 2 mg Pd/C was then added and the reaction mixture was put on a shaker to shake for 20 h at room temperature. ^{1}H-NMR showed the yield was still almost 100% (Figure **5.4**).

Figure 5.3. ^{1}H-NMR spectra of pure leucine and product from 50 mL reaction system

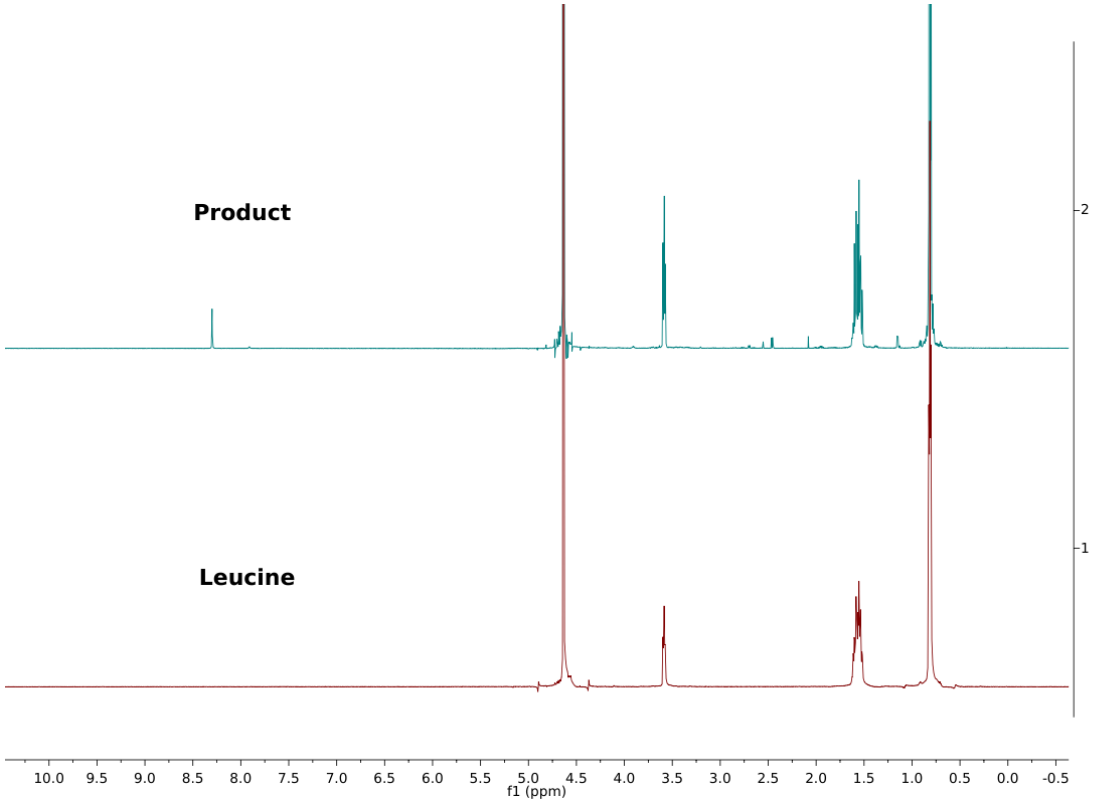

Figure 5.4. ^{1}H-NMR spectra of pure leucine and product from 1 mL reaction system

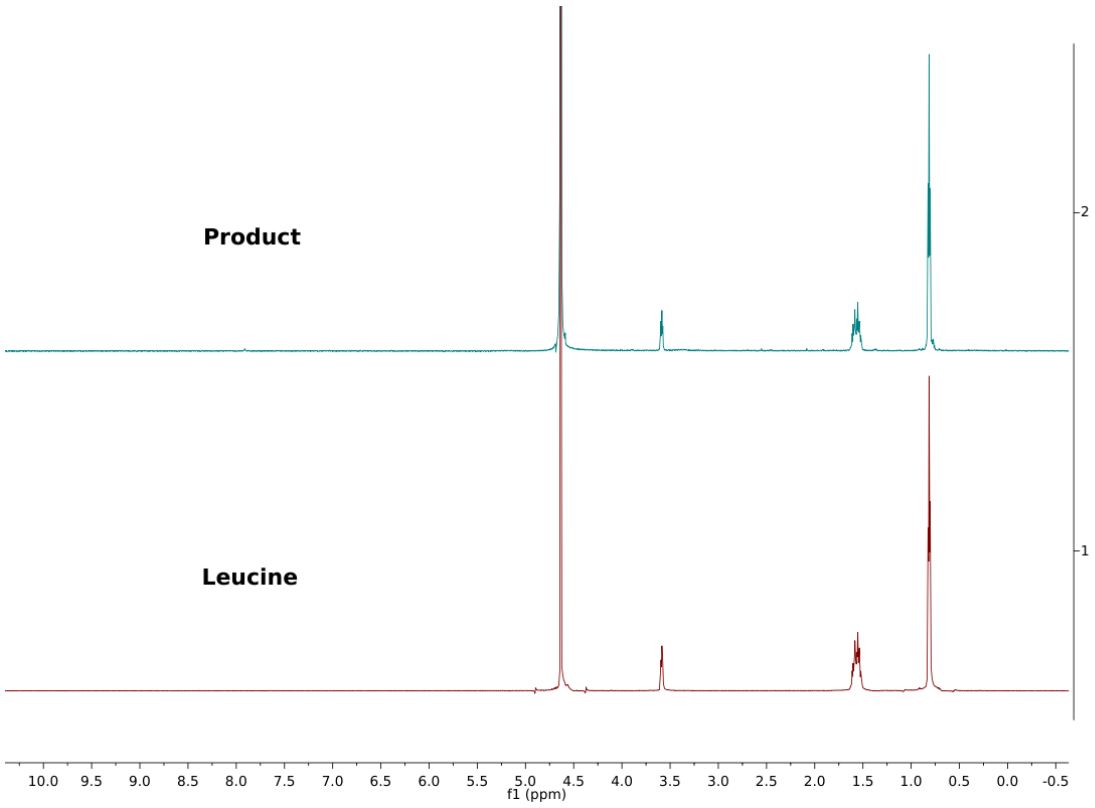

Then the fluorescent response of polymer probe toward the product was studied. Solvent was evaporated after the reaction and the crude product was dissolved in 1.5 mL BICINE buffer (25 mM, pH = 8.80) to make 4 mM reaction mixture solution (the total concentration of **5.1** and **5.3** were 4 mM). Then (*S*)- or (*R*)-**3.9** (50 μL, 1equiv., 1 mM in BICINE buffer) and $Zn(OAc)_2$ (50 μL, 2 equiv., 2 mM in water) was mixed with 125 μL product solution in BICINE. The mixture was allowed to stand at room temperature for 2h, then diluted to 5 mL using BICINE buffer to measure fluorescent. As shown in Figure **5.5**, The addition of product buffer solution led to similar fluorescence enhancement for (*S*) and (*R*) probe, proving the generation of racemic leucine. The fluorescence enhancement was weak, which was consistent with the previous fluorescence data of racemic leucine.

Figure 5.5. Fluorescence measurement of reaction mixture. (*S*)- or (*R*)-**3.9** (50 μL, 1 equiv., 1 mM in BICINE buffer) and $Zn(OAc)_2$ (50 μL, 2 equiv., 2 mM in water) was mixed with reaction mixture solution (125 μL, 10 equiv., 4 mM in BICINE buffer) (Reaction time: 2h, then dilute 100-fold with BICINE buffer. λ_{exc} = 320 nm. Slit: 5/5 nm).

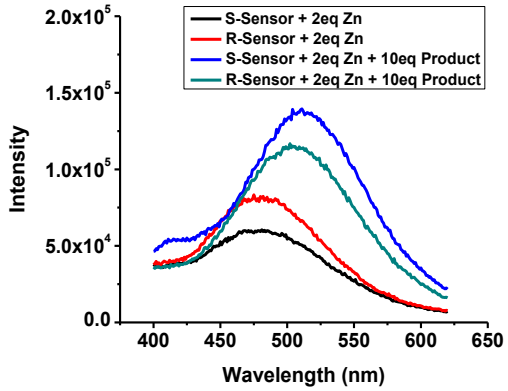

We used 1 mL reaction system for asymmetric catalyst screening experiment. We tried 12 different chiral alcohols, acids and sugars (**5.4**-**5.15**, Figure **5.6**) as chiral additives for the reaction. 0.006 mmol (1 equiv.) of each chiral additive was used. After reaction, the solvent was evaporated and the crude mixture was dissolved in 1.5 mL BICINE buffer. Then (*S*)- or (*R*)-**3.9** (50 μL, 1 equiv., 1 mM in BICINE buffer) and $Zn(OAc)_2$ (50 μL, 2 equiv., 2 mM in water) was mixed with 125 μL product buffer solution. The fluorescence measurement procedure was the same as described above. After measurement, only the addition of diisopropyl-L-tartrate (**5.7**) led to weak fluorescence enhancement for (*S*)- and (*R*)-**3.9**, and the fluorescence intensity are similar (Figure **5.7**). Therefore, the product was still racemic leucine and the addition of **5.7** did not increase the enantioselectivity of the reaction. There was no fluorescence enhancement for the addition of other chiral additives probably due to the low yield of leucine or the interference of additives.

Figure 5.6. Structure of chiral organic molecule additives

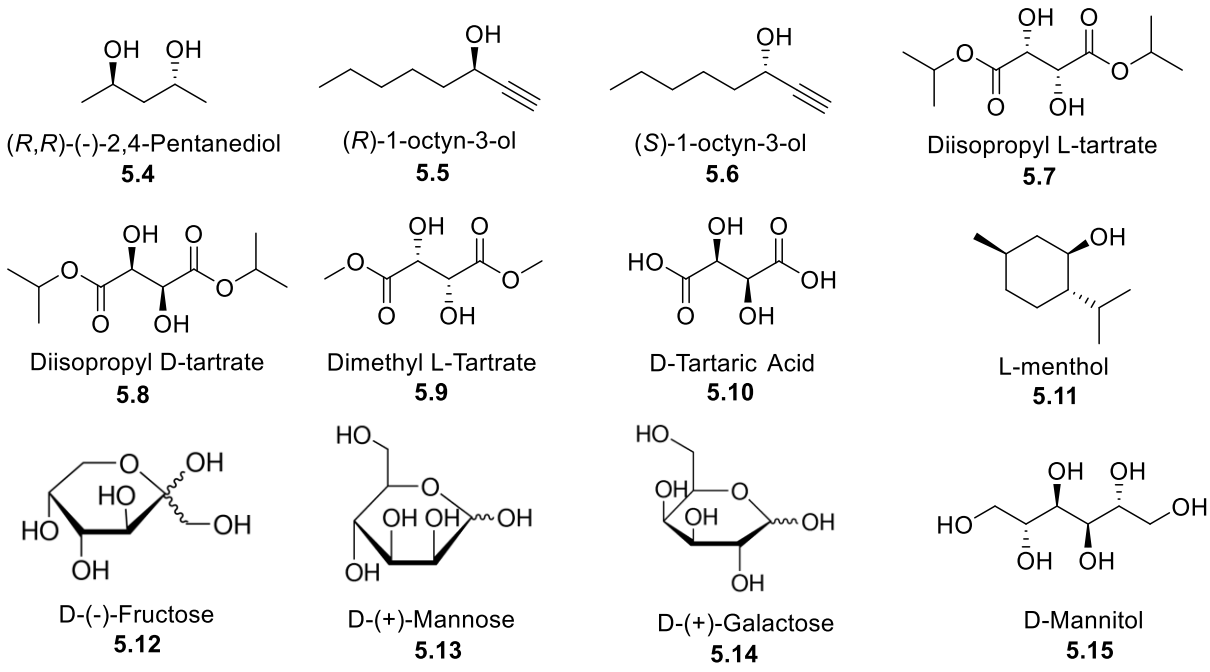

Figure 5.7. Fluorescence measurement of reaction mixture. (*S*)- or (*R*)-**3.9** (50 μL, 1 equiv., 1 mM in BICINE buffer) and $Zn(OAc)_2$ (50 μL, 2 equiv., 2 mM in water) was mixed with reaction mixture solution (125 μL, 10 equiv., 4 mM in BICINE buffer) (Reaction time: 2h, then dilute 100-fold with BICINE buffer. λ_{exc} = 320 nm. Slit: 5/5 nm).

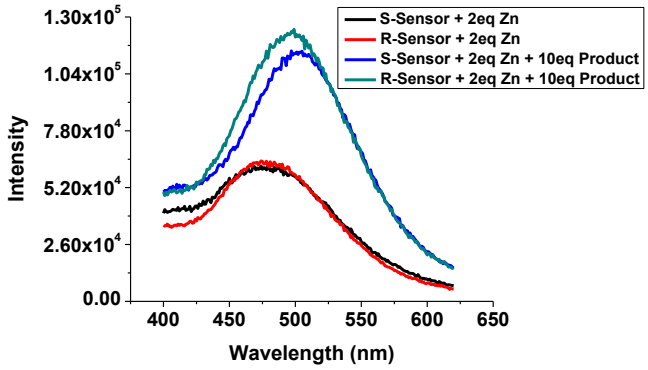

5.7 was chosen for further asymmetric catalysis study. Besides **5.7**, 20 different Lewis acids (Table **5.1**) were also added to the reaction mixture to see if the combination of **5.7** and Lewis acid could have a synergic effect on the enantioselectivity. However, no fluorescence

enhancement was observed after the addition of **5.7** and Lewis acid. This might be due to the low yield after the addition of Lewis acids. Small scale reactions, especially with heterogeneous catalyst Pd/C, was easy to be influenced by the component in the mixture. Therefore, we then try to increase the scale of the reaction to study the effect of **5.7** and Lewis acid on the enantioselectivity.

Table 5.1. 20 Lewis acids

$Zn(OAc)_2$	$Hg(OAc)_2$	AgOAc	$FeCl_3 \cdot 6H_2O$	$CuSO_4$
$MnCl_2 \cdot 4H_2O$	$Pb(NO_3)_2$	LiCl	NaCl	KCl
$CaCl_2$	$BaCl_2 \cdot 2H_2O$	$SnCl_2$	$Ni(NO_3)_2 \cdot 6H_2O$	$Mg(OAc)_2 \cdot 4H_2O$
$SnCl_4 \cdot 5H_2O$	$Yb(OTf)_3$	$Y(OTf)_3$	$La(OTf)_3$	$InBr_3$

We increased the volume of the solvent to 5 mL, 4-methyl-2-oxovaleric acid (3.9 mg, 0.03 mmol, 1 equiv.) and ammonium formate (13.2 mg, 0.21 mmol, 7 equiv.) were added to 5 mL methanol:water (9:1) solution in a vial. 8 mg Pd/C was then added to the mixture. The reaction mixture was stirred at room temperature for 20 h. ^{1}H-NMR showed almost 100% yield.

Then various amount of **5.7** and $Yb(OTf)_3$ were added into the reaction system and the fluorescence of the mixture was measured as described previously. The addition of 0.2, 0.5 and 1 equiv. of **5.7** and $Yb(OTf)_3$ led to 40%, 90% and 60% yield, respectively. The results of fluorescence measurement demonstrated that the products were still racemic as the fluorescence enhancements were similar for (*S*)- and (*R*)-**3.9** (Figure **5.8**). Therefore, the combination of chiral organic molecule with Lewis acid did not have an effect on the enantioselectivity of leucine synthesis reaction.

Figure 5.8. Fluorescence measurement of product. (*S*)- or (*R*)-**3.9** (50 μL, 1 equiv., 1 mM in BICINE buffer) and $Zn(OAc)_2$ (50 μL, 2 equiv., 2 mM in water) was mixed with 125 μL (10 equiv.) (a) no 5.7 and $Yb(OTf)_3$ (b) addition of 0.2 equiv. **5.7** and $Yb(OTf)_3$ (c) addition of 0.5 equiv. **5.7** and $Yb(OTf)_3$ (d) addition of 1 equiv. **5.7** and $Yb(OTf)_3$ reaction mixture solution (4 mM in BICINE buffer) (Reaction time: 2h, then dilute 100-fold with BICINE buffer. λ_{exc} = 320 nm. Slit: 5/5 nm).

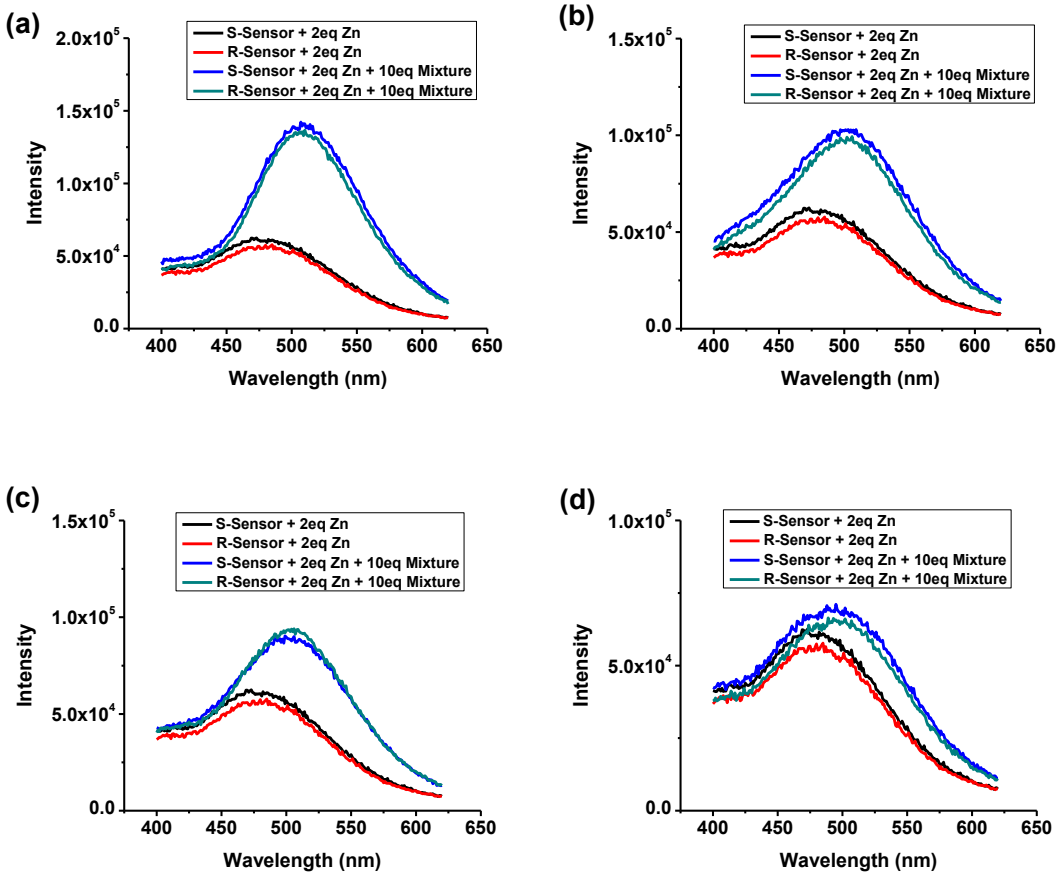

5.1.2.1. Asymmetric catalyst screening for the synthesis of amino alcohols

We also tried to use β-keto alcohol instead of α-keto acid to synthesize amino alcohols use similar reaction conditions. (*S*)- and (*R*)-**3.9** had highly enantioselective fluorescent response toward amino alcohols in water and methanol. Therefore, after reaction, the solution

could directly mix with water solution of polymer sensor and Zn(OAc)2 for fluorescence measurement without the evaporation of solvent.

Figure 5.9. Synthesis of alaninol

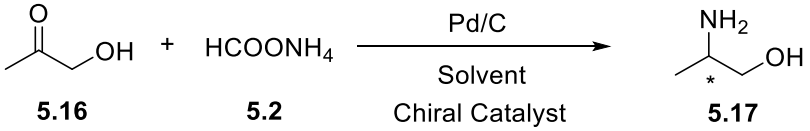

We chose acetol **5.16** as substrate for the synthesis of alaninol **5.17** (Figure **5.9**). Acetol (22.2 mg, 0.3 mmol, 1 equiv.), ammonium formate (189.2 mg, 3 mmol, 10 equiv.) and K_2CO_3 (31.1 mg, 0.75 equiv.) were added to 50 mL methanol:water (9:1) solution. 32 mg Pd/C was then added to the mixture. The reaction mixture was stirred at room temperature for 20 h, then the solvent was evaporated and the crude product was taken ^{1}H-NMR in D_2O. The peaks of the crude product were shifted to higher chemical shift compared with pure alaninol, probably due to the protonation of amine group (Figure **5.10**). The yield was over 95% due to the disappearance of acetol peak.

Figure 5.10. ^{1}H-NMR spectra of pure alaninol and product from 50 mL reaction system

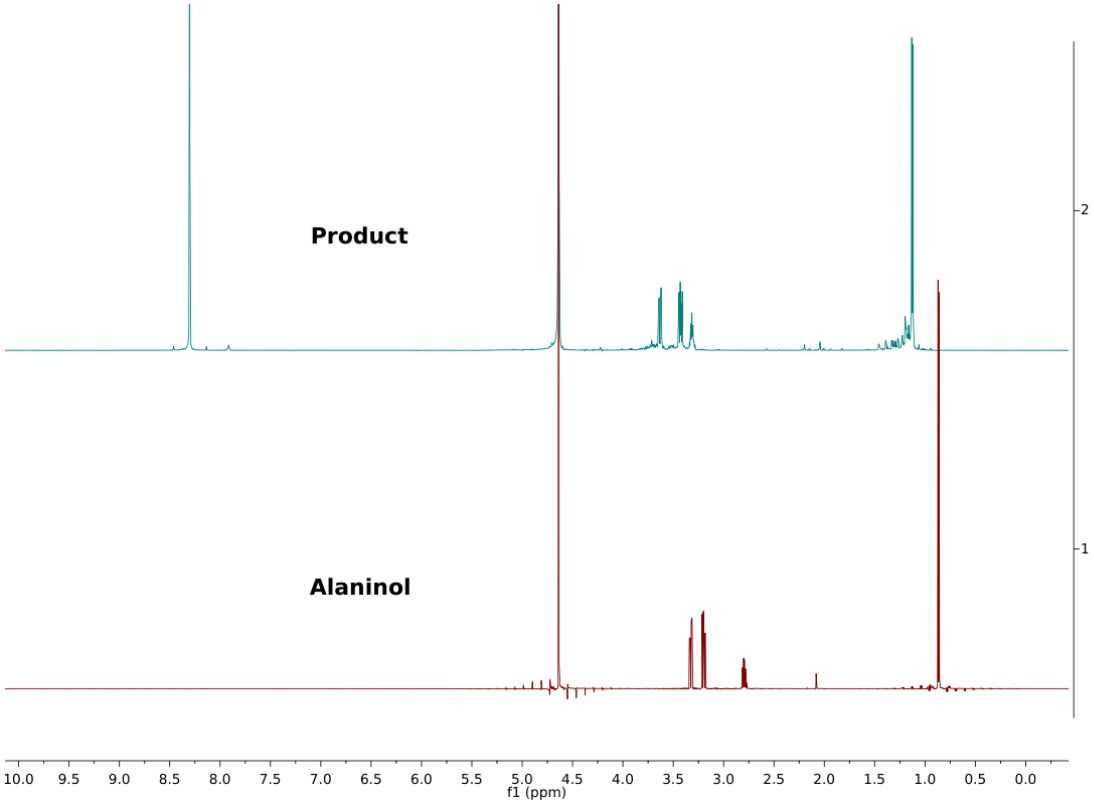

To study the fluorescent response of polymer probes, we first conducted a pseudo-reaction. We used (*S*)- and (*R*)-alaninol to add into separate reaction mixture instead of acetol. After 20 h, 83 μL solution (10 equiv.) was taken out to mix with (*S*)- or (*R*)-**3.9** (50 μL, 1 equiv., 1 mM in water) and $Zn(OAc)_2$ (50 μL, 2 equiv., 2 mM in water). After 2 h, the mixture was diluted to 5 mL using water for fluorescence measurement. No fluorescence enhancement was observed (Figure **5.11**), probably due to the protonation of amine group in alaninol. To deprotonate the amine group, 2 equiv. K_2CO_3 solid was added to the mixture before mixing with polymer probe and $Zn(OAc)_2$. High enantioselective fluorescence enhancements of (*S*)- and (*R*)-**3.9** were observed for both solutions that contained (*S*)- or (*R*)-alaninol (Figure **5.12**), which proved the feasibility of fluorescence measurement method.

Figure 5.11. Fluorescence measurement of reaction mixture. (*S*)- or (*R*)-**3.9** (50 μL, 1 equiv., 1 mM in water) and $Zn(OAc)_2$ (50 μL, 2 equiv., 2 mM in water) was mixed with (a) (*S*)-alaninol (b) (*R*)-alaninol reaction mixture solution (125 μL, 10 equiv., 4 mM in water) (Reaction time: 2h, then dilute 100-fold with BICINE buffer. λ_{exc} = 320 nm. Slit: 5/5 nm).

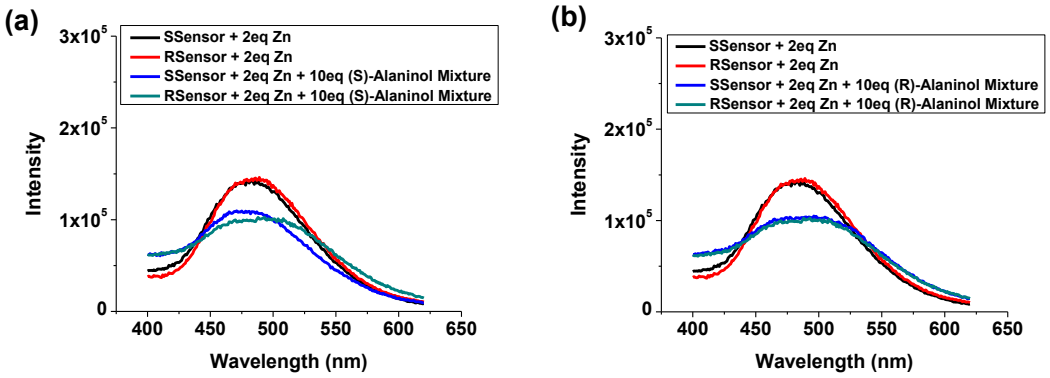

Figure 5.12. Fluorescence measurement of reaction mixture. 50 μL (1 equiv.) (*S*)- or (*R*)-**3.9** (1 mM in water), 50 μL (2 equiv.) $Zn(OAc)_2$ (2 mM in water) and 2 equiv. K_2CO_3 solid were mixed with 125 μL (10 equiv.) (a) (*S*)-alaninol (b) (*R*)-alaninol reaction mixture solution (4 mM in water) (Reaction time: 2 h, then dilute 100-fold with BICINE buffer. λ_{exc} = 320 nm. Slit: 5/5 nm).

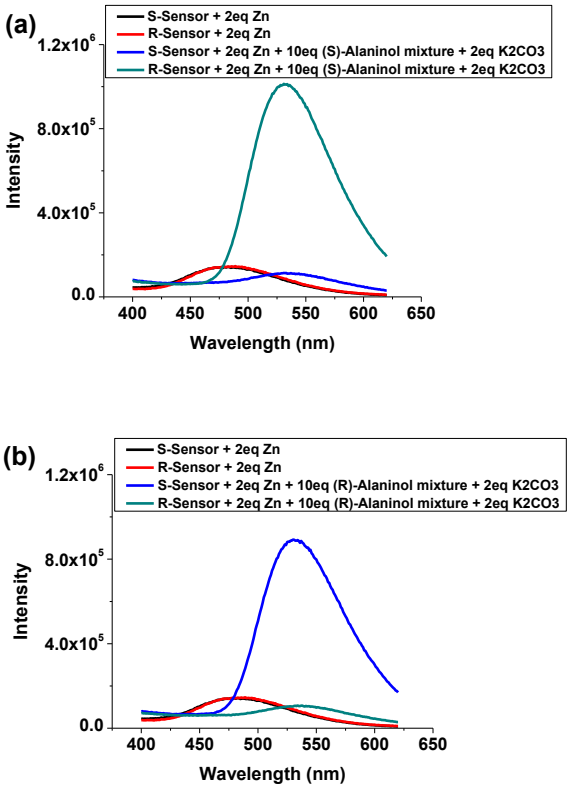

Then we studied the fluorescent response of probes toward reaction mixtures. The reaction was conducted as described above. After reaction, 83 μL solution (10 equiv.) was taken out to mix with (*S*)- or (*R*)-**3.9** (50 μL, 1 equiv., 1 mM in water) and $Zn(OAc)_2$ (50 μL, 2 equiv., 2 mM in water). After 2 h, the mixture was diluted to 5 mL using water for fluorescence measurement. No fluorescence enhancement was observed (Figure **5.13a**). After the addition of 2 equiv. K_2CO_3 solid, fluorescence enhancement was observed (Figure **5.13b**). The (*S*)- and (*R*)-**3.9** gave similar fluorescence enhancement, indicating that the product is racemic alaninol.

Figure 5.13. Fluorescence measurement of reaction mixture. (*S*)- or (*R*)-**3.9** (50 μL, 1 equiv., 1 mM in water) and $Zn(OAc)_2$ (50 μL, 2 equiv., 2 mM in water) were mixed with (a) before adding K_2CO_3 (b) after adding 2 equiv. K_2CO_3 solid into reaction mixture solution (125 μL, 10 equiv., 4 mM in water) (Reaction time: 2h, then dilute 100-fold with BICINE buffer. λ_{exc} = 320 nm. Slit: 5/5 nm).

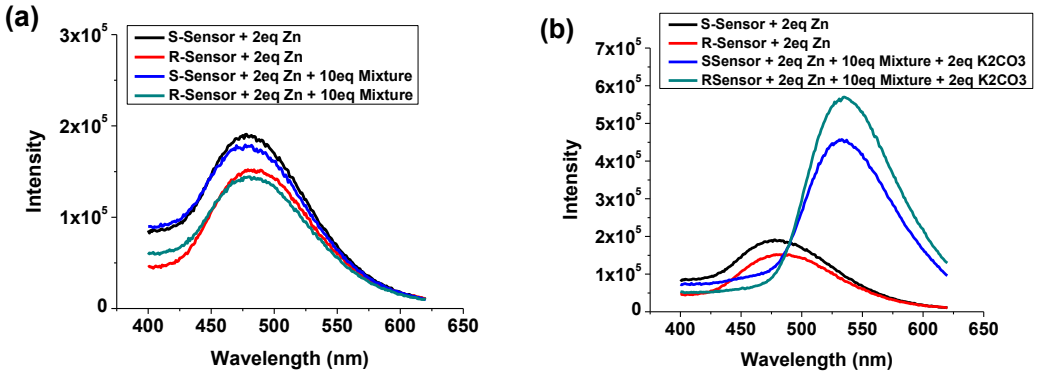

We also tried to use various chiral additives and Lewis acids for asymmetric synthesis of alaninol. 0.2 equiv. of compound **5.4-5.15** were added to the reaction mixture. After 20 h, fluorescence measurement was conducted (Figure **5.14**). It was found that **5.7** and **5.8** led to the opposite results. That is, for **5.7**, (*R*)-**3.9** had higher fluorescent response; for **5.8**, (*S*)-**3.9** had higher fluorescent response. In addition, **5.7** led to largest fluorescence intensity difference between (*S*) and (*R*) sensor. Therefore, **5.7** was chosen for further study. The amount of **5.7** was increased to 0.5, 1, and 2 equiv. However, the fluorescence intensity difference is small between the two probes (Figure **5.15**), which indicates poor enantioselectivity of the reaction.

Figure 5.14. Fluorescence measurement of reaction mixture. (*S*)- or (*R*)-**3.9** (50 μL, 1 equiv., 1 mM in water), $Zn(OAc)_2$ (50 μL, 2 equiv., 2 mM in water) and 2 equiv. K_2CO_3 solid were mixed with reaction mixture solution (125 μL, 10 equiv., 4 mM in water) (Reaction time: 2h, then dilute 100-fold with BICINE buffer. λ_{exc} = 320 nm. Slit: 5/5 nm).

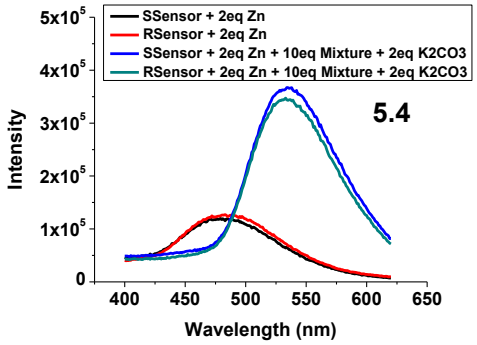
SSensor + 2eq Zn
RSensor + 2eq Zn
SSensor + 2eq Zn + 10eq Mixture + 2eq K2CO3
RSensor + 2eq Zn + 10eq Mixture + 2eq K2CO3
5.4
Intensity
Wavelength (nm)

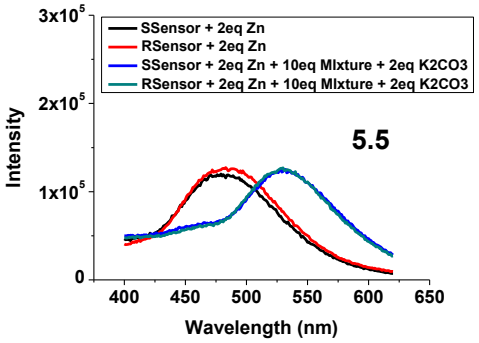
SSensor + 2eq Zn
RSensor + 2eq Zn
SSensor + 2eq Zn + 10eq MIxture + 2eq K2CO3
RSensor + 2eq Zn + 10eq MIxture + 2eq K2CO3
5.5
Intensity
Wavelength (nm)

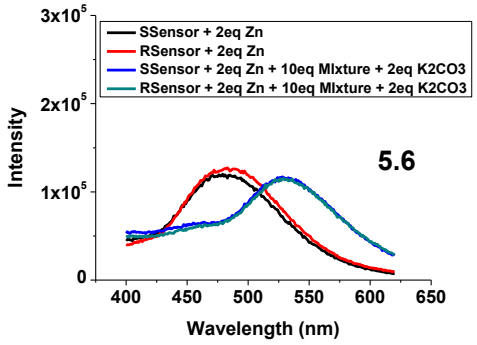
SSensor + 2eq Zn
RSensor + 2eq Zn
SSensor + 2eq Zn + 10eq MIxture + 2eq K2CO3
RSensor + 2eq Zn + 10eq MIxture + 2eq K2CO3
5.6
Intensity
Wavelength (nm)

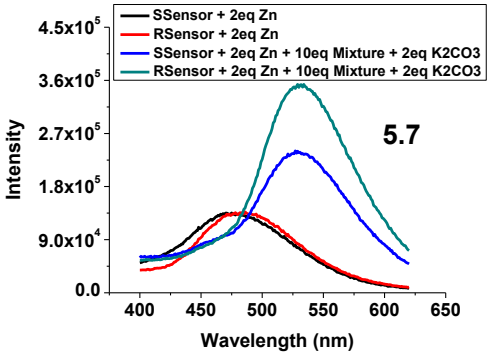
SSensor + 2eq Zn
RSensor + 2eq Zn
SSensor + 2eq Zn + 10eq Mixture + 2eq K2CO3
RSensor + 2eq Zn + 10eq Mixture + 2eq K2CO3
5.7
Intensity
Wavelength (nm)

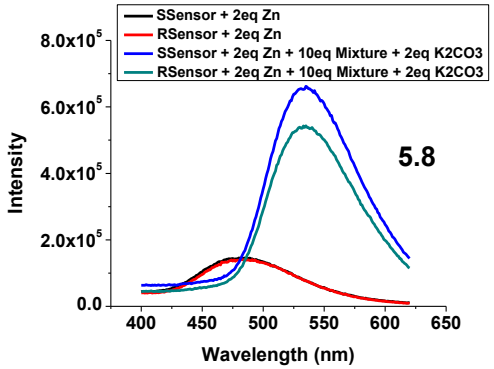
SSensor + 2eq Zn
RSensor + 2eq Zn
SSensor + 2eq Zn + 10eq Mixture + 2eq K2CO3
RSensor + 2eq Zn + 10eq Mixture + 2eq K2CO3
5.8
Intensity
Wavelength (nm)

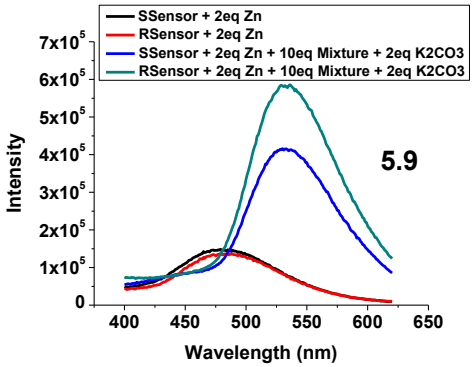
SSensor + 2eq Zn
RSensor + 2eq Zn
SSensor + 2eq Zn + 10eq Mixture + 2eq K2CO3
RSensor + 2eq Zn + 10eq Mixture + 2eq K2CO3
5.9
Intensity
Wavelength (nm)

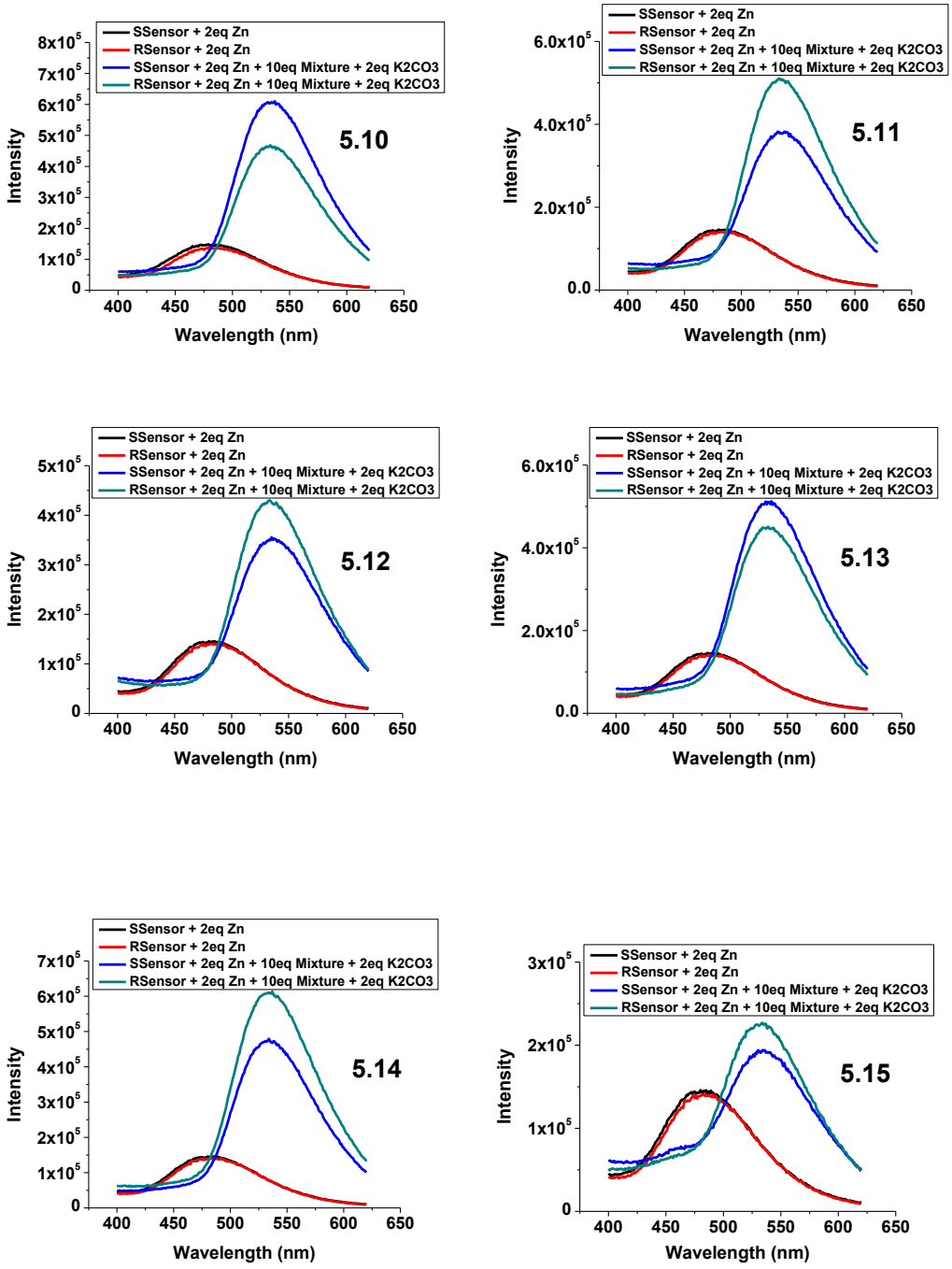

Figure 5.15. Fluorescence measurement of reaction mixture. 50 µL (1 equiv.) (*S*)- or (*R*)-**3.9** (1 mM in water), 50 µL (2 equiv.) $Zn(OAc)_2$ (2 mM in water) and 2 equiv. K_2CO_3 solid were mixed with 125 µL (10 equiv.) reaction mixture solution (4 mM in water) (a) 0.5 equiv. **5.7**, (b)

1.0 equiv. **5.**7, (c) 2.0 equiv. **5.7** (Reaction time: 2h, then dilute 100-fold with BICINE buffer. λ_{exc} = 320 nm. Slit: 5/5 nm).

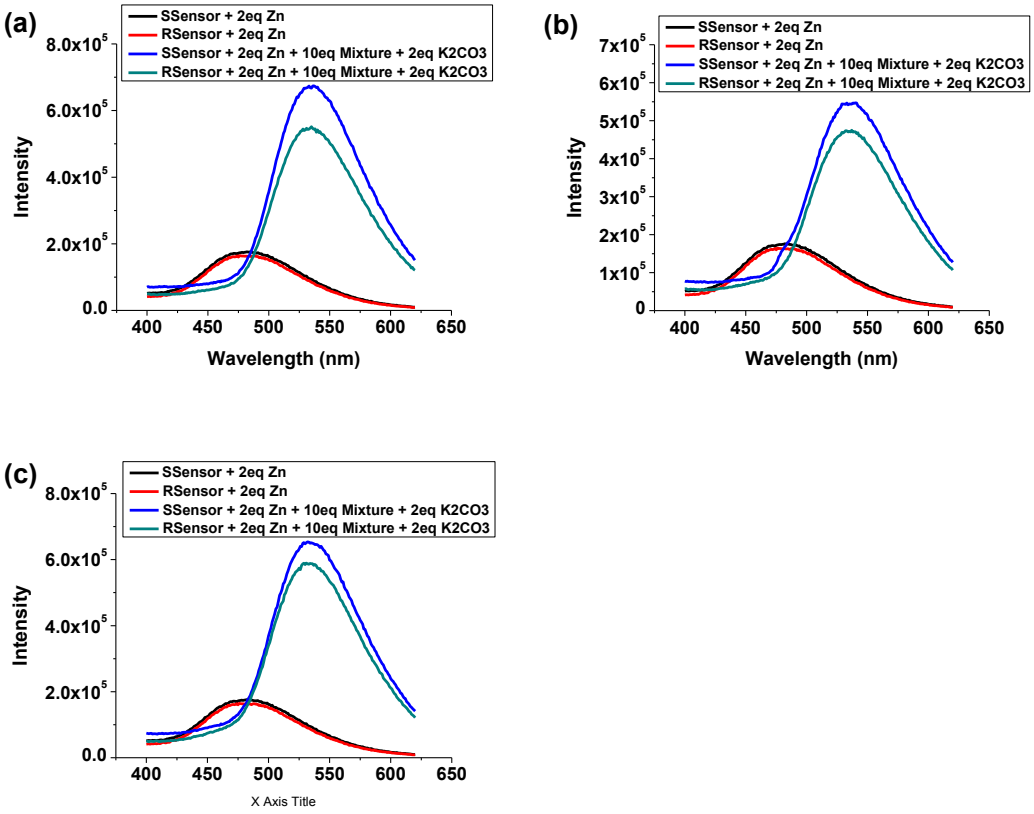

We decreased the reaction scale to 1 mL in the presence of **5.7**, 3 mg Pd/C was used. The reaction still went well and the yield was almost 100% from ^{1}H-NMR spectra. Therefore, we used 1 mL reaction scale and added Yb(OTf)$_3$, Y(OTf)$_3$ or La(OTf)$_3$ into reaction mixture in the presence of **5.7** to study the enantioselectivity of the reaction. As shown in Table **5.2**, different amount of **5.7** and Lewis acids were used. However, only weak fluorescence enhancement was observed for each of the reaction mixture due to the low yield of the reaction. The addition of other 17 Lewis acids (see Table **5.1**) led to no fluorescence enhancement, indicating that the reaction probably did not occur. These data demonstrated that Lewis acids may interfere with the reaction, especially when the reaction scale is small.

Table 5.2. Reaction yields with the addition of **5.7** and various Lewis acids

Diisopropyl L-Tartrate	Yb(OTf)3	Y(OTf)3	La(OTf)3
0.2 equiv.	0.2 equiv.	0.2 equiv.	0.2 equiv.
0.2 equiv.	0.5 equiv.	0.5 equiv.	0.5 equiv.
0.2 equiv.	1 equiv.	1 equiv.	1 equiv.
0.5 equiv.	0.2 equiv.	0.2 equiv.	0.2 equiv.
0.5 equiv.	0.5 equiv.	0.5 equiv.	0.5 equiv.
0.5 equiv.	1 equiv.	1 equiv.	1 equiv.
1 equiv.	0.2 equiv.	0.2 equiv.	0.2 equiv.
1 equiv.	0.5 equiv.	0.5 equiv.	0.5 equiv.
1 equiv.	1 equiv.	1 equiv.	1 equiv.

Reaction condition: Acetol (0.4 mg, 0.006 mmol, 1 equiv.), ammonium formate (3.8 mg, 0.06 mmol, 10 equiv.), K_2CO_3 (0.6 mg, 0.75 equiv.), **5.7** (various equiv.) and Lewis acids (various equiv.) were added to 1 mL methanol:water (9:1) solution. 3 mg Pd/C was then added to the mixture. The reaction mixture was shaken at room temperature for 20 h.

5.1.3. Conclusion

Asymmetric catalyst screening experiments were conducted for synthesis of leucine and alaninol. Racemic leucine and alaninol were synthesized with high yield by reductive amination of substrates by Pd/C catalyst. The addition of chiral additives and Lewis acids led to poor enantioselectivity of the reaction. New catalytic system needs to be developed to better improve the *ee* of the products.

5.2. Enantioselective Fluorescent Imaging of Amino Acids *in vivo*

5.2.1. Introduction

Zeng et al. reported enantioselective fluorescent imaging of free amino acids in living cells using SPINOL-based probe.[12] External amino acids needed to be added to cells and toxic Bu_4NOH was used for fluorescence measurement. The fluorescent probes need to be developed for better biocompatibility. Polymer probe **3.9** contains PNIPAM chains which is soluble in aqueous solutions and was used for enantioselective recognition of various amino acids in BICINE buffer (25 mM, pH = 8.80) in the absence of Bu_4NOH, which is a good candidate for fluorescent imaging *in vivo*. Recently, it was reported that various D-amino acids were found in mouse brain with much higher concentration than in blood. For example, the concentration of D-glutamine is 0.117 μg/mg, and is 7.9% of total glutamine in brain, which is over 100 times higher than in blood.[13] Therefore, it is possible that D-amino acids may accumulate in certain organs of mouse. We attempted to use polymer probe **3.9** for fluorescent imaging of amino acids in mouse.

5.2.2. Results and Discussion

5.2.2.1. Enantioselective fluorescent recognition of amino acids in HEPES buffer

As previously mentioned in Chapter 3, **3.9** had highly enantioselective fluorescent response toward leucine in HEPES buffer (25 mM, pH = 7.60). HEPES buffer with pH = 7.60 is much closer to the pH of the living system that BINCIE buffer with pH = 8.80. Therefore, various amino acids were tested for enantioselective fluorescent response by (*S*)-**3.9**.

For fluorescence measurement, HEPES buffer (25 mM, pH = 7.60) was freshly prepared. (*S*)-**3.9** (50 μL, 1 equiv., 1 mM in HEPES buffer) and $Zn(OAc)_2$ (50 μL, 2 equiv., 2 mM in water) were mixed with various volume of amino acids (4 mM in HEPES buffer). The

mixtures were allowed to stand at room temperature for 2 h and then diluted 100-fold using HEPES buffer (25 mM, pH = 7.60) for fluorescence measurement (Figure **5.16-5.32**). We found that polymer sensor (*S*)-**3.9** had highly enantioselective fluorescent response toward several free amino acids. The *ef* value was 11.2 for histidine, 9.3 for asparagine, 3.4 for arginine and 3.2 for glutamine, indicating high enantioselectivity.

Figure 5.16. Fluorescence spectra of (*S*)-**3.9** (1.0 mM) with various equiv of histidine, D-**3.11** or L-**3.11** (4.0 mM) in 25 mM HEPES buffer (pH = 7.60) in the presence of 2.0 equiv of $Zn(OAc)_2$ water solution (2.0 mM). Reaction time: 2 h, then diluted 100-fold using HEPES buffer. (λ_{exc} = 320 nm. Slit 5/5 nm. The fluorescence intensity at λ_{em} = 514 nm was used for each data point).

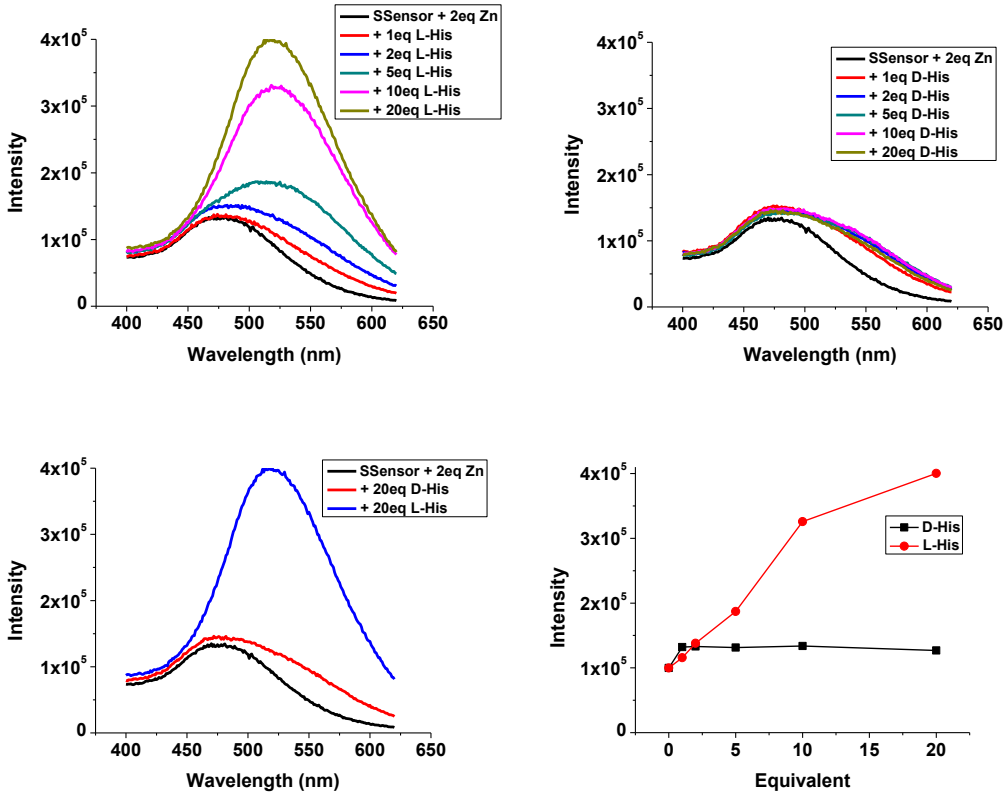

Figure 5.17. Fluorescence spectra of (*S*)-**3.9** (1.0 mM) with various equiv of glutamine, D-**3.12** or L-**3.12** (4.0 mM) in 25 mM HEPES buffer (pH = 7.60) in the presence of 2.0 equiv of

$Zn(OAc)_2$ water solution (2.0 mM). Reaction time: 2 h, then diluted 100-fold using HEPES. (λ_{exc} = 320 nm. Slit 5/5 nm. The fluorescence intensity at λ_{em} = 507 nm was used for each data point).

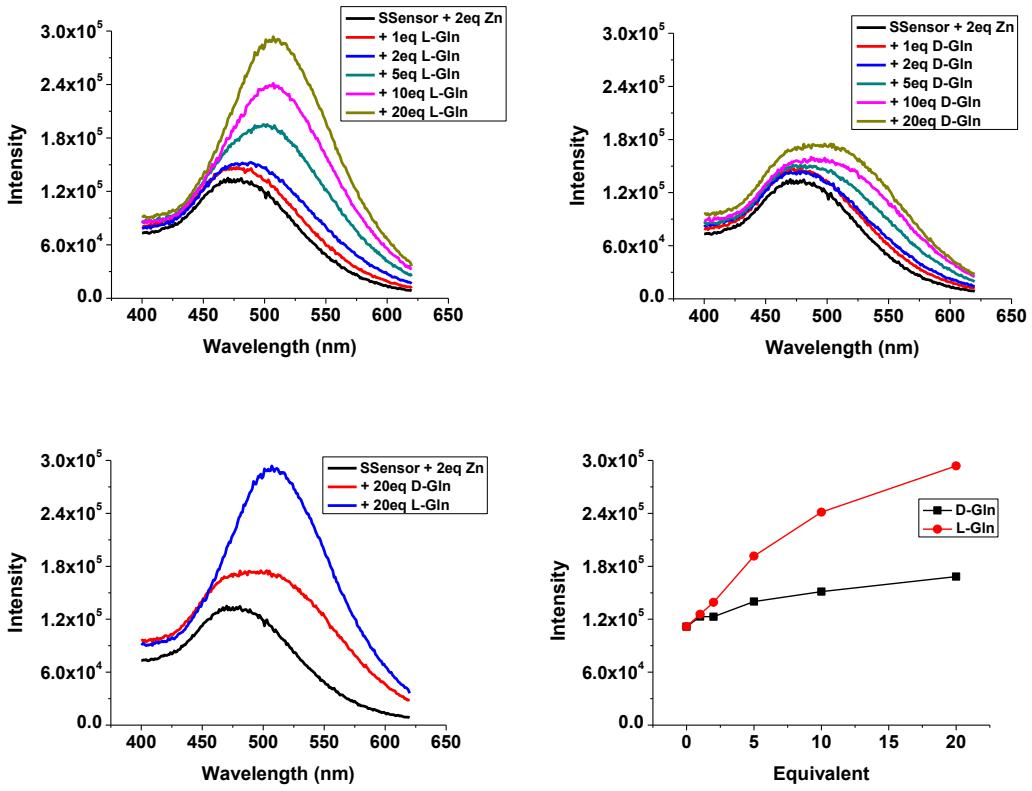

Figure 5.18. Fluorescence spectra of (*S*)-**3.9** (1.0 mM) with various equiv of arginine, D-**3.14** or L-**3.14** (4.0 mM) in 25 mM HEPES buffer (pH = 7.60) in the presence of 2.0 equiv of $Zn(OAc)_2$ water solution (2.0 mM). Reaction time: 2 h, then diluted 100-fold using HEPES. (λ_{exc} = 320 nm. Slit 5/5 nm. The fluorescence intensity at λ_{em} = 513 nm was used for each data point).

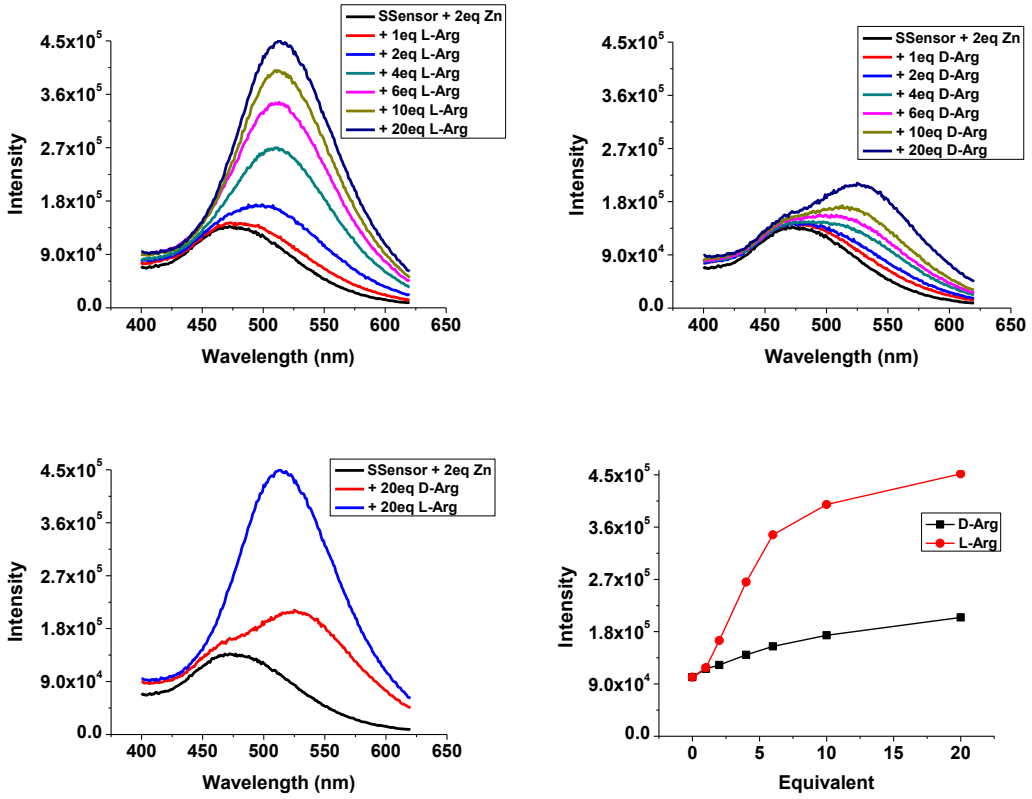

Figure 5.19. Fluorescence spectra of (*S*)-**3.9** (1.0 mM) with various equiv of asparagine, D-**3.18** or L-**3.18** (4.0 mM) in 25 mM HEPES buffer (pH = 7.60) in the presence of 2.0 equiv of $Zn(OAc)_2$ water solution (2.0 mM). Reaction time: 2 h, then diluted 100-fold using HEPES. (λ_{exc} = 320 nm. Slit 5/5 nm. The fluorescence intensity at λ_{em} = 506 nm was used for each data point).

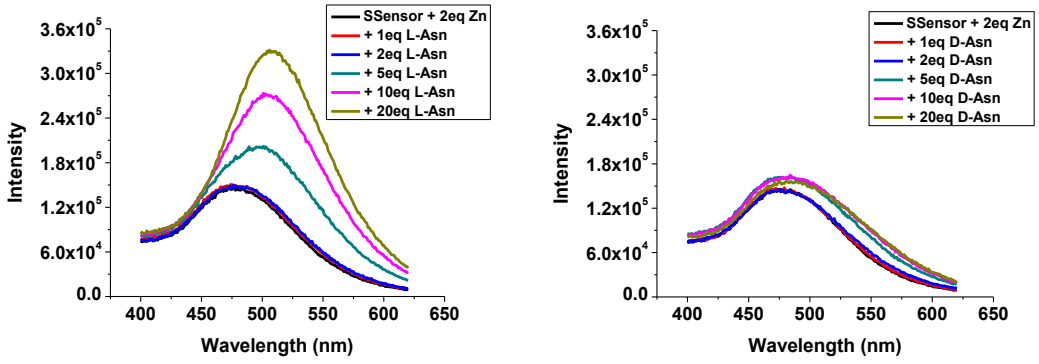

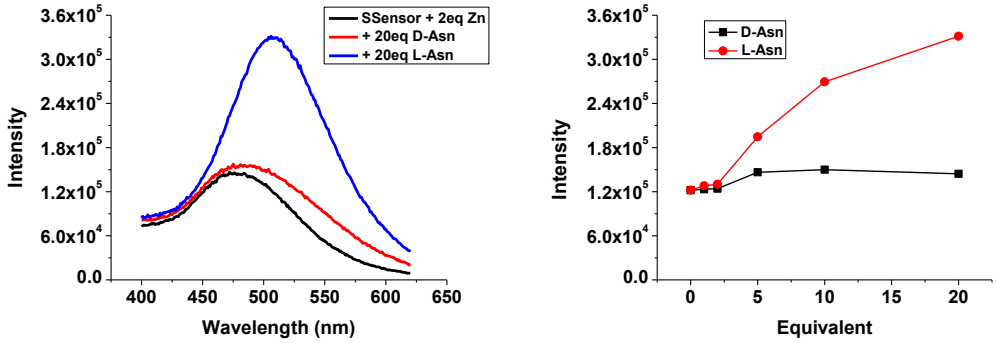

Figure 5.20. Fluorescence spectra of (*S*)-**3.9** (1.0 mM) with various equiv of leucine, D-**3.10** or L-**3.10** (4.0 mM) in 25 mM HEPES buffer (pH = 7.60) in the presence of 2.0 equiv of $Zn(OAc)_2$ water solution (2.0 mM). Reaction time: 2 h, then diluted 100-fold using HEPES. (λ_{exc} = 320 nm. Slit 5/5 nm. The fluorescence intensity at λ_{em} = 506 nm was used for each data point).

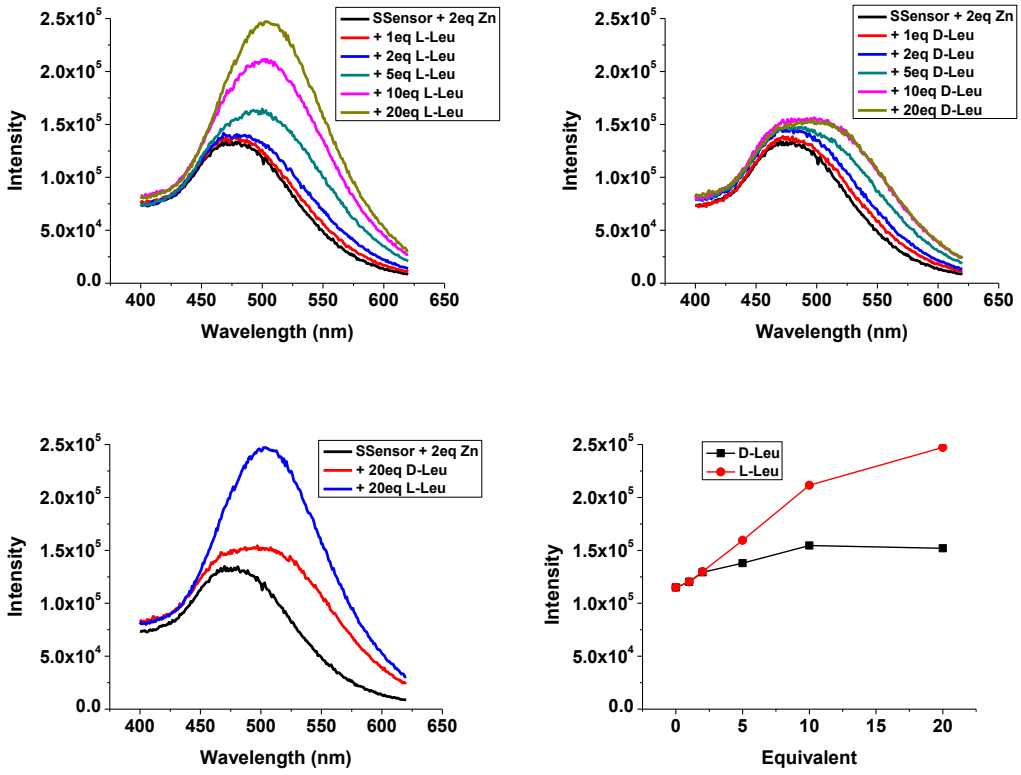

Figure 5.21. Fluorescence spectra of (*S*)-**3.9** (1.0 mM) with various equiv of serine, D-**3.17** or L-**3.17** (4.0 mM) in 25 mM HEPES buffer (pH = 7.60) in the presence of 2.0 equiv of $Zn(OAc)_2$

water solution (2.0 mM). Reaction time: 2 h, then diluted 100-fold using HEPES. (λ_{exc} = 320 nm. Slit 5/5 nm. The fluorescence intensity at λ_{em} = 502 nm was used for each data point).

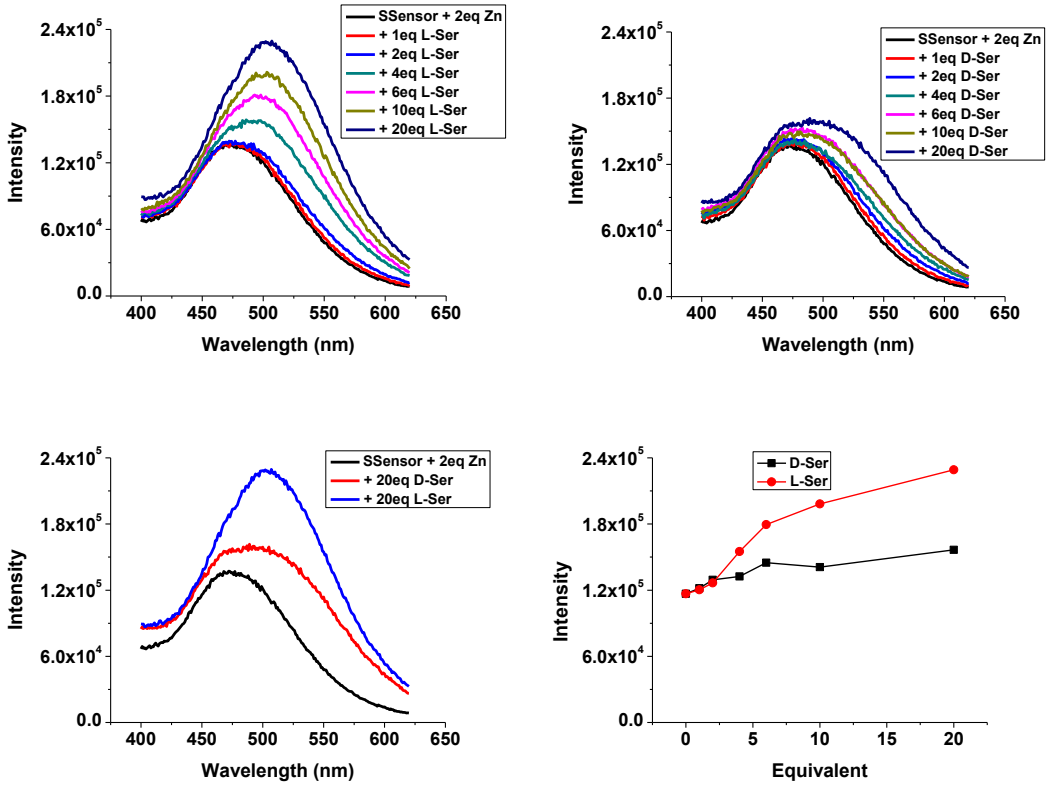

Figure 5.22. Fluorescence spectra of (*S*)-**3.9** (1.0 mM) with various equiv of phenylalanine, D-**3.15** or L-**3.15** (4.0 mM) in 25 mM HEPES buffer (pH = 7.60) in the presence of 2.0 equiv of $Zn(OAc)_2$ water solution (2.0 mM). Reaction time: 2 h, then diluted 100-fold using HEPES. (λ_{exc}=320 nm. Slit 5/5 nm. Fluorescence intensity at λ_{em} = 526 nm was used for each data point).

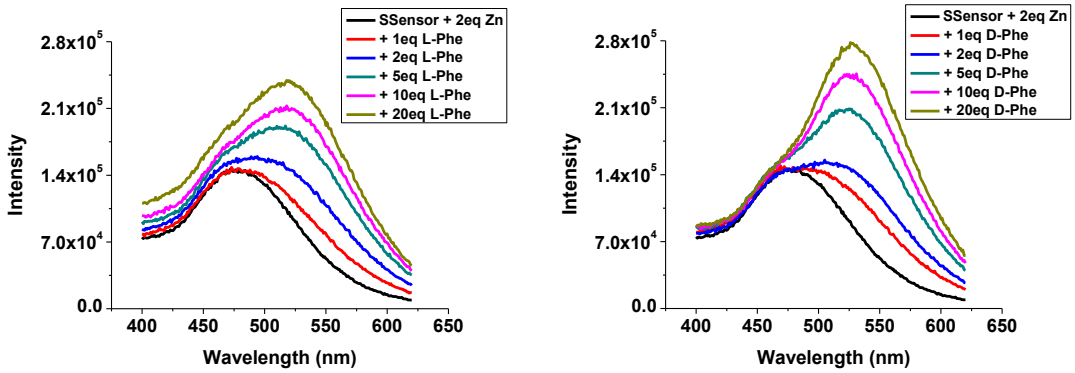

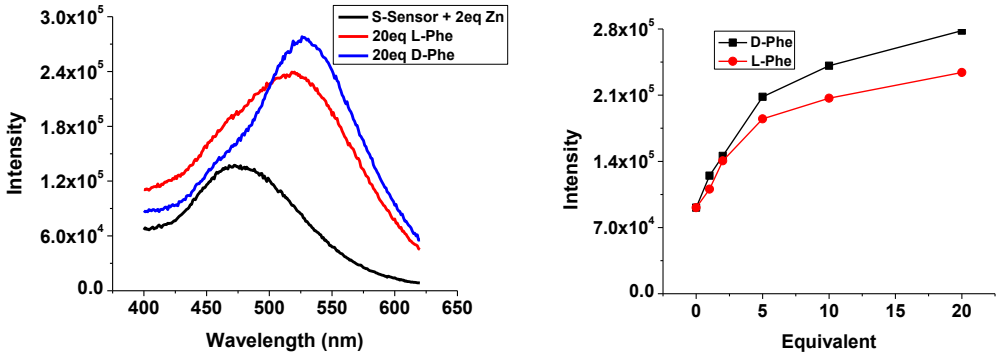

Figure 5.23. Fluorescence spectra of (*S*)-**3.9** (1.0 mM) with various equiv of threonine, D-**3.13** or L-**3.13** (4.0 mM) in 25 mM HEPES buffer (pH = 7.60) in the presence of 2.0 equiv of $Zn(OAc)_2$ water solution (2.0 mM). Reaction time: 2 h, then diluted 100-fold using HEPES. (λ_{exc} = 320 nm. Slit 5/5 nm. The fluorescence intensity at λ_{em} = 502 nm was used for each data point).

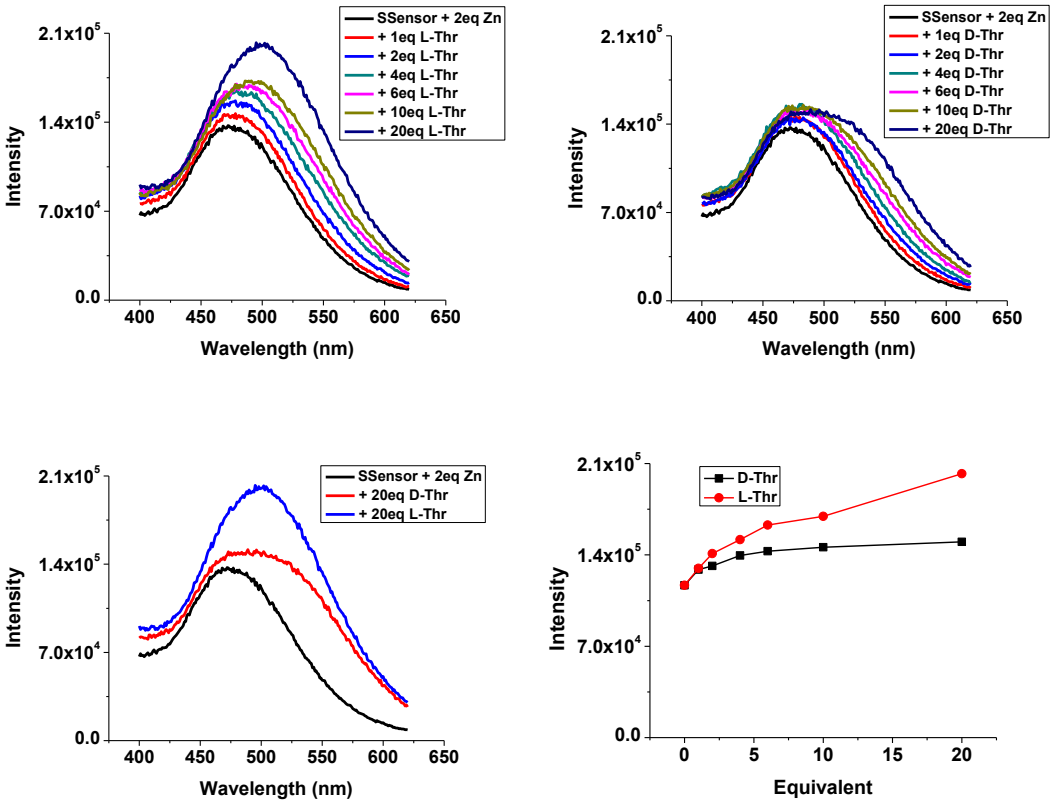

Figure 5.24. Fluorescence spectra of (*S*)-**3.9** (1.0 mM) with various equiv. of valine, D-**3.19** or L-**3.19** (4.0 mM) in 25 mM HEPES buffer (pH = 7.60) in the presence of 2.0 equiv of $Zn(OAc)_2$ water solution (2.0 mM). Reaction time: 2 h, then diluted 100-fold using HEPES. (λ_{exc} = 320 nm. Slit 5/5 nm. The fluorescence intensity at λ_{em} = 502 nm was used for each data point).

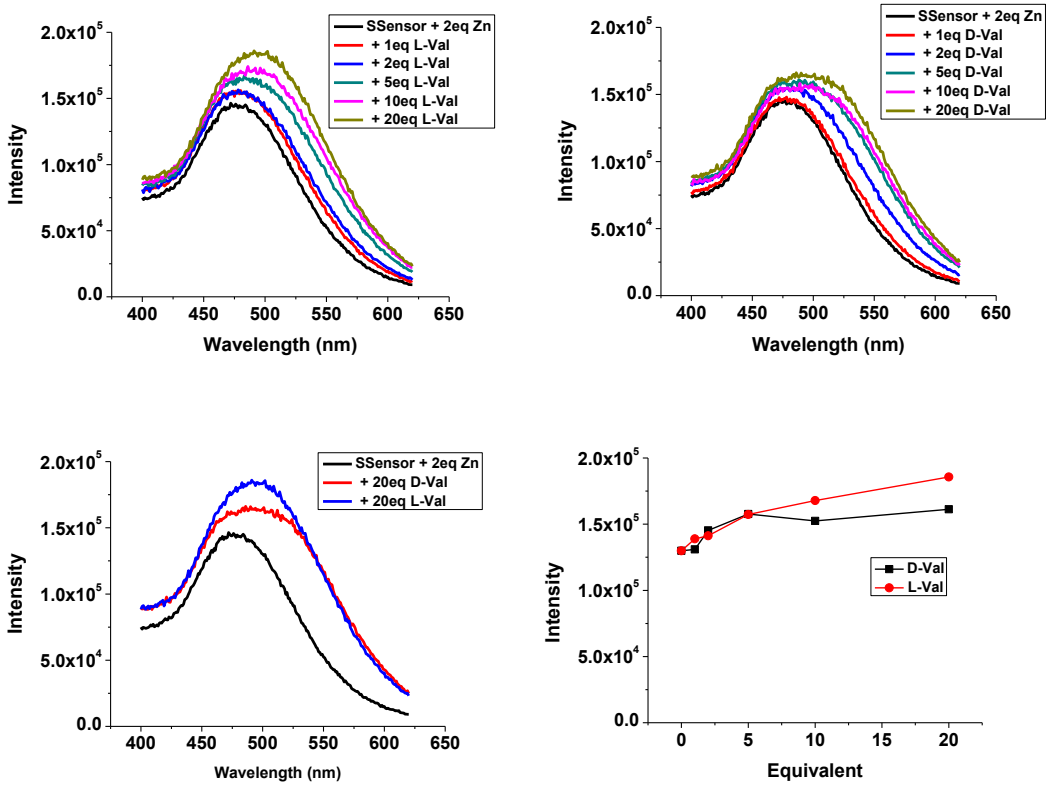

Figure 5.25. Fluorescence spectra of (*S*)-**3.9** (1.0 mM) with various equiv of tryptophan, D-**3.20** or L-**3.20** (4.0 mM) in 25 mM HEPES buffer (pH = 7.60) in the presence of 2.0 equiv of $Zn(OAc)_2$ water solution (2.0 mM). Reaction time: 2 h, then diluted 100-fold using HEPES. (λ_{exc} = 320 nm. Slit 5/5 nm. The fluorescence intensity at λ_{em} = 527 nm was used for each data point).

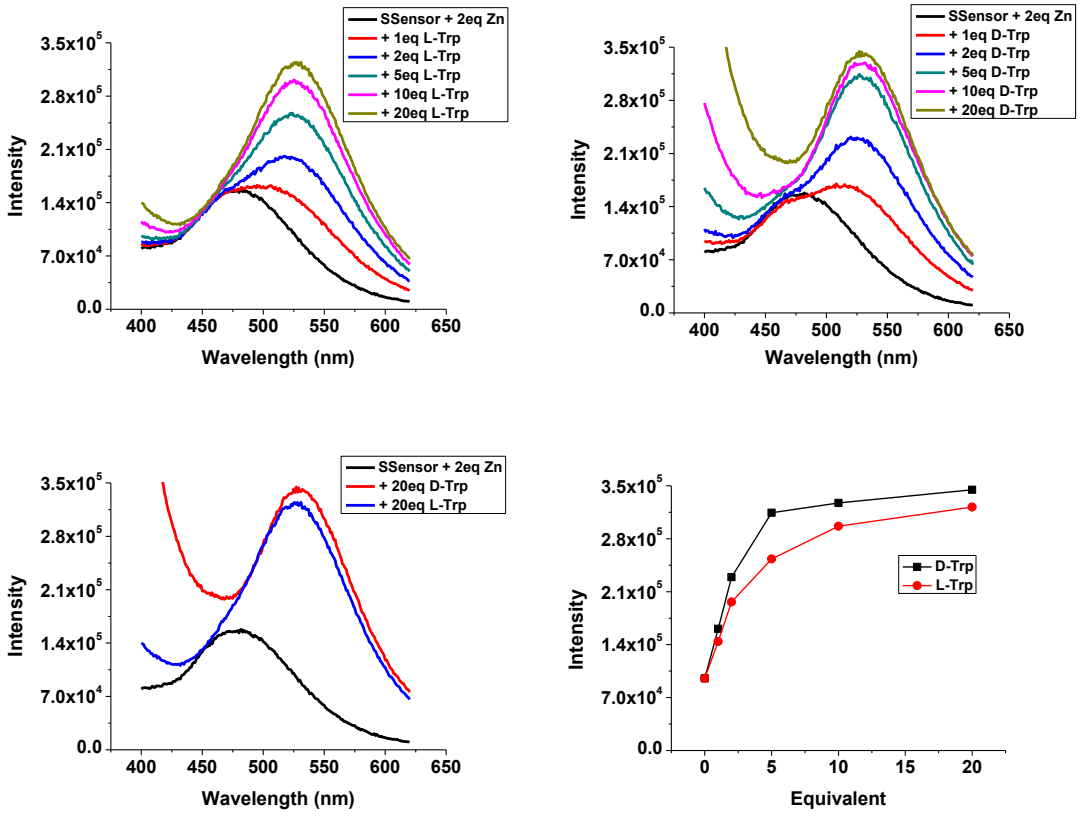

Figure 5.26. Fluorescence spectra of (*S*)-**3.9** (1.0 mM) with various equiv of methionine, D-**3.22** or L-**3.22** (4.0 mM) in 25 mM HEPES buffer (pH = 7.60) in the presence of 2.0 equiv of $Zn(OAc)_2$ water solution (2.0 mM). Reaction time: 2 h, then diluted 100-fold using HEPES. (λ_{exc}=320 nm. Slit 5/5 nm. Fluorescence intensity at λ_{em} = 509 nm was used for each data point)

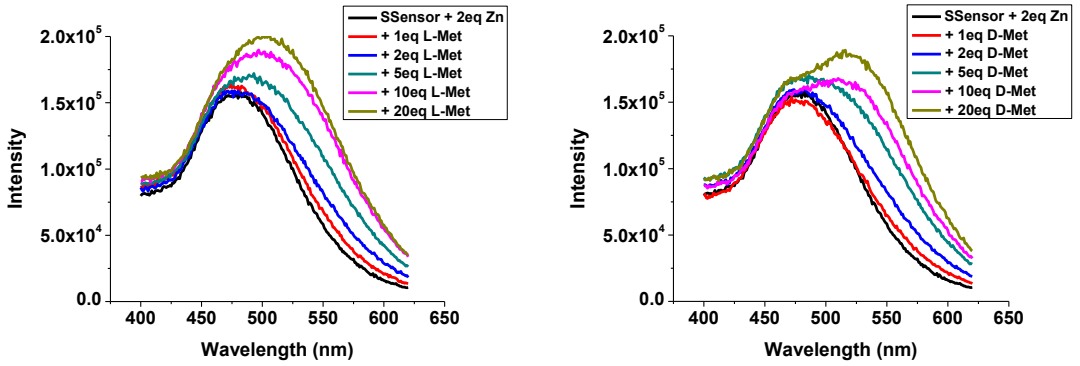

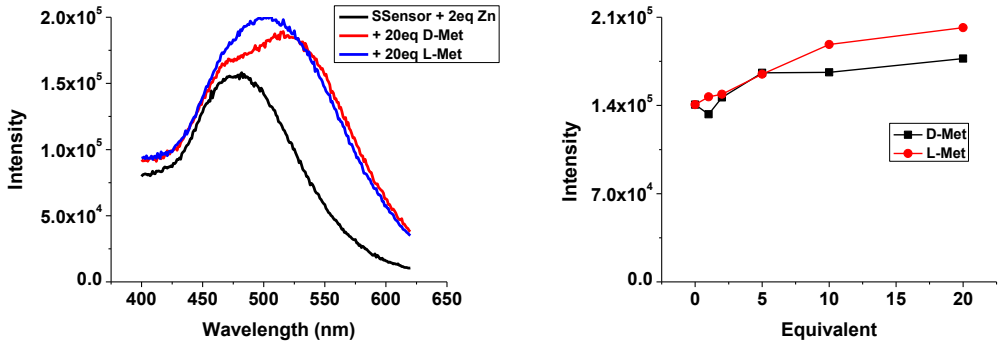

Figure 5.27. Fluorescence spectra of (*S*)-**3.9** (1.0 mM) with various equiv of tyrosine, D-**3.16** or L-**3.16** (2.0 mM) in 25 mM HEPES buffer (pH = 7.60) in the presence of 2.0 equiv of $Zn(OAc)_2$ water solution (2.0 mM). Reaction time: 2 h, then diluted 100-fold using HEPES. (λ_{exc} = 320 nm. Slit 5/5 nm. The fluorescence intensity at λ_{em} = 529 nm was used for each data point)

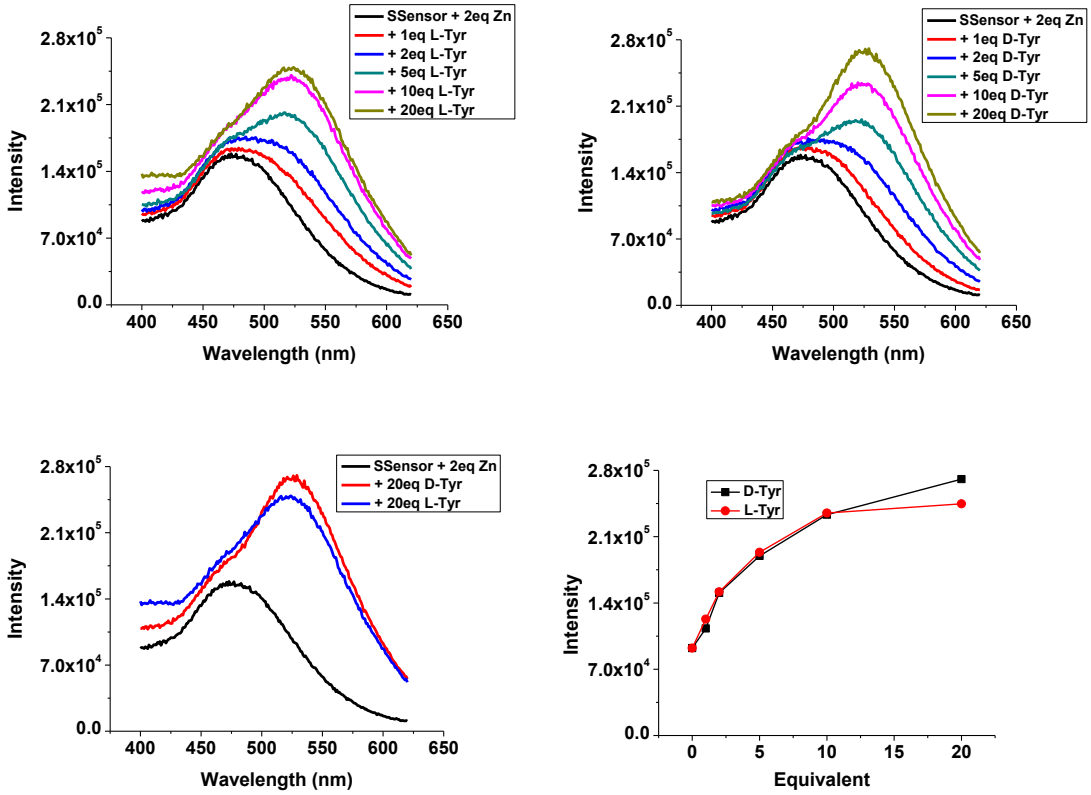

Figure 5.28. Fluorescence spectra of (*S*)-**3.9** (1.0 mM) with various equiv of lysine, D-**3.25** or L-**3.25** (4.0 mM) in 25 mM HEPES buffer (pH = 7.60) in the presence of 2.0 equiv of $Zn(OAc)_2$ water solution (2.0 mM). Reaction time: 2 h, then diluted 100-fold using HEPES. (λ_{exc} = 320 nm. Slit 5/5 nm. The fluorescence intensity at λ_{em} = 475 nm was used for each data point)

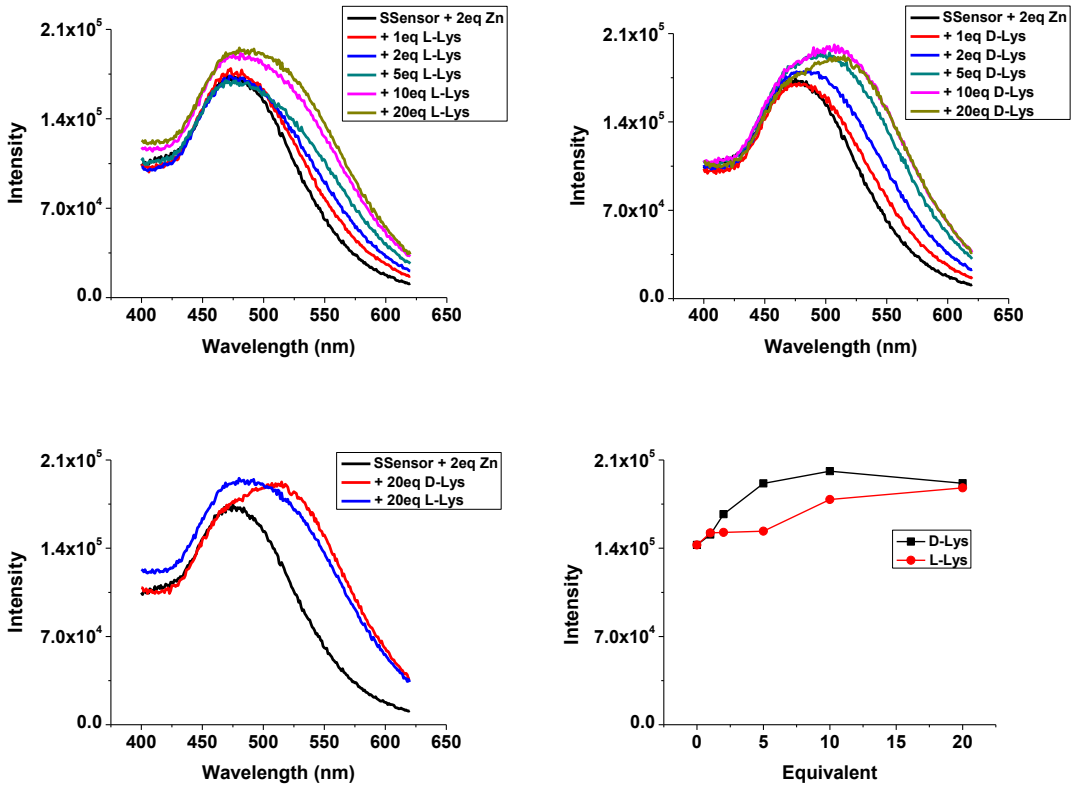

Figure 5.29. Fluorescence spectra of (*S*)-**3.9** (1.0 mM) with various equiv of alanine, D-**3.24** or L-**3.24** (4.0 mM) in 25 mM HEPES buffer (pH = 7.60) in the presence of 2.0 equiv of $Zn(OAc)_2$ water solution (2.0 mM). Reaction time: 2 h, then diluted 100-fold using HEPES. (λ_{exc} = 320 nm. Slit 5/5 nm)

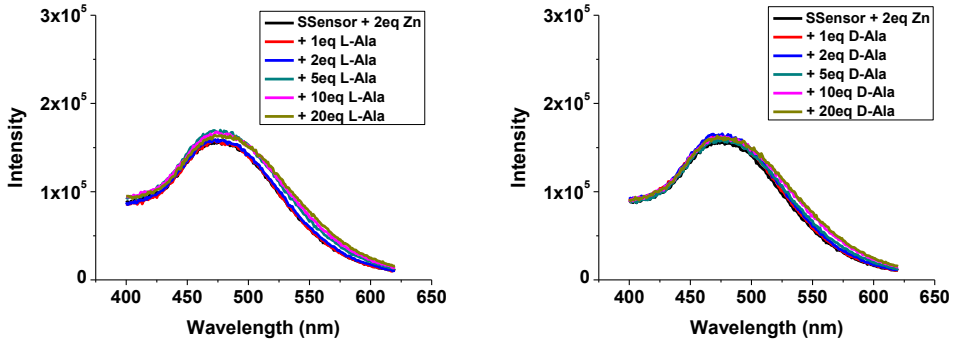

Figure 5.30. Fluorescence spectra of (*S*)-**3.9** (1.0 mM) with various equiv of proline, D-**3.23** or L-**3.23** (4.0 mM) in 25 mM HEPES buffer (pH = 7.60) in the presence of 2.0 equiv of $Zn(OAc)_2$ water solution (2.0 mM). Reaction time: 2 h, then diluted 100-fold using HEPES. (λ_{exc} = 320 nm. Slit 5/5 nm)

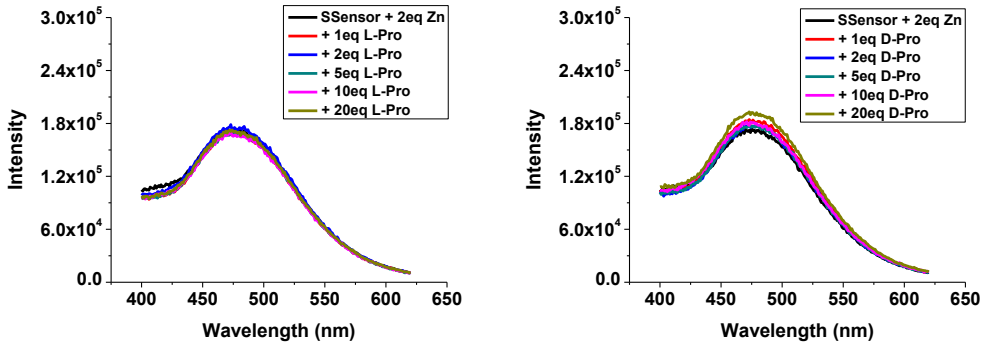

Figure 5.31. Fluorescence spectra of (*S*)-**3.9** (1.0 mM) with various equiv of aspartic acid, D-**3.26** or L-**3.26** (4.0 mM) in 25 mM HEPES buffer (pH = 7.60) in the presence of 2.0 equiv of $Zn(OAc)_2$ water solution (2.0 mM). Reaction time: 2 h, then diluted 100-fold using HEPES. (λ_{exc} = 320 nm. Slit 5/5 nm)

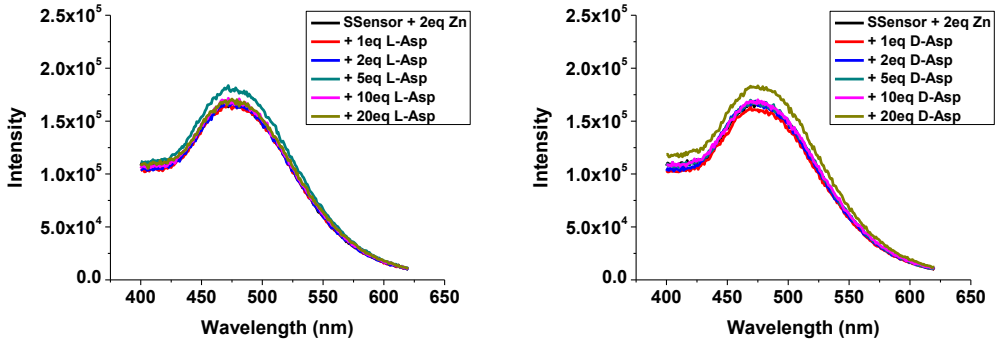

Figure 5.32. Fluorescence spectra of (*S*)-**3.9** (1.0 mM) with various equiv. of glutamic acid, D-**3.27** or L-**3.27** (4.0 mM) in 25 mM HEPES buffer (pH = 7.60) in the presence of 2.0 equiv of $Zn(OAc)_2$ water solution (2.0 mM). Reaction time: 2 h, then diluted 100-fold using HEPES. (λ_{exc} = 320 nm. Slit 5/5 nm)

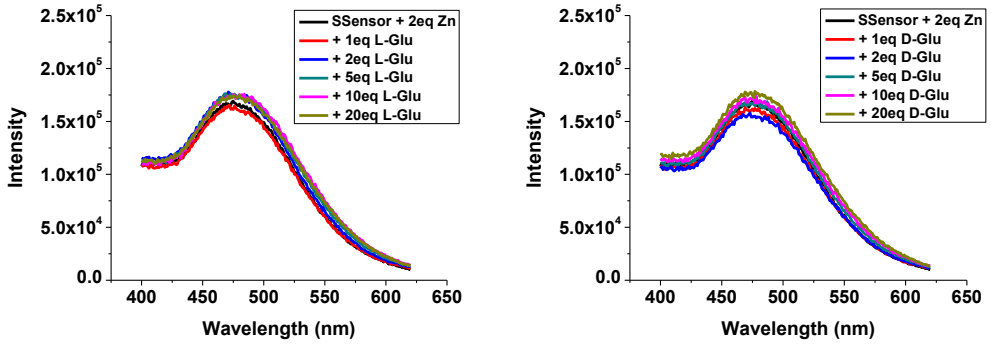

5.2.2.2. Enantioselective Fluorescent Imaging of Amino Acids in mouse

Polymer probes **3.9** had shown high enantioselectivity toward various amino acids in HEPES buffer. Therefore, we tried to use the probes in fluorescent imaging of amino acids in mouse.

0.2 mM and 1 mM (*S*)- and (*R*)-**3.9** HEPES buffer (25 mM, pH = 7.60) solution containing 0.4 mM and 2 mM Zn $(OAc)_2$ were freshly prepared. The volume of the blood in mouse is around 2 mL. Therefore, the concentration of probe was 10 μM if injecting 100 μL 0.2 mM solution into mouse body. We found that when the concentration of probe was larger

than 0.1 mM (200 μL 1mM **3.9** injection), mouse would die. Therefore, we chose the concentration of **3.9** in mouse as 10 μM (100 μL 0.2 mM **3.9** injection), 20 μM (200 μL 0.2 mM **3.9** injection) and 50 μM (100 μL 1mM **3.9** injection).

We first did the experiment on CD-1 normal male mice (at age of 5 weeks). The (*S*)- and (*R*)-**3.9** was 10 μM or 20 μM in mice. Perkin Elmer IVIS Spectrum In Vivo Imaging System was used for fluorescent imaging. Fluorescent imaging was conducted 10 min and 1 h after injection (Excitation: 430 nm; Emission: 500 nm). As shown in Figure **5.33**-**5.36**, all the mice exhibited fluorescence after injection of **3.9** with $Zn(OAc)_2$. Mice that injected (*S*)- or (*R*)-**3.9** did not have fluorescence intensity difference.

Figure 5.33. Fluorescent imaging of mice that have 40 μM $Zn(OAc)_2$ and 20 μM (*S*)-**3.9** (left) and 20 μM (*R*)-**3.9** (right) in the body. 10 min after injection.

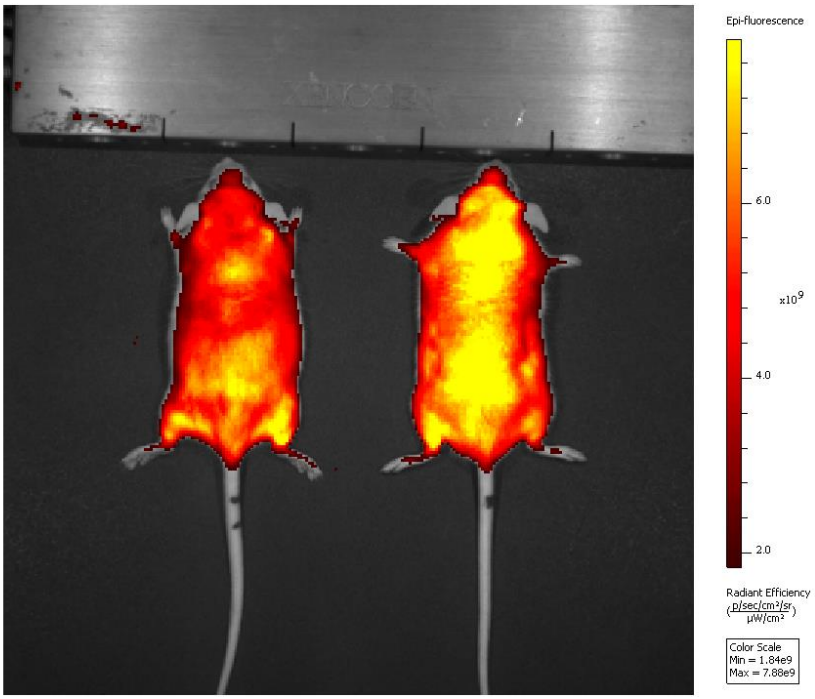

Figure 5.34. Fluorescent imaging of mice that have 40 μM $Zn(OAc)_2$ and 20 μM (*S*)-**3.9** (left) and 20 μM (*R*)-**3.9** (right) in the body. 1 h after injection.

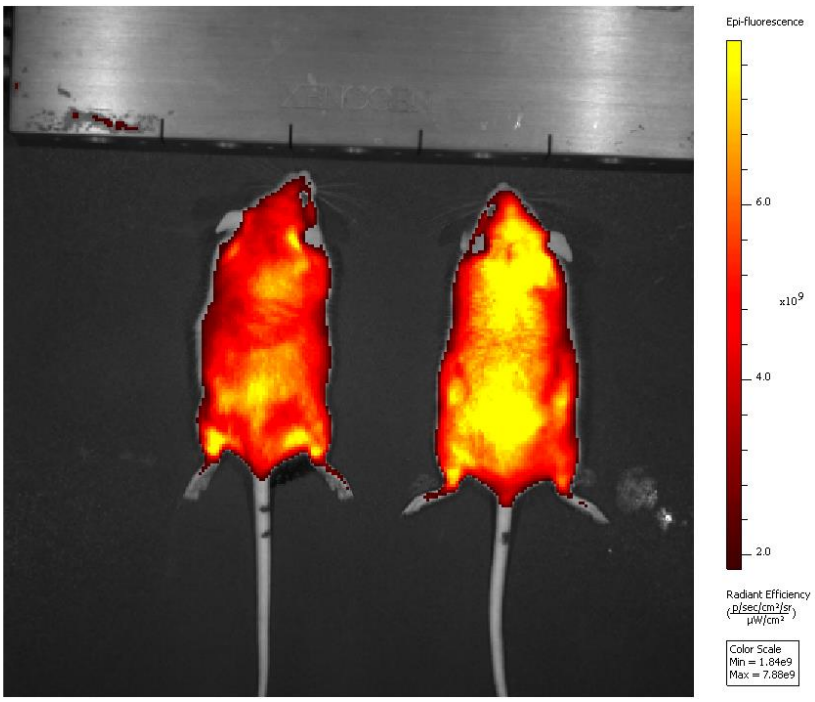

Figure 5.35. Fluorescent imaging of mice that have 20 μM $Zn(OAc)_2$ and 10 μM (*S*)-**3.9** (left) and 20 μM (*R*)-**3.9** (right) in the body. 10 min after injection.

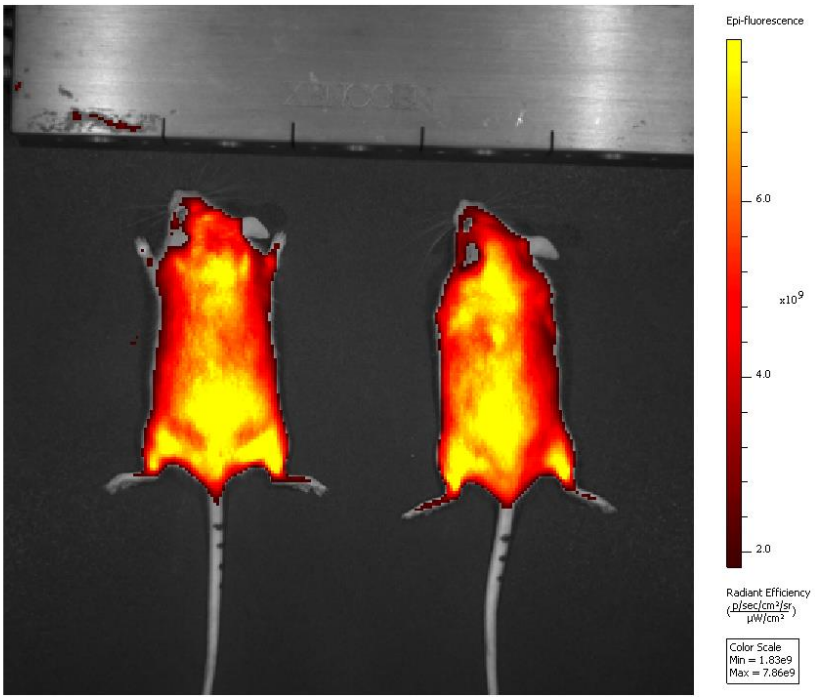

Figure 5.36. Fluorescent imaging of mice. From left to right: 20 μM $Zn(OAc)_2$ and 10 μM (*S*)-**3.9**; 40 μM $Zn(OAc)_2$ and 20 μM (*S*)-**3.9**; 20 μM $Zn(OAc)_2$ and 10 μM (*R*)-**3.9**; 40 μM $Zn(OAc)_2$ and 20 μM (*R*)-**3.9** in the body. 1 h after injection.

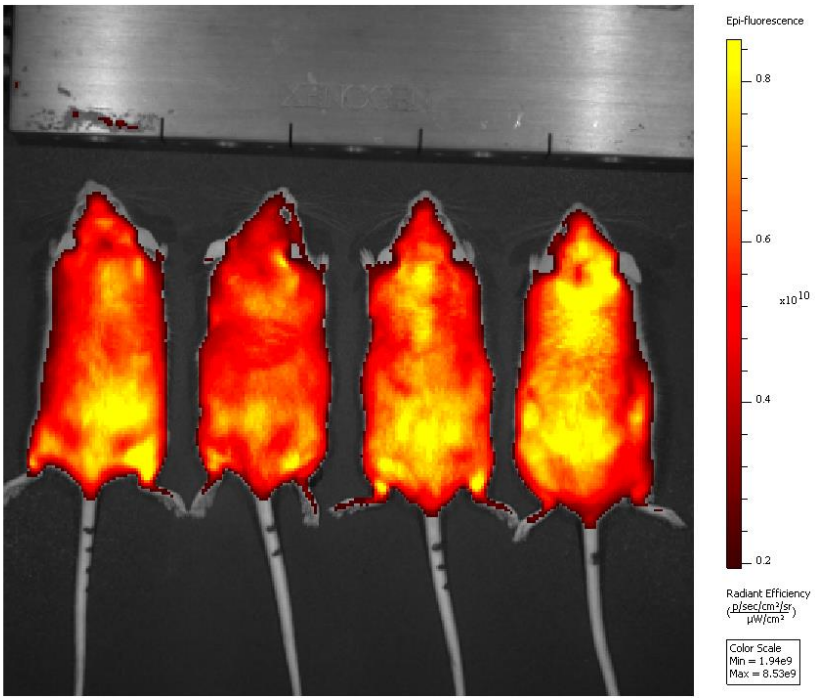

We then tried Rcn2-/- male mice at age of 20-22 weeks of age with dystonia (a condition of movement disorder). It was reported that mice with this disease may have higher percentage of D-amino acids.[14] Therefore, it is possible that D-amino acids may accumulated and have high concentration in certain region of mouse. (*S*)- or (*R*)-**3.9** with $Zn(OAc)_2$ were injected into the mice to make the concentration of probe as 10 μM or 20 μM. Then fluorescent imaging was conducted 10 min and 1 h after injection. However, no fluorescence was observed, probably because the light may be absorbed by the black fur and cannot penetrate the skin.

Therefore, we tried Nu/nu male nude mice (with prostate cancer xenograft tumor growing for 8-10 weeks) with no furs to see if better results can be obtained. D-amino acids may accumulate in the tumor part[15] and the probe may be able to turn on in tumor region.

(*S*)- or (*R*)-**3.9** with $Zn(OAc)_2$ were injected into the mice to make the concentration of probe as 10 μM or 50 μM. Fluorescent imaging was conducted 1 h and 25 h after injection. No fluorescence was observed in tumor region (close to right leg) (Figure **5.37**-**5.42**). The bright dots on the mice skin may be due to the contamination of the skin but not from the fluorescence of probes.

Figure 5.37. Fluorescent imaging of mice that have 20 μM $Zn(OAc)_2$ and 10 μM (*S*)-**3.9** in the body. Left two: tumor with moderate size; right: tumor with small size. 1 h after injection.

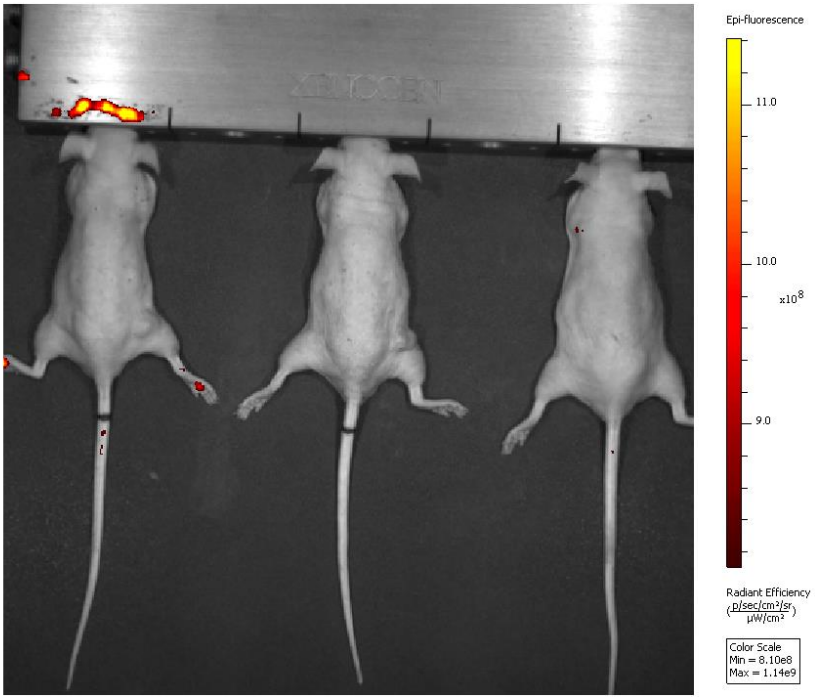

Figure 5.38. Fluorescent imaging of mice that have 20 μM $Zn(OAc)_2$ and 10 μM (*S*)-**3.9** in the body. Left two: tumor with moderate size; right: tumor with small size. 25 h after injection.

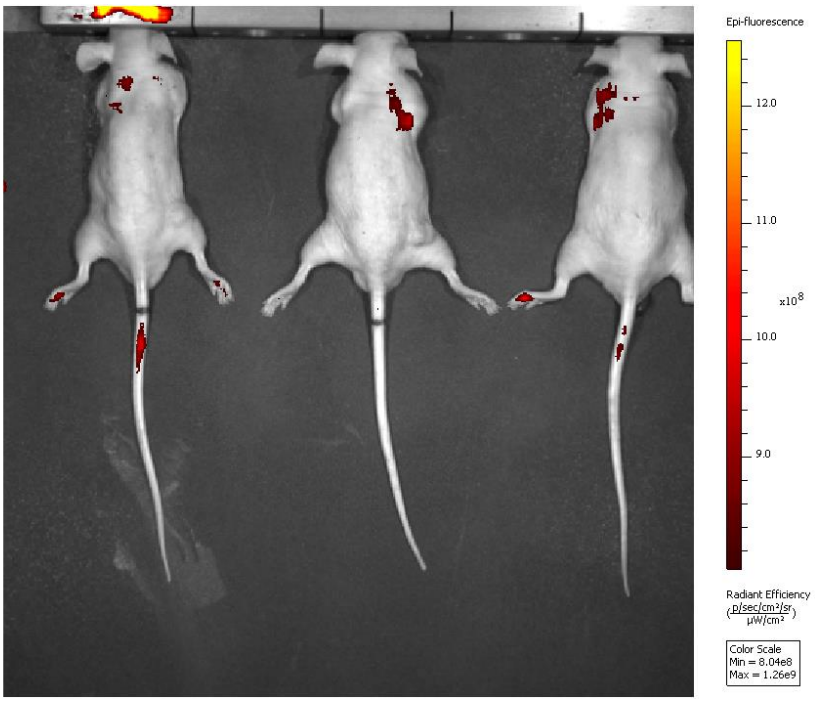

Figure 5.39. Fluorescent imaging of mice that have 20 μM $Zn(OAc)_2$ and 10 μM (*R*)-**3.9** in the body. Left two: tumor with moderate size; right: tumor with small size. 1 h after injection.

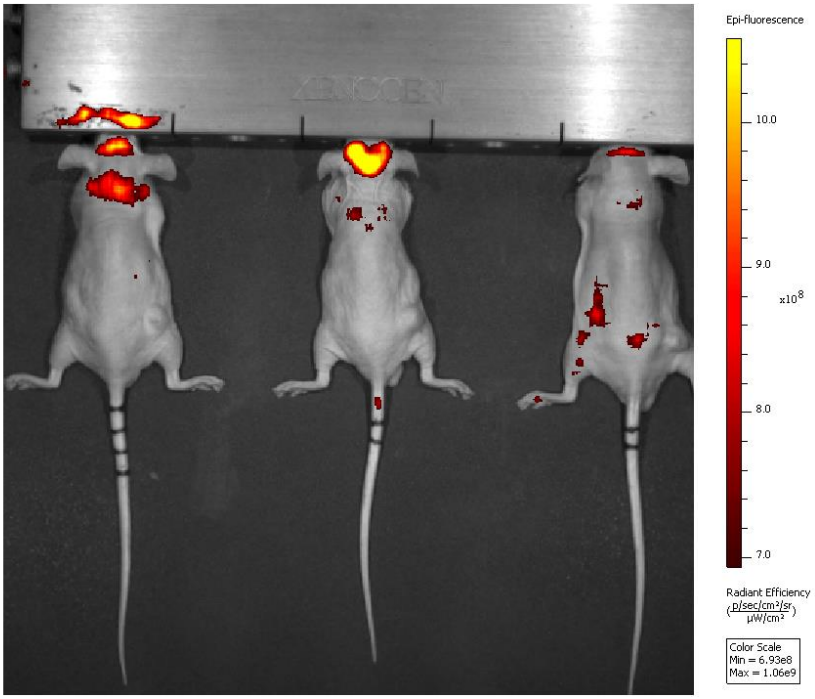

Figure 5.40. Fluorescent imaging of mice that have 20 μM $Zn(OAc)_2$ and 10 μM (*R*)-**3.9** in the body. Left two: tumor with moderate size; right: tumor with small size. 24 h after injection.

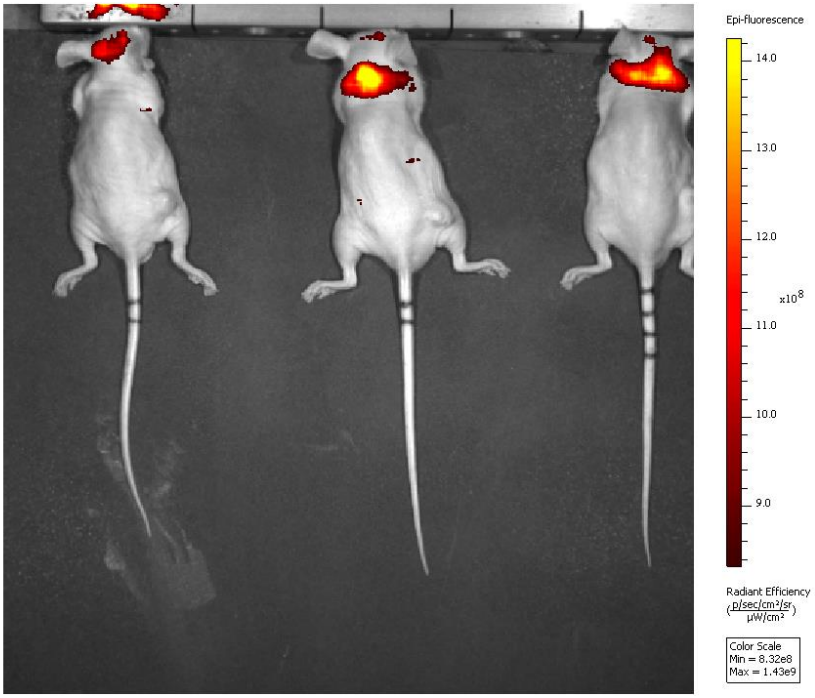

Figure 5.41. Fluorescent imaging of mice that have 100 μM $Zn(OAc)_2$ and 50 μM (*S*)-**3.9** (left) and (*R*)-**3.9** (right) in the body. 1 h after injection.

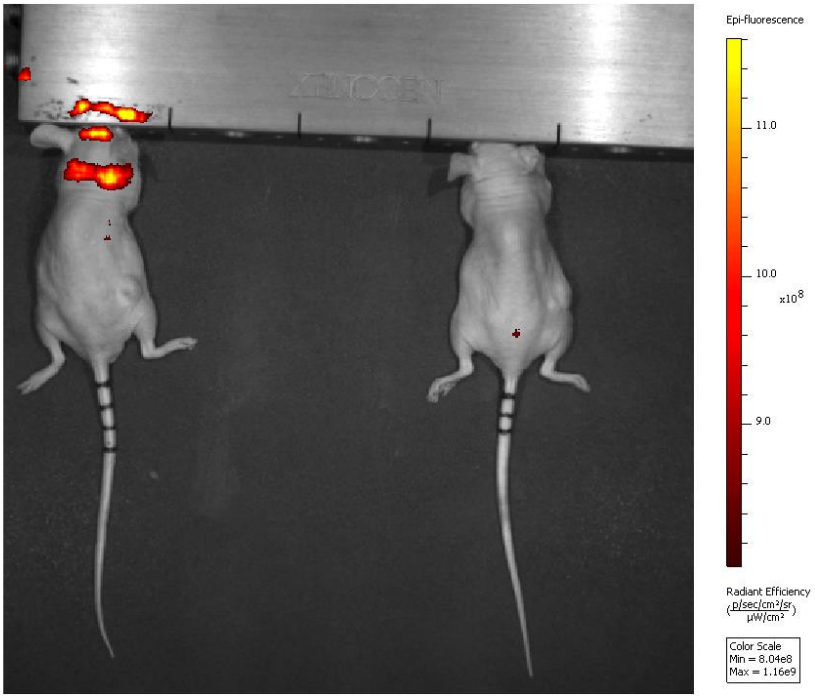

Figure 5.42. Fluorescent imaging of mice that have 100 μM $Zn(OAc)_2$ and 50 μM (*S*)-**3.9** (left) and (*R*)-**3.9** (right) in the body. 25 h after injection.

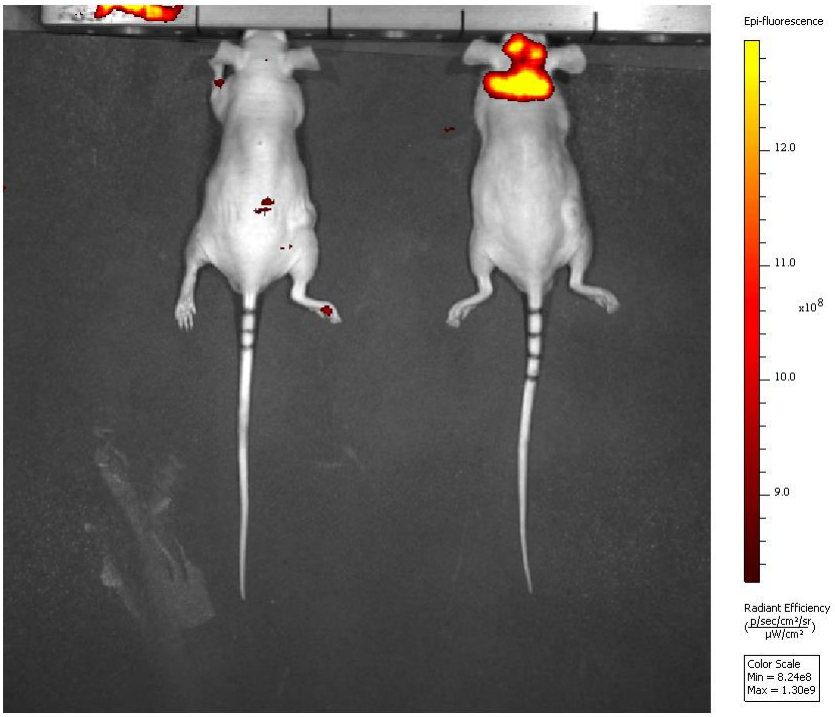

5.2.3. Conclusion

The *in vivo* imaging results demonstrated that the current probe might not be suitable for fluorescent imaging in animal at current conditions. The fluorescence observed in normal mice did not exhibit any particular pattern for useful biological information. No fluorescence was observed for the other two types of mouse models. These results suggested that the polymer probes do not have enough sensitivity for the fluorescent detection of amino acids in mice and that new probes need to be developed for *in vivo* use.

5.3. Experimental part

5.3.1. General information

All reactions were carried out under N_2 unless otherwise noted. All chemicals were purchased from Sigma Aldrich, Alfa Aesar or Thermo Fisher Scientific. NMR spectra were recorded on Varian-600 MHz spectrometer. Chemical shifts for ^1H NMR spectra were reported in parts per million relative to a singlet at 7.26 ppm for deuterated chloroform and a singlet at 4.79 ppm for D_2O. Chemical shifts for ^{13}C NMR were reported relative to the centerline of a triplet at 77.16 ppm for deuterated chloroform. Steady-state fluorescence emission spectra were recorded on Horiba FluoroMax-4 spectrofluorometer. Perkin Elmer IVIS Spectrum In Vivo Imaging System was used for fluorescent imaging of mice. pH measurements were performed on a Fisher Scientific Accumet AB15 pH meter.

5.3.2. Asymmetric catalyst screening experiment

Synthesis of leucine

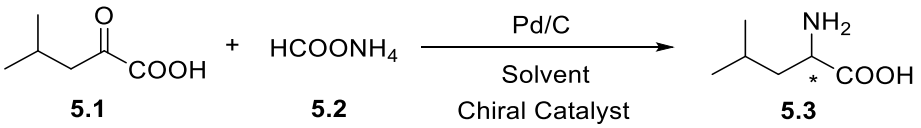

5.1 **5.2** **5.3**

4-methyl-2-oxovaleric acid (3.9 mg, 0.03 mmol, 1 equiv.), ammonium formate (13.2 mg, 0.21 mmol, 7 equiv.) and various equiv. of chiral additives and Lewis acids were added to 5 mL methanol:water (9:1) solution in a vial. were added. 8 mg Pd/C was then added to the mixture. The reaction mixture was stirred at room temperature for 20 h.

Synthesis of alaninol

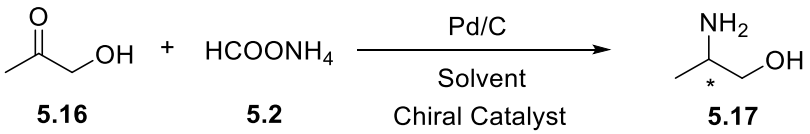

5.16 **5.2** **5.17**

Acetol (0.4 mg, 0.006 mmol, 1 equiv.), ammonium formate (3.8 mg, 0.06 mmol, 10 equiv.), K_2CO_3 (0.6 mg, 0.75 equiv.) and various equiv. of chiral additives and Lewis acids were added to 1 mL methanol:water (9:1) solution. 3 mg Pd/C was then added to the mixture. The reaction mixture was stirred at room temperature for 20 h.

5.3.3. Fluorescence measurement

Catalyst screening of leucine synthesis

Solvent was evaporated after the reaction and the crude product was dissolved in BICINE buffer (25 mM, pH = 8.80) to make 4 mM reaction mixture solution (the total concentration of **5.1** and **5.3** were 4 mM). Then 50 μL (1 equiv.) (*S*)- or (*R*)-**3.9** (1 mM in BICINE buffer) and 50 μL (2 equiv.) $Zn(OAc)_2$ (2 mM in water) was mixed with 125 μL product solution in BICINE. The mixture was allowed to stand at room temperature for 2h, then diluted to 5 mL using BICINE buffer to measure fluorescent.

Catalyst screening of alaninol synthesis

After reaction, 83 μL solution (10 equiv. (**5.16** and **5.17** in total)) was taken out to mix with (*S*)- or (*R*)-**3.9** (50 μL, 1 equiv., 1 mM in water), $Zn(OAc)_2$ (50 μL, 2 equiv., 2 mM in water) and 2 equiv. of K_2CO_3 solid. After 2 h, the mixture was diluted to 5 mL using water for fluorescence measurement.

Fluorescent response of (*S*)-3.9 toward amino acids

Stock solution of 1 mM polymer sensor (*S*)-**3.9** and 4 mM amino acids in HEPES buffer (pH = 7.60, 25mM) were freshly prepared. Stock solution of 2 mM $Zn(OAc)_2$ in water was freshly prepared. In the fluorescence enhancement study, a 50 μL solution of (*S*)-**3.9** (1 equiv.) was mix with 50 μL $Zn(OAc)_2$ solution (2 equiv.) and various equivalent of amino acids in 5 mL volumetric flasks. The resulting solution was allowed to stand at room temperature for 2 h before diluting to desired concentration (10 μM) using HEPES buffer. All the measurements were taken within 1 h.

5.3.4. Fluorescent imaging of mice

CD-1 normal male mice (at 5 weeks of age), Rcn2-/- male mice at 20-22 weeks of age with dystonia (a condition of movement disorder) and Nu/nu male nude mice (with prostate cancer xenograft tumor growing for 8-10 weeks) were obtained from Dr. Jiang He's lab in Department of Radiology and Medical Imaging at University of Virginia. The procedures were performed according to animal protocol approved by Institutional Animal Care and Use Committee, University of Virginia. 0.2 mM and 1 mM (*S*)- and (*R*)-**3.9** HEPES buffer (25 mM, pH = 7.60) solution containing 0.4 mM and 2 mM Zn $(OAc)_2$ were freshly prepared. The concentrations of **3.9** in mouse were 10 μM (100 uL 0.2 mM **3.9** injection), 20 μM (200 uL 0.2 mM **3.9** injection) and 50 μM (100 uL 1mM **3.9** injection). Mice were anesthetized using isoflurane. The different amount of (*S*)- and (*R*)-**3.9** with Zn $(OAc)_2$ HEPES buffer solutions were then injected from the mice tails. Fluorescent imaging was then conducted (λ_{Exc} = 430 nm, λ_{Em} = 500 nm was used for imaging).

References

(1) Maruoka, K.; Ooi, T. *Chem. Rev.* **2003**, *103* (8), 3013–3028.

(2) Nájera, C.; Sansano, J. M. *Chem. Rev.* **2007**, *107* (11), 4584–4671.

(3) Liang, J.; Ruble, J. C.; Fu, G. C. *J. Org. Chem.* **1998**, *63* (7), 3154–3155.

(4) Liu, Y. E.; Lu, Z.; Li, B.; Tian, J.; Liu, F.; Zhao, J.; Hou, C.; Li, Y.; Niu, L.; Zhao, B. *J. Am. Chem. Soc.* **2016**, *138* (34), 10730–10733.

(5) Alexandre, F.-R.; Pantaleone, D. P.; Taylor, P. P.; Fotheringham, I. G.; Ager, D. J.; Turner, N. J. *Tetrahedron Lett.* **2002**, *43*, 707–710.

(6) Park, H.; Kim, K. M.; Lee, A.; Ham, S.; Nam, W.; Chin, J. *Nature* **2007**, 1518–1519.

(7) Yuan, L.; Li, Y.; Zou, C.; Wang, C.; Gao, J.; Miao, C.; Ma, E.; Sun, T. *Bioorganic Med. Chem. Lett.* **2012**, *22* (6), 2216–2220.

(8) Shi, S. L.; Wong, Z. L.; Buchwald, S. L. *Nature* **2016**, *532* (7599), 353–356.

(9) Tang, T. P.; Volkman, S. K.; Ellman, J. A. *J. Org. Chem.* **2001**, *66* (26), 8772–8778.

(10) Schoenheimer, R.; Ratner, S. *J. Biol. Chem.* **1939**, *127* (1), 301–313.

(11) Ogo, S.; Uehara, K.; Abura, T.; Fukuzumi, S. *J. Am. Chem. Soc.* **2004**, *126* (10), 3020–3021.

(12) Zeng, C.; Zhang, X.; Pu, L. *Chem. - A Eur. J.* **2017**, *23* (10), 2432–2438.

(13) Weatherly, C. A.; Du, S.; Parpia, C.; Santos, P. T.; Hartman, A. L.; Armstrong, D. W. *ACS Chem. Neurosci.* **2017**, *8* (6), 1251–1261.

(14) Fuchs, S. A.; Berger, R.; Klomp, L. W. J.; De Koning, T. J. *Mol. Genet. Metab.* **2005**, *85* (3), 168–180.

(15) Miller, J. A. *Cancer Res.* **1950**, *10* (2), 65–72.

Appendix

Appendix for Chapter 3

GPC Data for (*S*)-**3.9** (Top) and (*R*)-**3.9** (Bottom)

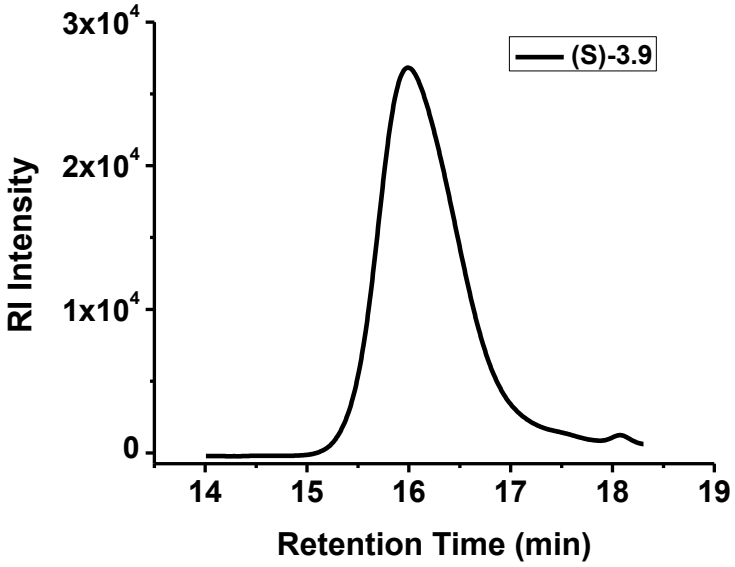

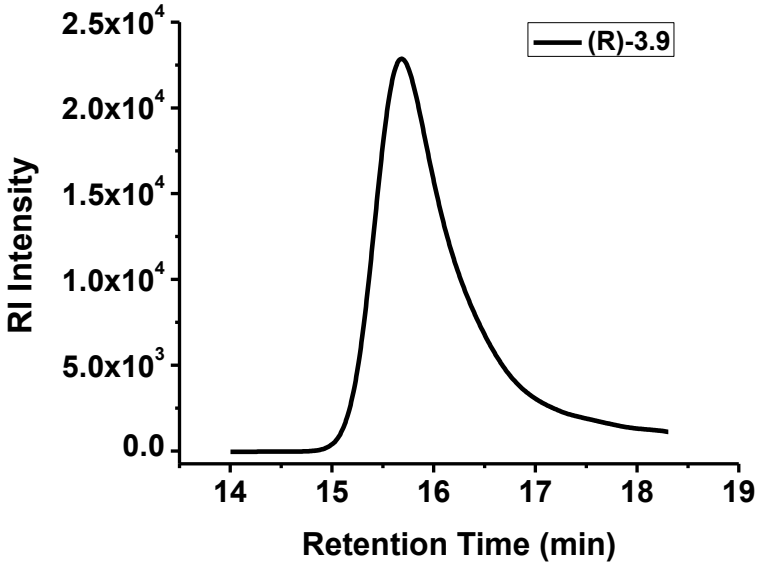

^{1}H and ^{13}C NMR spectra

^{1}H NMR spectra of (*S*)-**3.4**

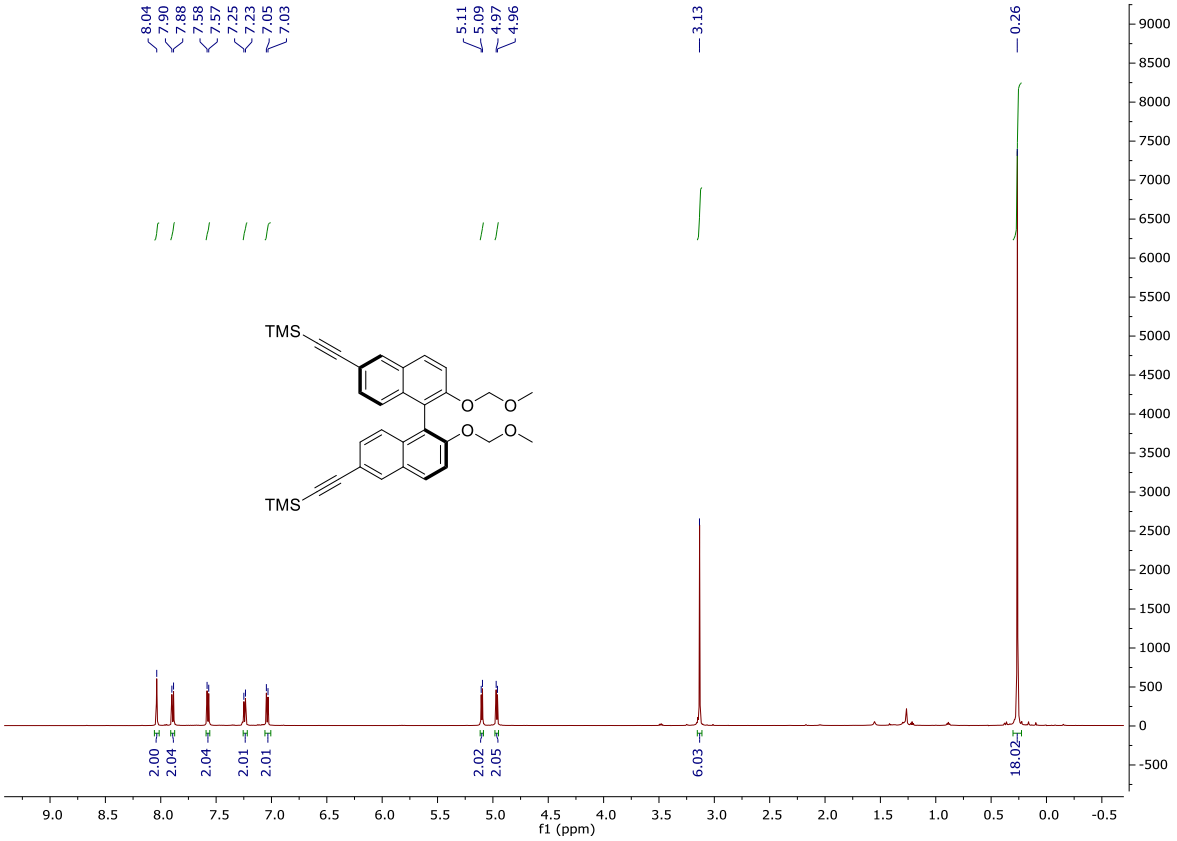

^{13}C NMR spectra of (*S*)-**3.4**

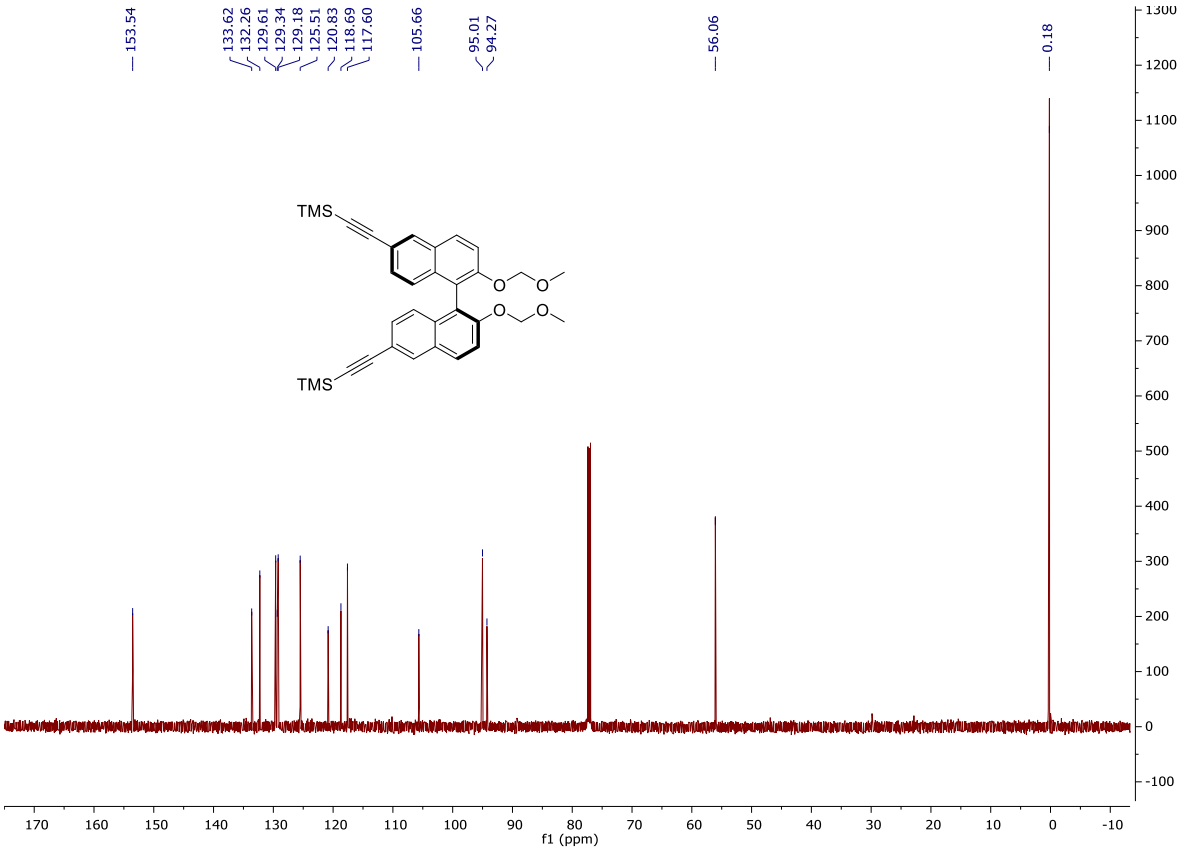

^{1}H NMR spectra of (*R*)-**3.4**

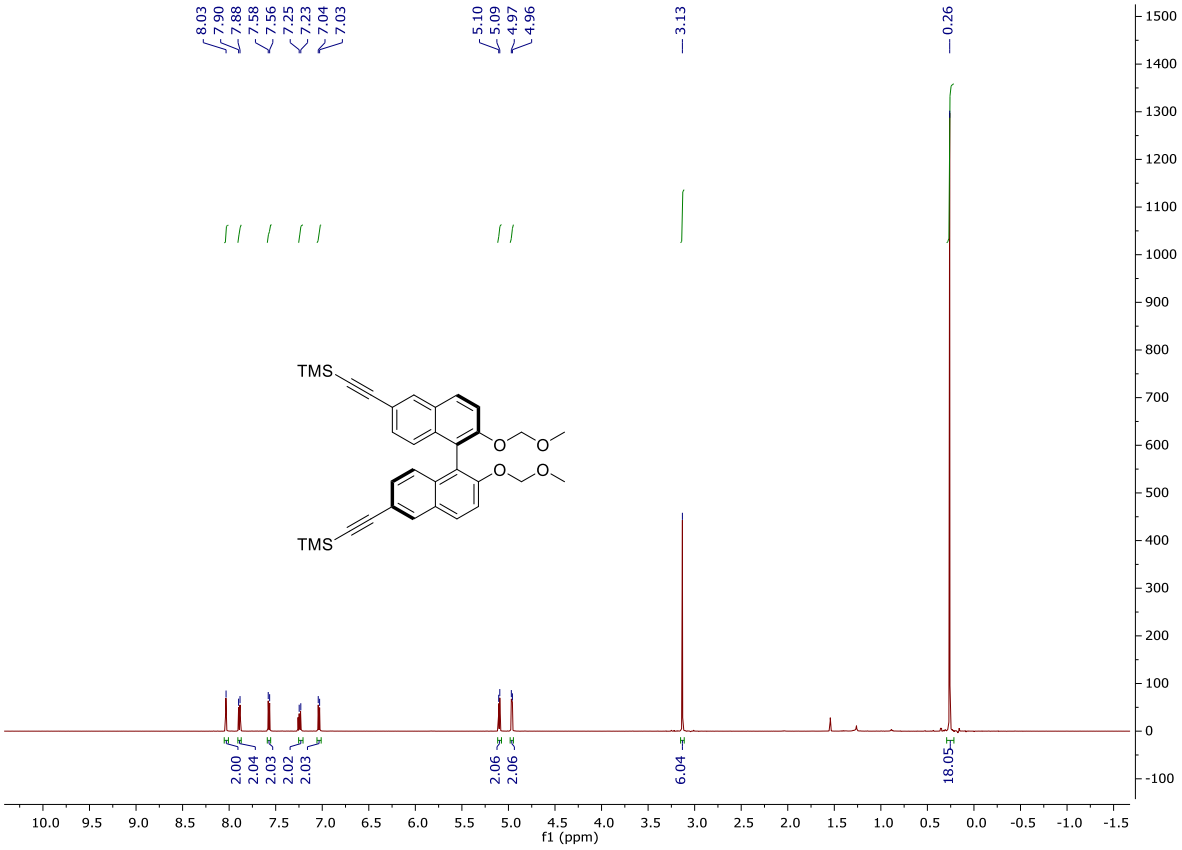

^{13}C NMR spectra of (*R*)-**3.4**

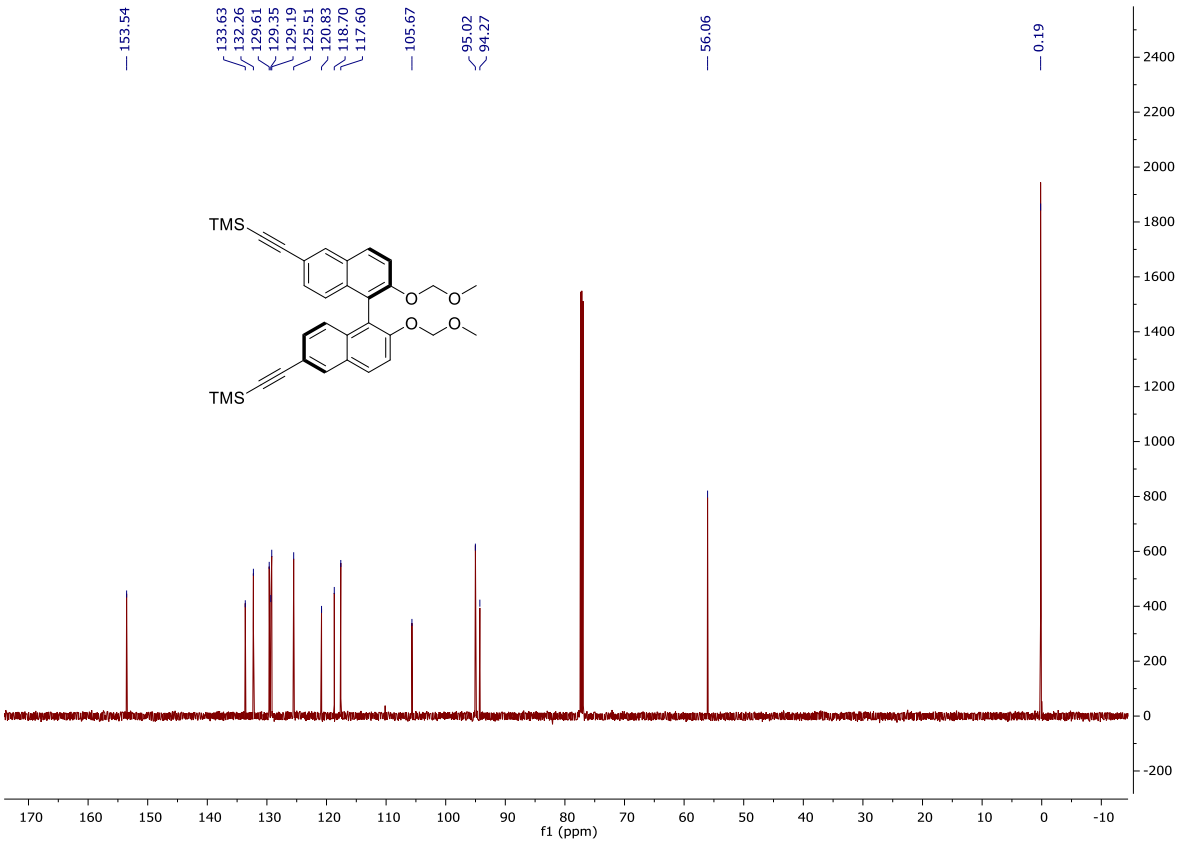

^{1}H NMR spectra of (*S*)-**3.5**

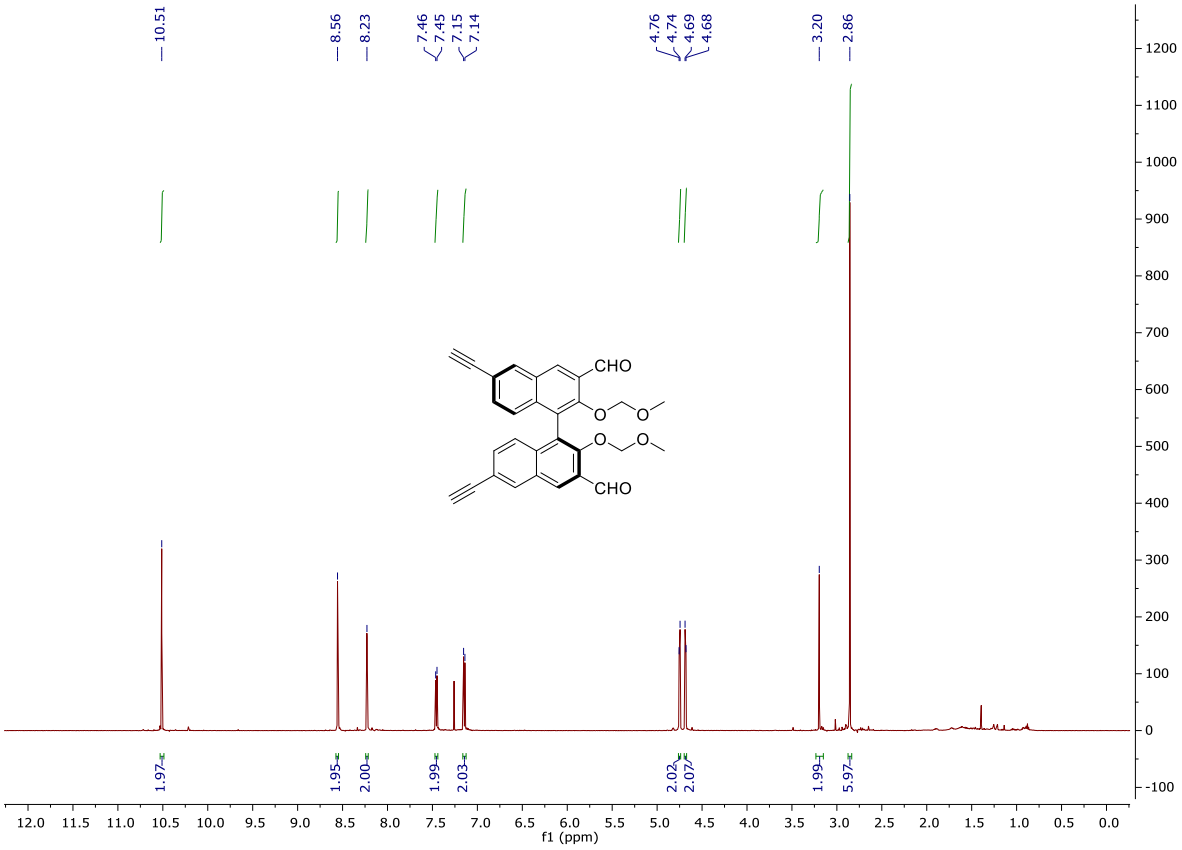

^{13}C NMR spectra of (*S*)-**3.5**

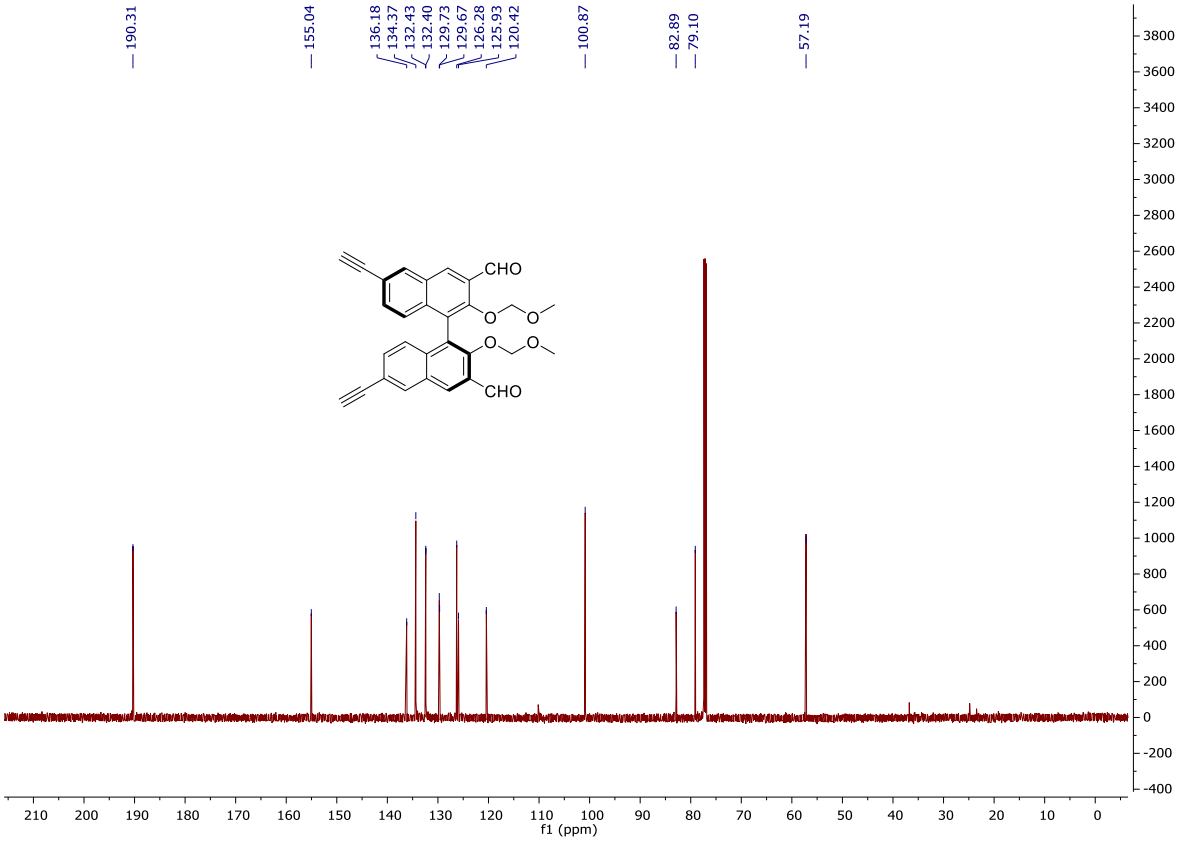

^{1}H NMR spectra of (*R*)-**3.5**

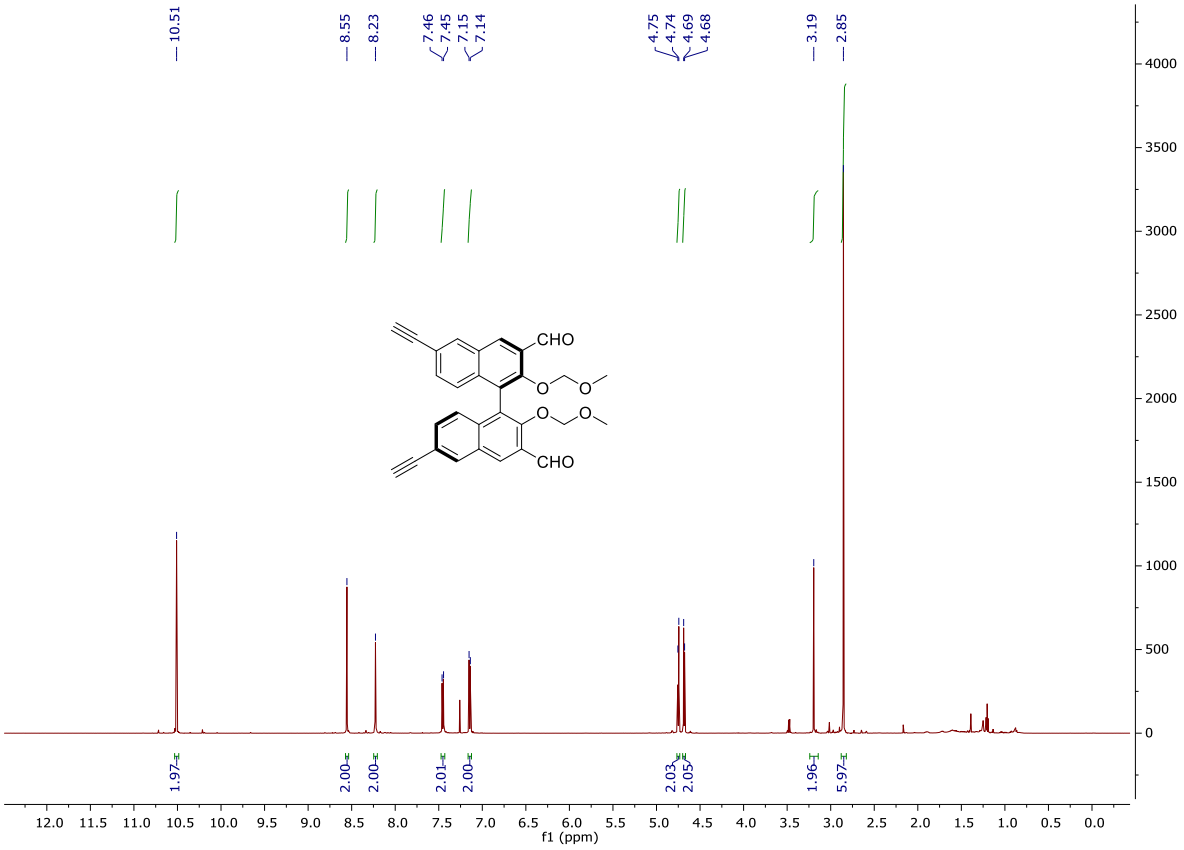

^{13}C NMR spectra of (*R*)-**3.5**

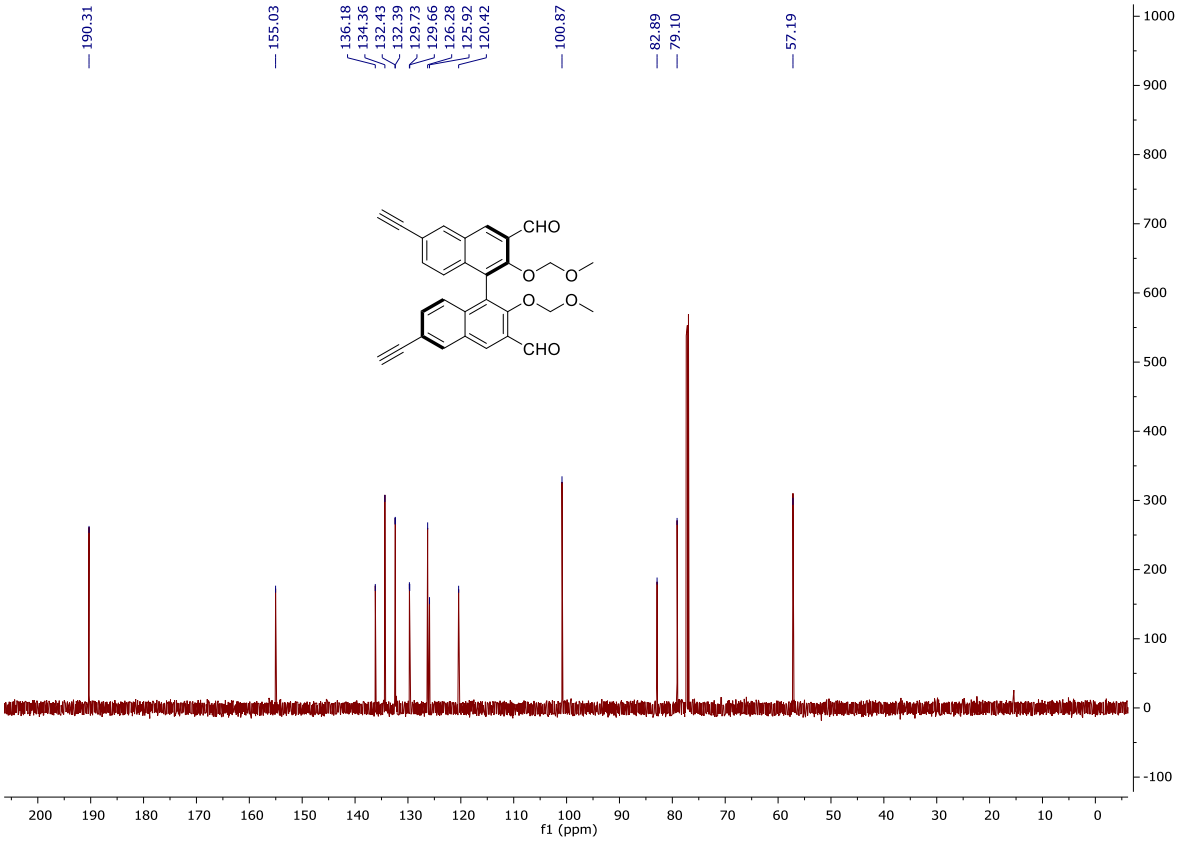

^{1}H NMR spectra of (*S*)-**3.6**

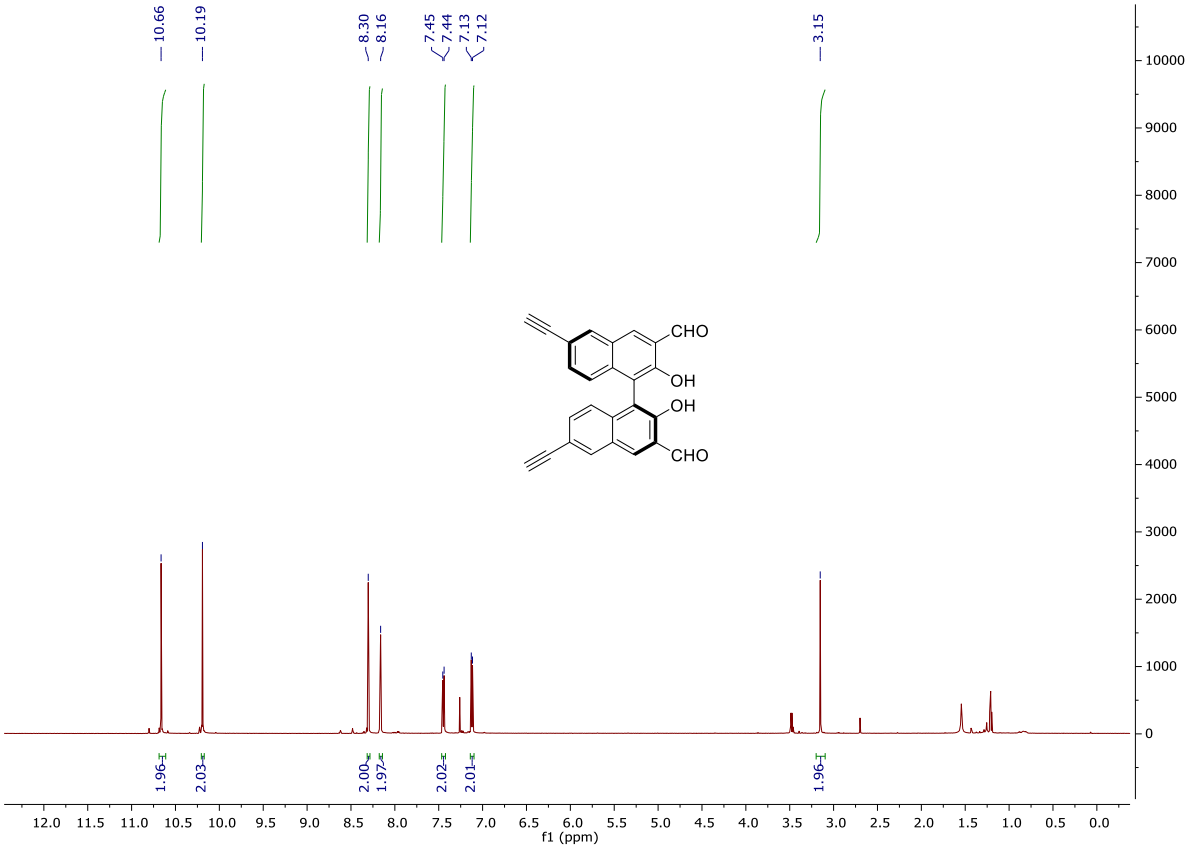

^{13}C NMR spectra of (*S*)-**3.6**

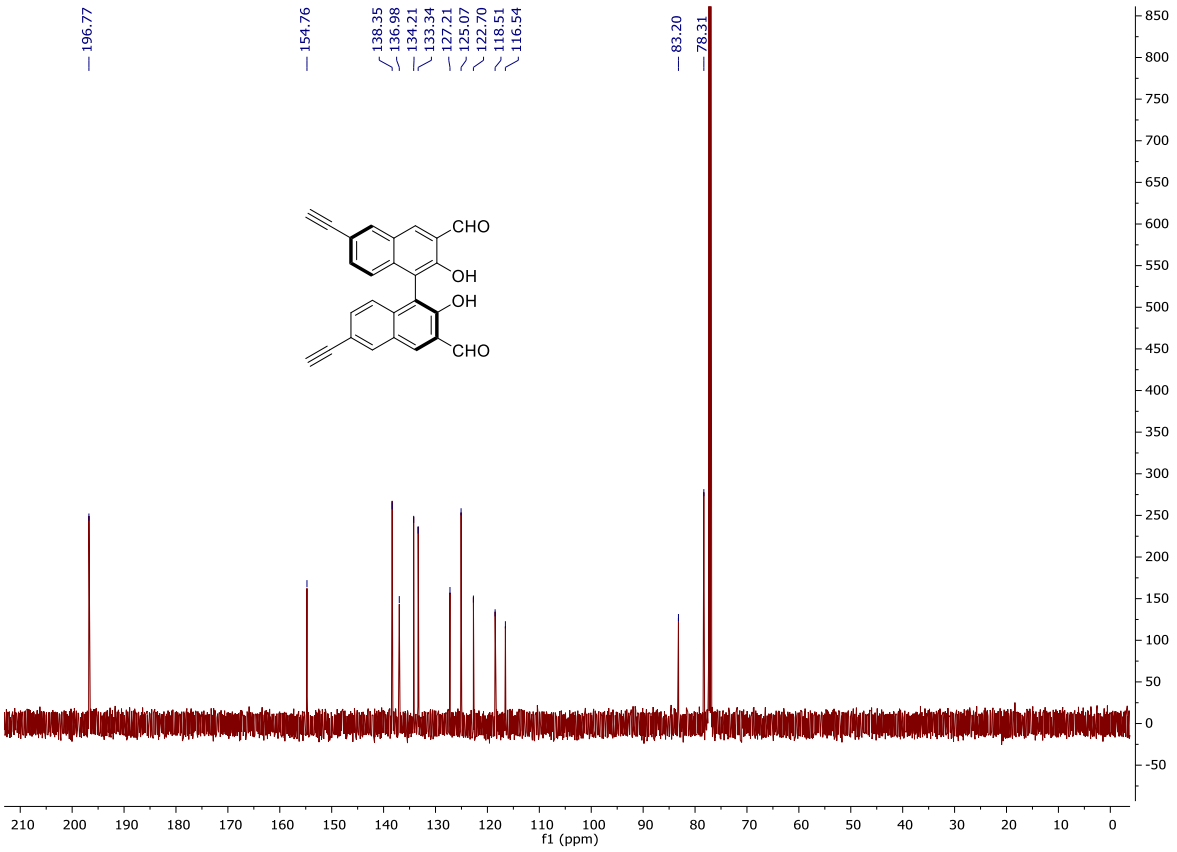

^{1}H NMR spectra of (*R*)-**3.6**

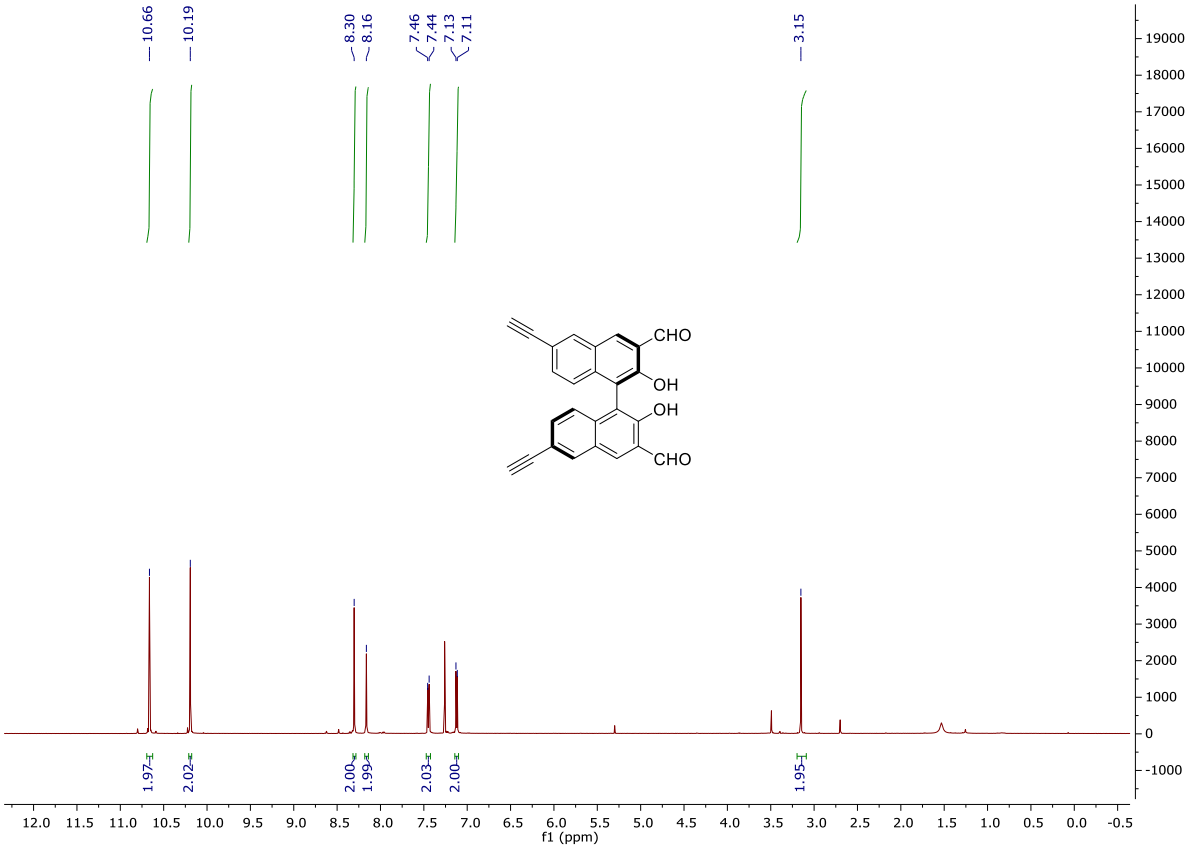

^{13}C NMR spectra of (*R*)-**3.6**

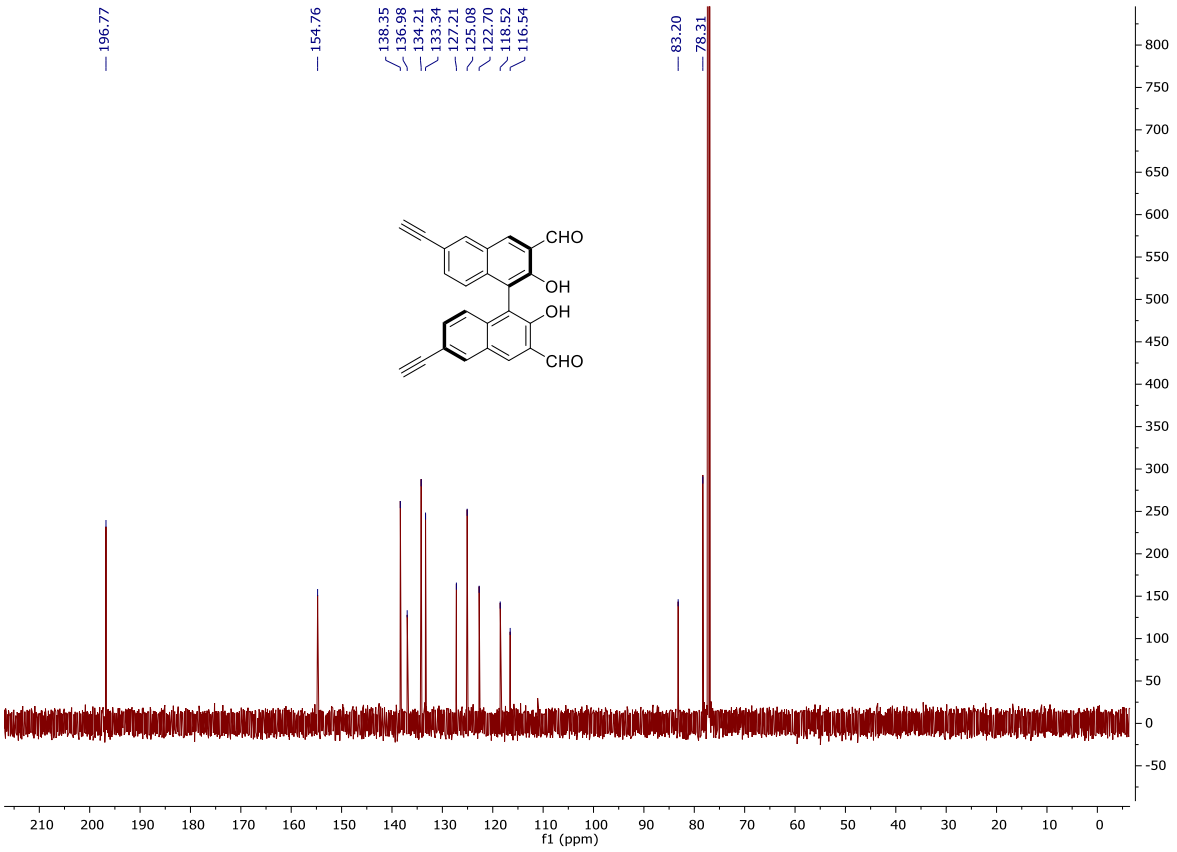

^{1}H NMR spectra of 2-azidoethyl 2-chloropropanoate **3.7**

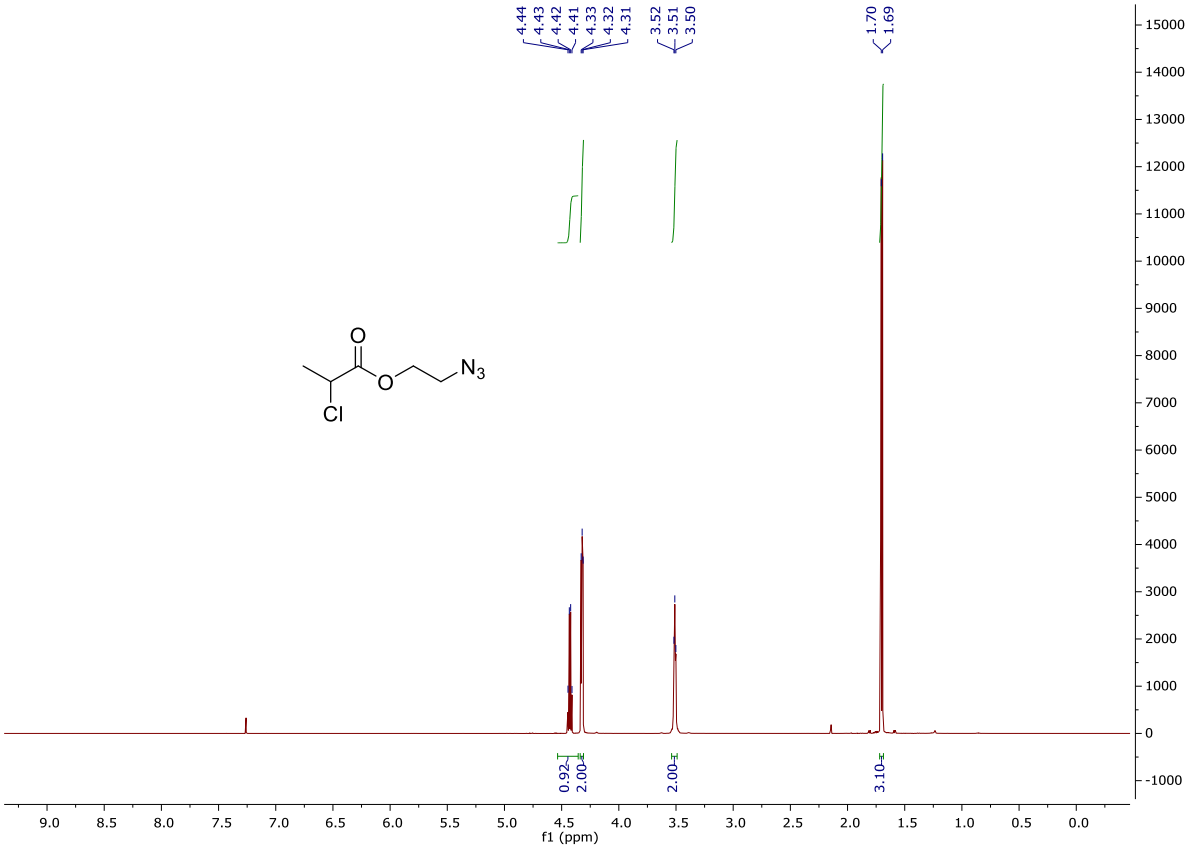

^{13}C NMR spectra of 2-azidoethyl 2-chloropropanoate **3.7**

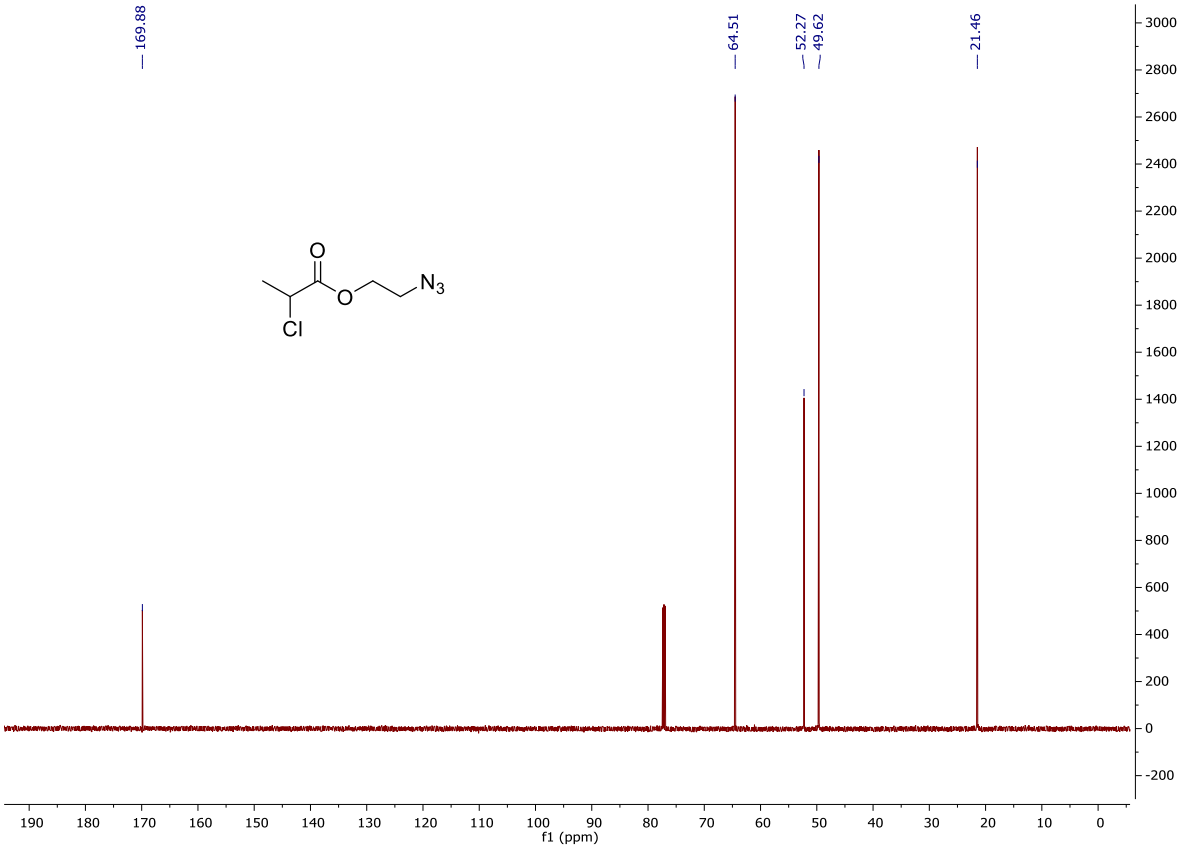

^{1}H NMR spectra of (*S*)-**3.8**

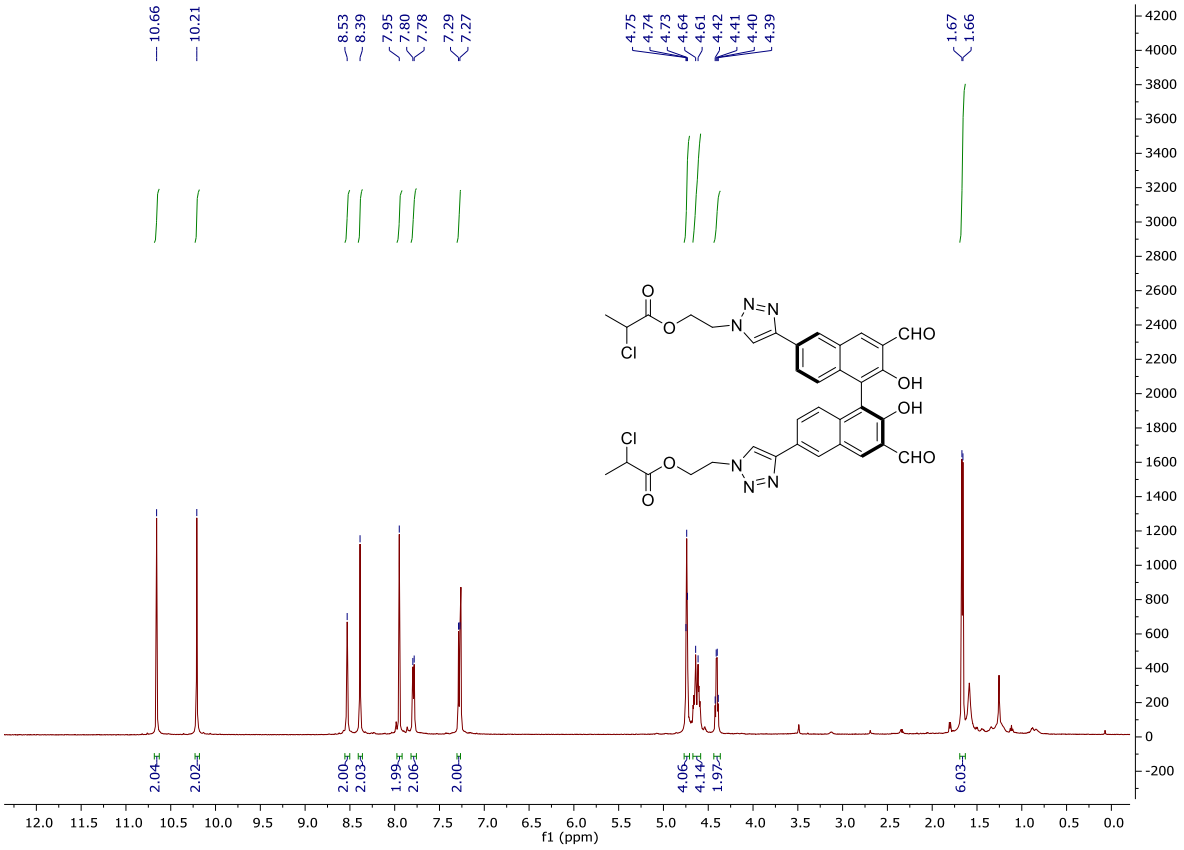

^{13}C NMR spectra of (*S*)-**3.8**

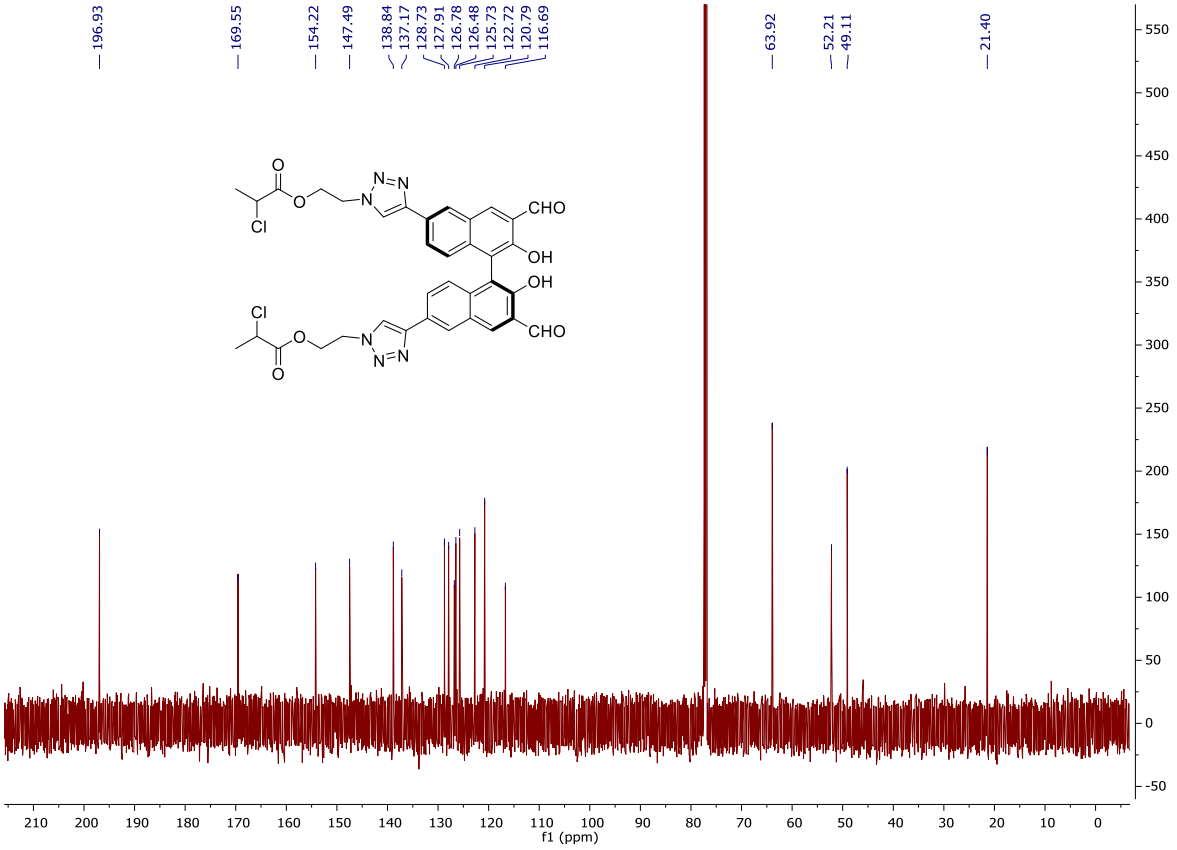

^{1}H NMR spectra of (*R*)-**3.8**

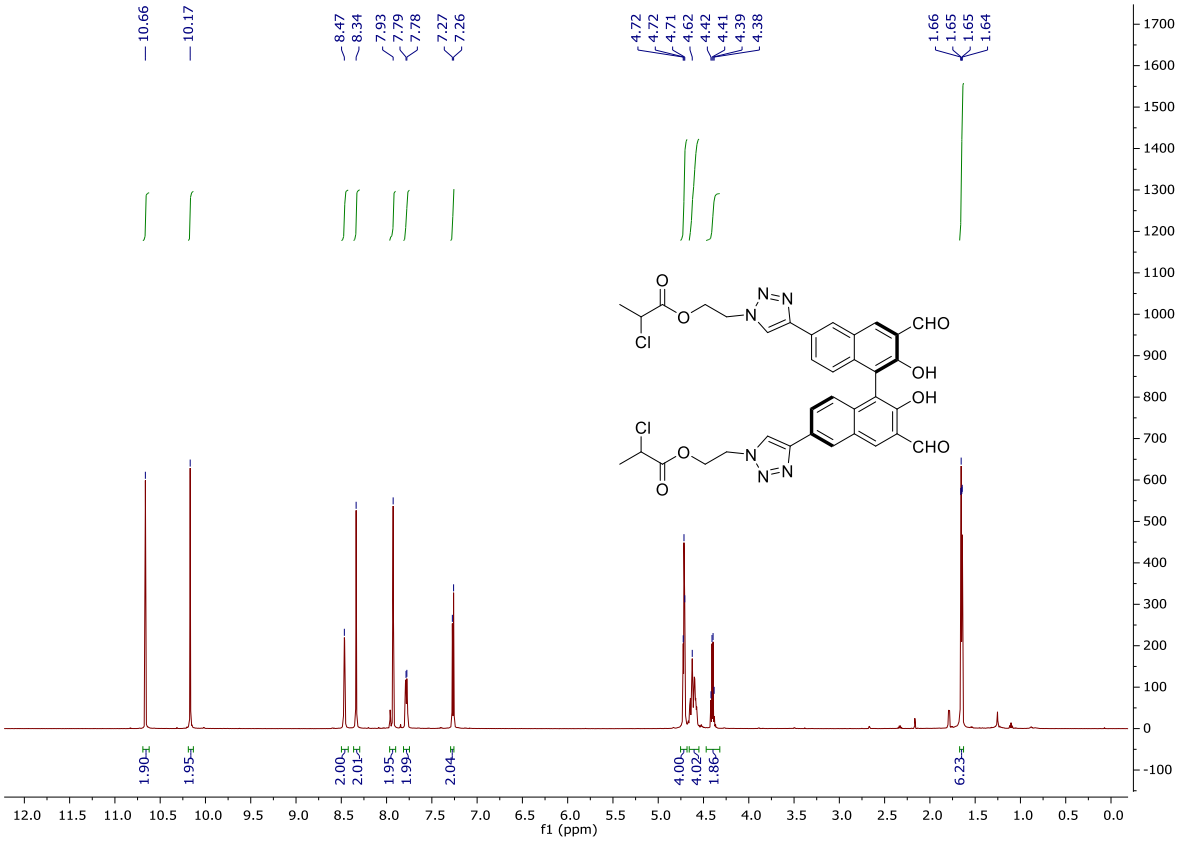

^{13}C NMR spectra of (*R*)-**3.8**

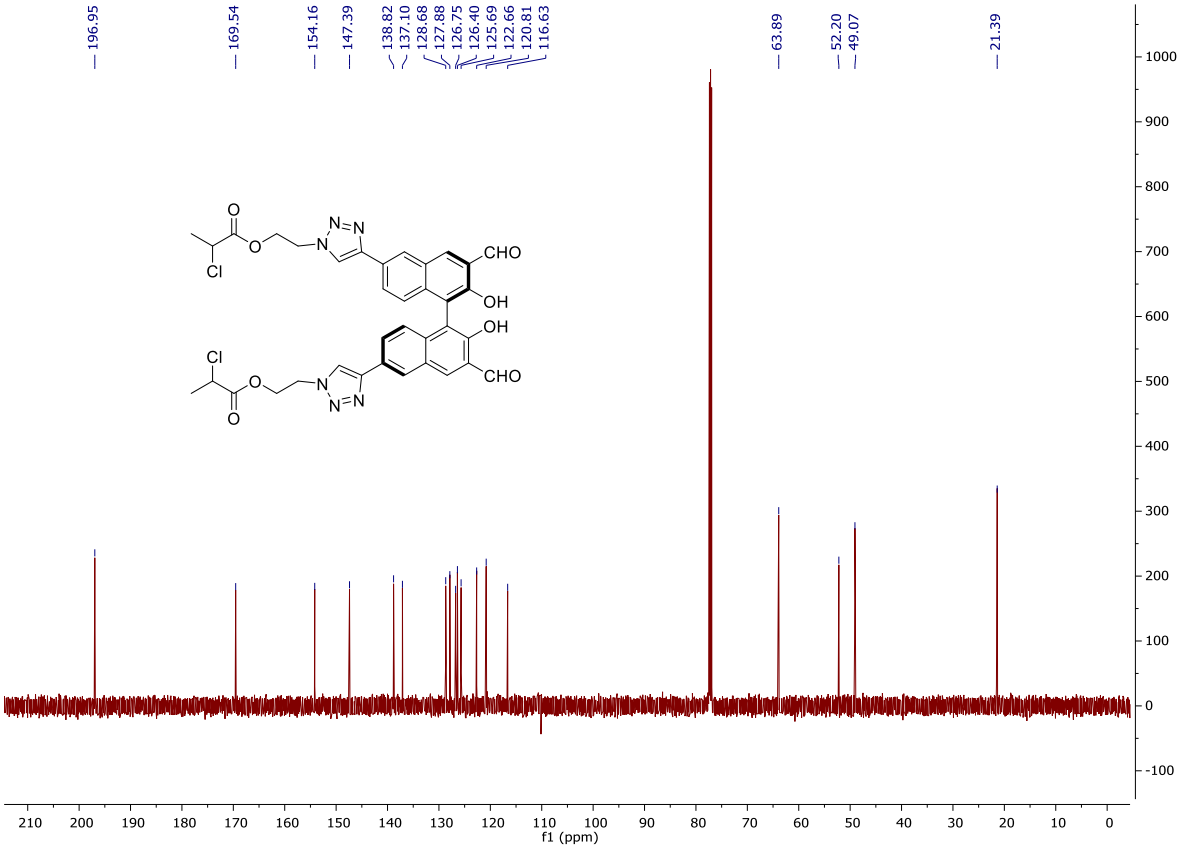

^{1}H NMR spectra of (*S*)-**3.9** in $CDCl_3$

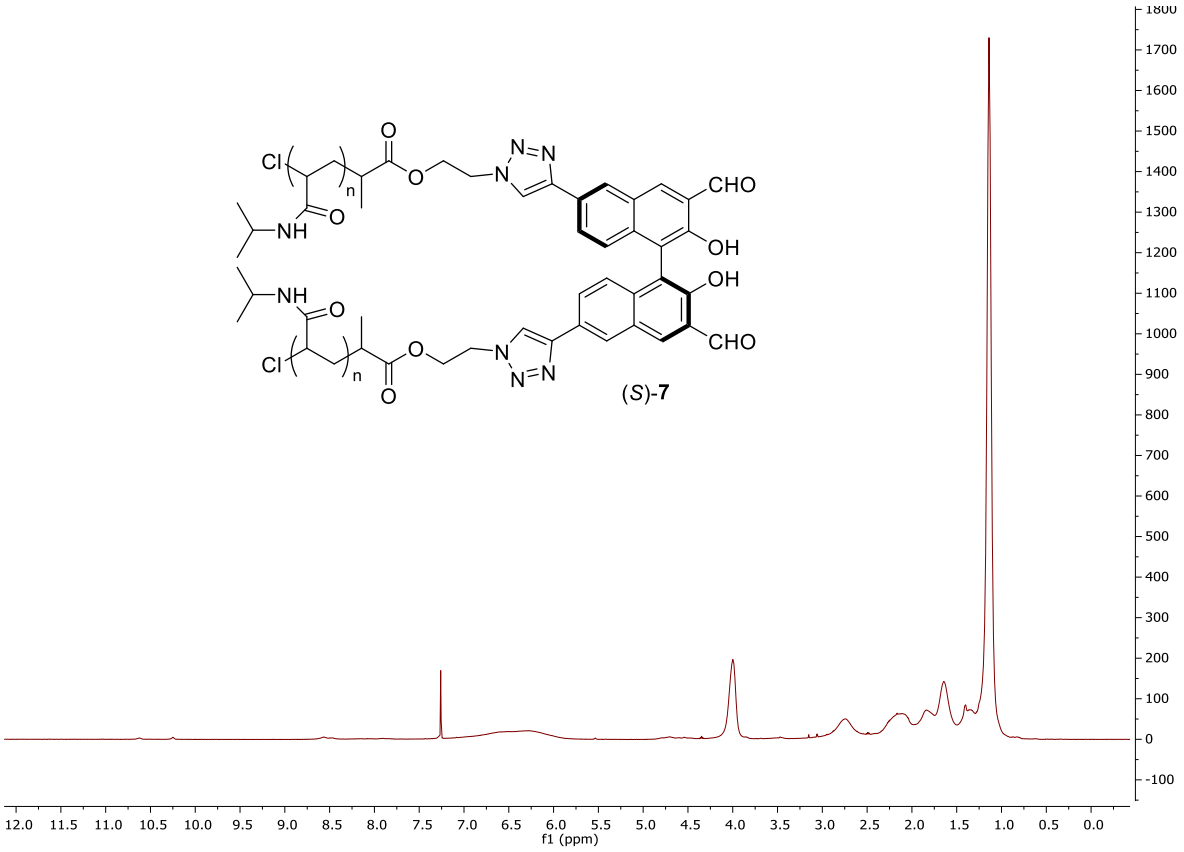

Zoom in of ^{1}H NMR spectra of (*S*)-**3.9**

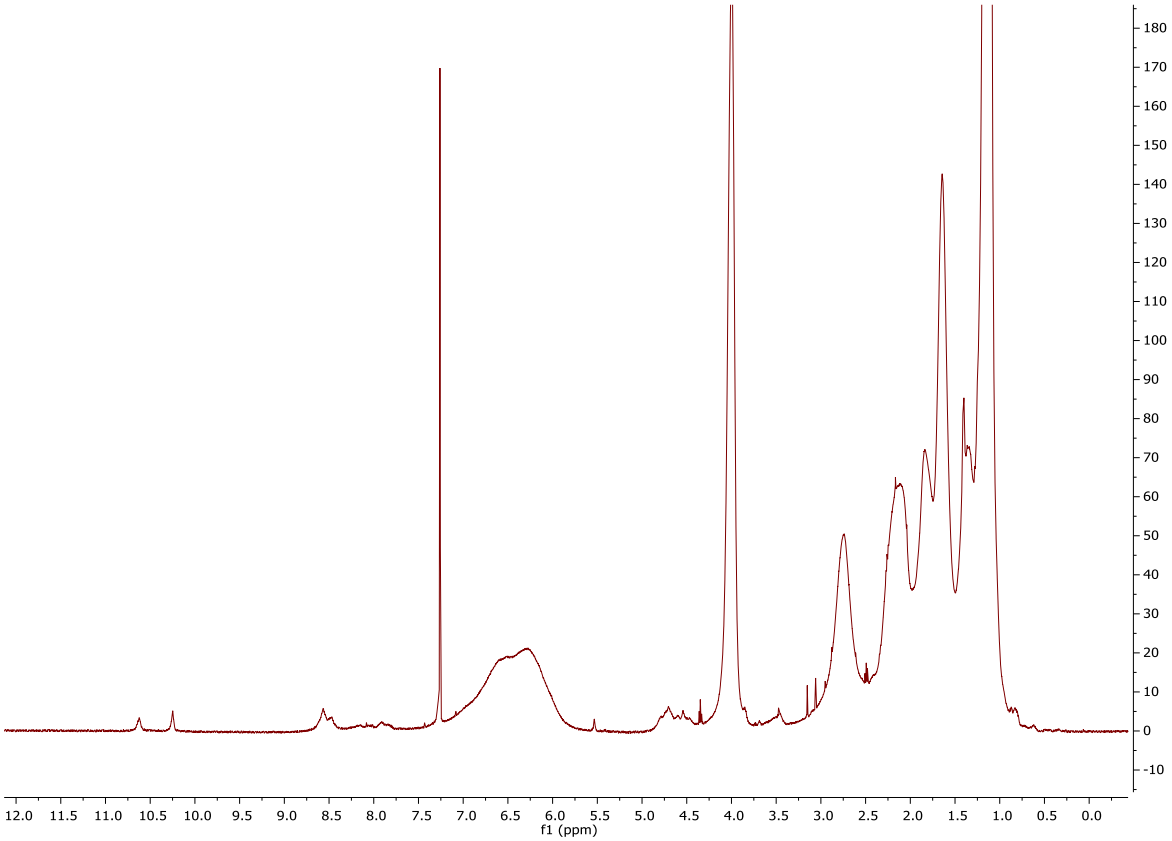

^{1}H NMR spectra of (*R*)-**3.9** in $CDCl_3$

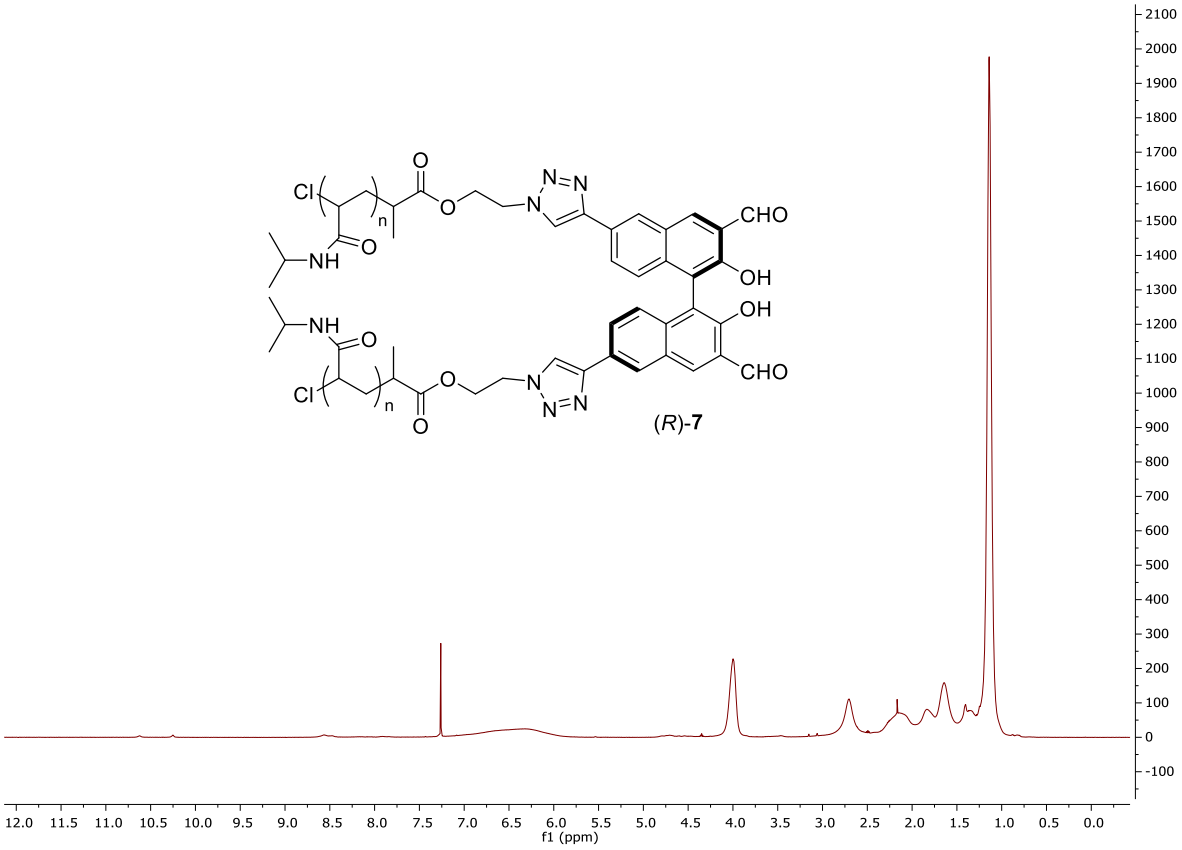

Zoom in of ^{1}H NMR spectra of (*R*)-**3.9**

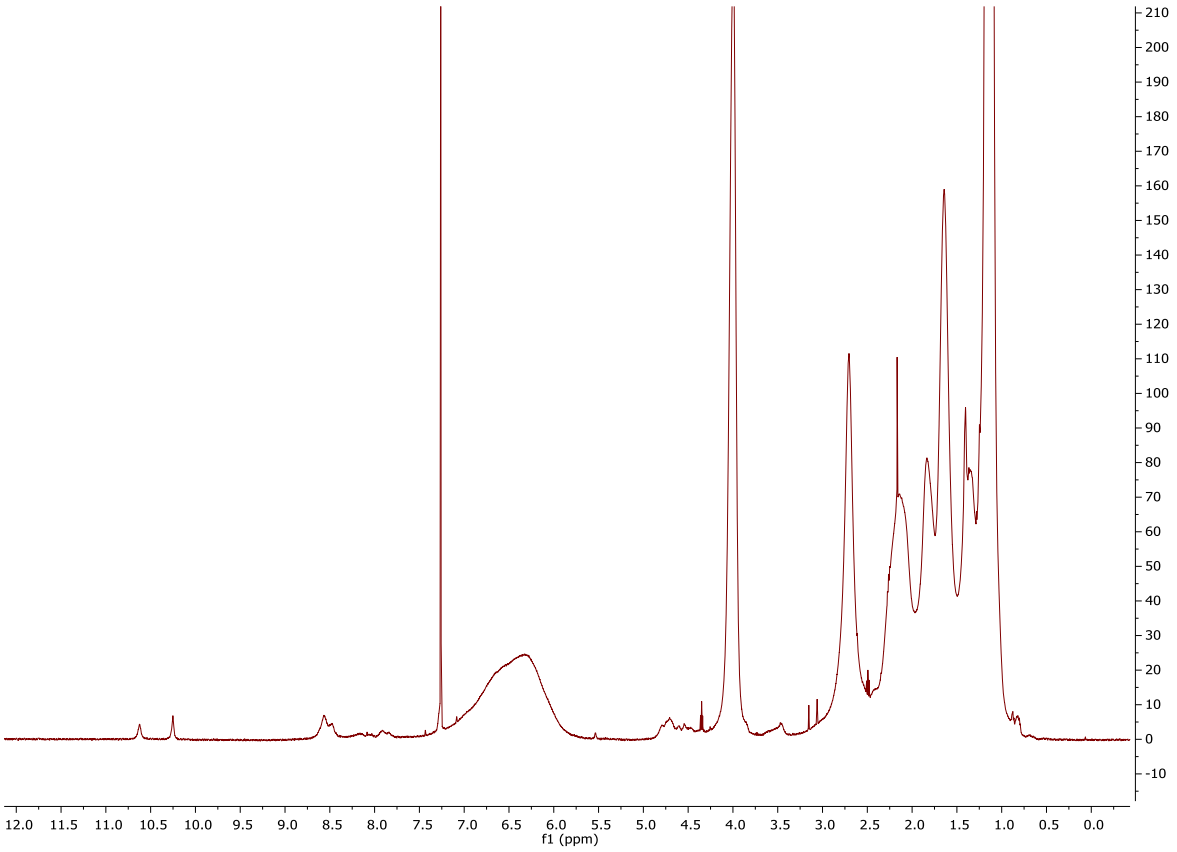

Appendix for Chapter 4

GPC Data for *Rac*-**3.9**

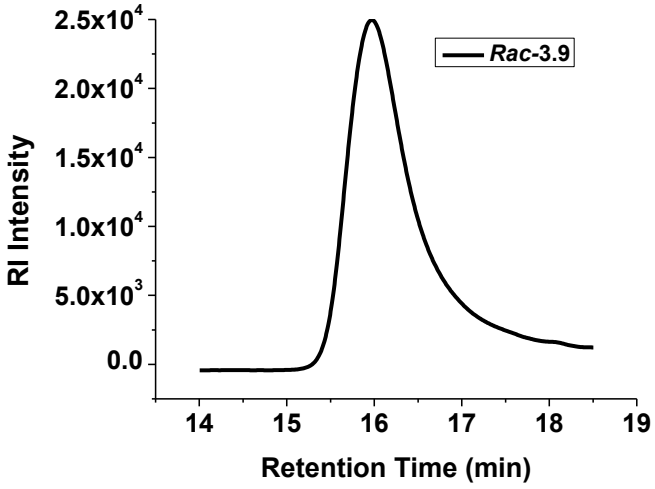

^{1}H and ^{13}C NMR Data

^{1}H NMR spectra of *Rac*-**3.9** in $CDCl_3$

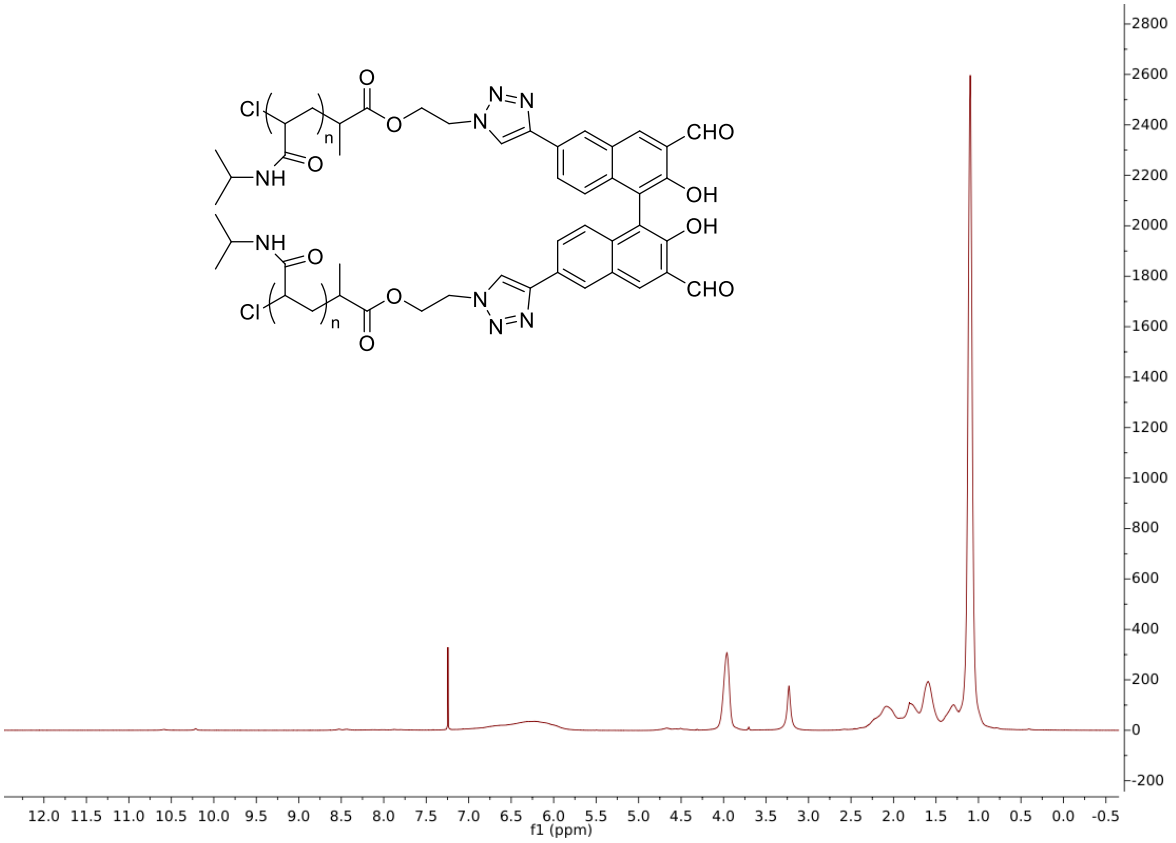

Zoom in of ^{1}H NMR spectra of *Rac*-**3.9** in $CDCl_3$

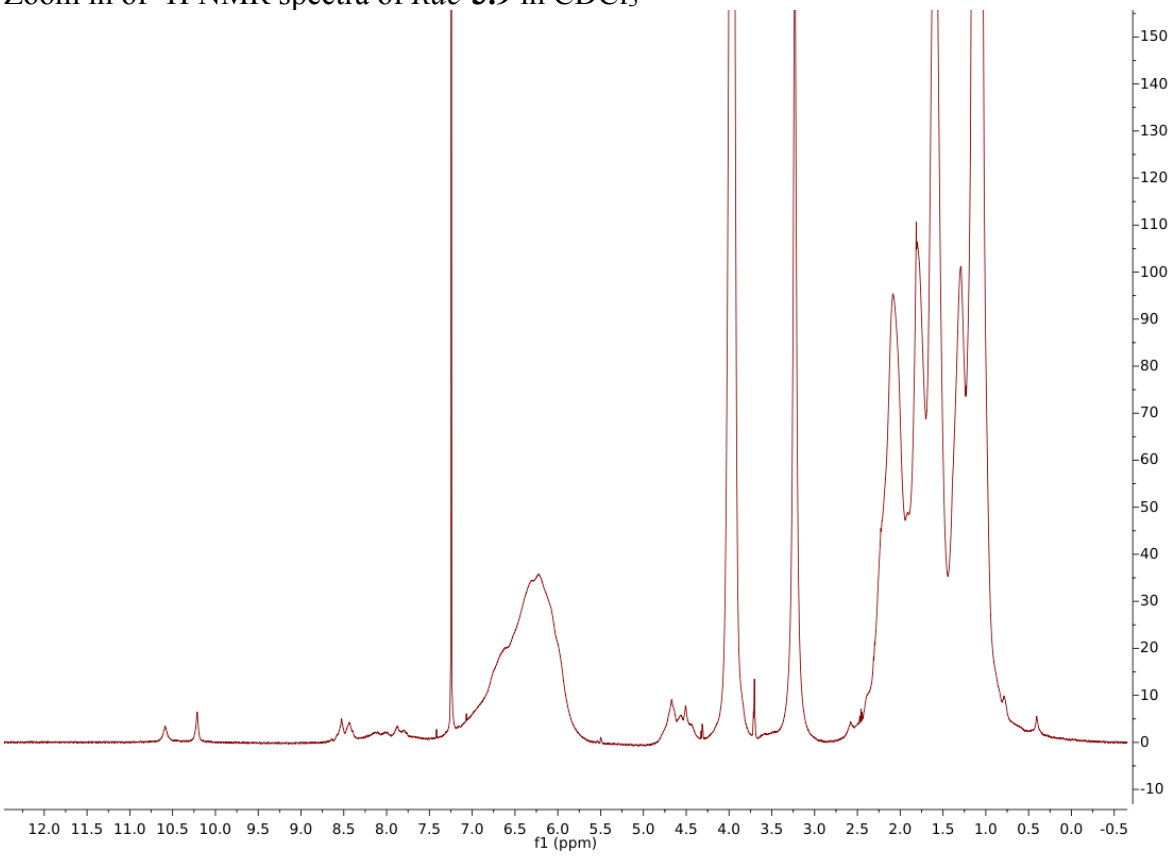

^{13}C NMR spectra of *Rac*-**3.9** in $CDCl_3$

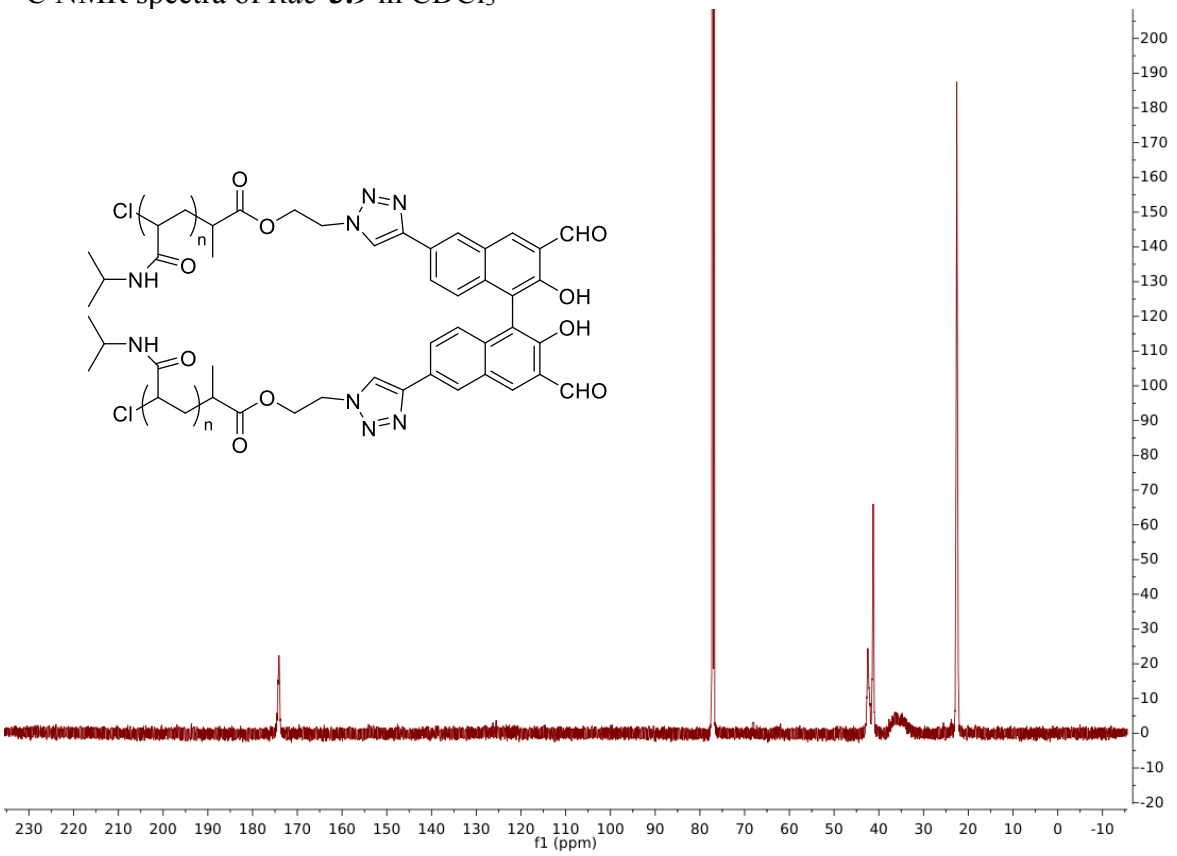

^{1}H NMR spectra of **4.6** in $CDCl_3$

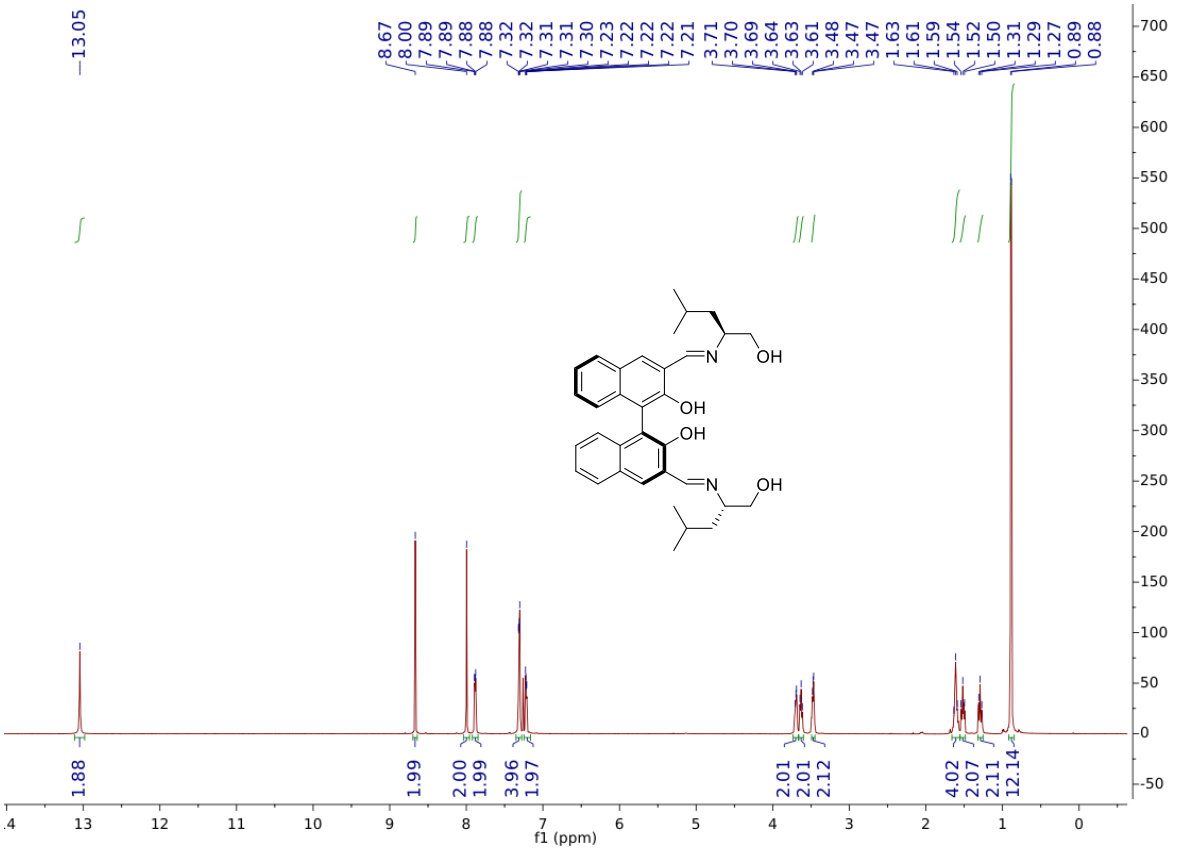

^{13}C NMR spectra of **4.6** in $CDCl_3$

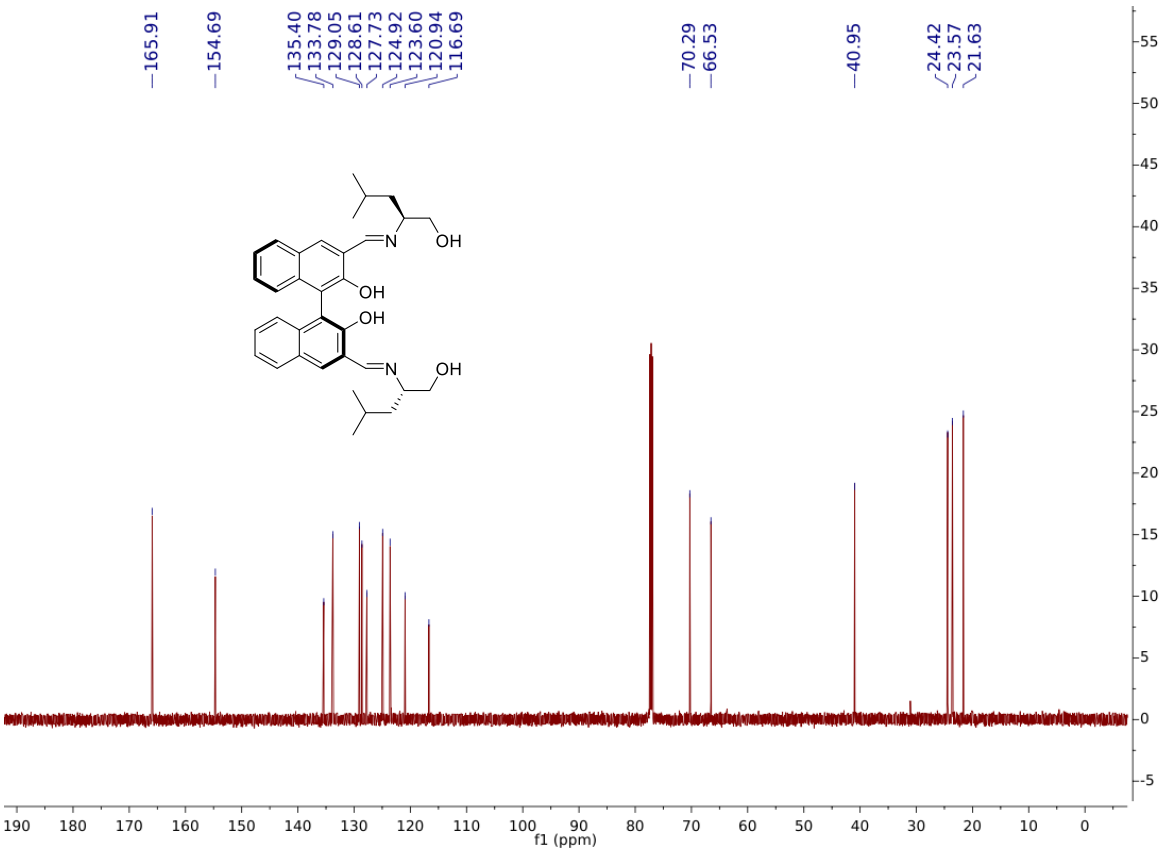

^{1}H NMR spectra of **4.7** in $CDCl_3$

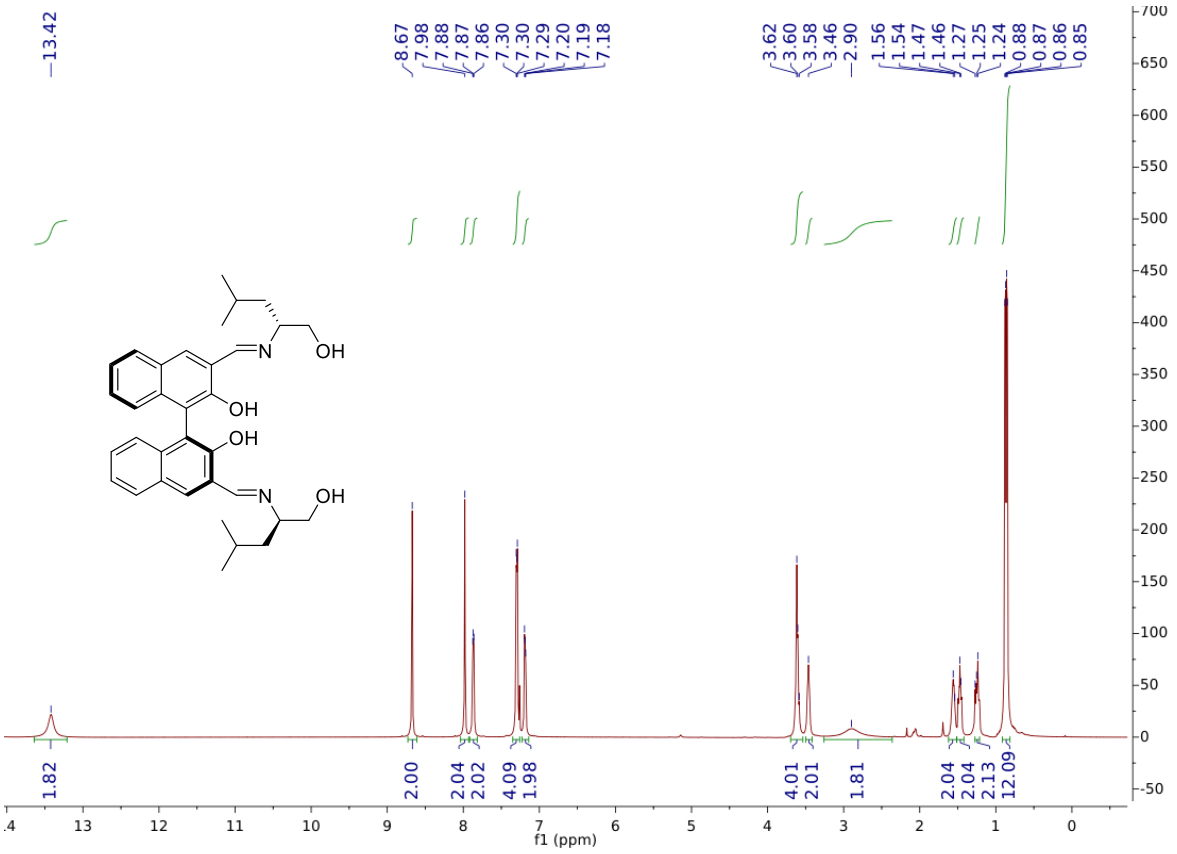

^{13}C NMR spectra of **4.7** in $CDCl_3$

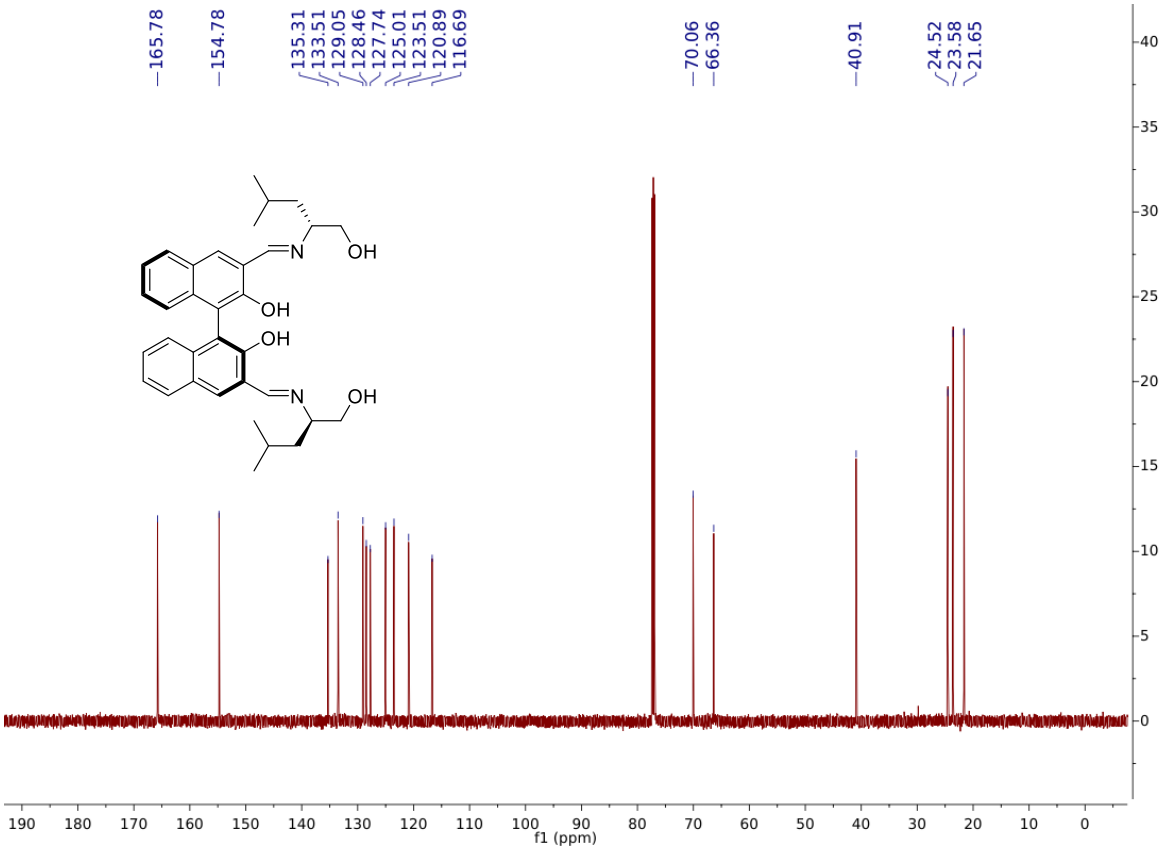

^{1}H NMR spectra of **4.8** in $CDCl_3$

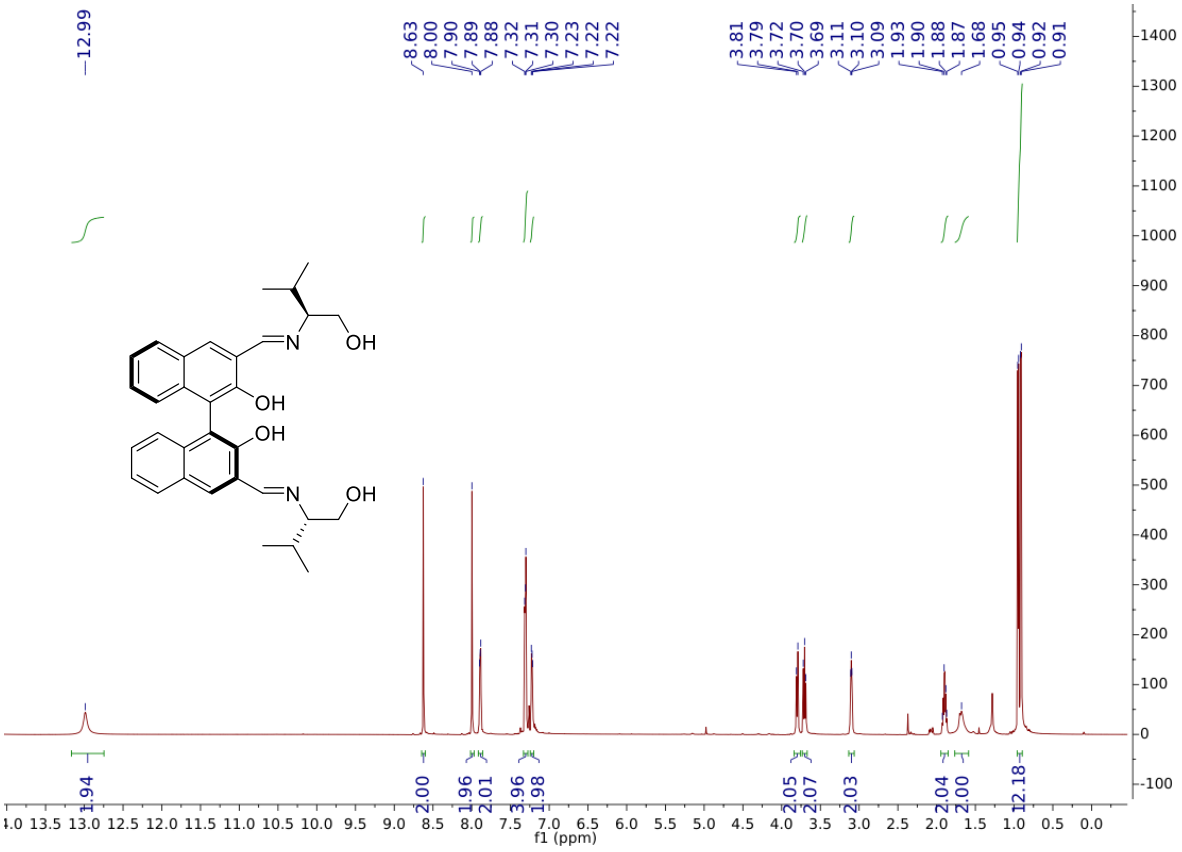

^{13}C NMR spectra of **4.8** in $CDCl_3$

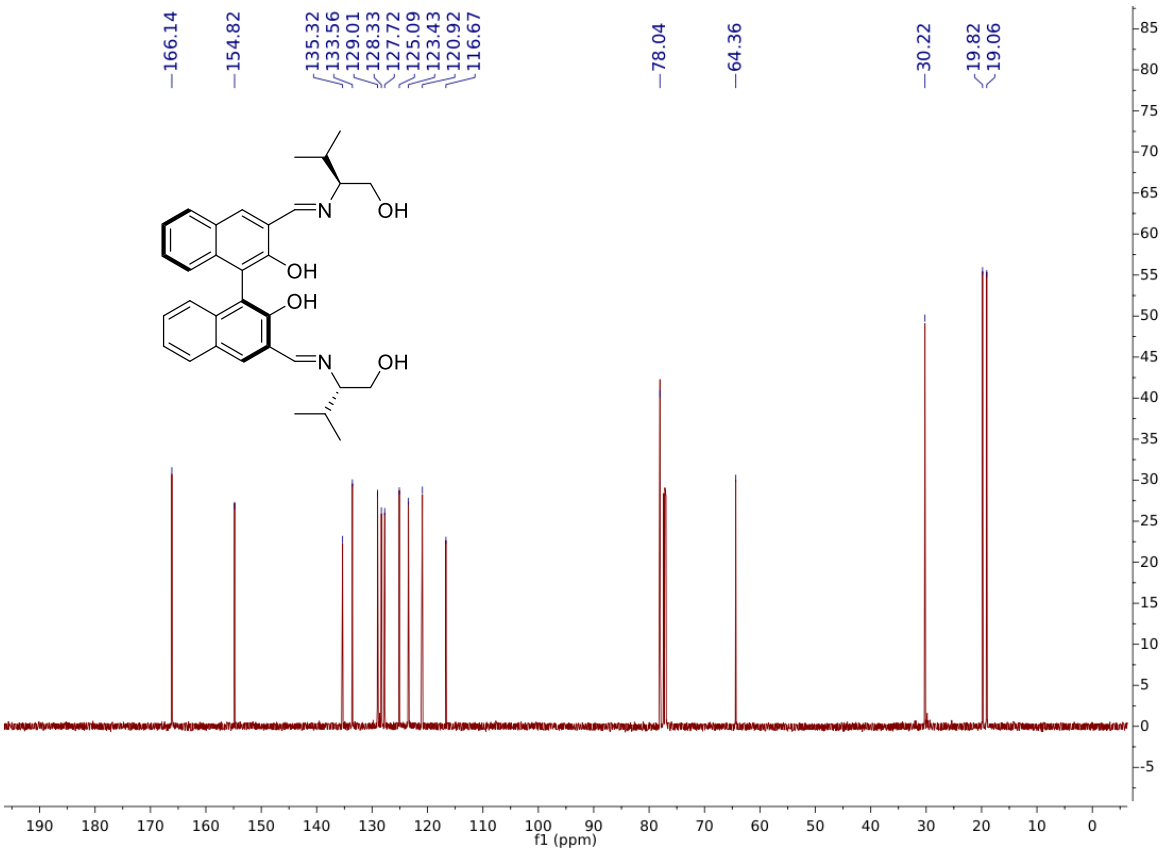

^{1}H NMR spectra of **4.9** in $CDCl_3$

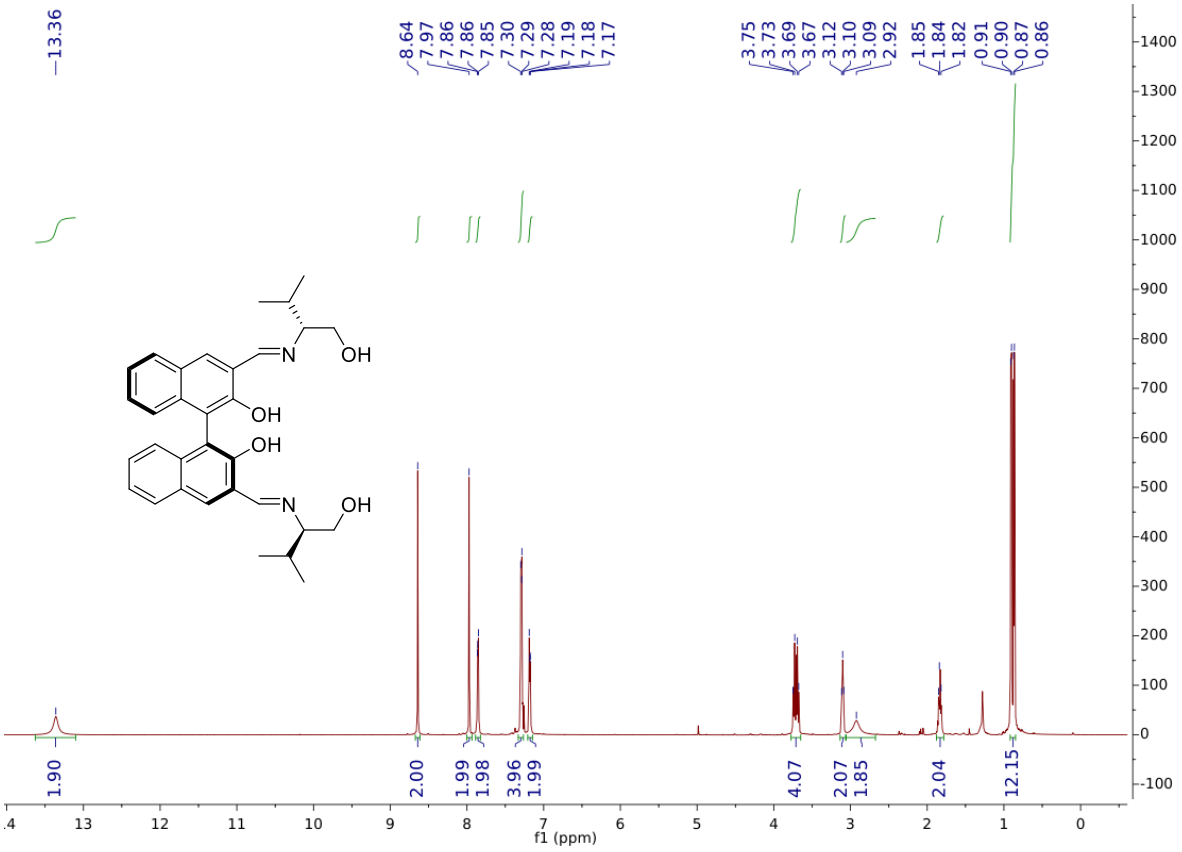

^{13}C NMR spectra of **4.9** in $CDCl_3$

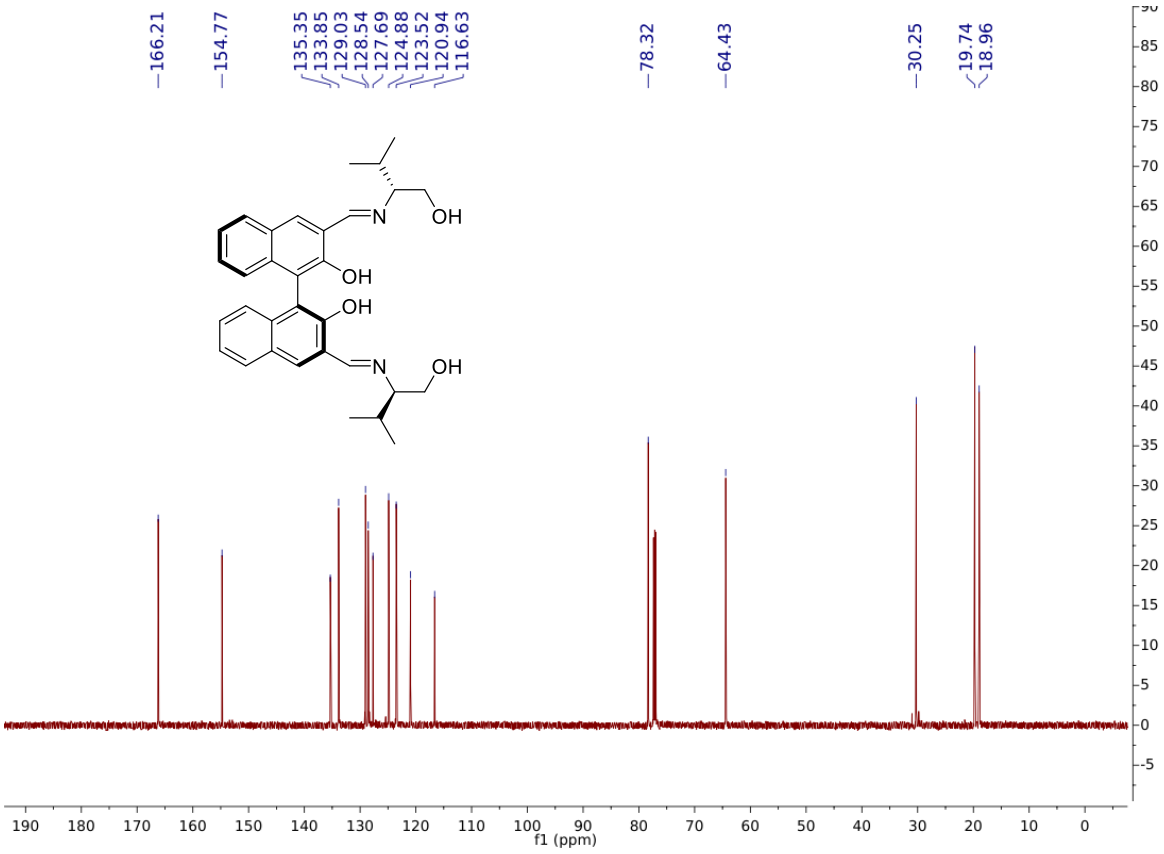

Title:	Simultaneous Determination of Both the Enantiomeric Composition and Concentration of a Chiral Substrate with One Fluorescent Sensor
Author:	Shanshan Yu, Winston Plunkett, Michael Kim, et al
Publication:	Journal of the American Chemical Society
Publisher:	American Chemical Society
Date:	Dec 1, 2012

PERMISSION/LICENSE IS GRANTED FOR YOUR ORDER AT NO CHARGE

This type of permission/license, instead of the standard Terms & Conditions, is sent to you because no fee is being charged for your order. Please note the following:

- Permission is granted for your request in both print and electronic formats, and translations.
- If figures and/or tables were requested, they may be adapted or used in part.
- Please print this page for your records and send a copy of it to your publisher/graduate school.
- Appropriate credit for the requested material should be given as follows: "Reprinted (adapted) with permission from (COMPLETE REFERENCE CITATION). Copyright (YEAR) American Chemical Society." Insert appropriate information in place of the capitalized words.
- One-time permission is granted only for the use specified in your request. No additional uses are granted (such as derivative works or other editions). For any other uses, please submit a new request.

If credit is given to another source for the material you requested, permission must be obtained from that source.

BACK CLOSE WINDOW

Title: Enantioselective Fluorescent Recognition in the Fluorous Phase: Enhanced Reactivity and Expanded Chiral Recognition

Author: Chao Wang, Elaine Wu, Xuedan Wu, et al

Publication: Journal of the American Chemical Society

Publisher: American Chemical Society

Date: Mar 1, 2015

PERMISSION/LICENSE IS GRANTED FOR YOUR ORDER AT NO CHARGE

This type of permission/license, instead of the standard Terms & Conditions, is sent to you because no fee is being charged for your order. Please note the following:

- Permission is granted for your request in both print and electronic formats, and translations.
- If figures and/or tables were requested, they may be adapted or used in part.
- Please print this page for your records and send a copy of it to your publisher/graduate school.
- Appropriate credit for the requested material should be given as follows: "Reprinted (adapted) with permission from (COMPLETE REFERENCE CITATION). Copyright (YEAR) American Chemical Society." Insert appropriate information in place of the capitalized words.
- One-time permission is granted only for the use specified in your request. No additional uses are granted (such as derivative works or other editions). For any other uses, please submit a new request.

If credit is given to another source for the material you requested, permission must be obtained from that source.

Title:	Structurally Rigid and Optically Active Dendrimers
Author:	Qiao-Sheng Hu, Vincent Pugh, Michal Sabat, et al
Publication:	The Journal of Organic Chemistry
Publisher:	American Chemical Society
Date:	Oct 1, 1999

PERMISSION/LICENSE IS GRANTED FOR YOUR ORDER AT NO CHARGE

This type of permission/license, instead of the standard Terms & Conditions, is sent to you because no fee is being charged for your order. Please note the following:

- Permission is granted for your request in both print and electronic formats, and translations.
- If figures and/or tables were requested, they may be adapted or used in part.
- Please print this page for your records and send a copy of it to your publisher/graduate school.
- Appropriate credit for the requested material should be given as follows: "Reprinted (adapted) with permission from (COMPLETE REFERENCE CITATION). Copyright (YEAR) American Chemical Society." Insert appropriate information in place of the capitalized words.
- One-time permission is granted only for the use specified in your request. No additional uses are granted (such as derivative works or other editions). For any other uses, please submit a new request.

If credit is given to another source for the material you requested, permission must be obtained from that source.

BACK CLOSE WINDOW

Title: Enantioselective Fluorescent Recognition of a Soluble "Supported" Chiral Acid: Toward a New Method for Chiral Catalyst Screening

Author: Zi-Bo Li, Jing Lin, Ying-Chuan Qin, et al

Publication: Organic Letters

Publisher: American Chemical Society

Date: Aug 1, 2005

PERMISSION/LICENSE IS GRANTED FOR YOUR ORDER AT NO CHARGE

This type of permission/license, instead of the standard Terms & Conditions, is sent to you because no fee is being charged for your order. Please note the following:

- Permission is granted for your request in both print and electronic formats, and translations.
- If figures and/or tables were requested, they may be adapted or used in part.
- Please print this page for your records and send a copy of it to your publisher/graduate school.
- Appropriate credit for the requested material should be given as follows: "Reprinted (adapted) with permission from (COMPLETE REFERENCE CITATION). Copyright (YEAR) American Chemical Society." Insert appropriate information in place of the capitalized words.
- One-time permission is granted only for the use specified in your request. No additional uses are granted (such as derivative works or other editions). For any other uses, please submit a new request.

If credit is given to another source for the material you requested, permission must be obtained from that source.

BACK CLOSE WINDOW